# ABSTRACT

Title of dissertation: NUCLEAR STRUCTURE STUDIES OF $^{78,80}$Ge AND ADJACENT NUCLEI

Anne Marie Forney
Doctor of Philosophy, 2018

Dissertation directed by: Professor William B. Walters
Department of Chemistry and Biochemistry

The main topic of this thesis concerns the unusual features of the nuclear structure of $^{78}$Ge. The discovery of a sequence of levels separated by one unit of angular momentum for which the expected crossover transitions carrying two units of angular momentum are not observed. This result stands in contrast to the neighboring even-even Ge and Se nuclei, as well as the results of most model calculations. The level structures of adjacent $^{82,80}$Ge are also studied to place the results for $^{78}$Ge in context. Likewise, shell-model calculations are performed as comparisons with the structures for all three nuclei.

The data come from experiments at Argonne National Laboratory using the Gammasphere detector array. These experiments are important because of the broad interest in the structure of $^{76}$Ge and neighboring nuclei, owing to a world-wide effort in the search for neutrinoless double $\beta$ decay. Owing to the unusual features of this level sequence, it is labelled as a $\kappa$ band, taken from the Greek word $\kappa\alpha\iota\nu o\acute{\upsilon}\rho\gamma\iota o\varsigma$, meaning new. The results pose a challenge to theorists to find ways to develop

models that can fit both these features, as well as the other aspects of the structure of $^{78}$Ge. In addition, this study is important determining why no sequence like this has been found in any of the adjacent nuclei.

# NUCLEAR STRUCTURE STUDIES OF $^{78,80}$Ge AND ADJACENT NUCLEI

by

Anne Marie Forney

Dissertation submitted to the Faculty of the Graduate School of the
University of Maryland, College Park in partial fulfillment
of the requirements for the degree of
Doctor of Philosophy
2018

Advisory Committee:

Professor William B. Walters, Advisor, Chair
Professor Alice C. Mignerey
Professor Amy S. Mullin
Professor John M. Ondov
Professor William F. McDonough
Representing the Dean of the Graduate School

# Dedication

I dedicate this dissertation to my husband and best friend, David Colman.

# Acknowledgments

First and foremost, I would like express my special appreciation to my supervisor, Bill Walters. Working with Bill these past few years has given me an invaluable opportunity to contribute to meaningful research under the watchful eye of a leader in the field of nuclear structure. Bill was always there to share with me the excitement of each new discovery in a wide range of nuclei, the implications, and the extensive history of every research group in the field. The enthusiasm Bill exhibits provides an important model of how one can be an involved, long-term player in this field. I have greatly benefited from his support of my interest in Health Physics related topics, while encouraging me to become engaged in the future of detector arrays, such as GRETA. It has been an honor to be his PhD student and I look forward to joining the ranks his many successful graduates.

I am deeply grateful to Robert Janssens, who has acted as a mentor without equal. He has been a major supportive force throughout my PhD with unmatched attention to detail and a knack for limiting my use of unsubstantiated jargon. I am indebted to him for his valuable guidance and blunt honesty.

I would like to acknowledge Chris Chiara, for his keen eye and willingness to share his time and expertise far beyond angular correlations: into every piece required to achieve a truly rigorous analysis of the data.

Special thanks to Akaa Daniel Ageanakaa who helped make this paper easier to read, providing insights towards my writing and formatting. It has been a pleasure to work with him.

I cherish the genuine camaraderie shared with Barbara Walters in our days of teaching young undergraduates and one another.

I also want to express my appreciation to all of my colleagues within the nuclear structure community. This impactful group continually strives to build a strong cohort of informed scientists through meetings, training, and networking. Special thanks to Alex Brown at MSU for the support with his NuShellX code, to Heather Crawford and the group at LBNL for their tireless dedication to the future of $\gamma$-ray spectroscopy, and to Shaofei Zhu and the group at ANL for keeping Gammasphere running and their assistance with experiments (especially the 3 a.m. phone calls for help).

I gratefully acknowledge the Marie Curie Fellowship Programme and Professor Dimitris Emetzoglou. My time in Greece not only initialized this PhD odyssey but also served as a formative year on a personal level.

Numerous funding sources made this PhD possible, but I am particularly grateful for Department of Energy support which allowed me to focus on this research full-time. This work is supported by the U.S. Department of Energy, Office of Science, Office of Nuclear Physics, under contract Nos. DE-AC02-06CH11357 (ANL) and DE-AC02-98CH10886 (BNL), and grants No. DE-FG02-94ER40834 (Maryland), DE-FG02-97ER41041 (UNC), DE-FG02-97ER41033 (TUNL). This research used resources of ANLs ATLAS facility, which is a DOE Office of Science User Facility.

These past years, I could easily have been focused only on a half-life but friends at and outside the University of Maryland provided an important balance to my

academic pursuits. To the members of Faith Lutheran Church thank you for teaching me what it means to be a leader and and to understand the common ties that bind a community. To my fellow Team Z'ers - I am grateful for the companionship and wonderful memories punctuated by hundreds of pool laps, long runs, and even longer bike rides. The motto "you'll never know... unless you tri" has been applicable to much more than triathlons. Seven years ago, I could not have imagined that I would be a two-time IronMan finisher getting her PhD!

Lastly, I owe so much to my family for their unwavering support and guidance throughout my PhD path. To my grandparents, Dr. Robert C. Forney and Mrs. Marilyn G. Forney, for setting a high standard for the family. To my parents, Gerald Forney and Irene Ludwig, who have always encouraged me to enrich my life through education, travel, culture, and service. To my mom, who would come up with math problems to keep me occupied during church sermons. To my dad, who has an answer for any question. They raised me with a love of science and encouraged me every step of the way. Most of all, much thanks to my loving, patient, and supportive husband David. He has been along for a roller-coaster, especially in these final stages of this PhD but will not have the title to prove it. Thank you.

Anne Marie Forney

University of Maryland College Park

October 2018

# Table of Contents

# List of Tables

# List of Figures

LIST OF ABBREVIATIONS

# List of Abbreviations

| | |
|---|---|
| $\alpha$ | Alpha |
| AC | Angular correlation |
| ANL | Argonne National Laboratory |
| ATLAS | Argonne tandem linear accelerator system |
| $B(E2)$ | Reduced transition probability |
| $\beta$ | Beta |
| $\beta$-$n$ | Beta-delayed neutron |
| BGO | Bismuth germanate |
| CLARA | Clover detector array at Legnaro, Italy |
| Co | Cobalt |
| Cu | Copper |
| DDD | Delay-Delay-Delay coincidence |
| DIS | Deep-inelastic scattering... MNT |
| ECR | Electron cyclotron resonance |
| EDF | Energy density functional |
| $\gamma$ | Gamma |
| Ge | Germanium |
| gsb | Ground-state band |
| HBF | Gogny-Hartree-Fock-Bogoliubov |
| HF | Hartree-Fock |
| HPGe | High-purity Germanium |
| $J^{\Pi}$ | Angular momentum (spin) and parity |
| Kr | Krypton |
| MNT | Multi-nucleon transfer... DIS |
| Ni | Nickel |
| PAC | Program advisory committee |
| Pb | Lead |
| PDD | Prompt-Delay-Delay coincidence |
| PPP | Prompt-Prompt-Prompt coincidence |
| PRISMA | Magnetic spectrometer for heavy ions at Legnaro, Italy |
| Pt | Platinum |
| RHB | Hartree-Bogoliubov |
| SCMF | self-consistent-mean-field |
| Se | Selenium |
| Zn | Zinc |

# Chapter 1: Introduction

## 1.1 Overview

The nuclear shell model is the main theoretical model to describe the structure of nuclei close to closed shells. This paradigm has evolved from a simplistic view such as the atomic shell model to include the spin-orbit interaction and deformation of the potential well. It has been developed mainly by the study of stable nuclei. The model has made it possible to identify extra stability in groups of nuclei that have a closed nuclear orbital (shell), which are considered "magic" nuclei. More recently, studies of "semi-magic" nuclei which exist on a sub-shell closure have further tested the nuclear shell model. An important discovery resulting from such investigations is that not all nuclei are spherical and described in shell-model terms.

Atomic nuclei exist in a variety of shapes, with closed-shell ones adopting spherical symmetry, and those between closed shells possessing varying degrees of spheroidal deformation. For most deformed nuclei, the ground states are characterized by axially-symmetric configurations with equilibrium shapes corresponding to either prolate or oblate ellipsoids. In many cases, strong deviations from axial symmetry in the nuclear mean field have been observed. These nuclei are described as triaxial, owing to reduced axial symmetry.

Theoretical nuclear structure models predict the possibility of over 3000 nuclei within the limits of the neutron and proton drip lines. However, only half have been observed. Specific experimental setups have been dedicated to study non-stable (exotic) isotopes for further insight into the underlying physics of the nucleus. From these experiments, collectivity, shape coexistence, triaxiality, and intruder states have been discovered in nuclei near the $N = 40$ and $N = 50$ oscillator shell closures.

Experimental nuclear spectroscopy is used to determine the characteristics of the different quantum states of the nuclear system including: energy, spin, and parity. It is not enough to know the characteristics of the excited states, but also the manner of decay and electromagnetic static moments. In this work, nuclear excited states were populated through deep-inelastic collisions between a beam and a target with the Argonne Tandem Linear Accelerator System (ATLAS) at Argonne National Laboratory. The subsequent decay of the nuclear excited states was detected using the Gammasphere high-purity germanium detector array.

A wide variety of shapes have been postulated for stable $^{72,74,76}$Ge. Some nuclei of these nuclei indicate the presence of multiple shapes, some of which may be triaxial. The focus of this thesis is the structure of $^{78}$Ge whose static properties, meaning level energies, appear to be similar to those in the lighter Ge nuclei, but whose dynamic properties, that is their decay modes are completely different. A sequence of states in $^{78}$Ge has been observed in this work to decay strictly through $\Delta J = 1$ transitions, while similar sequences is other Ge nuclei decay through both $\Delta J = 1$ and 2 transitions.

Calculations have been performed using the NuShellX program to determine

if the $\Delta J = 2$ transitions are diminished theoretically whose results do not show diminished $E2$ strength. Due to the failure of the shell model to describe the absence of such transitions, other models which describe triaxiality were considered. The Davydov-Filippov-Rostovsky (DFR) model describes a rigid-triaxial rotor with a deformation parameter, $\gamma$. When $\gamma$ is maximized at 30°, the probability of $\Delta J = 2$ transitions becomes zero. Although there are other aspects of the DFR calculations that are not in accord with such observations, these calculations are the sole source in which the $\Delta J = 2$ transitions have a probability of zero. The DFR model over-predicts the excitation energy of such states, which is persistent problem with many theoretical models.

## 1.2 Properties of nuclei

The nucleus can be characterized in terms of static and dynamic properties. Static properties include nuclear size, mass, spin, and also electric and magnetic moments. The time-dependent dynamic properties of nuclei arise from transitions between excited levels, and also transitions between excited levels and the ground state.

This dissertation focuses on the nuclear static properties of $^{82,80,78}$Ge as a result of the population of excited nuclear states and the dynamic properties of the decay of one sequence of levels. Nuclear $\gamma$-ray spectroscopy provides a means to study the structure of these Ge nuclei. Studies of nuclear structure are important in understanding the role of each individual nucleon, impacting the shape, stability, decay,

and the excitation energies of the nucleus. The addition or removal of an individual nucleon can have unexpected effects on experimentally observed phenomena. Some of these effects are hard to account for in a single model,, including the changes in the excited states within an isotopic chain at mid-shell and closed shell.

## 1.3 Nucleons

In the twentieth century, the development of high-energy projectiles allowed further study of individual nucleons. One such study in the early 1960s, produced the unexpected result that the magnetic moment of a proton is not equal to a magneton, and also suggested that a neutron has magnetic properties. These observations implied that nucleons are comprised of smaller entities. The entities include quarks and gluons which are bound together to create a particle called a hadron. Quarks have an electric charge of $2/3$ or $-1/3$, and gluons are a type of boson that holds together the nucleon. The types of hadrons found in nature are mesons and baryons. Mesons are comprised of a quark and an anti-quark, and they make up particles such as pions or kaons. Baryons are comprised of three quarks, and some examples include protons, neutrons, and anti-protons. A neutron is comprised of two down (d) $-1/3$ and one up (u) $2/3$ quarks for a total charge of 0. Similarly, a proton has two up (u) and one down (d) quarks combining to a charge of $+1$. The discovery of quarks complicates the quantum mechanical description of the nucleus, because each nucleon requires a three-body interaction to describe its behavior.

## 1.4 Development of nuclear structure models

In this work, nucleons are treated as the fundamental building blocks of the nucleus. Nuclear interactions lead to the experimentally-observed nuclear phenomena. Nuclei may be comprised of hundreds of nucleons moving in orbitals, with a diameter of $10^{-14}$ to $10^{-15}$ m. The nucleus can be described in short-hand as ${}^{A}_{Z}\mathrm{X}_{N}$ with X representing the element (based on proton number), and nuclear mass number, $A$, which is the sum of the number of protons ($Z$) and neutrons ($N$). Confining these protons and neutrons in such a small space requires a force far stronger than the Coulomb repulsive force that repels protons, and thus it is named the strong nuclear force.

The development of models for nuclear structure only started in 1932 with the discovery of the neutron. Shortly thereafter, the liquid drop formulation of nuclear masses and binding energies was promulgated by von Weizsäcker in his famous formula:

$$E_B = a_V A - a_s A^{2/3} - a_C \frac{Z(Z-1)}{A^{1/3}} - a_A \frac{(A-2Z)^2}{A} + \partial(A,Z) \qquad (1.1)$$

In the liquid drop model, the binding in the nucleus is described by a strong, contact nuclear force (proportional to its volume, $a_V A$), whose effects are reduced by Coulomb repulsion between protons ($-a_C \frac{Z(Z-1)}{A^{1/3}}$), loss of binding energy at the surface ($-a_s A^{2/3}$), and the imbalance between numbers of neutrons ($N$ or $\nu$) and protons ($Z$ or $\pi$) ($-a_A \frac{(A-2Z)^2}{A}$). In addition, a pairing term ($\partial(A,Z)$) accounts for strong pairing between nucleons that lead all nuclei with even numbers of both neu-

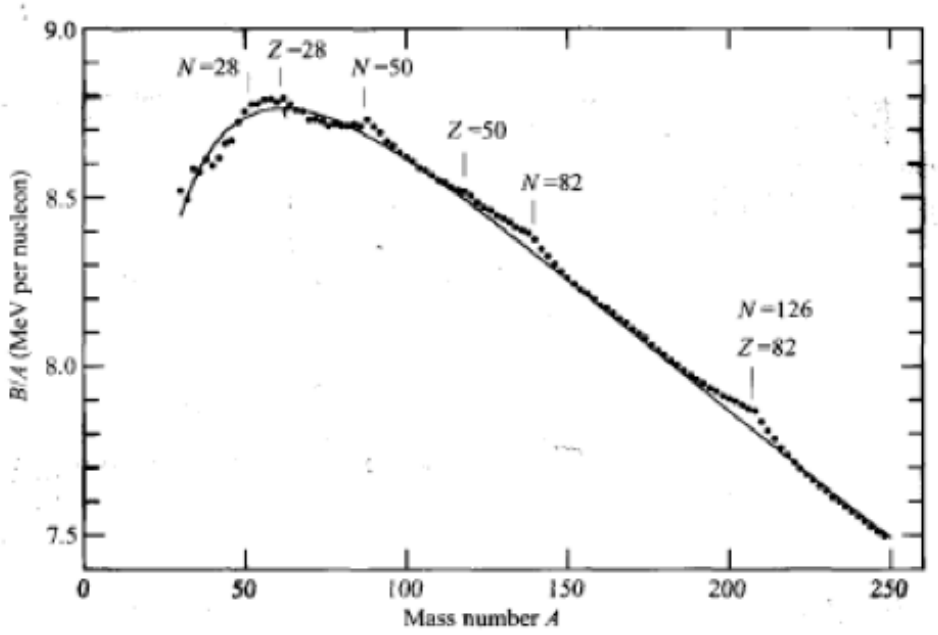


Figure 1.1: Binding energy per nucleon dependent on mass number from Ref. [7].

trons and protons to exhibit zero ground state angular momentum. The result is a general description of binding energy per nucleon ($BE/A$) that is shown in Fig. 1.1, which describes the stability of the nucleus by the nuclear binding energy, which is a measure of the force required to break a nucleus into its neutron and proton components. From this, it is assumed that nuclei are approximately spherical like a liquid drop or a basketball. The power of this model is that it can explain processes such as fission.

As more precise nuclear masses became available, small peaks in the BE/A curve (Fig. 1.1) were identified at nucleon numbers $28, 50, 82$, and $126$. Vilen M. Strutinsky showed that the inclusion of shell corrections provided a much better description of fission [8]. Quantum mechanical approximations using both a square-

well and a harmonic-oscillator (H.O.) potential could not reproduce these peaks. In 1949, Maria Mayer, formerly of Argonne National Laboratory (ANL), initiated the shell-model description of nuclear structure in which strong spin-orbit coupling dominated the filling of nuclear orbitals along with strong pairing. The nuclear shell model describes the configuration of the nucleus through orbitals and levels. Like the atomic shell model, there are orbitals with different radial properties, which can hold a certain number of nucleons.

The Bohr planetary model for electrons in the atom describes the quantization of atoms, and it is a precursor to the full quantum-mechanical description of the atom with a central potential. Four quantum numbers emerge from the full quantum mechanical description: $n$, $\ell$, $\ell_m$, and $s$. The principle quantum number, $n$, designates the size of the nuclear orbital. The angular momentum and directional numbers, $\ell$ and $\ell_m$, refer to the shape of the orbital and its orientation in a magnetic field. Lastly, the spin, $s$ is an intrinsic angular momentum value limited to $\pm 1/2$. These four basic atomic descriptors of nuclei provide insight into certain properties in the the nucleus such as the rise of strong stability.

The main difference between the atomic model and nuclear shell model is that the atomic shell model assumes a central potential, while the nuclear shell model assumes a spherically symmetric mean field potential. Two basic mechanisms can be used to describe excited states at low energy. These are single-particle excitation and collective excitation. Single-particle excitation is included in the independent particle model, which focuses on the wavefunction of the unpaired particle. A simple example of this model is an odd nucleus whose ground state is due to the unpaired

nucleon. Additional excited states can be created by moving that nucleon to a higher single particle orbital. Collective excitation is comprised by the excitation of multiple nucleons. The term "closed shell" was coined to describe a filled nuclear orbital (Table 1.1).

The four quantum numbers to describe a nuclear state are N, $\ell$, $J$, and $J_m$. N is the principle quantum number, which designates the size of the orbital. The angular momentum of a level is denoted by $\ell$, whereas the total nuclear angular momentum, $J$, is defined by $J = \ell \pm s$. Orbitals with $J = \ell + s$ are significantly lowered in energy with respect to nuclei with $J = \ell - s$. The occupancy of each level is dependent on the degeneracy, described by $J_m = 2J + 1$.

The standard shell-model diagram is shown in Fig. 1.2. The properties of an odd-mass nucleus reflect the properties of the last unpaired neutron or proton, due to strong pairing. In the absence of an external magnetic field, the states with the same $J$ are degenerate, where multiple states occur at the same energy. For her work on this topic, Maria Mayer was awarded the Nobel Prize in 1963. Further use of the shell model suggests that it describes the nuclei near closed shells well, but it is unable to describe nuclei away from a filled orbital.

Table 1.1: Parity and capacity of nuclear orbitals.

| Orbital | $\ell$ | J | Nucleons for each J | Total Nucleons | Natural Parity |
|---|---|---|---|---|---|
| s | 0 | 1/2 | 2 | 2 | + |
| p | 1 | 1/2, 3/2 | 2, 4 | 6 | - |
| d | 2 | 3/2, 5/2 | 4, 6 | 10 | + |
| f | 3 | 5/2, 7/2 | 6, 8 | 14 | - |
| g | 4 | 7/2, 9/2 | 8, 10 | 18 | + |
| h | 5 | 9/2, 11/2 | 10, 12 | 22 | - |
| i | 6 | 11/2, 13/2 | 12, 14 | 26 | + |

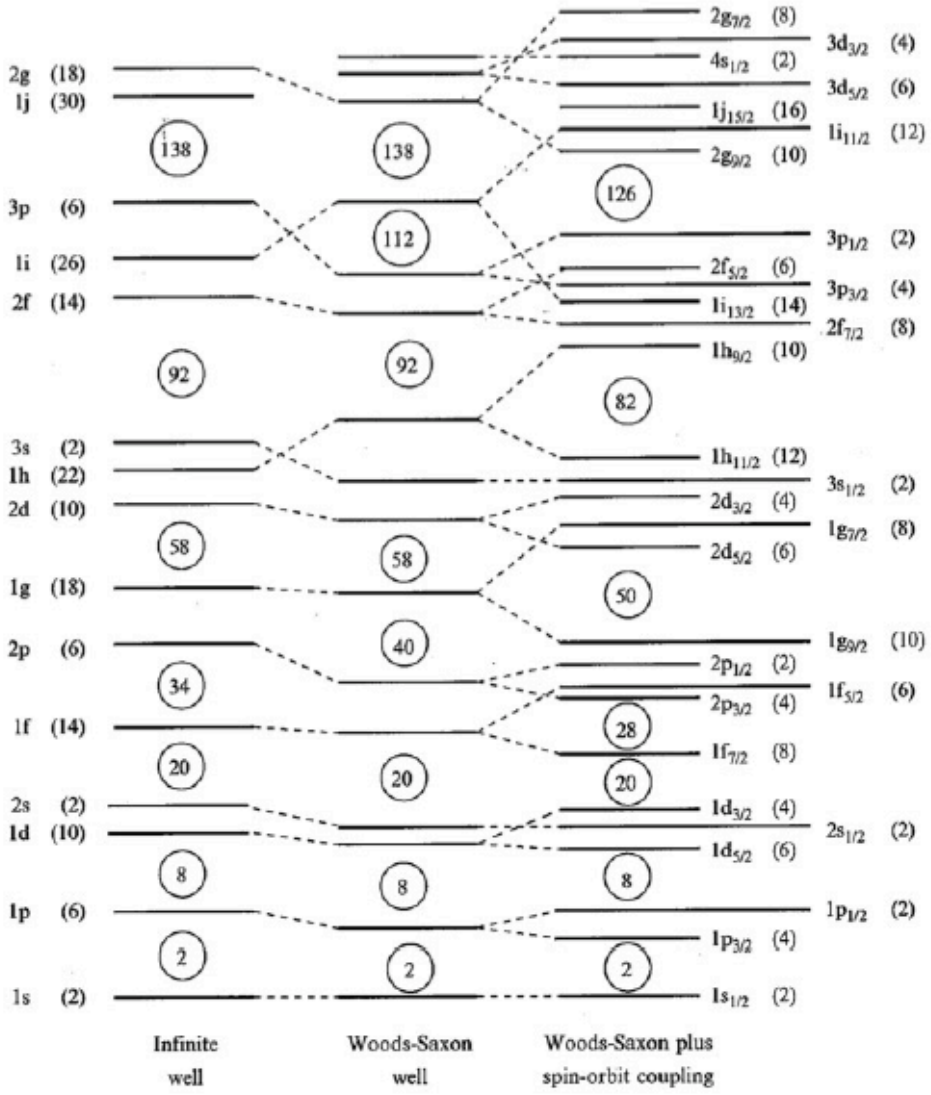


Figure 1.2: Shell model approximations with the infinite well, Woods-Saxon well, and Woods-Saxon plus spin-orbit coupling. The numeric-alphabetical value on the left is the quantum number N and its corresponding orbital (s,p,d,...). Numbers in parentheses describe the occupation available in each orbital.

## 1.5 Stability and interactions within nuclei

Nuclear separation energies act as a measure of stability, provide information on the outermost nucleon, and also describe the characteristics of the nuclear force near the edge of the nucleus. The separation energies, $S(p)$ for protons and $S(n)$ for neutrons, are defined as the energy required to remove the last (valence) nucleon from the nucleus. This energy results from the fact that nucleons seem to favor pairing. The observation that nucleons favor pairing is basic to the field of quantum chromodynamics (QCD), which investigates the fundamental properties that make up nucleons, and aims to describe the source of the fundamental nuclear force. The range of the nuclear force is on the order of $10^{-15}$ m (on the same order of magnitude as the diameter of a nucleus), so it does not affect electrons or other nuclei in a molecule. In most mass calculations, the strength of the nuclear force is set at a constant value of 14 MeV/nucleon.

A similar measure for stability is the nuclear binding energy, which is a measure of the force required to break a nucleus into its neutron and proton components. Certain neutrons and protons demonstrate high separation energies and binding energies (Fig. 1.1), implying an underlying stability in the nucleus shown by the difficulty in removing a nucleon. This increased stability has been found with nucleon numbers of $8, 20, 28, 50, 82$, and 126.

Nucleons interact with one another in three different mechanisms. The first type is between two protons (p-p), the second is between two neutrons (n-n), and the third is between one proton-one neutron (p-n). The nuclear force does not

distinguish between p-p and n-n interactions, which can be observed by the similarity of level structure in mirror nuclei which have the same mass numbers but inverted neutron and proton numbers. The principle that governs pp-nn interactions is the Pauli principle. Data on nucleon separation energies show the p-n interaction as attractive and strong when both are particles. Data also show that there is a direct correlation between an increase in $N$ or $Z$ with the separation energy of $S(N)$ or $S(P)$, respectively.

## 1.6 Nuclear excited state production

Gamma-ray ($\gamma$-ray) decay occurs with the emission of electromagnetic radiation (a photon) when a nucleus is in a state other than its ground state. The $\gamma$ ray must connect the initial and final states of the nucleus, remove energy, and possibly change the total angular momentum from the higher, initial excited state. The wavefunction of each state is dependent on the behavior, $(-1)^{\ell}$, of the spherical harmonic under oscillation. The nuclear properties of an energy state are best described by a definite energy ($E$), angular momentum (often denoted as spin, $J$), and parity ("$\pi$"). All levels of a given harmonic oscillator shell have the same parity. Positive parity is associated with even $\ell$ values, and negative parity with odd $\ell$ values. The even or odd value of $\ell$ determines the symmetry of the nuclear state wavefunction. Each nucleon has its own quantum properties, and protons and neutrons occupy separate orbitals, denoted as $\pi$ and $\nu$, respectively. For example, the $46^{th}$ neutron in the $^{78}$Ge nucleus can be described as $\nu 1g_{9/2}$, where $\nu$ designates a neutron, $1g$ is

the smallest $g$ orbital in the nucleus, and 9/2 is the total angular momentum of that $g$ orbital. This state would be a $9/2^+$ level, where the parity is governed by $\ell = 4$.

Each gamma transition has a multipolarity that quantifies the amount of angular momentum carried away as well as the change in parity. If one unit of angular momentum is carried away, it is called a dipole photon. When two units are removed it is referred to as a quadrupole, and when three units are removed it is an octupole (Table 1.2). If the final and initial states have the same parity, $\Delta\pi = 0$, they are colloquially referred to as "no". States are described in the form of $J^{\pi}_{\#}$, where the subscript number identifies the state $J$ value starting at 1 (the first instance), and increasing with the excitation energy.

Table 1.2: Gamma ray multipolarities determined by change in angular momentum and parity.

| Radiation Type | Name | $\ell = \Delta J$ | $\Delta\pi$ |
|---|---|---|---|
| 1 | Electric Dipole | 1 | (yes) |
| 1 | Magnetic Dipole | 1 | (no) |
| 2 | Electric Quadrupole | 2 | (no) |
| 2 | Magnetic Quadrupole | 2 | (yes) |
| E3 | Electric Octupole | 3 | (yes) |
| M3 | Magnetic Octupole | 3 | (no) |

The rate of electromagnetic transition ($\lambda$) is governed by the gamma energy ($E_\gamma$), the mass number ($A$), the change in angular momentum, and change in parity as shown in Table 1.3. Since $\lambda$ is proportional to $E_\gamma$ and inversely proportional to $J$, the lowest multipolarity with the highest energy will be favored. In nuclear structure, the yrast band is defined by the quantum state with the lowest energy for a given angular momentum. This topic is discussed in further detail in Section 1.7.

From the proportionality of $\lambda$ to the $\gamma$-ray energy, low-energy transitions are much slower than high-energy transitions due to the strong energy dependence of the transition rates as shown in Table 1.3 [9]. The Weiskopf estimates are the shell model estimations of the electromagnetic transition rates due to single particle orbital change. The half-life of a state ($t_{1/2}$) is related to $\lambda$ by: $\lambda = ln(2)/t_{1/2}$.

Table 1.3: Transition rates ($\lambda$) in excited states: Weisskopf estimates for electric (E) and magnetic (M) transitions.

| Multipole | E, $\lambda(s^{-1})$ | M, $\lambda(s^{-1})$ |
|---|---|---|
| 1 | $1.03 \times 10^{14}\ A_{2/3}\ E_\gamma^3$ | $3.15 \times 10^{14}\ E_\gamma^3$ |
| 2 | $7.28 \times 10^{7}\ A^{4/3}\ E_\gamma^5$ | $2.24 \times 10^{7}\ A^{2/3}\ E_\gamma^5$ |
| 3 | $3.39 \times 10^{1}\ A^{2}\ E_\gamma^7$ | $1.04 \times 10^{1}\ A^{4/3}\ E_\gamma^7$ |
| 4 | $1.07 \times 10^{-5}\ A^{8/3}\ E_\gamma^9$ | $3.27 \times 10^{-6}\ A^{2}\ E_\gamma^9$ |
| 5 | $2.40 \times 10^{-12}\ A^{10/3}\ E_\gamma^{11}$ | $7.36 \times 10^{-13}\ A^{8/3}\ E_\gamma^{11}$ |

Table 1.3 shows that with each extra unit of angular momentum carried away, the transition is slowed by a factor of roughly $10^6$.

## 1.7 Yrast states

Heavy ion reactions can produce nuclei with high total angular momentum. The term "yrast" states has been coined from the Danish word for "dizzy" to denote the state with lowest energy for a particular angular momentum value. As higher angular momentum values require more broken pairs, the location of the "yrast states" increases in energy with angular momentum as shown in Figure 1.3. In addition to the yrast states, many other states are populated. As the nucleus de-excites it loses energy and reduces its angular momentum. This is depicted as a downward movement in Figure 1.3 and eventually feeds the yrast band. The yrast

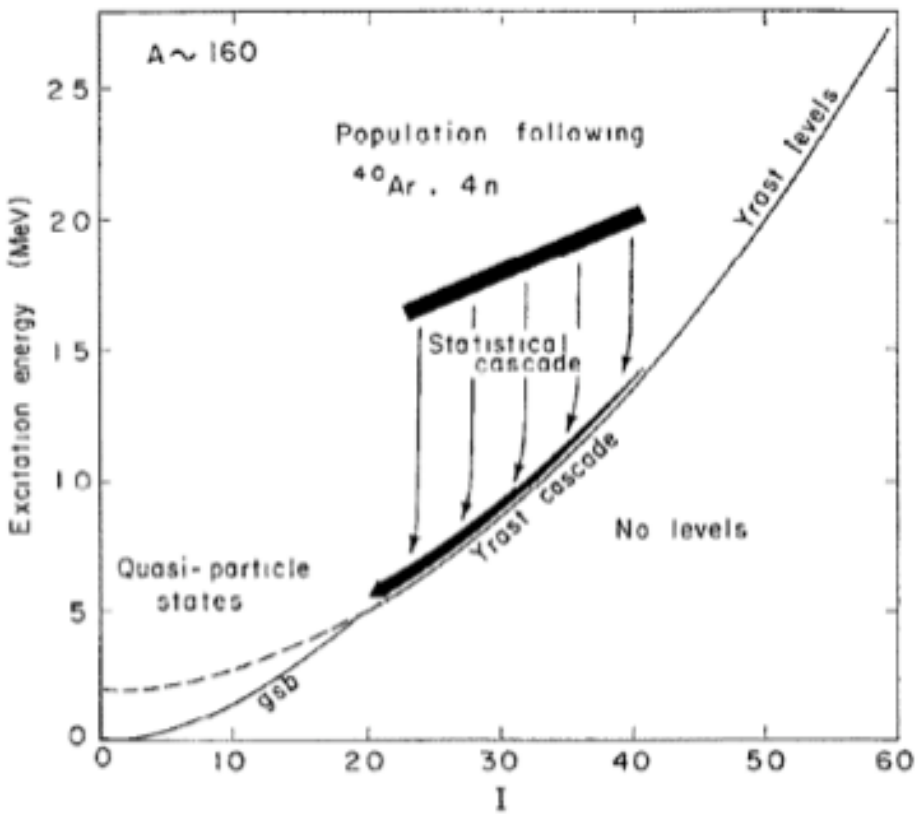


Figure 1.3: Statistical cascade from higher angular momentum into yrast states and ground state band (gsb). Adapted from Ref. [10].

band is the pathway for the energetically unstable nucleus to remove a maximum amount of energy for a minimum change in angular momentum. Transitions between nuclear states with a maximum change in angular momentum ($\Delta J = 2$) are called "stretched". The transitions that make up the yrast band are comprised of these stretched transitions. Stretched transitions are favored because they remove energy and angular momentum quickly. If the only transition moves angular momentum with little energy available (typically $< 400$ keV), the initial nuclear state will have a lifetime and the transition is hindered.

## 1.8 Beyond the shell-model description

The shell model assumes that the nuclear charge in closed shells is spherically symmetric, and this leads to a lack of an electric dipole or quadrupole moment. In 1950, James Rainwater at Columbia University suggested that nuclei might not be spherical, but could take on other shapes. Aaga Bohr, son of Niels Bohr, was a post-doctoral worker at Columbia University at the time, and he took this idea back to Copenhagen where he was joined by Ben Mottelson. Mottelson was a new post-doctoral employee, having finished his studies at Purdue University and Harvard University. This Copenhagen group soon proposed a new model for deformed nuclei. For these ideas, Rainwater, Bohr, and Mottelson were awarded the 1975 Nobel Prize in Physics. Ironically, the standard terminology for this model bears the name of a Copenhagen graduate student, Sven Gösta Nilsson. After graduation, Nilsson returned to the Lund University in Sweden.

## 1.9 Deformed Nuclear Model

The main feature of the Nilsson model is breaking the degeneracy in the deformed field so that favored orbitals are those whose wavefunctions align with the deformed field. As a result the nucleus can be either prolate (football shaped) or oblate (doorknob shaped). Bohr and Mottelson introduced the quadruople oscillation (deformation), and is measured by $\beta$. This parameter describes the deviation from sphericity. Both vibrations and rotations were introduced, each having a $\beta$

value $< 0.2$ or $> 0.2$, respectively.

Nuclei that are near closed shells tend to exhibit quantized vibrational structure in which excitations occur at approximately equal energy intervals as seen in Fig. 1.4. In a vibrational description, the first excited state is a quadrupole vibration with a spin and parity of $2^+$. The second vibrational excitation consists of two such $2^+$ vibrations with $J$ values of $0, 2$, and 4. The second group has approximately twice the energy of the first $2^+$ level. A third group has spins and parities of $0^+, 2^+, 3^+, 4^+$, and $6^+$ with approximately three times the energy of the first $2_1^+$ level. Such sequences are shown in Figure 2 in the Physical Review Letter by Ani Aprahamian, a Freimann Professor at Notre Dame University [12].

More highly deformed nuclei will exhibit a rotational structure in addition to the vibrational structure, where the energy dependence is proportional to $J(J+1)$. The rotational motion is similar to that of the tumbling of a football. In such a scheme, the $4_1^+$ level would be at 3.3 times the energy of the $2_1^+$ level.

Many nuclei have a second excited state with spin and parity of $2^+$ [13, 14]. For spherical nuclei, this state should be vibrational and lie close to the $4^+$ level. In nuclei where this second $2_2^+$ is depressed relative to the $4^+$ state, the depression is attributed to the loss of axial symmetry and described by parameter $\gamma$ [15]. In this formulation, $\gamma$ describes the deviation by an angle where $\gamma = 0°$ as prolate (football) and $\gamma = 60°$ as oblate (doorknob).

Few nuclei actually have the vibrational energy ratio of the first $4^+$ state to first $2^+$ state ($E_4/E_2$) as 2.0. This suggests that the straightforward vibrational approach may be over-simplified. In contrast, football-shaped, prolate nuclei have

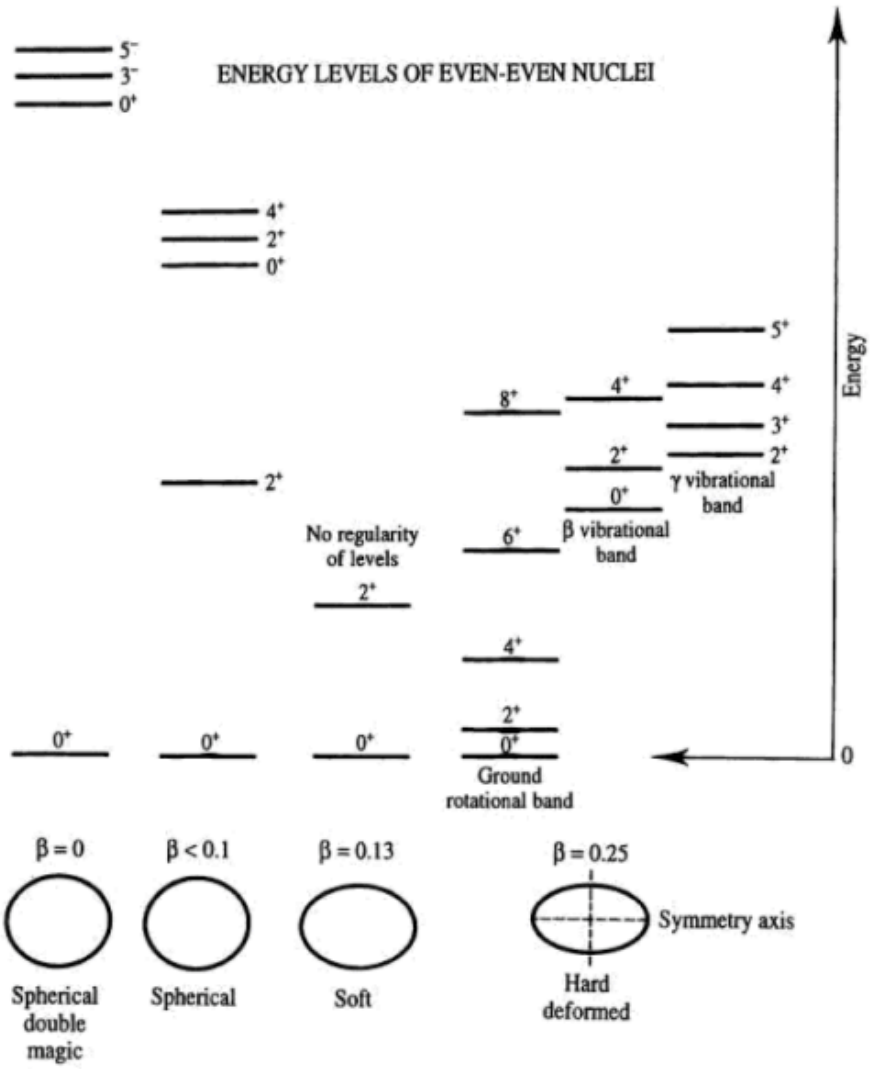


Figure 1.4: Dependence on energy level spacing on shape of the nucleus from Ref. [11].

been identified across the chart of the nuclides. Oblate structures are poorly defined and are not often discussed in literature. In other words, $\gamma$ usually varies between $0° \rightarrow 30°$, and $30° \rightarrow 60°$ are less commonly observed. When the nucleus is neither perfectly oblate (0°) or prolate (60°), it is considered to have a triaxial shape, meaning all three axes of the nucleus are necessary to its description.

Deviations from sphericity (near a closed shell) typically require a minimum of four neutron or four proton holes. As a result they are referred to as "far from" a closed shell. In 1955, Bohr and Mottelson described nuclei whose proton-neutron numbers are not near closed shells and therefore may not be spheroid but could have either prolate- (football) or oblate- (doorknob) shaped ground states [16]. The Nilsson model calculates the bound states in a deformed nuclear potential. The degree to which $\beta$ varies affects the shell model energies. The model is often depicted in a single plot referred to as a Nilsson diagram as in Fig. 1.5, where the nucleon occupation can be predicted. This model is often used when comparing a nuclear state with counterparts in isotonic or isotopic nuclei.

## 1.10 Implications of $\gamma$ deformation

Maurice Jean and Lawrence Wilets visited Copenhagen in 1956. They noted the presence of a large number of nuclei where the second $2^+$ level, labeled as $2_2^+$ was depressed. The $2_2^+$ was found at an excitation energy below that of the first $4_1^+$ level. Additionally, they observed instances in which the energy of the $4_1^+$ level was approximately 2.5 times the energy of the $2_1^+$ level. This energy ratio is about

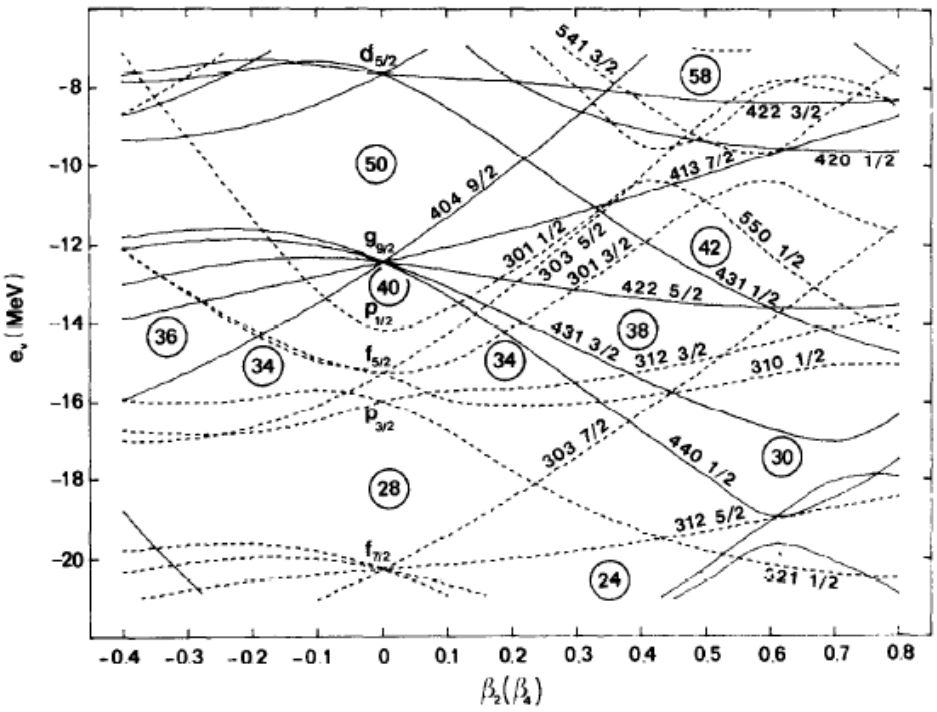


Figure 1.5: Nilsson plot in N or $Z = 40$ region from Ref. [17].

half way between the extreme vibrational and rotational values. Wilets and Jean suggested that such nuclei had rather low $\beta$ values, meaning that these nuclei were slightly deformed, and were relatively insensitive to the loss of axial symmetry. In other words, $\gamma$-soft by the allowance of $\gamma$ to fluctuate without major change. For example, a partially inflated balloon can be pushed into a variety of shapes. A small $\gamma$ value might describe the slightly deflated football of New England Patriot's quarterback Tom Brady [18]. This football returned to its symmetric prolate shape with a spiral arc once released.

In 1958 in Moscow, Professor Alexander S. Davydov and his student G.F. Filippov described nuclei with larger $\beta$ values, where loss of symmetry could lead to rigid structures at the point $\gamma = 30°$. Davydov and Filippov outlined the rotation of "triaxial" nuclei [19]. In the Davydov-Fillipov rigid-triaxial rotor model, a collective potential is assumed which has a stable minimum at a certain value of $\gamma$ causing it to be $\gamma$-rigid. The main feature of this model predicts that, at 30°, the low-lying nuclear states are described by simplified equations and $\Delta J = 2$ transitions disappear. In a follow-up paper, Davydov and Rostovsky published equations that extend the Davydov-Fillipov rigid-triaxial states to higher spins, referred to as the DFR model in this thesis [20]. A key feature of this elaboration is the appearance near and at $\gamma = 30°$ of a third $4^+$ level in close proximity to the $4_2^+$ level. In his textbook [21], Richard Casten commented that although these simple ideas were attractive, no nucleus has been found in which they are exhibited. An example of this behavior would be if Tom Brady deflated his football to the point that upon release, it maintained the loss of axial symmetry and would only tumble meaninglessly on

its path. In other words, the DFR model describes a rigid body with no axis of symmetry.

## 1.11 Geometric or shape-specific nuclear models

Nuclei can be grouped into two limiting categories which are spherical and deformed. However, many nuclei fall somewhere in between. The shape of the nucleus is dependent on the distribution of the nucleons. In the compact space of the nucleus, each nucleon interacts with between $6 - 10$ of its neighbors [21]. The shape in turn, determines the excitation levels within the nucleus (Fig. 1.4). The behavior of the nucleus is dependent on the pairing interactions between nucleons in the same orbit and also the valence proton-neutron interaction. Interactions between protons and neutrons control the onset of deformation and collectivity, configuration mixing, magic numbers, and single-particle states.

The basic measure of collectivity is the $B(E2)$ value that is often related to single particle transition rates described by Weiskopf [9]. Transition rates are a product of matrix elements and an energy factor, so the $B(EL)$ (or $B(ML)$ for magnetic transitions) value is used as the energy factor is removed. Collective rates are faster than single particle rates and the magnitude of the faster rate is a measure of the degree to which the transition is "collective".

The spherical shell model (Figure 1.2) for the nucleus is constructed from a mean field potential of individual nucleons and also the spin-orbit coupling between the nucleons. The mean field potential describes the nuclear and Coulomb

interactions. It is possible that this potential can be approximated by the sum of translational, rotational (rigid rotor model), and vibrational (harmonic oscillator) parts.

Deformation occurs when there is a rearrangement of nucleons into different configurations with a lower energy than the spherical arrangement. Stable deformation is experimentally shown by the existence of rotational bands and large quadrupole moments [22]. The quadrupole moment is a major indicator of deformation, and it can be determined via atomic hyper-fine splitting, where $R_0$ is the average nuclear radius, $Y_{\ell,m}$ are the spherical harmonics, and $\theta, \phi$ are the angles from the nuclear center to the surface [23].

## 1.12 Deformed nuclear measures

Both the Wilets and Jean, as well as the Davydov and Filippov models predict similar excitation energies and $B(E2)$ values for transitions within the ground-state rotational band. Both models describe a sequence of levels, $2^+$, $3^+$, $4^+$, $5^+$... associated with the second $2_2^+$ level arising from varying degrees of loss of axial symmetry. The $\gamma$ band of a nucleus shows higher sensitivity to triaxiality and demonstrates different level staggering for $\gamma$-rigid and $\gamma$-soft triaxial states. The question of rigidity in triaxial nuclei was addressed by Zamfir and Casten. They defined the "staggering factor", $S(4,3,2)$ (or $S(4)$) as the energy difference between the $4^+$ and $3^+$ levels, minus the $3_1^+$ and $2_2^+$ energy difference, divided by the $2_1^+$ energy [24].

$$S(J) = \frac{[E(J) - E(J-1)] - [E(J-1) - E(J-2)]}{E(2_1^+)} \tag{1.2}$$

Negative values for S were considered as $\gamma$-soft systems while positive values were an indication of rigidity. The question is whether the $3^+$ state is closer to the $2^+$ level or closer to the $4^+$ one? An extensive discussion of S values was provided by McCutchan et al. who found several nuclei with slightly positive S values in the rare-earth region [25].

Low-energy characteristics of triaxiality include a $2_2^+$ state lower in energy than the $4_1^+$ state and a low-lying $3_1^+$ state. Triaxial structures identified at high energies are given various labels including those of chiral and wobbling bands. Strong chirality results in the presence of two identical rotational bands with intra-band transitions. Wobbling involves a change in the axial collective motion away from the principal axis, or the axis with the largest moment of inertia. Wobbling is seen experimentally in nuclei with similar intrinsic band structures, but with different spin and parity (e.g. a $4^+$, $6^+$, $8^+$ band would be coupled to a $5^-$, $7^-$, $9^-$ band).

Shape coexistence occurs where there are multiple shapes in a single nucleus. These structures are separated by a barrier up to the point that keeps particles separated by a barrier that inhibits mixing. Shape coexistence is possible by different configurations close in energy [6]. These configurations are caused by the promotion of nucleons across shell gaps. Typically, one of the shapes will be considerably closer to sphericity and the other shape will be considerably more deformed, with the latter involving both protons and neutrons shifting into different shells.

## 1.13 Nuclear model calculations

Observation of nuclear properties has resulted in various nuclear models. These models simplify the basic interactions between nucleons, but do not accurately describe more complex nuclear systems. Statistical models such as the liquid-drop model assume a uniform spherical nucleus, while the shell model is comprised of a spherical nucleus whose nucleons occupy orbitals. The independent particle model also describes the nucleus and the nucleons in their orbits and interactions. The fundamental success of the nuclear shell model is that it "provides a well-defined procedure for the calculation of basic nuclear observables" [21]. The predictive power of existing nuclear structure models is limited because of their development from observables of nuclei close to stability. This underlines the importance of understanding the behavior of the nucleus away from stability.

Nuclear modeling is often conducted using computational power, and the model utilized is often dependent on the mass-region. Nuclear modeling has several different approaches. These include self-consistent microscopic models with an underlying nucleon-nucleon interaction (*ab initio*), models which use calculated shell and pairing corrections (self-consistent mean-field (SCMF), shell model theories), macroscopic models which use empirical data (liquid drop), algebraic expressions based on the nuclear shell model (interacting boson model (IBM)), and neural networks [26]. Each approach has its own merit, but many are beyond the computer power currently available for the germanium nuclei. In the following chapters, this work will describe the experimental data using the traditional shell model with ef-

fective interactions. For cases within the A=60-100 region the JUN45 and jj44b interactions in the jj44 model space are commonly used. This model space includes the proton and neutron $2p_{3/2}$ $2p_{1/2}$, $1f_{5/2}$, and $1g_{9/2}$ orbitals, excludes the filled $1f_{7/2}$ orbitals below $Z, N = 28$ and also the empty orbitals in the *gddsh* shell states above $Z, N = 50$.

The *ab initio* methods start from a given nucleon-nucleon potential which describes nucleon-nucleon scattering data by an effective nucleon interaction. In this model, the core of the nucleus is assumed to be largely repulsive where the nuclear matter is a strongly correlated quantum liquid. Such "no-core" shell models with current computational power are only available for nuclei with $A \leq 12$. For example, Green's Function Monte Carlo (GFMC) is a solution of the many-body Schrödinger equation, but certain difficulties arise with the application of the Coulomb potential and the requirement of Fermi antisymmetry [27]. Heavier systems require an inert core to be assumed and effective residual interactions between the nucleons. The self-consistent mean-field (SCMF) theory approaches the many-body nucleon problem by an average effect of one nucleon on the rest of the nucleons in the nucleus. The main interactions which use SCMF are the Gogny, Skyrme, and relativistic mean field interactions.

The shell model presented here can be applied by assuming the presence of a nuclear core to simplify the multi-body system. The nuclear core is a closed-shell group of nucleons into and out of which nucleon excitations are not allowed. The individual nucleons, or valence nucleons, are those above the core. The core consists of both protons and neutrons in filled orbitals. The simplest model of

nuclear structure is the independent particle model, which assumes that the single unpaired nucleon is solely responsible for the nuclear properties. The independent particle model is most successful in predicting level sequences when the nucleus is near a closed shell. Above the core, the configurations of the nucleons determine the behavior and characteristics of the nuclear excited state.

## 1.14 Nucleon configurations near $^{78}$Ge

The configuration of the nucleons in the shell-model framework is a powerful tool to compare the theoretical characteristics of a particular state to experimental results. These include the spin, parity, and level energy.

A simple way to create an excited state in an even-even nucleus is to break a pair of nucleons, and move one nucleon of these into an unfilled orbital. Table 1.4 shows possible configurations available for broken pairs of protons and neutrons in the region near $^{78}$Ge. Experimental pairing energies are around 2 MeV in nuclei near mass $A = 80$ [22]. Measurements in even-even nuclei show that the first excited state nearly always has a spin and parity of $2^+$. This energy is far below 2 MeV, which suggests a role for collective motion [23]. Hence, these $2^+$ states are depressed in energy by a mixing of the wave functions of many broken pairs. Further multiple-pair excitations including core-coupled excitations require additional mathematics which can be calculated by programs such as NuShellX. The configurations presented in this thesis should be viewed as an extreme simplification of the occupancy of the nucleons in each orbital. The jj44 model space of the NuShellX code calculates the

Table 1.4: Parity possibilities of mixed-shell configurations

| | Group | Shell | Parity Possibilities |
|---|---|---|---|
| 2 protons | $[pf7]$ | $f_{5/2}f_{5/2}$ | $2^+, 4^+$ |
| | $[pf7]$ | $p_{3/2}f_{5/2}$ | $1^+, 2^+, 3^+, 4^+$ |
| | $[pf7]$ | $p_{3/2}p_{3/2}$ | $2^+$ |
| | $[pf11]$ | $p_{1/2}f_{5/2}$ | $2^+, 3^+$ |
| | $[pf11]$ | $p_{3/2}p_{1/2}$ | $1^+, 2^+$ |
| 2 neutrons | | $g_{9/2}g_{9/2}$ | $2^+, 4^+, 6^+, 8^+$ |
| | | $g_{9/2}p_{1/2}$ | $4^-, 5^-$ |
| | | $g_{9/2}p_{3/2}$ | $3^-, 4^-, 5^-, 6^-$ |
| | | $g_{9/2}f_{5/2}$ | $2^-, 3^-, 4^-, 5^-, 6^-, 7^-$ |
| 2 broken proton pairs | | $f_{5/2}f_{5/2} \circ f_{5/2}p_{3/2}$ | $1^+, 2^+, 3^+, 4^+, 5^+, 6^+$ |
| | | $f_{5/2}f_{5/2} \circ p_{3/2}p_{3/2}$ | $1^+, 2^+, 3^+, 4^+, 5^+, 6^+$ |

occupancy of the nucleons in each of the $f_{5/2}$, $p_{3/2}$, $p_{1/2}$, and $g_{9/2}$ orbitals (the *fpg* shell). NuShellX also calculates the average occupancies for each orbital, and the decomposition for different total angular momentum couplings between protons and neutrons. Further discussion of NuShellX can be found in Section 3.7.

In this thesis, "groups" of configurations are designated with one broken proton pair as [pf7] or [pf11] as shown in Table 1.4. The [pf7] group consists of a single $1^+$ state, a single $3^+$ state, three $2^+$ levels, and two $4^+$ levels. The [pf11] group includes the [pf7] states from the $f_{5/2}$ and $p_{3/2}$ orbitals, and also an additional four positive-parity configurations. These additional states result from the involvement of the $p_{1/2}$ orbital. These four states lie at higher energies, and include a single $1^+$ level, two $2^+$ states, and a $3^+$ level. The separation for $29 \leq Z \leq 35$ between the upper four levels is a direct consequence of the spin-orbit splitting between the $p_{3/2}$ and $p_{1/2}$ states. This is particularly important in model calculations that use widely different values for this spin-orbit splitting.

Note that Table 1.4 shows five different ways to make a $2^+$ state with a proton pair and only one way with a neutron pair. The maximum spin created with one broken proton pair is 4. Table 1.4 shows that the creation of a $6^+$ state is not possible by breaking a single pair of protons, but it is possible with a pair of neutrons. Additionally, a broken pair of neutrons can create $2^+, 4^+, 6^+, 8^+$ states as well as negative-parity states ranging from $2^-$ to $7^-$. The only two-neutron configuration that can result in a $7^-$ state is from a $g_{9/2}f_{5/2}$ coupling. The excitation energy of this configuration can act as a measure of nucleon paring and single-particle energies. States from multiple broken proton pairs are in the lower section of Table 1.4.

The subsequent sections discuss the neutron-hole and proton-particle structures of this region in more detail.

## 1.15 Neutron Hole Structures

The isotopes of $^{74-77}$Ni with the closed $Z = 28$ orbital are presented to exemplify structures due to neutron holes as shown in Fig. 1.6. The single-hole structure of $^{77}_{28}\mathrm{Ni}_{49}$ is unknown beyond the presence of a $g_{9/2}$ ground state. The expected excited states for the $p_{1/2}$, $f_{5/2}$, and $p_{3/2}$ orbitals in the jj44b model space are at 1084, 1914, and 2144 keV, respectively. In Fig. 1.6, the experimental and theoretical structures of the two-hole nucleus, $^{76}$Ni, are shown, along with the four-hole system, $^{74}$Ni.

In the $^{76}$Ni nucleus, the $2^+$, $4^+$, $6^+$, and $8^+$ positive-parity states are possible by breaking a neutron pair, and positioning the nucleons in an empty orbital. These

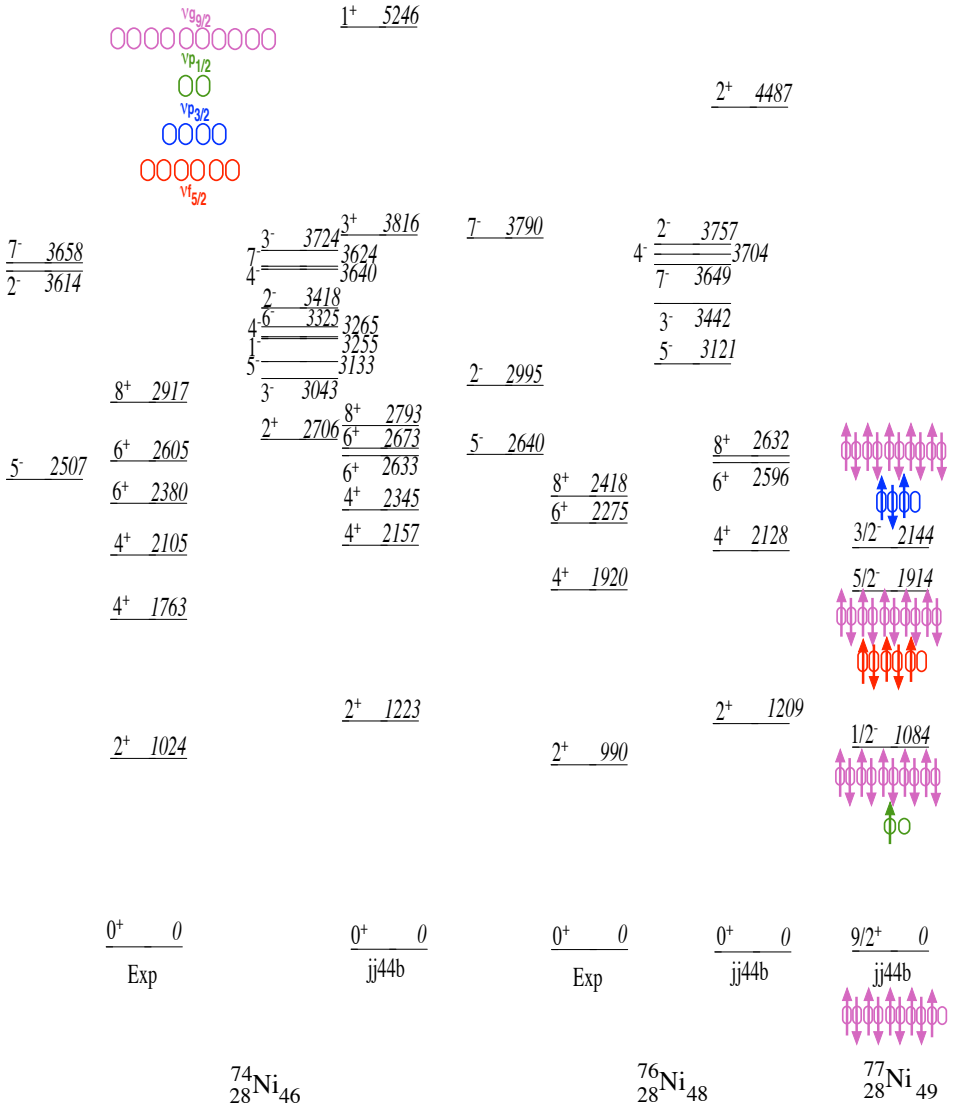


Figure 1.6: Experimental [28] and jj44b calculated levels for $^{74-77}$Ni. The full model space is shown on the upper left of the figure with each circle corresponding to a space for occupation of a nucleon. The the specific single-hole states are shown along the right edge. The neutron configurations are displayed for calculated $^{77}$Ni with up and down arrows to depict the pairing between neutrons.

four states are well known due to the isomeric character of the $8^+$ level. The $2_2^+$ state is calculated in the jj44b model space at a much higher energy (4487 keV) than the $8^+$ level. This is because the $Z = 28$ proton core cannot be broken (in the NuShellX code), and the breaking of a deep hole $f_{5/2}$ neutron pair is repaired together with the alignment of the two neutron holes.

Negative-parity $5^-$ and $4^-$ levels can be produced by the breaking of a deeper neutron-hole pair with configuration $g_{9/2}^{-1}p_{1/2}^{-1}$. Additional negative-parity states occur by breaking a pair in the deeper $p_{3/2}$ or $f_{5/2}$ orbitals. The maximum angular momentum of a negative-parity state with one broken pair is a $7^-$ level with an aligned $g_{9/2}^{-1}f_{5/2}^{-1}$ state. The calculated level energies from the jj44b interaction, are higher than those observed for the positive-parity levels. However the code produces the negative-parity states well within the expected energy range.

For the four-hole nucleus, $^{74}$Ni, the observed and calculated level schemes are more complex. This is due to the presence of seniority-four configurations (breaking of two nucleon pairs) at low energies (Fig. 1.6). The calculated $2_2^+$, $4_2^+$, and $6_2^+$ levels are found at low energies in the same region as the seniority-two levels. Seniority-two levels involve the breaking of one nucleon pair, with resulting mixed configurations. The theoretical negative-parity levels are found within a reasonable range when compared to experimental levels. The odd-spin positive-parity levels lie at much higher excitation energies (above 3800 keV), as seniority-four levels. Such states were not possible in $^{76}$Ni, due to the presence of only a single neutron-pair hole.

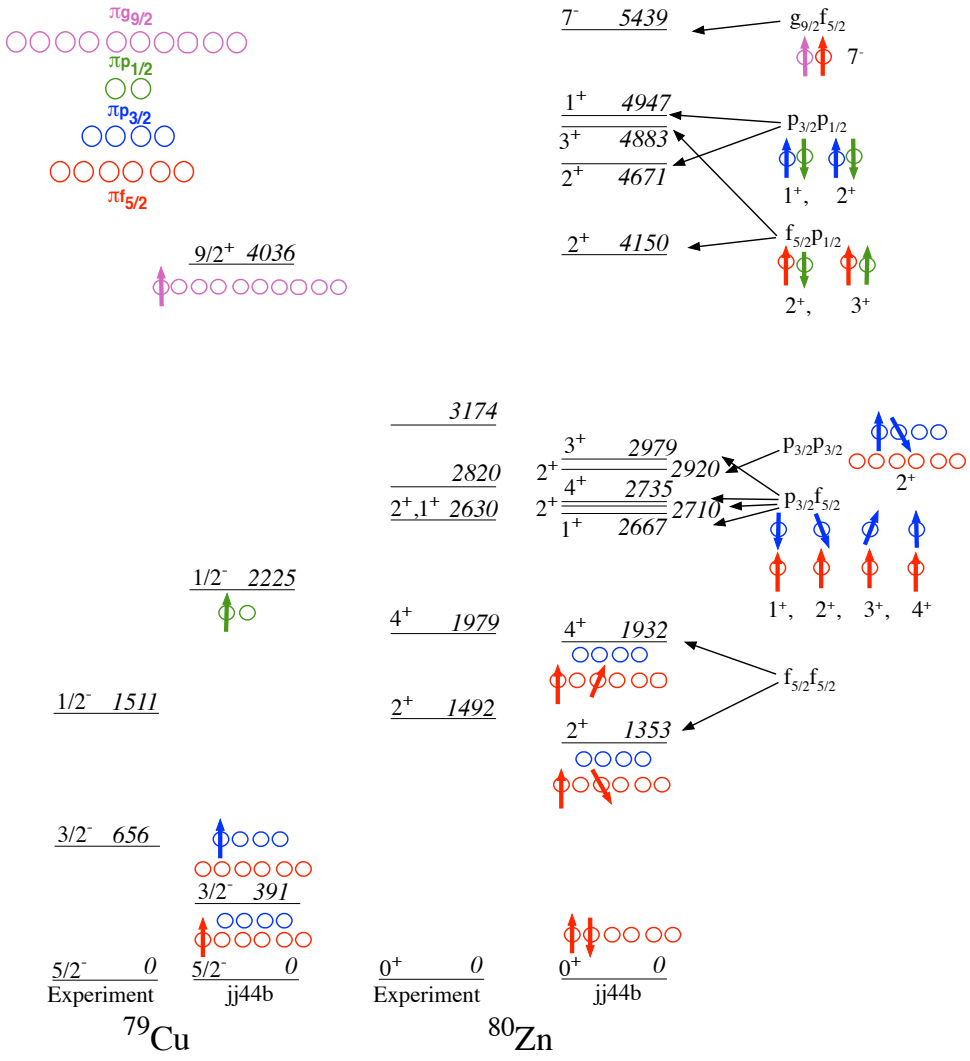


Figure 1.7: Experimental [29,30] and calculated levels for $^{79}$Cu and $^{80}$Zn. The proton configurations are displayed for each calculated level.

## 1.16 Proton-Particle Structures

The observed levels in $^{79}$Cu with a single proton beyond double-magic $^{78}$Ni are presented in Fig. 1.7. This figure includes the levels for $^{80}$Zn, a nucleus with a single pair of protons beyond $^{78}$Ni. The monopole-driven inversion of the $p_{3/2}$ and $f_{5/2}$ levels was observed in $^{75}$Cu (Refs. [31, 32]). This result raised the question of the separation size for a single proton beyond double-magic $^{78}$Ni. The observed 656-keV separation in $^{75}$Cu is lower than most calculated values. The exception is the jj44b interaction, which predicts the $p_{3/2}$ state as low as 391 keV. The separation between the $p_{3/2}$ and the $p_{1/2}$ orbitals arises from the spin-orbit splitting and is measured to be 855 keV, but is calculated to be 50% larger. This experimental value is consistent with the spin-orbit splitting of 988 keV observed in $^{131}$In [33]. The energy of the $2_1^+$ first excited state in $^{78}$Ni has not been formally published. However, preliminary data from the RIBF facility at RIKEN (Japan) indicate that the state is about 2500 keV, nearly the same energy as in double-magic $^{56}$Ni. The low-energy of the $1/2^-$ level in $^{79}$Cu at 1511 keV could be caused by an admixture of another state (a core-coupled $1/2^-$ level).

The shell-model states of $^{80}$Zn are presented in Fig. 1.7. There are eleven positive-parity states (the [pf11] group), and the lowest negative-parity state, a $7^-$ level is at 5439 keV. For nucleon configurations of one proton pair produce positive-parity levels with spin $> 4$, and are not possible below about 8 MeV. The calculated $6^+$ and $8^+$ levels lie at 10314 and 10350 keV, respectively. These arise from promoting a pair of protons (which requires $\sim 4$ MeV) to the $g_{9/2}$ orbital. An

additional broken a pair requires two more MeV. The calculations reproduce the observed levels accurately. The $4_1^+$ level is calculated to lie in close proximity to the observed state, and the three higher-energy states are in the same energy range as the states involved in breaking of the lone pair, and the promotion of one proton in the $p_{3/2}$ orbital.

# Chapter 2: Motivation

The search for neutrinoless double $\beta$ decay is currently one of the most expensive nuclear physics projects in the world. Such a discovery will only occur if the neutrino is both massless and its own antiparticle. A nucleus for which such a property might be found is $^{76}$Ge. The properties of this single nucleus and those with adjacent odd-mass have been the subject of extensive study over the last 15 years. At Argonne National Laboratory (ANL), John Schiffer and Ben Kay undertook many studies of the single-particle properties of adjacent $^{75,77}$Ge using transfer reactions. Starting in 2009, the University of Maryland College Park-Argonne collaboration pursued studies of the structure of $_{28}$Ni nuclei. These experiments used deep inelastic scattering (DIS) or multi-nucleon transfer (MNT) reactions to populate levels in Ga and Ni. The work was initiated by a post-doctoral worker, Dr. Irina Stefanescu, now in the detector group at Lund University and was carried on by Maryland Assistant Research Scientist, Dr. Chris Chiara. A visitor to ANL from Japan, Dr. Yusuke Toh, was interested in "triaxial nuclei" and used these data to provide new information for stable $^{76}$Ge. The result was a "featured" Rapid Communication in Physical Review C, that hypothesized that $^{76}$Ge exhibits features of rigid triaxiality [34].

In 1977-1978, Nilsson's group at Lund published a paper and also a review which demonstrated that at $\gamma = 30°$, gaps appear in the moderately deformed single-particle levels at nucleon numbers $26, 32, 44$, and $46$ [35,36]. They singled out two nuclei $^{58}Fe_{32}$, and $^{76}Ge_{44}$ as examples using just the first 3 levels in each nucleus to demonstrate thise effect. For the former nucleus, they suggested a triaxially deformed minimum with $\beta = 0.26$, and $\gamma = 25°$ and for the latter one a similar minimum with $\beta = 0.27$ and $\gamma = 35°$. The aurthors concluded that these gaps would provide effective shell closures at $\gamma = 30°$ with stabilized structures. These papers vanished into the dark recesses of the scientific literature and were not cited by any of the authors who discussed triaxiality in the subsequent 40 years, including the Toh *et al.* paper on $^{76}$Ge [34].

Owing to the interest in double $\beta$ decay, numerous theoretical papers were published, nearly all of which indicated that $^{78}Ge_{46}$, with two additional neutrons beyond $^{76}Ge_{44}$, would be a dull nucleus with no features of interest. However, heavier $^{80}Ge_{48}$ and $^{82}Ge_{50}$ were extensively studied by scientists interested in properties of nuclei near closed spherical shells, in this case, $N = 50$. One surprising result was the identification of a low-energy second $0^+$ level in $^{80}$Ge that was attributed to shape coexistence with structures across the $N = 50$ closed shell [6].

## 2.1 Closed shells

The properties of nuclei in the vicinity of closed shells and subshells provide insight into the hierarchy of the nuclear orbitals. These are succinctly described

within the shell-model framework. In particular, studies on doubly-magic $_{8}$O, $_{20}$Ca, $_{28}$Ni, $_{50}$Sn, $_{82}$Pb and their surrounding nuclei provide insight into the role of major closed shells. The predictive power of present nuclear structure models is limited due to the development of such models from observables obtained from nuclei close to stability. This emphasizes the importance of the behavior of the nucleus away from stability.

A comprehensive description of the shell structure of the semi-magic number 32 described by a full valence $2p_{3/2}$ orbital within the shell-model framework is necessary to establish shell evolution. This in turn, affects changes in the structure of the shell model. The subshell closure at $Z = 32$ can be attributed to the magnitude of the spin-orbit splitting that drives the $1f_{5/2}$ orbital a full MeV above the $2p_{3/2}$ one. The spin-orbit splitting of the $2p_{3/2}$ and $2p_{1/2}$ orbitals also places the $2p_{1/2}$ state well above that of the $2p_{3/2}$, isolating the $2p_{3/2}$ orbital. Above $N = 40$, the $Z = 32$ subshell closure disappears when the $1g_{9/2}$ neutrons weaken the $\pi 1f_{7/2} - \nu 1f_{5/2}$ splitting, which allows for the $1f_{5/2}$ orbital to become the ground state in $^{75}$Cu. A similar inversion, due to the monopole interaction, is seen in the mirror-case of $^{54}_{28}$Ti$_{32}$ [37]. Additionally, strong shell effects were identified in $_{19}$K$_{32}$ [38], $_{20}$Ca$_{32}$ [39, 40], and $_{21}$Sc$_{32}$ [41].

With 32 protons, germanium nuclei lie just above the $Z = 28$ major closed shell. Excited states in Ge isotopes are known over $N = 30$ to $N = 54$, that is across the closures of the $N = 40$ subshell and $N = 50$ shell. The degree of collectivity versus single-particle characteristics of the other Ge nuclei is affected by the ability of theoretical models to accurately describe the excited states. Certain features,

such as the excitation energy of the $2_1^+$ state, challenge the shell-model picture that includes a $N = 40$ subshell closure. The subshell at $N = 40$ is an oscillator-shell boundary between odd-parity $L = 3$ orbitals and even-parity $L = 4$ ones. However, the $2p_{1/2}$ orbital is the highest one in the $N = 3$ oscillator shell, and it has little influence on the collectivity of the nucleus. Therefore, collective properties are also weak at both N and $Z = 38$ as evidenced by the properties of $^{88}$Sr and $^{90}$Zr, along the $N = 50$ closed neutron shell. With enough energy, the $2p_{1/2}$ orbital will play a role in contributing to excited states. Hence, overall collective properties show a maximum at $N = 42$ as evidenced by the Coulomb excitation data shown in Figure 2.1 from Gürdal *et al.* [42]. Collectivity is a much more significant contributor to the Sr and Kr nuclei when compared to the Ge and Zn.

## 2.2 Collectivity and Deformation

The energy of the lowest $2^+$ state has historically served as a basic gauge for collectivity and deformation. Owing to the subshell closure at $N = 40$, a considerable gap is expected between the ground and the first excited state. In the Ge isotopes, the excitation energy of the $2_1^+$ level varies between 902 and 1039 keV for $N = 32 - 38$ nuclei. At that point the excitation energy drops to 834 keV at $N = 40$ and continues to drop until it stabilizes around 600 keV for $N = 42 - 48$. When the $N = 50$ shell is reached, the expected higher $2_1^+$ excitation energy at 1348 keV appears. Coulomb excitation studies of Zn, Se, Kr, as well as Ge also show that $N = 42$ is the mid-shell location of a maximum in collectivity [43]. Wilets and Jean

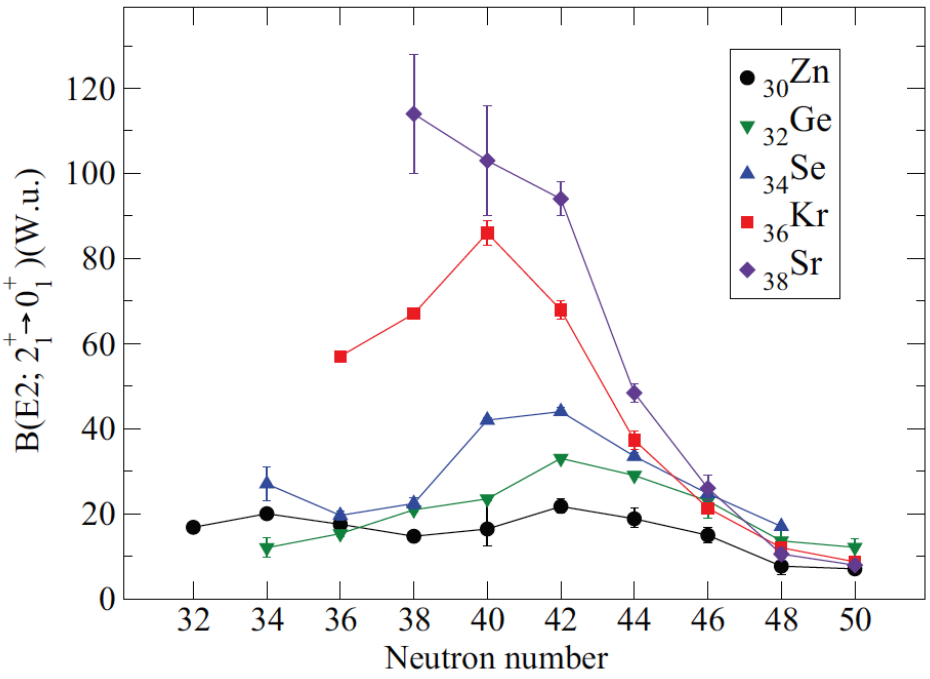


Figure 2.1: Quadrupole transition values ($B(E2)$) of Zn, Ge, Se, Kr, and Sr in the $N = 40$ region. From Ref. [42].

noted a group of nuclei whose second $2^+$ level fell well below the first $4^+$ levels, and they ascribed the presence of these states to a loss of axial symmetry [13]. To describe such triaxial systems, three degrees of freedom are required. In these cases, the $2_2^+$ state is interpreted as the band head of a $\gamma$ band [44]. Bohr and Mottelson, in their introduction to geometric models of the nucleus, described both vibrational and rotational nuclei. They recognized a need for a second deformation parameter, to describe further departures from axial symmetry for rotational nuclei and collective vibration. This results in a loss of axial symmetry that leads to the creation of the $\gamma$ parameter.

The change in characteristics in even-A Ge nuclei toward the $N = 50$ shell closure can be examined through the study of the nuclear structure and associated decay patterns. Such a study provides insight into the strength of the shell closures at $N = 50$ and $Z = 32$. Above the $N = 40$ subshell closure, the Ge isotopes exhibit a variety of characteristics that include increasing collectivity [45], competition between intrinsic shapes associated with unique configurations [46, 47], as well as low-spin properties related to specific intruder excitations [6, 48] across the $Z = 28$ shell gap, and also evidence of substantial triaxiality [34, 49]. The fact that triaxialty is considered in $^{76}$Ge and $^{78}$Ge, should come as no surprise as gaps for $\gamma = 30°$ were predicted at 32, 44, and 46 nucleon numbers by Larsson *et al.* and also Ragnarsson, Nilsson and Sheline [35, 36].

## 2.3 Structures and deformation in $Ge_{40-50}$

There have been extensive studies of the systematic features of the low-lying states in even-A Ge nuclei above $N = 40$. The ratio of energies of the $4^+$ state to the $2^+$ state, $E_{4^+}/E_{2^+}$ is often used as a gauge of deformation (as discussed in Chapter 1). The $E_{4^+}/E_{2^+}$ energy ratios in $^{74,76,78,80}$Ge are approximately 2.5. This ratio is above the value representative of vibrational nuclei and significantly below that of rotational ones. However, Wilets and Jean took interest in this specific feature [13]. In turn, this instability can bring intruder states close to the Fermi surface. As a result, the energy of the first excited $0^+$ state has been investigated by many scientists. These include the research group of T. Fortune [50] and also has been reported by Van den Berg *et al.* [51]. With increasing neutron number the $0_2^+$ level decreases from 1215 keV in $^{70}$Ge to 692 keV in $^{72}$Ge and it rises again to 1483 keV in $^{74}$Ge. The $0_2^+$ state is at a local minimum within the isotopic chain at $N = 40$ in $^{72}$Ge and it is also the first excited state in the nucleus. In contrast, the $2_1^+$ level is consistently the first state in the heavier isotopes. In $^{74}$Ge, the $0_2^+$ state doubles in energy, and it becomes the fourth excited state in the nucleus, even above the yrast $4_1^+$ state. The state in $^{76}$Ge reaches a maximum at 1911 keV above an additional state, the $3_1^+$ level. In $^{78}$Ge, the $0_2^+$ state drops below the $3_1^+$ and $4_1^+$ states to an energy of 1547 keV. Described as an intruder state [6], a $0_2^+$ level has been reported in $^{80}$Ge at 639 keV, the lowest $0^+$ occurrence in the isotopic chain. The only excited $0^+$ state known in $^{82}$Ge has an excitation energy of 2333 keV, and in heavier isotopes no excitation of this type has been observed.

The region around $^{76}$Ge is important in the interpretation of double-$\beta$-decay studies. The process of $\beta$ decay normally occurs between two adjacent nuclei. In the case of $^{76}$Ge, $\beta$ decay is energetically unfavorable to $^{76}$As, as it lies at a higher energy. Experimentally, $^{76}$Ge has been observed to decay directly to $^{76}$Se by the release of two $\beta$ particles. Double $\beta$-decay studies are frequently conducted to determine whether or not the neutrino is its own antiparticle, as would be indicated by the identification of neutrinoless double $\beta$ decay. If this decay is found in $^{76}$Ge, a complete characterization of the $^{76}$Ge wavefunctions will be necessary to extract information on this process.

### 2.3.1 Brief Overview of Experimental Findings

Although important in study of shell evolution of the Ge isotopes, the $^{70,72,74,76}$Ge nuclei are only briefly mentioned in this work. Here is an outline of significant findings in these nuclei.

**$^{70}$Ge**: The $^{70}$Ge nucleus has been interpreted to have a spherical shape by the filled $p_{3/2}$ and $f_{5/2}$ orbitals, and has been the basis of shape transition studies [52, 53].

**$^{72}$Ge**: The newly reported $^{72}$Ge structure suggests that there are two coexisting shapes present, both of which may be triaxial [46]. This nucleus has also been described to have a $\gamma$-soft triaxiality [49].

**$^{74}$Ge**: Sun *et al.* determined $^{74}$Ge to have a triaxial, mainly collective structure [49]. Further corrections to this scheme have been presented by the University of Mary-

land group [54].

**$^{76}$Ge**: Triaxiality in the $^{76}$Ge nucleus was described as $\gamma$-rigid in Refs. [34, 49, 55].

**$^{78-82}$Ge**: The study of the nuclear structure of $^{78-82}$Ge forms the basis of this work and it is presented and discussed in Chapters 4 and 5. Previously works described $^{78}$Ge as prolate [56], but subsequent investigation (as part of this thesis) has produced evidence for a structure that has not been previously observed, nor is easily described theoretically [57]. A second nuclear configuration in $^{80}$Ge was reported by Gottardo *et al.*, and indicated a $0^+$ intruder state [6]. $^{82}$Ge has a high first excited state at 1348 keV, indicating an increased stability since the nucleus lies on the $N = 50$ closed shell.

In closing, further studies on the nuclear structure of the Ge isotopes are warranted to further realize a theoretical model that accurately describes all experimental observations.

# Chapter 3: Experimental Methods and Analysis

## 3.1 Deep inelastic scattering

Deep inelastic scattering (DIS) was first used as a technique in nuclear reaction experiments before it was used in the field of nuclear structure. In a DIS reaction, complete fusion between the nuclei in the beam and target does not take place. Instead, when the nuclei come in partial contact, neutrons and protons are exchanged along a contact boundary creating beam-like and target-like residual nuclei. Depending on the beam energy, which is usually kept in a range $20-50\%$ above the Coulomb barrier, the deeper collisions exchange more particles. Generally, the nuclei that have the highest probability of creation are near the initial nuclei, and also nuclei which lie on a line between the target and beam nuclei (see Fig. 3.1). DIS is a valuable means of producing neutron-rich nuclei by bombarding a neutron-rich target with a neutron-rich beam [58, 59].

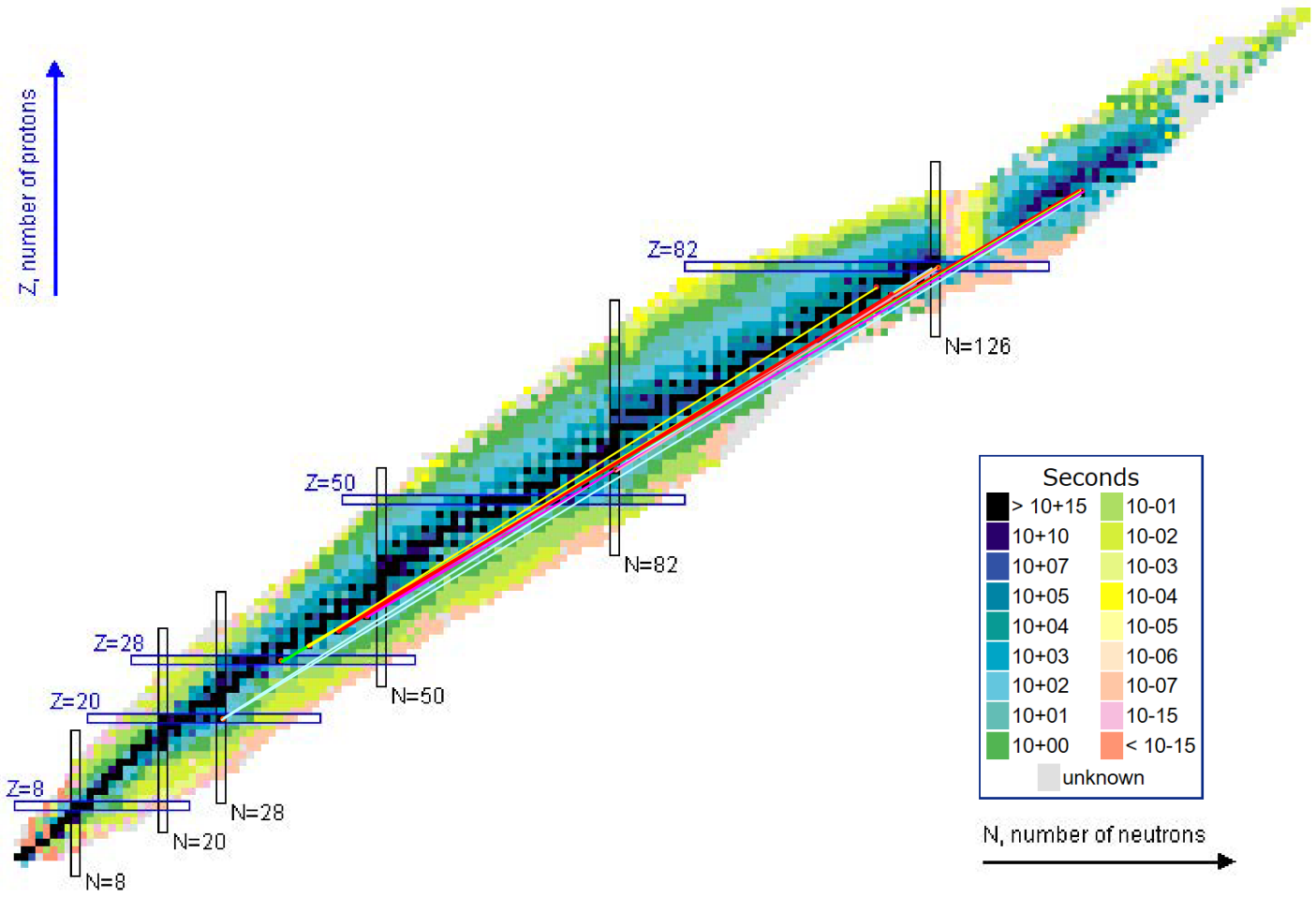


Figure 3.1: Chart of the nuclides colored by nuclide half-life. Lines between beam-target combinations for available data (Tab. 3.1) are made for beams $^{48}$C (light blue), $^{64}$Ni (green), $^{70}$Zn (yellow), $^{76}$Ge (red), $^{82}$Se (magenta) and $^{136}$Xe (light pink) to their respective targets. Adapted from Ref. [28].

## 3.2 ATLAS and Gammasphere

### 3.2.1 ATLAS

The Argonne Tandem Linear Accelerator System (ATLAS) is housed at Argonne National Laboratory (ANL). It was developed in the 1970s, and it proved to be the world's first superconducting accelerator for projectiles heavier than the electron. ATLAS is a Department of Energy (DOE) nuclear physics national user facility, and it provides experimental means to explore questions in nuclear structure, nuclear dynamics, nuclear astrophysics, low-energy tests of the Standard Model, and applications of low-energy nuclear physics. ATLAS can provide light in-flight radioactive beams, and also beams from heavy neutron-rich Cf fission products. Stable beams up to uranium (U) with intensities approaching 10 p$\mu$A are also available at ATLAS. These stable beams have energies ranging from $\sim$ 0.5 MeV/u to 10-20 MeV/u, depending on the mass and charge state of the projectile.

### 3.2.2 Gammasphere

The Gammasphere (GS) spectrometer is a powerful tool to study nuclear spectroscopy across the chart of nuclides including those far from stability. Paired with other detector systems, the GS array can be used to detect heavy ion reaction partners (CHICO), low-mass particles (MicroBall), and to separate reaction products (Fragment Mass Analyzer (FMA) and AGFA). GS was developed and assembled at Lawrence Berkeley National Laboratory (LBNL) by a collaboration involving many

universities and national laboratories. With the advancement of ATLAS and the various available beams and energies, GS was relocated to its present location at ANL.

Gammasphere is a $4\pi$ detector array comprised of high-purity germanium (HPGe) n-type detectors paired to bismuth germanate (BGO) detectors [61]. The experimental setup is shown in Figure 3.2. The BGO scintillators act as Compton suppressor shields to the Ge detectors. This ensures that if a $\gamma$ ray deposits its energy through multiple scattering events and the photon scatters out of the detector and is detected in the BGO shield then the event is deleted. This is an important factor, because within GS, approximately half of the total number of events occur within the Ge detectors and the other half within the BGO shield [62]. The leading interaction mode between 50 keV to 8 MeV is Compton scatterin (Fig. 3.3). As seen in Fig. 3.4, Compton-scattered $\gamma$ rays overwhelm the spectrum of fully-absorbed $\gamma$ rays within the Ge crystal. The peak-to-total (P/T) ratio compares the response of the full-energy peak of a mono-energetic $\gamma$ ray interacting with a detector to the total number of counts within the spectrum. This ratio using Ge only is approximately 20%, while including the BGO material increases this value to 68% [60].

The absolute efficiency of the HPGe detectors varies with the energy of the $\gamma$ ray detected. X-rays can be inhibited by absorbers of various thickness and materials in front of the detectors, making Gammasphere most effective for $\gamma$ rays above 100 keV. The absorber effect drops off below 2000 keV where detector efficiency drops rapidly. The detector sphere has a central focal point, where the target material is mounted. If auxiliary detectors are included in GS experiments, they are often

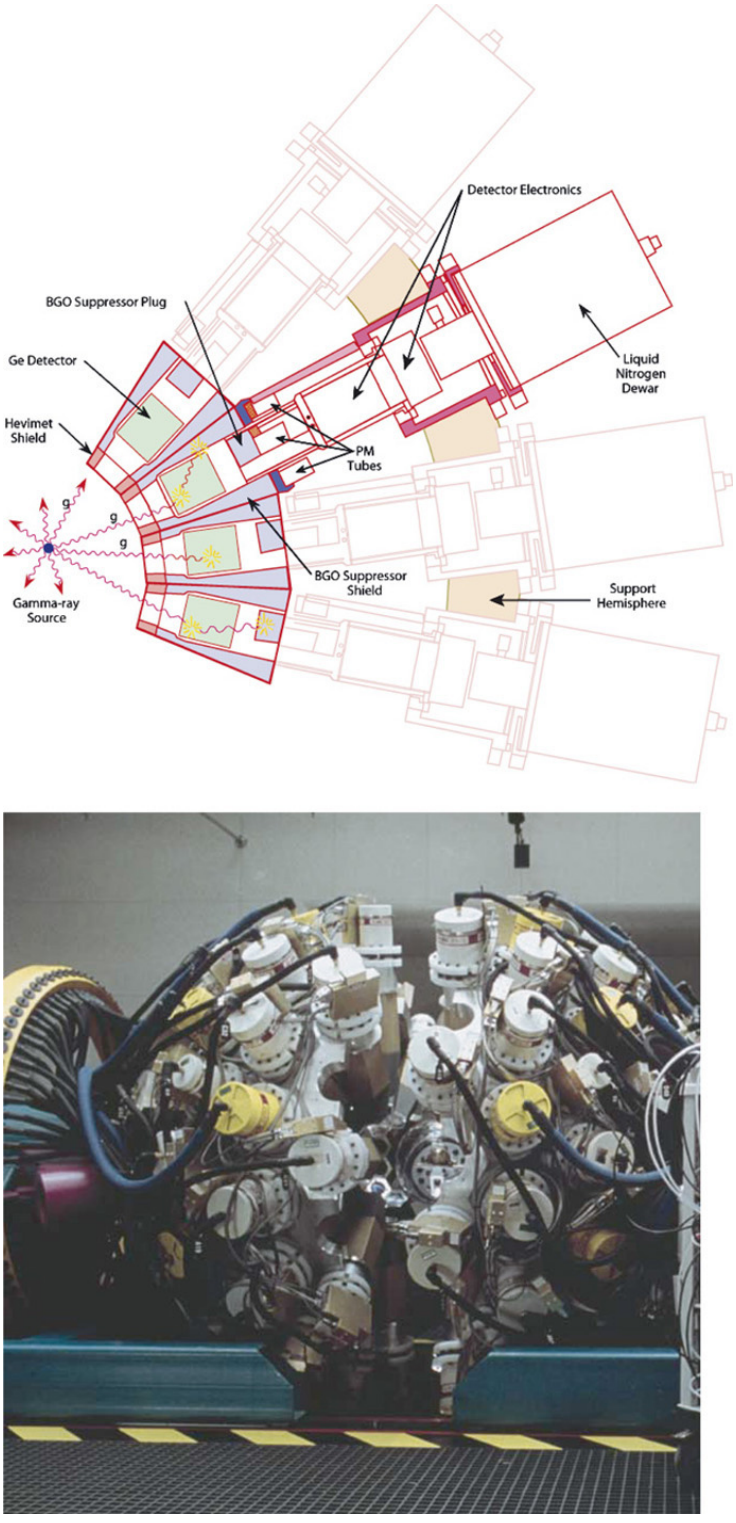


Figure 3.2: Experimental setup of the Gammasphere array. From Ref. [60].

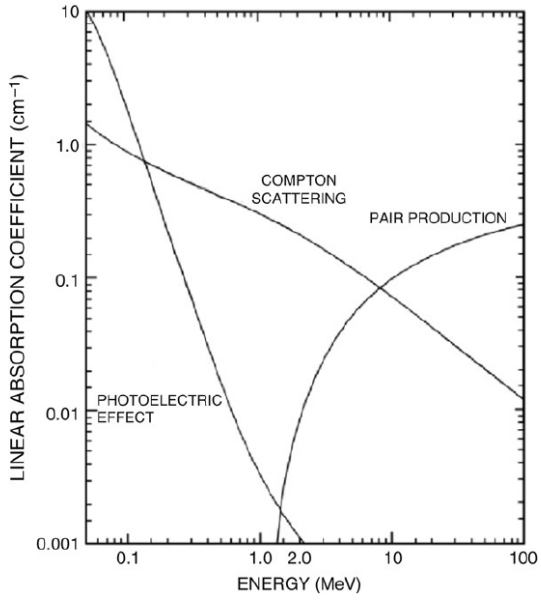


Figure 3.3: Attenuation coefficients of $\gamma$ rays interacting with germanium as a function of the $\gamma$-ray energy. Interactions include the photoelectric, Compton, and pair production. From Ref. [60].

placed at the focal point. The fixed frame of the Gammasphere can hold up to 110 detector-shielding pairs. Each detector unit can be replaced for maintenance without affecting the reproducibility of the system. This large number of detectors maintains a small solid angle for each individual detector. This is important to enable Doppler corrections over a small angular range. In addition, events arising from the summing in a single detector of two $\gamma$ rays from a single event are minimized.

Germanium is used as a bulk semiconductor material in high-purity germanium (HPGe) detectors. A high level of purity in germanium is required to produce a high quality detector because of depletion depths that correspond with the highly-

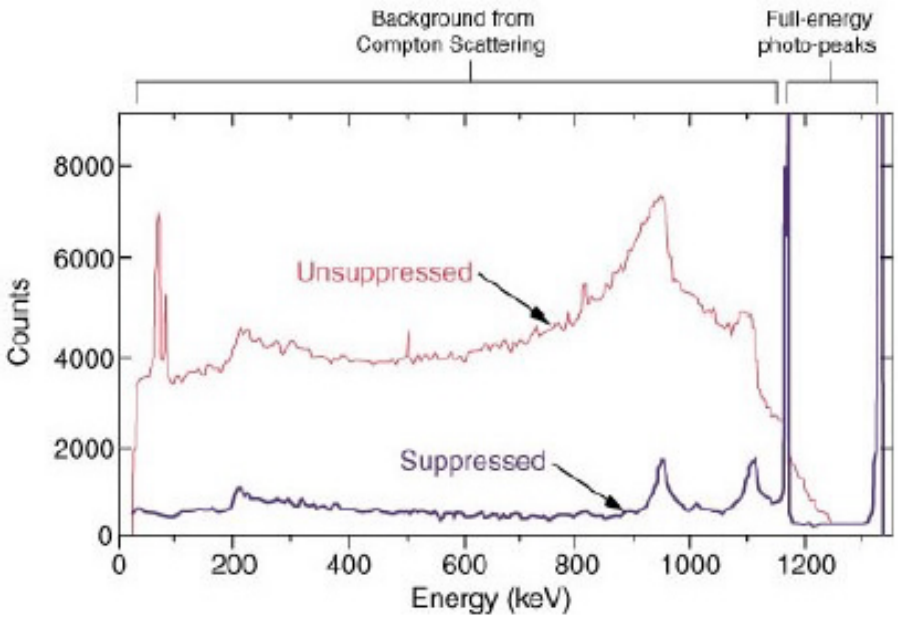


Figure 3.4: Background from Compton scattering within Gammasphere. The unsuppressed spectrum (red) includes subsequent events detected in the surrounding BGO, whereas the suppressed spectrum (black) eliminates the contribution from the Compton-scattered $\gamma$-rays.

penetrating $\gamma$ rays. The depletion depth thickness is given by

$$d = \left(\frac{2\epsilon V}{eN}\right)^{0.5}, \tag{3.1}$$

where N is the net impurity in the bulk semiconductor material and V is the reverse bias voltage. A high reverse bias voltage or an ultra-pure (with an impurity level on the order of $10^{10}$ atoms/cm$^3$) semiconductor material is necessary to expand the depletion depth to a few centimeters. The germanium crystals in the detectors must be cooled to liquid nitrogen temperatures (77° K) to avoid leakage current due to the small band gap. A close-ended coaxial configuration can incorporate more crystal volume, and this in turn can detect higher energy $\gamma$ rays. This configuration also avoids leakage currents and has a lower capacitance than a planar geometry. Unlike less expensive sodium-iodide detectors, high-purity large-volume Ge detectors achieve high peak efficiency and sharp energy resolution.

## 3.3 Experiments in Gammasphere

Thick targets were used in the Gammasphere data sets used in the analysis of this work. As the beam nucleus progresses through the target, it loses energy, leading to progressively shallower collisions and transfer of fewer nucleons. Ultimately, the projectile-like fragment is stopped in the target. A disadvantage is some $\gamma$ rays are emitted before the fragment has stopped. The resulting $\gamma$-ray peak is smeared in energy and is not observed unless it has higher intensity or unless there is a "slow" decay that feeds into the level of interest.

Once the beam strikes the target, excited nuclei are formed. Then the decaying $\gamma$ rays are detected by the HPGe detectors of GS as depicted in Fig. 3.2. Next, a preamplifier for each Ge detector reads the flow of electrons as a current. With each event, a timestamp is included. The signal then moves from the preamplifier to the DAQ (data acquisition) system which is connected to all the preamplifiers. Here, the DAQ compiles the timestamps and converts the currents to energies of the individual photons, $E_\gamma$. The DAQ system includes many other processes such as pulse-shape analysis, which will not be described in this work.

## 3.4 Gammasphere Data and Coincidence Cubes

The beam from ATLAS was directed onto the target in pulses of about 1 ns width every 82 ns. Only every fifth pulse was used, and this left a $\sim$ 410 ns time difference between events caused by the nuclear reactions. Each data set of Table 3.1 can be called a "cube" because the data is sorted into three-fold coincidence events. A three-fold coincidence is three successive signals recorded within 1 $\mu$s of the first signal [63]. Any additional Compton-suppressed $\gamma$ rays within this time frame are also included as events. For each detected $\gamma$ ray, a timestamp relative to the RF beam pulse was recorded (Fig. 3.5). An example of how multiple data cubes are used in the analysis of a gate can be found in Appendix A.1.

Events occurring with the initial flash of radiation from a beam pulse, are categorized as "prompt". Events recorded between subsequent beam bursts are categorized as "delayed". During the microsecond of signals recorded after the beam burst

Table 3.1: Gammasphere deep inelastic scattering data*

| gsfma label | Beam | Target | Beam Energy (MeV) | Date |
|---|---|---|---|---|
| 089 | $^{48}$Ca | $^{208}$Pb | 305 | 01-2000 |
| 118 | $^{48}$Ca | $^{238}$U | 330 | 08-2003 |
| 145 | $^{82}$Se | $^{208}$Pb,$^{238}$U | 525 + 630 | 09-2004 |
| 166 | $^{64}$Ni | $^{238}$U | 430 | 10-2005 |
| 223 | $^{76}$Ge | $^{238}$U | 425 + 530 | 10-2008 |
| 245 | $^{76}$Ge | $^{208}$Pb | 450 | 02-2009 |
| 266 | $^{76}$Ge | $^{198}$Pt | 450 | 11-2010 |
| 287 | $^{70}$Zn | $^{197}$Au | 430 | 02-2012 |
| 291 | $^{70}$Zn | $^{208}$Pb,$^{238}$U | 440 | 03-2012 |
| 299 | $^{70}$Zn | $^{208}$Pb | 440 | 07-2012 |
| 314 | $^{136}$Xe | $^{208}$Pb | 450 | 04-2014 |

* Available for analysis in this work.

events can be correlated on the order of hundreds of nanoseconds. Such correlations are useful in examining $\beta$-decay transitions, prompt transitions, and transitions above and below isomers. GS coincidence data have also been organized in four classes: prompt-prompt-prompt (PPP), delayed-delayed-delayed (DDD), prompt-delayed-delayed (PDD), and prompt-prompt-delayed (PPD). The PPP coincidence events occur when all three $\gamma$ rays occur within the flash of radiation associated with the beam pulse and when they are within $\sim$ 40 ns of one another (Region 1 of Fig. 3.5). DDD coincidence relationships occur with a delay from the initial beam pulse (Region 2 or 3 of Fig. 3.5). PDD and PPD coincidence events occur when one or two events occur with the beam pulse (Region 1 of Fig. 3.5), and the other(s) occur after a delay (Region 2 or 3 of Fig. 3.5). Events from the simultaneous emission of three $\gamma$ rays from radioactivity will be observed across the entire time spectrum. Owing to the narrow time window for Region 1, most such events are observed in

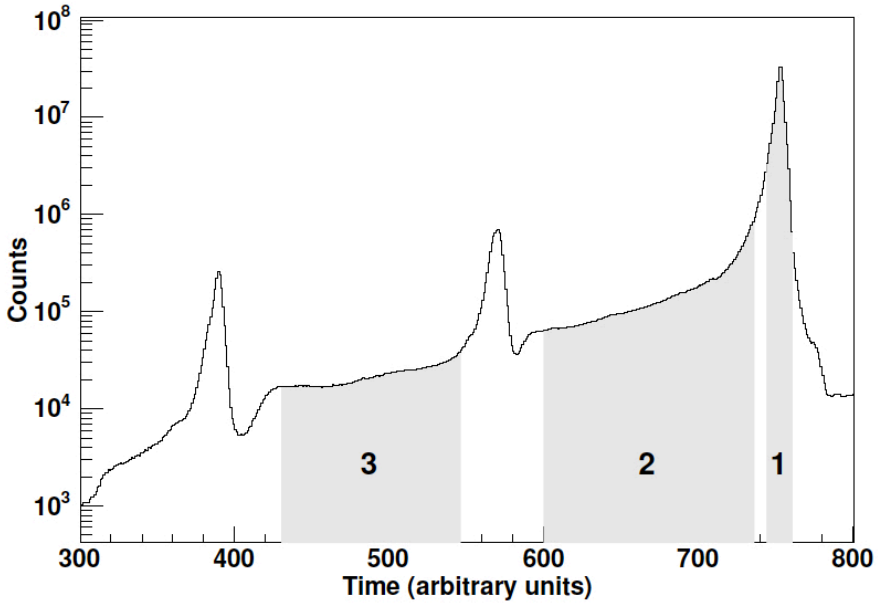


Figure 3.5: Plot of the counts over the time on a logarithmic scale with respect to the RF beam pulse. Region 1 indicates a "Prompt" event, which occurs during the initial flash of radiation and is emitted as the beam hits the target [63]. Regions 2 and 3 indicate a "Delayed" event which occur between subsequent beam bursts, but are products of the initial beam burst. From Ref. [63].

Regions 2 and 3, along with the isomeric decay produced by the initial beam flash. Therefore, a delayed event can be associated with the beam burst for data sets of PDD and PPD. Figure 3.5 shows that the best data quality is in the PPP cube and the worst in DDD.

### 3.4.1 Cross-correlations and complementary nuclei

Following each deep-inelastic scattering event, two excited nuclei are created, and they are unique to the beam-target combination. If this reaction is treated as a two-body system, they are produced at the same time. Therefore, $\gamma$ rays

emitted from both fragments are coincident and are considered complementary to one another. Additional transitions are found by gating on a transition from a target-like nucleus and its complementary, projectile-like nucleus. Transitions from the target-like nucleus will appear in the spectrum of transitions within the projectile-like nucleus due to their coincident nature. In the $^{76}$Ge beam on $^{238}$U target run (Ge/U), each event in which a $^{78}$Ge nucleus is formed, there also is a complementary $^{236}$U nucleus. Transitions from this complementary nucleus are present in the $^{78}$Ge spectrum (Fig. 4.13). Although this is a simple mechanism in theory, there are complications such as isomers in one member of the two-body system. A list of complementary transitions found in cross-correlation are shown in Tab. 3.2. For higher-spin states, where deeper inelastic collisions take place, neutron evaporation may occur. The observation of a complimentary nucleus with three or four fewer neutrons than expected is a common result.

Table 3.2: Commonly observed transitions (in keV) in the beam, target, and complementary nuclei of Ge cubes.

| $^{238}$U | $^{236}$U | $^{208}$Pb | $^{206}$Pb | $^{198}$Pt | $^{196}$Pt | $^{76}$Ge |
|---|---|---|---|---|---|---|
| 159.0 | 160.3 | 883.6 | 537.5 | 407.2 | 326.3 | 562.9 |
| 210.6 | 212.46 | 1609.3 | 803.1 | | 333.0 | 847.2 |
| 257.0 | 260.1 | 2614.5 | | | 355.7 | 1639.9 |
| 300.6 | 303.0 | | | | 393.3 | |
| 338.8 | 642.3 | | | | 521.2 | |
| 927.2 | 1006.0 | | | | 594.7 | |
| 1042.4 | 1014.1 | | | | 604.6 | |
| 1223.3 | | | | | | |
| 1370 | | | | | | |
| 1470 | | | | | | |

## 3.5 Data Analysis

### 3.5.1 RADWARE

RadWare, developed by Dr. David Radford is a software package designed to analyze $\gamma$-ray coincidence data [64]. This package includes three major programs: gf3, escl8r and levit8r. These programs can manipulate one-dimensional (1-D), two-dimensional, and three-dimensional spectra, respectively. The gf3 program is a least-squares peak-fitting program that allows for interaction with one-dimensional spectra. The features include the fitting of peaks, the comparison of spectra (with overlay), the addition of multiple spectra (with AS- add spectrum), as well as many other capabilities described in Ref. [65]. The escl8r program [66] analyzes two-dimensional matrices, and is useful in creating level schemes and comparing the angular correlation between two transitions. The levit8r programs allows for the analysis of triple-$\gamma$ coincidence relationships by organizing data from one-dimensional spectra into three-dimensional cubes. A fourth program, 4dg8r, creates hypercubes that allow for coincidence events of higher degrees. Figure-plotting programs are available for graphical visualization and construction of level schemes (xmlev) as well as angular correlations (gnuplot).

### 3.5.2 Coincidence gates and spectra

Coincidence spectra were used to analyze the data in this thesis. A spectrum is created by gating on one or two transitions in this type of analysis. When gating

on any transition, $\gamma_1$, a spectrum is produced with peaks (lines) at energies of all other $\gamma$ rays that are detected when $\gamma_1$ is observed. These other peaks are called "coincident peaks", and each correspond to a coincident $\gamma$ ray. The gating on a single transition is called a "single gate", and it can be useful identifying the transitions in the partner nucleus of the reaction. Since hundreds of different nuclei are present, there is a high likelihood that a certain transition, $\gamma_1$ will be found in multiple nuclei. Hence, most singles gates are not very useful.

Although a single $\gamma$ ray may be present in many nuclei, the likelihood of two coincident $\gamma$ rays or three $\gamma$ rays is much smaller. A "double" gate is a spectrum created from two transitions coincident with one another, e.g. $\gamma_1$ and $\gamma_2$. In Fig. 3.6 panel (a), $\gamma_3$ would show up as a peak in the the coincidence spectrum in a gate on $\gamma_1$ and $\gamma_2$ (shortened to $\gamma_1/\ \gamma_2$). These three $\gamma$ rays are said to be in coincidence with one another. This is the method used to identify new transitions (like $\gamma_3$) in a nucleus. If a new transition is identified, it is important to verify that it belongs in the nucleus of interest. First, the process of "back-gating" ensures that the three transitions are coincident with one another. As a $\gamma_1/\gamma_2$ gate was used to find $\gamma_3$, a subsequent gate on $\gamma_1/\gamma_3$ should return $\gamma_2$ as well as a $\gamma_2/\gamma_3$ gate should return $\gamma_1$. If other, stronger transitions are present in the gate, this is a clear indication that this set of $\gamma$ rays is also found in another nucleus. The second step to ensure that $\gamma_3$ is not in another nucleus is to check the National Nuclear Data Center website (NNDC) [28] in the "Levels and Gammas Search" of the NuDat tab. A third step in this type of analysis is to check data from a different reaction to see if $\gamma_3$ is found in coincidence. These three steps were used to scrutinize the placement of

new transitions to establish new states in $^{78,80,82}$Ge.

In Fig. 3.6 panel (b), a double gate on $\gamma_1/\gamma_5$ should produce a peak at $\gamma_7$ in the coincidence spectrum. However, a gate on $\gamma_1/\gamma_4$ will not return $\gamma_7$ in their spectrum because $\gamma_1$ and $\gamma_4$ are not coincident. The two transitions both feed into the same state, but are independent of one another. For example, $\gamma_4$ and $\gamma_7$ are coincident with one another, but a third transition on top of state E is necessary in the data analysis. In Fig. 3.6 panel (c) has a more complicated level scheme, including a transition feeding into state E. Here, $\gamma_{12}$ should be found in the following gates: $\gamma_7/\gamma_5$, $\gamma_7/\gamma_4$, $\gamma_7/\gamma_1$, and $\gamma_6/\gamma_1$. Since there is no pathway between $\gamma_{12}$ to $\gamma_2$, $\gamma_3$, $\gamma_9$, $\gamma_{10}$, $\gamma_{11}$, and $\gamma_{13}$, these transitions are not coincident with $\gamma_{12}$. States like $\Delta$ and H are the highest-energy state in their respective sequences. Therefore, higher confidence in the level energy can be made through multiple gates. An example of this is when $\gamma_{11}$, $\gamma_{12}$, $\gamma_{13}$ all initiate at state H, and through gates using each of these transitions, the level energy for H should end up being the same, independent of the coincidence path used.

## 3.6 Angular Correlations

Since the 1940s the method of angular correlations between two $\gamma$ rays has been used to assign nuclear spins. The relationship between two successive $\gamma$ rays emitted from an excited nuclear state can be assessed through their anisotropy (directional correlation). Since there is no preferred orientation of fragments following a collision, the correlation between two coincident $\gamma$ rays can be expressed in terms of the

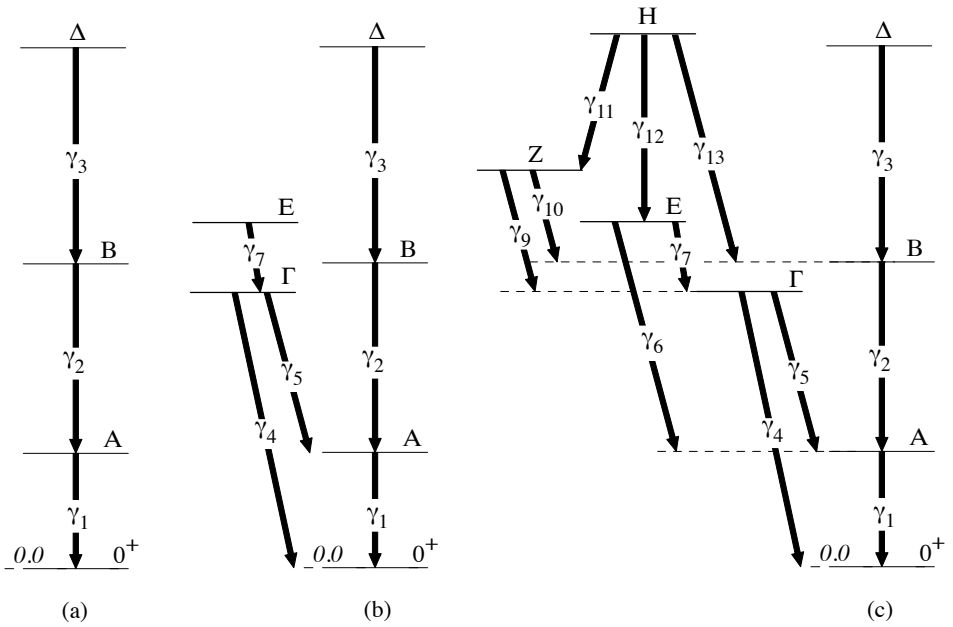


Figure 3.6: Example level schemes to show double, triple, and higher-fold coincidence events.

angular distribution probability, $W(\theta)$, a Legendre polynomial ($P_k(\cos\theta)$ of order $k$),

$$W(\theta) = \sum_{k=0,2,4}^{2L} a_k P_k(\cos\theta) \tag{3.2}$$

where the $a_k$ are coefficients dependent on the angular momentum removed by the transition (multipolarity), the nuclear spins of the states involved, and the mixing ratios of the transitions. The first five Legendre polynomials are listed in Table 3.3.

The angular distribution probability, $W(\theta)$, and its error, $\delta W(\theta)$ can be measured experimentally using either the movement of one detector through a range of angles (a method not used in this work) or by using multiple angles between detec-

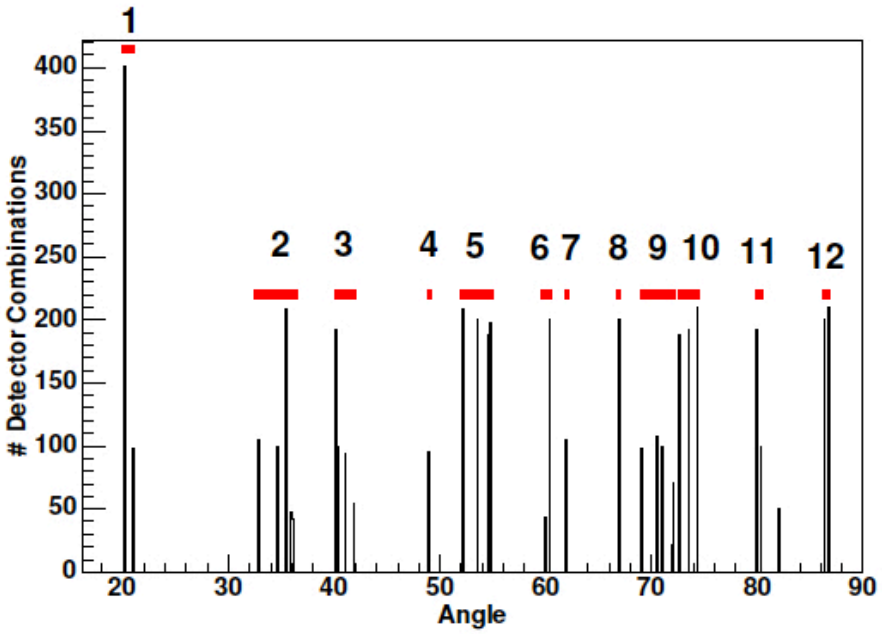


Figure 3.7: Distribution angles between 100 detectors in GS as the corresponding bin numbers (1-12). From Ref. [63].

Table 3.3: Legendre Polynomials

| Legendre Polynomial Order | Form |
|---|---|
| $P_0(\cos\theta)$ | $1$ |
| $P_1(\cos\theta)$ | $\cos\theta$ |
| $P_2(\cos\theta)$ | $\frac{1}{2}(3\cos\theta^2 - 1)$ |
| $P_3(\cos\theta)$ | $\frac{1}{4}(5\cos\theta^3 - 3\cos\theta)$ |
| $P_4(\cos\theta)$ | $\frac{1}{8}(35\cos\theta^4 - 30\cos\theta^2 + 3)$ |

tors in fixed positions as seen in Fig. 3.7. The various methods to analyze $W(\theta)$ and sources of discrepancies that can affect experimental results are described by Robinson [67]. Beyond the straight-forward quadrupole and dipole transitions, a $\gamma$ ray can be emitted by competing modes of de-excitation. This de-excitation has a multipole mixing ratio, $\delta$ which is described as the square root of the ratio of the number of $E2$ transitions per second by the number of $M1$ transitions per second.

$$W(\theta) = a_0[1 + \frac{a_2}{a_0}P_2(\cos\theta) + \frac{a_4}{a_0}P_4(\cos\theta)] \tag{3.3}$$

The general rules for the angular distribution of $\gamma$ rays are as follows: a $\Delta J = 2$, stretched quadrupole transition, has an $a_2 \approx 0.3$ and $a_4 \approx -0.1$. For a $\Delta J = 1$, stretched dipole transition, the values are typically $a_2 \approx -0.2$ and $a_4 = 0$. For a mixed transition with dipole and quadrupole multipolarities, $a_4 < 0$ and the transition is $\Delta J = 1$. Figure 3.8 shows an example of an $E2$ transition in Panel (a) and an $E1$ transition in Panel (b). Note that the $E2$ transition decreases with angle, while an $M1$ transition increases with angle. A second mechanism for determining the multipolarity of a transition is the use of an ellipse comparison plot with $a_2$ against $a_4$ (Fig. 3.9). This approach assumes that one of the two transitions in the

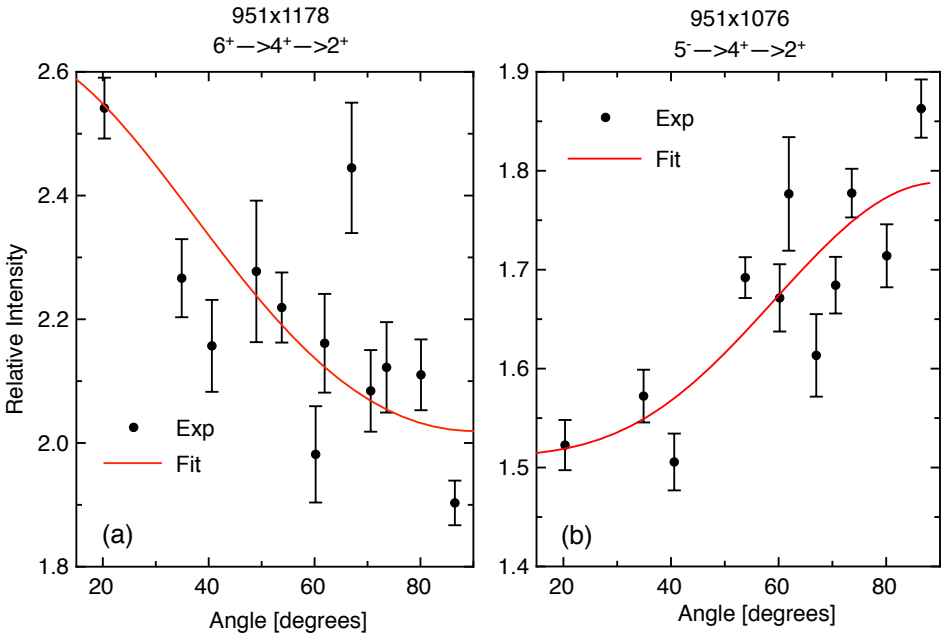


Figure 3.8: Two angular correlations from the $^{78}$Ge analysis. The angular correlation between the 950.6-keV $4_1^+ \rightarrow 2_2^+$ and 1178.4-keV $6_1^+ \rightarrow 4_1^+$ transitions is shown in Panel (a). This is an example of an $E2$ transition, within the ground state band. Panel (b) has the angular correlation between 950.6-keV $4_1^+ \rightarrow 2_2^+$ and the 1076.0-keV $5_1^- \rightarrow 4_1^+$ transitions. This dipole transition is concluded to be $E1$ in character owing to other properties of the level.

angular correlation is of pure multipolarity (either dipole or quadrupole). A list of values with a range of mixing ratios can be plotted (Ref. [68]). The nature of the transition can be determined if the the experimental $a_2$ and $a_4$ intersect with one of the ellipses.

### 3.6.1 Relative Intensities

DIS creates many nuclei, some of which contain transitions of similar energy. In order to determine intensities in a nucleus of interest, two transitions ($\gamma_1$ and

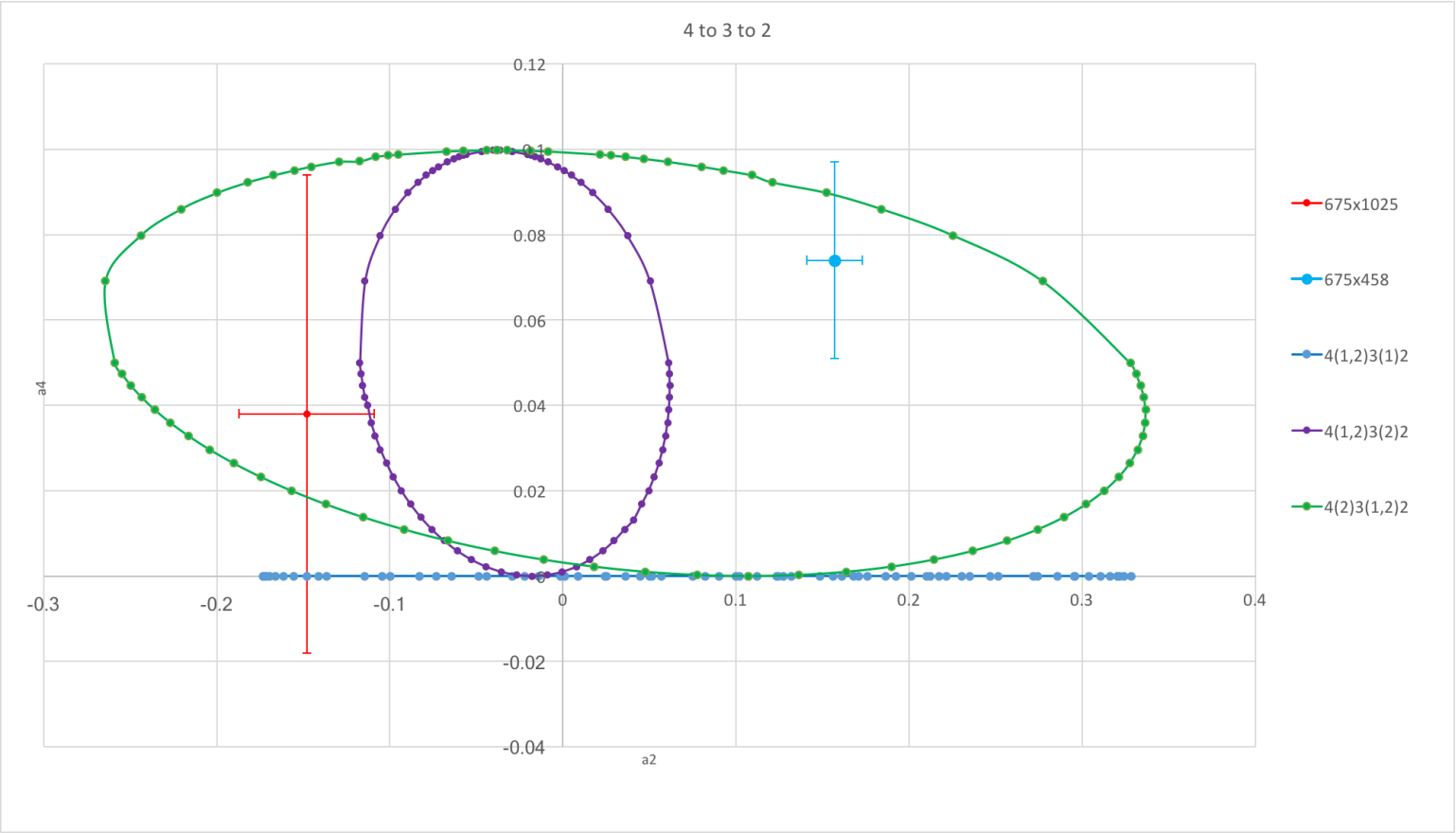


Figure 3.9: Ellipse comparison to determine the multipolarity of the 675-keV $\gamma$ ray in $^{78}$Ge compared to the 1025- and 458-keV $\gamma$ rays. Values for a mixed $4 \rightarrow 3$ and pure dipole $3 \rightarrow 2$ decay are plotted in dark blue, for a mixed $4 \rightarrow 3$ and pure quadrupole $3 \rightarrow 2$ decay are plotted in yellow, and a pure quadrupole $4 \rightarrow 3$ and mixed $3 \rightarrow 2$ decay are plotted in green. Once the value crossed is determined, the $\delta$ value for that $a_2, a_4$ combination is listed in Ref. [68]. The value for the light blue 675-keV $\gamma$ ray in the 458-keV gate is in agreement with a pure 675 keV $E2$ transition, with a mixed 458-keV transition. The ellipse comparison for red experimental $a_2, a_4$ value does not provide insight as to the nature of the transition. For a pure dipole transition, the value of $a_4$ is zero.

$\gamma_2$) must be used. These two $\gamma$ rays are both assigned an intensity of 100. A coincidence spectrum using $\gamma_1$ is created, and the areas of other coincident peaks can be collected (including $\gamma_2$). The measured area and the uncertainty of a peak are then corrected for detector efficiency. The intensity of each peak is reported relative to the intensity of $\gamma_2$ ($I_2$). Corrections to some transitions must be made when they do not decay to the ground state through the $\gamma_1 - \gamma_2$ sequence. In these cases, other gates on transitions which decay through $\gamma_1$ or $\gamma_2$ are used, and a conversion factor is necessary. These data are useful in obtaining branching ratios from a single level. The overall intensities will be sensitive to both the target and projectile used, and also to the energy of the particle. These types of experiments can also use thin targets with mass gating. Thin target data are sensitive to the energy of the beam and the thickness of the target. The branching ratios are independent of the method of production, and are therefore quite useful across experiments.

## 3.7 Shell-model calculations

Configuration-Interaction (CI) codes such as NuShellX, require a specific scheme to build a complete basis. Once the basis is created, matrix elements of the Hamiltonian are calculated and the eigenvalues and eigenvectors are identified. The basis may be populated by a fixed value $J$ (angular momentum), $T_z$ (isospin), or $M$ (where $J_z = M$). The design of the basis is important to minimize computer processing time. A fixed total $M$ and $T_z$ value is called the M-pn (proton-neutron) scheme. The J-pn scheme has a fixed total $J$ and $T_z$ value. The NuShellX code

uses the J-pn scheme, while another well-cited code in this mass region, ANTOINE, uses a M-pn basis. In the region of Zn, Ge, and Se nuclei, the jj44b and jun45 Hamiltonians within the jj44 model space are often cited in literature. NuShellX is able to provide the following information for this nuclear analysis: a level scheme, transitions between states of the same parity (no $E1$ transitions are allowed), and $B(E2)$ values. The information in this section was obtained from Alex Brown and Ed Simpson [69].

The jj44 model space for the jj44 Hamiltonian is a truncation of the shell model. It is comprised of an inert core of $^{56}$Ni, with 28 protons and 28 neutrons. The excitations within the nucleus can occur within the following valence orbitals: $1f_{5/2}$, $2p_{3/2}$, $2p_{1/2}$, and $1g_{9/2}$. The dimension of the matrix is on the order of $10^{11}$ entries. The M-scheme dimension is on the order of $10^6$. Within the jj44 model space, different interactions or Hamiltonians can be used, but this work focuses on jj44b and jun45. The jj44b interaction assumes a mass dependence of $(A/58)^{-0.3}$, and it uses two-body matrix elements (TBME) obtained with a renormalized Bonn-C potential. It also uses the single-valued decomposition (SVD) method (an effective Hamiltonian) to constrain the TBME in nuclei with $Z = 28 - 30$ ($N = 28 - 50$) and $N = 48 - 50$ ($Z = 28 - 50$). There is also a correction in the binding energy in the Skyrme energy-density functional calculation.

When the "shell" program is run within NuShellX, a "batch" file (*.bat) and an answer file (*.ans) are created to run the shell-model calculation. These files execute and display the commands for the program in which two main options "lpe" and "dens" are used. The "lpe" routine calculates the complex many-body wavefunctions

with a preset value to return the first ten eigenstates, which correspond to the first ten levels. The "dens" routine calculates the one-body transition densities, which return the transition probabilities ($B(E2)$ values) between states.

The model space and interaction are identified within "lpe" and the proton and mass numbers are given to identify the nucleus. The minimum and maximum angular momentum of the final states are inputs that define calculation parameters. The parity (even, odd, or both) is specified as to which levels are produced. Each wavefunction is comprised of the partitions of valence nucleons in available orbits in a reduced model space (e.g. jj44). The configuration of a partition in the reduced model space is more commonly known as a Slater determinant. The wave function is a sum over these Slater determinants. The routine returns the calculated levels of the input nucleus in a *.lpt file. It also incorporates the experimental data for this nucleus from the National Nuclear Data Center at Brookhaven National Laboratory (BNL) [28]. The experimental levels are reported alongside the calculated levels, useful for comparison.

Once the many-body wave functions have been calculated for each state, the "dens" command calls on these wavefunctions and then calculates the overlaps between two wavefunctions. "Dens" calculates the radial wave functions for each potential and also calculates $B(EL)$, $B(ML)$ and $B(GT)$ reduced transition probabilities from one-body transition density (*.obd) files. The $M1$ and $E2$ matrix elements are found in a *.den (or *.dei for gamma decay) file. In this thesis, the "t" option is chosen to calculate the two-body matrix elements. This produces the *.obd files for all transitions. The *.den file can be edited in order to use a different

potential from the harmonic oscillator (HO) and also to change the effective operators of the free-nucleon values. The other methods available to calculate the matrix elements are the Woods-Saxon and Skyrme energy-density functionals. The $\gamma$-ray decay scheme is constructed from the $M1$ and $E2$ results and also the magnetic and quadrupole moments for each states.

Files with an *.lpe output provide average occupancies for each orbital and also the decomposition for different total angular momentum couplings of protons and neutrons. This type file provides a list of neutron and proton partitions to describe each nuclear configuration.

Table 3.4: Occupation of 4 protons and 18 neutrons in a specific excited nuclear state.

| $\pi 1f_{5/2}$ | $\pi 2p_{3/2}$ | $\pi 2p_{1/2}$ | $\pi 1g_{9/2}$ |
|---|---|---|---|
| 2.1457 | 1.3729 | 0.3121 | 0.1693 |

| $\nu 1f_{5/2}$ | $\nu 2p_{3/2}$ | $\nu 2p_{1/2}$ | $\nu 1g_{9/2}$ |
|---|---|---|---|
| 5.2928 | 3.8208 | 1.6077 | 7.2785 |

The occupation numbers in Table 3.7 show one full pair of protons always sits in the $f_{5/2}$ orbital. The second pair has the following orbital occupancy: 1/6 in the $p_{3/2}$, 1/6 in the $p_{1/2}$, 1/12 in the $f_{5/2}$ and 1/12 in the $g_{9/2}$. The $p_{3/2}$, $f_{5/2}$, $p_{1/2}$, and $g_{9/2}$ orbitals hold a total of 22 nucleons. For $N = 46$, seen in Table 3.7, there are four holes, 2 of which always reside in the $g_{9/2}$ orbital, with the other two holes vary between the $f_{5/2}$ and $p_{1/2}$ orbitals. The occupancy in the $\nu p_{3/2}^{-1}$ (hole) is shown as 3.82, meaning that it is close to the full value of 4, as it is deep within the core of the nucleus. In $N = 46$ isotone, $^{75}$Cu, the monopole migration has lead to a near degeneracy of the $\pi f_{5/2}$ and $\pi p_{3/2}$ proton orbitals [31, 32].

# Chapter 4: Experimental Results

This chapter contains the results for $^{78,80,82}$Ge obtained in this work. The closed-neutron-shell nucleus $^{82}$Ge is presented first. This will provide an example of the relative simplicity found in closed-shell systems. This simplicity is demonstrated by the fact that many of the states can be described by two- and four-particle configurations with minimal collectivity. $^{80}$Ge, with two neutron holes in the $N = 50$ shell, has an influx of more levels and complexity compared to $^{82}$Ge. Fewer states can be assigned to a specific particle configurations with relative certainty. In $^{78}$Ge, with four neutron holes, seniority-four neutrons states and seniority-four proton states are both present. With this added complexity, configurations are not presented as the majority would be speculative.

A brief review of previous characterizations for each nucleus is found in Background Sections 4.1.1, 4.2.1, 4.3.1 and compiled in graphical form in Figs. 4.1, 4.5, 4.10. Published data sets are available from the National Nuclear Data Center (NNDC) website [28]. Other data sets are not included in the NNDC evaluation because they are found in unpublished theses. Sections 4.1.2, 4.2.2, 4.3.2 include key examples of coincidence spectra used in the analysis of this data. Many unmarked peaks appear in the spectra because they did not pass the scrutiny of the back-gating

analysis. The "Levels" sections discuss the reported (seen and unseen in this work) levels in the $^{78,80,82}$Ge nuclei to be used in conjunction with previously reported levels from Figs. 4.1, 4.5, 4.10. The level schemes compiled in this thesis are found in Figs 4.2, 4.6, 4.11. Uncertainties in the level energies are presented with each level. The energies of levels that were not seen in this work are not stated with an error. There is higher uncertainty in level energies that require multiple transitions to the ground state (uncertainty determined through error propagation). There is also higher uncertainty with levels which decay through Doppler-broadened peaks. Established spins and parities are presented here without parentheses, whereas a state with a $(J^{\pi})$ label is a tentative assignment, as it lacks sufficient evidence to be certain of the spin or parity.

## 4.1 $^{82}$Ge

### 4.1.1 Background

Fig. 4.1 depicts the historical evolution of the reported level structures for $^{82}$Ge. The unstable $^{82}$Ge nucleus lies at the $N = 50$ major shell closure in the shell model. Even-even $N = 50$ isotones have been thoroughly examined between $^{86}$Kr and $^{100}$Sn. These nuclei can be populated in a variety of nuclear reactions with light and medium-mass nuclei. A theoretical description of these levels was published by Wildenthal and others long before extensive experimental data were available from the nuclei in and near the valley of stability around $^{88}$Sr and $^{90}$Zr [81–83]. On the other hand, scant data are available for $^{84}$Se, $^{82}$Ge, and $^{80}$Zn, and there is currently

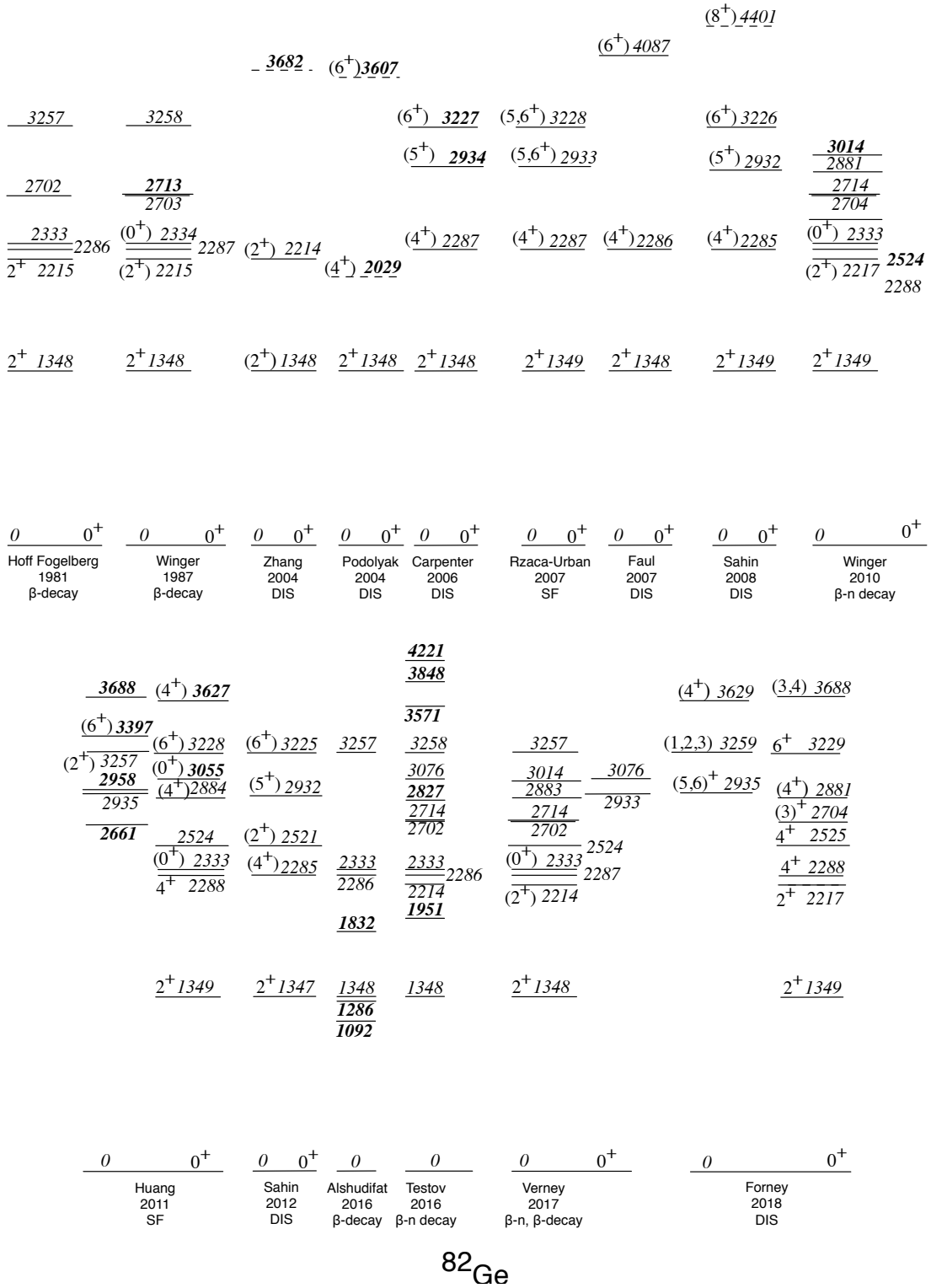


Figure 4.1: Level schemes reported (Refs. [1, 3, 4, 70–80]) for $^{82}$Ge with energies in keV.

no published structure for double-magic $^{78}$Ni. These nuclei are necessary for a comprehensive overview of the role of protons in even nuclei between $Z = 28 - 50$. Hoff and Fogelberg were the first to study $^{82}$Ge in 1981 by the $\beta$ decay from $^{82}$Ga [1]. Their work is abbreviated as HF81 in this thesis due to its importance and the frequency of comparison. The HF81 work identified eight transitions in total, and described the first two states as $2^+$. The authors identified three states near 2.3 MeV (shown in Fig. 4.1) along with two states at higher energy. The ground-state spin of $^{82}$Ga had not been determined at that time, so the authors assumed a parent with $J = (1, 2, 3)$ by the states that were fed.

In 1987, Winger performed a $\beta$-decay study from $^{82}$Ga into $^{82}$Ge. He expanded the level scheme proposed in HF81 by resolving a doublet at 2700 keV and he also included a spectrum of the results [70]. The new level in this doublet (2713.7 keV) decayed directly into the ground state, and also into the $2^+_1$ state limiting it to a $J = 1, 2$. From angular correlations, Winger supported the HF81 hypothesis that the first two excited states were $2^+$, and he presented the 2333-keV state as a $(0^+)$. Winger performed shell-model calculations for the $N = 50$ isotones, and argued that the $\beta$-parent $^{82}$Ga ground state could range from $0^- \rightarrow 4^-$. He favored an assignment of $1^-$ because the shell model predicted two low-lying $4^+$ states that were not seen.

Over fifteen years passed without additional work on the structure of $^{82}$Ge. The first $\beta$-delayed neutron ($\beta$-$n$) experiment on $^{82}$Ge was included in a work by Perru *et al.* in 2003 [84]. The authors presented a strong $\beta$-$n$ channel comprised of 40% of the $^{83}$Ga $\beta$ decay, which established an opportunity to study $^{82}$Ge further

by $\beta$-$n$ decay. Although no new levels were established in this work, a coincidence spectrum solidified the observation that the 938-keV $\gamma$ ray is coincident with the 1348 keV $2_1^+ \rightarrow$ ground state transition. Perru *et al.* were limited by the scope of their data, and they were unable to observe the weaker $2_2^+ \rightarrow 2_1^+$ 866-keV transition in coincidence with the 1348-keV $\gamma$ ray.

Two papers following a single deep-inelastic scattering experiment with a $^{82}$Se beam on a $^{192}$Os target were published in 2004. These included data on $^{82}$Ge, as it was a "beam-like" nucleus produced in the reaction. Podolyák *et al.* observed the first $2^+$ state and presented tentative 681- and 1578-keV transitions from the $(4^+)$ and $(6^+)$ levels in $^{82}$Ge [3]. A followup work, by Zhang *et al.* used cross $\gamma$-ray coincidences. This technique uses one transition from the "target-like" nucleus and another from the "beam-like" one to study the levels in $^{82}$Ge. Zhang *et al.* confirmed the 2214-keV $2^+$ level, and they presented a new tentative level at 3682 keV to decay by a 1468-keV $\gamma$ ray atop the 2214-keV state. They also observed the 681- and 1578-keV transitions seen in the Podolyák work, but mentioned that these coincident $\gamma$ rays had also been observed in $^{87}$Kr.

In 2005, a deep-inelastic scattering experiment of $^{82}$Se on $^{208}$Pb and $^{238}$U targets in GS was reported by Carpenter *et al.* [72]. Using the coincidence method, Carpenter identified three new transitions at 940, (293) and 646 keV with a double gate on the 1348/939-keV lines. He was able to determine the presence of a second 940-keV $\gamma$ ray coincident as a $(6_1^+)$ level at 3228 keV. Within the same coincidence gate, a 646- and a tentative 293-keV transitions were found. Separate from the 940-keV doublet, the 646 keV transition was attributed to the decay from the $(5^+)$

state.

Returning to his thesis subject 23 years later, Winger *et al.* studied the decay of $^{83,84,85}$Ga nuclei into Ge [75] through direct $\beta$ decay and $\beta$-delayed neutron decay. This work reported a probability of neutron emission of $P_n = 62.8\%$, which is much higher than the value presented by the Perru thesis. Winger *et al.* introduced three new states at 2524, 2883, and 3015 keV, none of which directly feed into the ground state (therefore $J < 2$). The work used a $J^\pi$ value for the $^{83}$Ga parent of $5/2^-$, which was later confirmed [85].

$^{82}$Ge was studied through $\beta$ decay under the assumption that the $^{82}$Ga parent had a $J = (1, 2, 3)$. Laser spectroscopy measurements by Cheal *et al.* tentatively assigned the parent a $J = 2$, with first forbidden transitions to levels with $J = (1^+, 2^+, 3^+)$ [86]. The assignment of the Ga parent was changed to a firm $J^\pi = 2^-$ by Alshudifat *et al.* [78]. They found the $\log(ft)$ values for each level which lie in the first forbidden range, and this implies that there is a parity change from the parent nucleus and so the populated spins will be $1^+, 2^+, 3^+$. The positive-parity results agree with theoretical calculations that have no reasonable configurations available at low energy for negative-parity levels in $^{82}$Ge.

Sahin *et al.* examined $N = 50$ nuclei through a multi-nucleon transfer (MNT) reaction of a $^{82}$Se beam on a $^{238}$U target. By charge and mass selection, they published a spectrum of $^{82}$Ge containing $\gamma$-ray peaks at 647, 938, 940, 1174, and 1347 keV [77]. The current spin-parity assignments adopted by NNDC are a result of the angular distributions reported in this work. Through a similar reaction, Faul observed numerous transitions in a single gate which are listed in Table 4.2. Most

recently, in 2017, Verney *et al.* confirmed many of the known states through $\beta$ and $\beta$-$n$ decays after mass separation [80]. Due to inconsistencies in the Verney 2013 paper on $^{80}$Ge [5], conclusions from the Verney 2017 work on $^{82}$Ge will not be weighed heavily [80].

Table 4.1: $^{82}$Ge excitation energies $E_{lev}$, $\gamma$-ray energies $E_\gamma$, branching ratios and spin-parity assignments $I_i^\pi \rightarrow I_f^\pi$ of initial and final states for $\gamma$ rays placed in $^{82}$Ge from the experimental prompt data. The states with reliable reproducibility are shown. **States reported with a precision of 0.1 keV were seen in this work**.

| $E_{lev}$ (keV) | $E_\gamma$ (keV) | B.R. % | $J_i^\pi \rightarrow J_f^\pi$ |
|---|---|---|---|
| 1348.6[a-c] | 1348.6 | 100 | $2_1^+ \rightarrow 0_1^+$ |
| 2217.2[a-c] | 868.4 | 33(17)[f], 29[g], 38(7)[*] | $2_2^+ \rightarrow 2_1^+$ |
| | 2217.2 | 67(24)[f], 71[g], 62(11)[*] | $2_2^+ \rightarrow 0_1^+$ |
| 2288.2[a-d] | 939.6 | 100 | $4_1^+ \rightarrow 2_1^+$ |
| 2333[a-d] | 984 | 100 | $0_2^+ \rightarrow 2_1^+$ |
| 2525.0[b,d] | 1176.4 | 100 | $4_2^+ \rightarrow 2_1^+$ |
| 2703.6[a,b] | 415.4 | 31(3)[f], 27[g] | $(3_1^+) \rightarrow 4_1^+$ |
| | 486.4 | 10(7)[f], 12[g] | $(3_1^+) \rightarrow 2_1^+$ |
| | 1355.0 | 59(3)[f], 61[g] | $(3_1^+) \rightarrow 2_1^+$ |
| 2714[a,b] | 1365 | 62(14)[f], 70[g] | $(1_1^+) \rightarrow 2_1^+$ |
| | 2714 | 38(12)[f], 30[g] | $(1_1^+) \rightarrow 0_1^+$ |
| 2881.4[b,d] | 356.7 | | $(4_3^+) \rightarrow 4_1^+$ |
| | 595 | | $(4_3^+) \rightarrow 4_2^+$ |
| 2934.7[c] | 408.6 | | $(5,6)^+ \rightarrow 4_2^+$ |
| | 645.5 | | $(5,6)^+ \rightarrow 4_1^+$ |
| 3014[b] | 726 | 100 | $(4,5)^+ \rightarrow 4_1^+$ |
| 3055[d] | 1707 | | $(0)^+ \rightarrow 2_1^+$ |
| 3076[e] | 1727 | 67(4)[f] | $(2)^+ \rightarrow 2_1^+$ |
| | 3076 | 33(7)[f] | $(2)^+ \rightarrow 0_1^+$ |
| 3228.7[c] | 940.5 | 100 | $6^+ \rightarrow 4_1^+$ |
| 3258.7[a,d] | 1909.1 | 100 | $(2^+) \rightarrow 2_1^+$ |
| 3397[d] | 513 | | $(6^+) \rightarrow (4^+)$ |
| 3629.1[d] | 370.4 | | $(4^+) \rightarrow (2^+)$ |
| 3688.1[d] | 1470.9 | | $\rightarrow (2^+)$ |
| | 756.2 | | $\rightarrow (5,6)^+$ |

[*] indicates branching ratios identified in this work
[a] from HF81 [1]
[b] from Ref. [87]
[c] from Ref. [73]
[d] from Ref. [76]
[e] from Ref. [78]
[f] from Ref. [80]
[g] from Ref. [88]

Table 4.2: Transitions in $^{82}$Ge observed in CLARA-PRISMA experiments from Table 3.5 in the thesis by Faul [4].

| $E_\gamma$ (keV) | $I_{\text{rel}}$ | $R_{\text{asym}}$ |
|---|---|---|
| 203.5(2)* | 37(6) | |
| 608.5(14)* | 78(40) | |
| 644.7(13) | 47(17) | |
| 938.7(1) | 77(14) | 2.10(77) |
| 949.5(8)* | 38(12) | |
| 1348.1(9) | 100(12) | 1.53(45) |
| 1800.6(10) | 18(13) | 2(1) |

* Likely a contaminant.

### 4.1.2 Spectra

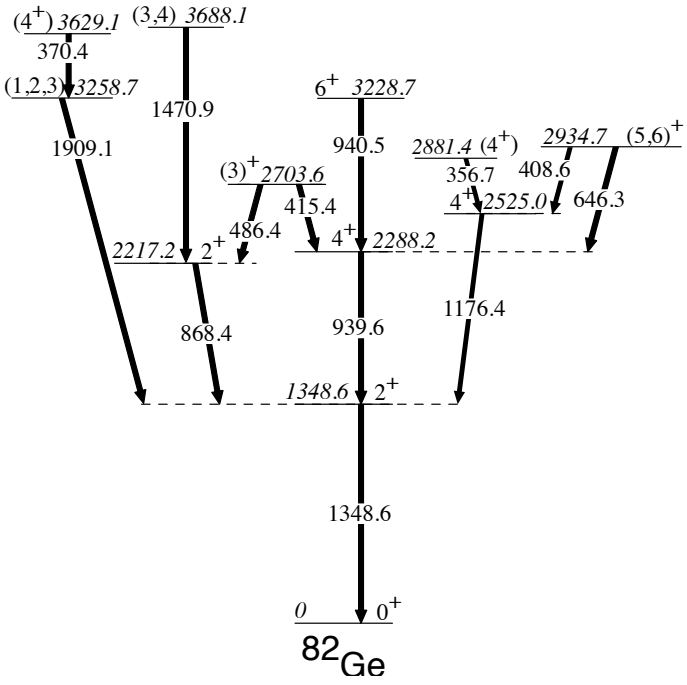


Figure 4.2: Transitions in $^{82}$Ge observed in this work using the Se/U data with energies in keV.

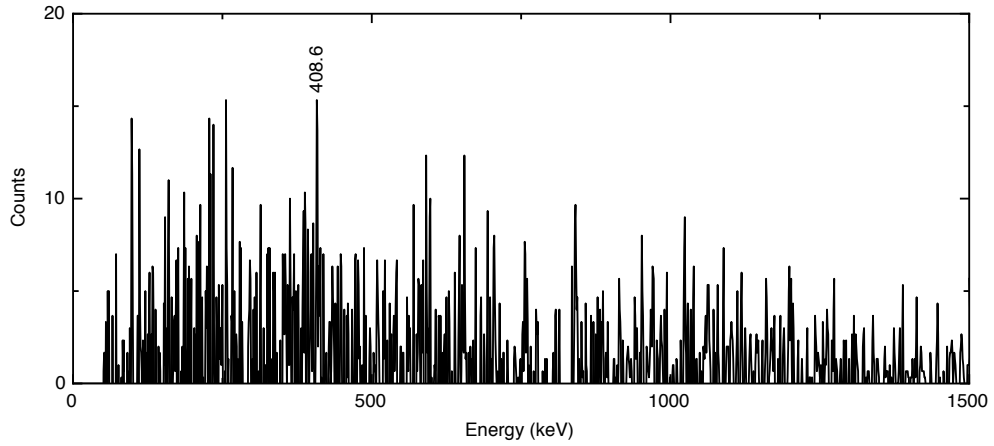


Figure 4.3: Coincidence gate on $^{82}$Ge 1176.4- and 1348.6-keV transitions in Se/U data.

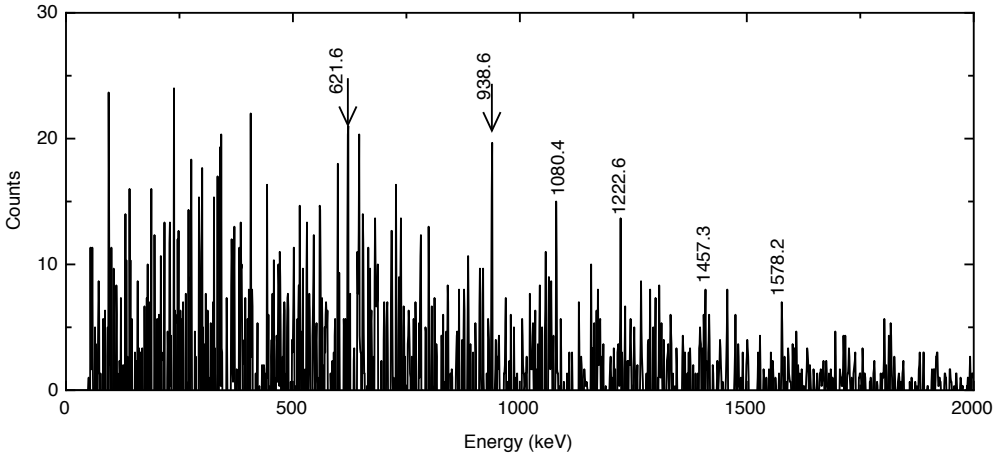


Figure 4.4: Coincidence gate on $^{82}$Ge 1348.6- and 645.5-keV transitions in Se/U data.

### 4.1.3 $^{82}$Ge Levels

Different types of experiments will populate a distinct range of angular momentum. The allowed states seen in direct $\beta$ decay have spins of $1, 2, 3$ from the $2^-$ $^{82}$Ga parent [1]. These authors also observed the $4_1^+$ state at 2282 keV through first-forbidden unique and unobserved secondary feeding. The spontaneous fission work and multi-nucleon transfer reactions [3,71,73,77] produce states of higher spin. States seen in those reactions, but not observed in $\beta$ or $\beta$-$n$ decay, are considered higher-spin states ($\geq 4$).

**1348.6 (1) keV, $2_1^+$.** This state is accepted as the yrast $2^+$ state with a $B(E2)$ of 12.1(21) W.u. [45,89,90]. This thesis confirms the presence of the of the 1348.6 keV peak in a $\gamma - \gamma$ gate on each pair of coincident transitions in Fig. 4.2.

**2217.2 (1) keV, $2_2^+$.** The identification of the 868.4-keV $\gamma$ ray in gates on the 1348.6-keV $2_1^+ \rightarrow 0^+$ transition with the 486.4-keV $(3_1^+) \rightarrow 2_2^+$ and 1470.9-keV transitions confirmed this state in the present work. The reported 2216-keV transition to the ground state was not observed. This state was identified by HF81 as a $2_2^+$ level and in the Winger thesis to be either a $(1^+)$ or $(2^+)$ one.

**2288.2 (1) keV, $4_1^+$.** This state was confirmed by the 939.6-keV $\gamma$ ray feeding into the yrast $2^+$ state through coincidence gates on the 1348.6- with the 415.4-keV and 645.5-keV transitions. The 939.6-keV transition has also been observed in the deep inelastic scattering experiments of Faul [4].

**2333 keV, $0_2^+$.** This level decays by a 984-keV transition to the $2_1^+$ state, but was not observed in the present work [1, 87]. This state was determined to have

$(0^+)$ quantum numbers initially in the Winger thesis by angular correlations [70]. A $0_2^+ \rightarrow$ ground-state transition has yet to be reported.

**2525.0 (1) keV, $4_2^+$.** This work observed this state through the decay of a 1176.4-keV $\gamma$ ray in a coincident gate on the 1348.6 keV line with the 408.6- and 356.7-keV transitions. The 2525-keV state is proposed as a $J^\pi = 4^+$ instead of a $5^+$ level because it is fed by the $5/2^-$ parent in $\beta$-delayed neutron decay, but not by the $2^-$ parent in $\beta$ decay experiments (which allow for $J = 1, 2, 3$). Hwang *et al.* proposed this state is a $(2^+)$ level as they identified a transition directly to the ground state [76]. They also reported a 191.4-keV transition from this level to the $0_2^+$ level at 2333 keV. If the 2525-keV level was a $2^+$ state, it should be seen in the direct $\beta$-decay work by Hoff and Fogelberg [1]. Confirmation of the two transitions is necessary to limit the $J^\pi$ values of this state to $1^+$, $1^-$ or $2^+$. Additionally, Verney *et al.* were unable to identify either the 191.4- nor 2524.7-keV transitions reported by Hwang *et al.* [76]. Angular correlations were reported by Ref. [77] on the 1176-keV transition to have an $a_2 = 0.31(17)$ coefficient, but the $\gamma$-ray multipolarity could not be determined. The angular correlation has a smaller slope than the other $E2$ transitions of the yrast band, allowing the 1176-keV $\gamma$ ray to be either a stretched quadrupole or a strongly mixed dipole transition.

**2703.6 (4) keV, $(3)^+$.** This state was observed to decay via both direct $\beta$ decay [1] and $\beta$-delayed neutron decay [87] by 415.4 and 1354-keV transitions into the yrast sequence and also a tentative 487-keV transition [88] to the $2_2^+$ state. Verney *et al.* confirmed a weak line at 487 keV [80]. This level is a likely candidate for the $(3^+)$ state as it feeds $J^\pi = 2$ states, but not the ground state. A 415.4-keV transition into

the $4^+$ state was seen in a 1348.6/939.6-keV coincidence gate and the 486.4-keV $\gamma$ ray was observed in the 1348.6/868-keV gate. During the investigation for the third previously reported transition, a 1307.1-keV transition was found coincident with a 1352.5-keV one. It was not possible in this work to determine if the 1307.1-keV transition is also coincident with the 415.4- and 486.4-keV transitions that were observed. If the 1352-keV $\gamma$ ray has the highest intensity reported by Verney *et al.*, a weaker 1307.1-keV transition may not be observed due to the low number of counts in a 1349/1354-keV coincidence gate. **2714 keV,** $(1^+)$**.** This state was observed is seen in direct $\beta$ decay following the fission of $^{238}$U [88]. It feeds the $2_1^+$ level and ground state, restricting it to a spin of 1 or 2, but it was not identified in this work. This thesis favors a $(1^+)$ assignment, as a $1^+$ state is expected in this energy region by the 2627-keV state in isotonic $^{80}$Zn. Verney *et al.* were unable to identify the 596.4-keV transition reported by Winger *et al.*, but they were able to identify the 1365.4- and 2713.4-keV transitions [80].

**2881.4 (2) keV,** $(4_3^+)$**.** The 356.7- and 593.2-keV transitions which are included in the decay of this state both feed $4^+$ levels as observed in $\beta - n$ decay [87], but no states of lower spin. In this work, this state is observed to decay by a 356.7-keV transition to the 2525-keV level (first identified by Ref. [76]) in a 1176.4/1348.6-keV coincidence gate in the DDD Se/U cube. **2934.7 (2) keV,** $(5^+)$**.** The 646-keV transition was observed in spontaneous fission by Hwang *et al.* [76] and Rzaca-Urban *et al.* [73], and it was confirmed in this work. A newly identified, second transition decaying from this state by a 408.6-keV $\gamma$ ray to the 2525-keV $4^+$ state was identified in the present work by a coincidence gate on the 1348.6- and 1176.4-keV

transitions(Fig. 4.3). As this state was not seen in either $\beta$ decay or $\beta$-delayed neutron decay (except in Verney *et al.* [80]), the spin is likely $> 4$. This level has the same decay pattern as the 2881-keV ($4_3^+$) state, limiting it to a spin $\leq 6$ value. Unable to separate the doublet at 940 keV, the relative intensities calculated by Faul describe the 645.5-keV transition as larger than the 940 keV one [4]. Sahin *et al.* reported a relative intensity of the 940-keV transition ($6^+ \rightarrow 4^+$) as 37(8) units compared to the 646 keV intensity as 22(7) [77], and the present work agrees within uncertainty. Sahin *et al.* also calculated an angular correlation which showed the 646-keV transition to have a dipole character, supportive of a $5_1^+$ assignment [77]. The 646.3-keV and 408.6-keV transitions were observed in the prompt data to decay to the 2288-keV state and to the 2525 keV states. Evidence for the the 408.6-keV line is observed in a coincidence gate with either the 1348.6- or 1176.4-keV transitions. The 645.5-keV transition was confirmed by the presence of the 939.6-keV $\gamma$ ray in a 1348/646-keV coincidence gate as in Fig. 4.4.

**3014 keV.** A 727-keV transition was observed in $\beta$-delayed neutron decay [87] from this state (to the $4_1^+$ level), but it was not confirmed by in the present study.

**3228.7 (2) keV, $6^+$.** This state was designated as the yrast $6^+$ level by Refs. [73, 74,77] and it decays by a 940.5-keV transition to the $4^+$ state at 2282.2 keV. Ref. [77] also determined that the 940.5-keV transition was quadrupole in nature. Through coincidence gates, this thesis determined that the 940.5-keV line is the strongest transition in the 1348.6/939.6-keV gate. The presence of a tentative 293-keV transition was previously reported using the same data set by Carpenter *et al.*(Ref. [72]). This is not included in the present thesis due to lowthe low number of counts in the

gate.

**3258.7 (2) keV,** $(2^+)$**.** This level, initially identified by the $\beta$-decay study of HF81 [1], was assigned as $(2^+)$ by Ref. [76]. A 1909.1-keV transition decays from this state in the 370.4/1348.6-keV coincidence gate. This gate was determined by the 1908.9- and 369.6-keV transitions reported by Hwang *et al.* [76]. That group also reported that this level decayed by a 201.9-keV transition, which was not seen in the present work nor in the previous work by Verney *et al.* [80].

**3629.1 (3) keV,** $(4^+)$**.** A transition with 370.4 keV energy is found in coincidence with the 1909.1-keV one which subsequently decays into the 1348.6-keV $2_1^+$ state, in agreement with Ref. [76].

**3688.1 (3) keV,** $(3, 4)$**.** The present work observed a 1470.9-keV transition on top of the 2217.2-keV level in agreement with Refs. [3,71]. An additional decay from this state via a 756-keV transition to the 2935-keV $(5)^+$ state was reported by Ref. [76] without a $J^\pi$ assignment. **4402 keV** Currently included in the NNDC-evaluated file on $^{82}$Ge, this state was reported by Sahin [74] in 2008 through the decay of a 1176-keV transition into the $6_1^+$ state. Subsequently, Sahin *et al.* published a more thorough investigation on the same nuclei and data with an adjustment in location of the 1176-keV transition [77]. Further support for this adjustment is shown in the coincident gates in Fig. 4 (middle panel) of Ref. [77], where the 1176-keV transition was not found to be coincident with either transition in the 940-keV doublet.

**6063 keV** This level is reported to decay to the $3^+$ state by a 3360.6-keV transition by Alshudifat *et al.* [78]. It is possible that a second transition, described by the same work as 3848.4 keV could decay from this state into the 2215-keV $2_2^+$ state.

This observation was strictly determined from the energy differences between the states.

### 4.1.4 Level Configurations

Table 4.3: Possible configurations for states in $^{82}$Ge.

| $E_{\text{lev}}$ (keV) | $J^\pi$ assignment | Particle configuration |
|---|---|---|
| 1348.6 | $2^+$ | $\pi f_{5/2}^{+1} f_{5/2}^{+1}$ |
| 2288.2 | $4_1^+$ | $\pi f_{5/2}^{+1} f_{5/2}^{+1}$ |
| 2217.2 | $2_2^+$ | $\pi p_{3/2}^{+1} f_{5/2}^{+1}$ |
| 2525.0 | $4_2^+$ | $\pi f_{5/2}^{+1} p_{3/2}^{+1}$ |
| 2703.6 | $3^+$ | $\pi f_{5/2}^{+1} p_{3/2}^{+1}$ |
| 2714 | $1^+$ | $\pi f_{5/2}^{+1} p_{3/2}^{+1}$ |
| 2881.4 | $4_3^+$ | $\pi f_{5/2}^{+1} f_{5/2}^{+1} f_{5/2}^{+1} p_{3/2}^{+1}$ |
| 2934.7* | $5^+$ | $\nu g_{9/2}^{-2} \circ d_{5/2}^{+2}$ |
| 3228.7 | $6^+$ | $\pi f_{5/2}^{+1} f_{5/2}^{+1} f_{5/2}^{+1} p_{3/2}^{+1}$ |

* Configuration as described by Seija and Nowacki [91].

## 4.2 $^{80}$Ge

### 4.2.1 Background

$^{80}$Ge was first investigated by Hoff in 1981 by the $\beta - n$ decay of $^{81}$Ga with a ground state spin of $(5/2^-)$ [92]. Hoff and Fogelberg (HF81), published in the same issue and presented data on the $\beta$ decaying isomer of $^{80}$Ga produced with their mass separator. On the basis of their observations, they proposed a spin $J$ of 3 for $^{80}$Ga and a half-life of 1.676 s [1]. HF81 mentioned the likelihood of isomerism due to the

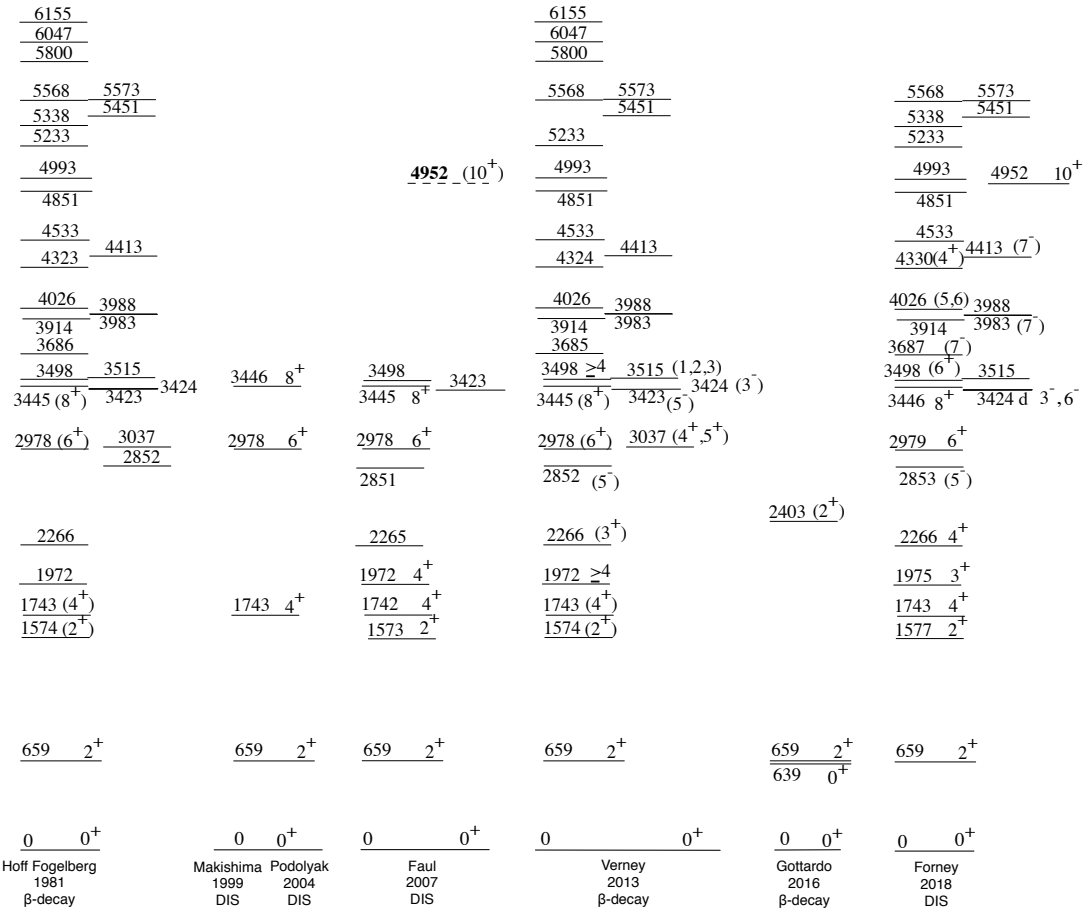


Figure 4.5: Level schemes reported (Refs. [1–6]) for $^{80}$Ge with energies in keV.

proximity of the $p_{1/2}$ and $g_{9/2}$ neutron configurations. However, they were unable to identify two $\beta$-decaying states in $^{80}$Ga through multi-spectrum analysis. The authors suggested this was because the isomer might have a half-life similar to that of the ground state. The HF81 evaluation of the spin parent of $^{80}$Ga was determined by the strong, allowed feeding of the $2^+$ levels, in addition to the observed $4^+$ state at 1742 keV which would require the spin to be between 3 and 5.

In a study of $^{80}$Zn, Winger *et al.* suggested a ground state of $3^+$ for $^{80}$Ga. The positive parity was inferred by the log*ft* values in the allowed $\beta$ decay [75]. The ground-state two-quasi-particle configuration for a $J = 3^+$ assignment would be a $\pi f_{5/2}\nu p_{1/2}$.

Cheal *et al.* performed colinear laser spectroscopy on $^{80}$Ga and they found a low-lying isomeric state with a half-life much longer than 200 ms [86]. Through multiple theoretical models, they determined that the isomeric and ground-state structures have spins of 3 and 6, but they could not distinguish between the two. Cheal *et al.* agreed that the earlier HF81 work was correct in the prediction that there were two $\beta$-decaying states. The structure of $^{80}$Ga was resolved by Lică *et al.* who established a $6^-$ ground state and a $3^-$ $\beta$-decaying isomer at only 22.4 keV [93].

Makishima *et al.* populated the $^{80}$Ge yrast transitions through deep-inelastic collisions of a 743-MeV $^{82}$Se beam on a enriched 4.3 $mg/cm^2$ thick $^{198}$Pt target [2]. They proposed that the yrast states up to $8^+$ can be ascribed to the two-hole states $\nu g_{9/2}^{-2}$ for the $N = 50$ closed shell. They discovered that a second high-spin, $7^-$ $^{80}$Ga parent accounted for the observation of the $8^+ \rightarrow 6^+$ and $6^+ \rightarrow 4^+$ transitions in the HF81 work [1]. Makishima *et al.* reported a $8^+ \rightarrow 6^+$ B(E2) value of $< 3$ W.u. [2].

The the ground-state sequence up to $8^+$ by lifetime measurements was conducted by Mach *et al.* [94] who reported a 2.95(6) ns half-life for the $8^+ \rightarrow 6^+$ transition.

Faul populated states in $^{80}$Ge in mass- and Z-gated deep-inelastic scattering reaction using a $^{82}$Se beam on a $^{238}$U target, with transitions presented in Table 4.4. Faul used a gate on a single transition to extend the yrast band to the $8^+$ state to include a tentative 1506.2-keV transition decaying from the $(10^+)$ state. Multiple near-yrast transitions not observed in previous studies were also identified [4]. All of the levels identified in the HF81 work below 3913 keV were subsequently confirmed in the 1983 mass-excess experiment conducted by Wiedner *et al.* [95].

Verney *et al.* attempted, with only partial success, to assign $\gamma$ rays to either 1.9(1) and 1.3(2) s isomers [5]. Two levels at 2323 keV were identified, each separately fed from the isomers.

Table 4.4: Transitions in $^{80}$Ge observed in CLARA-PRISMA experiments from Table 3.4 in the Faul thesis [4].

| $E_\gamma$ (keV) | $I_{\text{rel}}$ | $R_{\text{asym}}$ |
|---|---|---|
| 203.86(7)* | 9.0(4) | |
| 352.01(81)* | 1.5(2) | |
| 374.01(99)* | 1.3(2) | |
| 385.51(17)* | 0.7(2) | |
| 466.76(57) | 9.5(5) | 1.05(26) |
| 523.03(23) | 17.8(8) | 0.67(10) |
| 659.01(14) | 100(2) | 1.68(9) |
| 913.60(16) | 12.1(9) | $> 1$ |
| 1082.95(36) | 72(2) | 1.17(9) |
| 1108.68(57) | 12.6(8) | |
| 1234.98(14) | 22(1) | 2.10 (34) |
| 1314.28(94) | 10.3(7) | 6(2) |
| 1506.23(86) | 7.7 (9) | |

* Likely a contaminant.

### 4.2.2 Spectra

The level scheme compiled in this thesis work is shown in Fig. 4.6. In Fig. 4.7, $^{80}$Ge was populated in MNT reactions of $^{76}$Ge + $^{238}$U (Ge/U, blue, left axis) and $^{82}$Se + $^{238}$U (Se/U, red, right axis). More $^{80}$Ge is populated in the Se data set, and different uranium lines are populated between the two reactions. Within the Se/U reaction, there are strong differences in the states populated in prompt (PPP) or delayed (DDD) data sets as seen in Fig. 4.8. The establishment of the states feeding into the 2853-keV $5^-$ state is presented in Fig. 4.9.

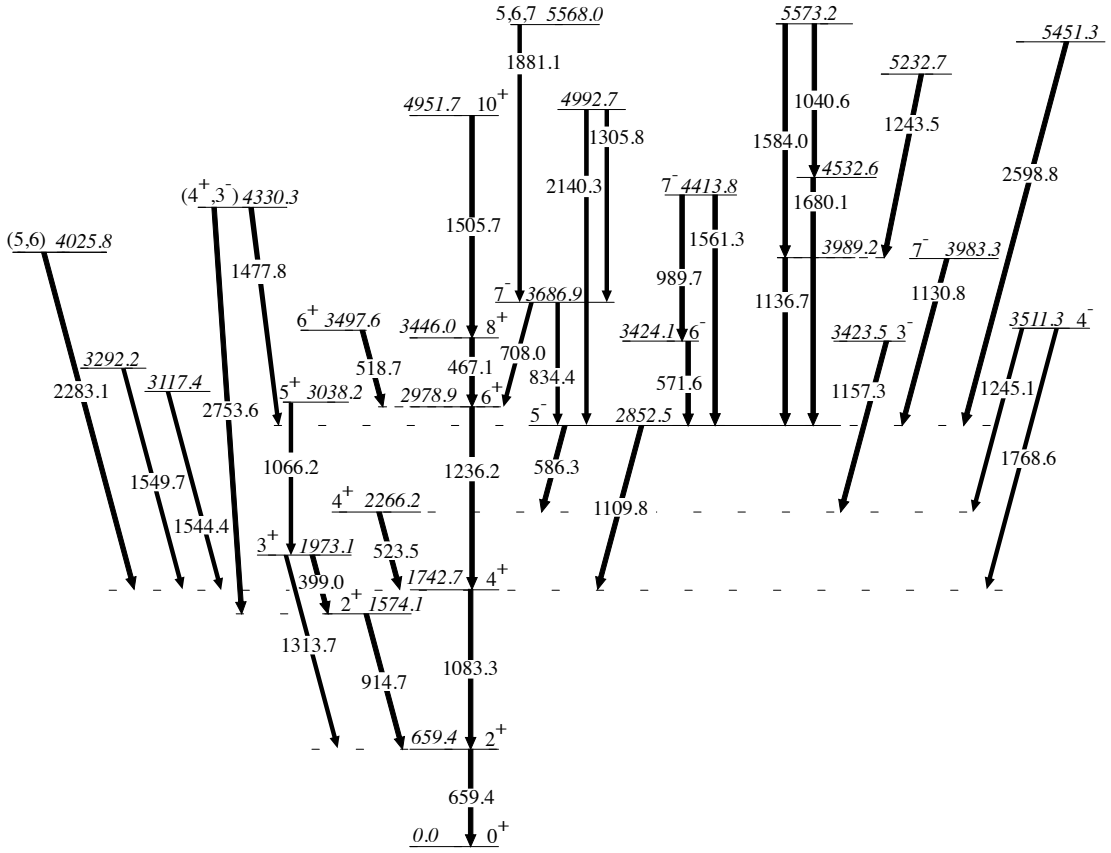


Figure 4.6: Level Scheme of $^{80}$Ge from transitions observed in this work with energies in the Se/U data set. Energies are reported inkeV.

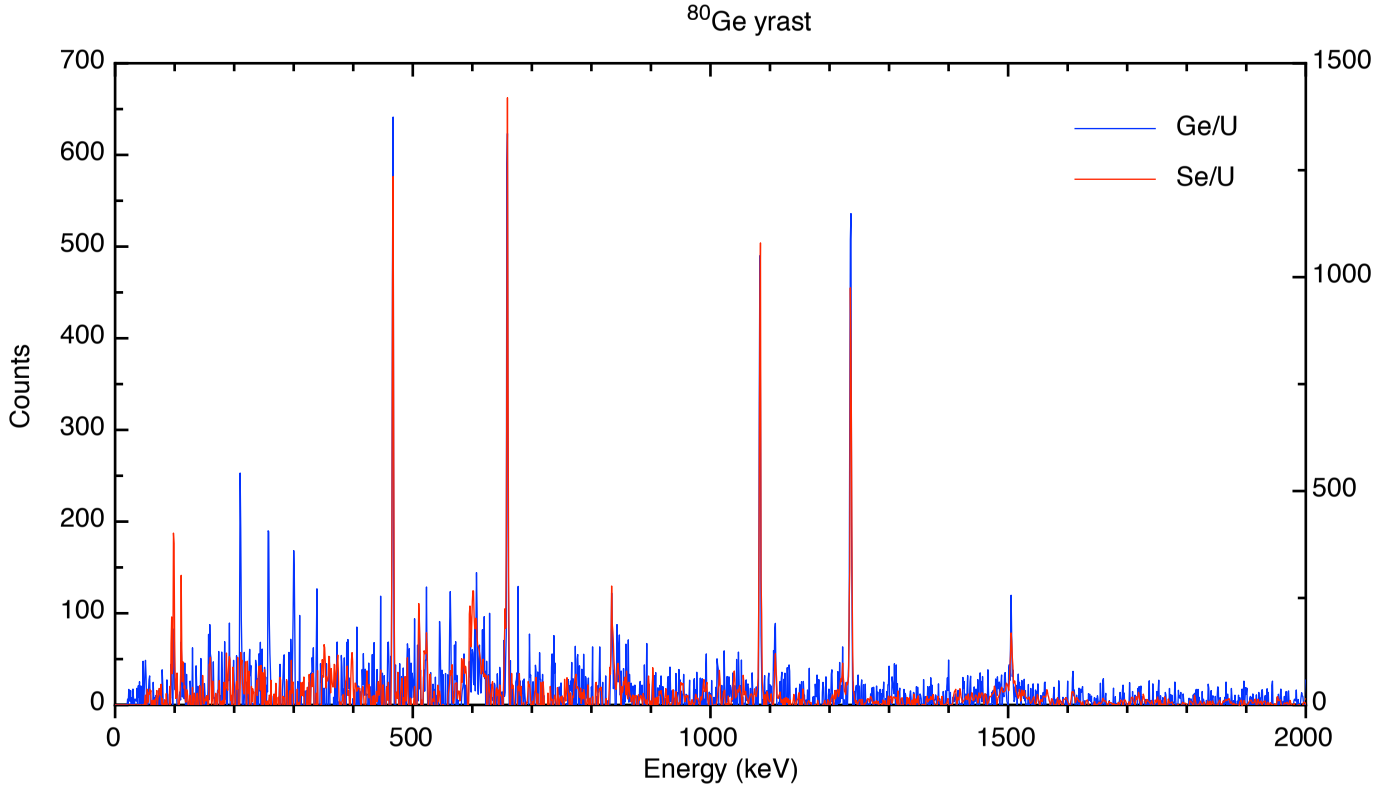


Figure 4.7: Coincidence spectra of transitions in the $^{80}$Ge yrast band. These spectra are summed gates between transitions with energies of 659.4, 1083.3, 1236.2, 467.1, 1505.7 keV. The $^{76}$Ge + $^{238}$U (Ge/U) spectrum is in blue with the y-axis on the left, whereas the $^{82}$Se + $^{238}$U (Se/U) data is in red with the y-axis on the right. The cross-correlated rotational states in U are clearly seen in the Ge/U data, whereas the Pu x rays are seen in the Se/U data.

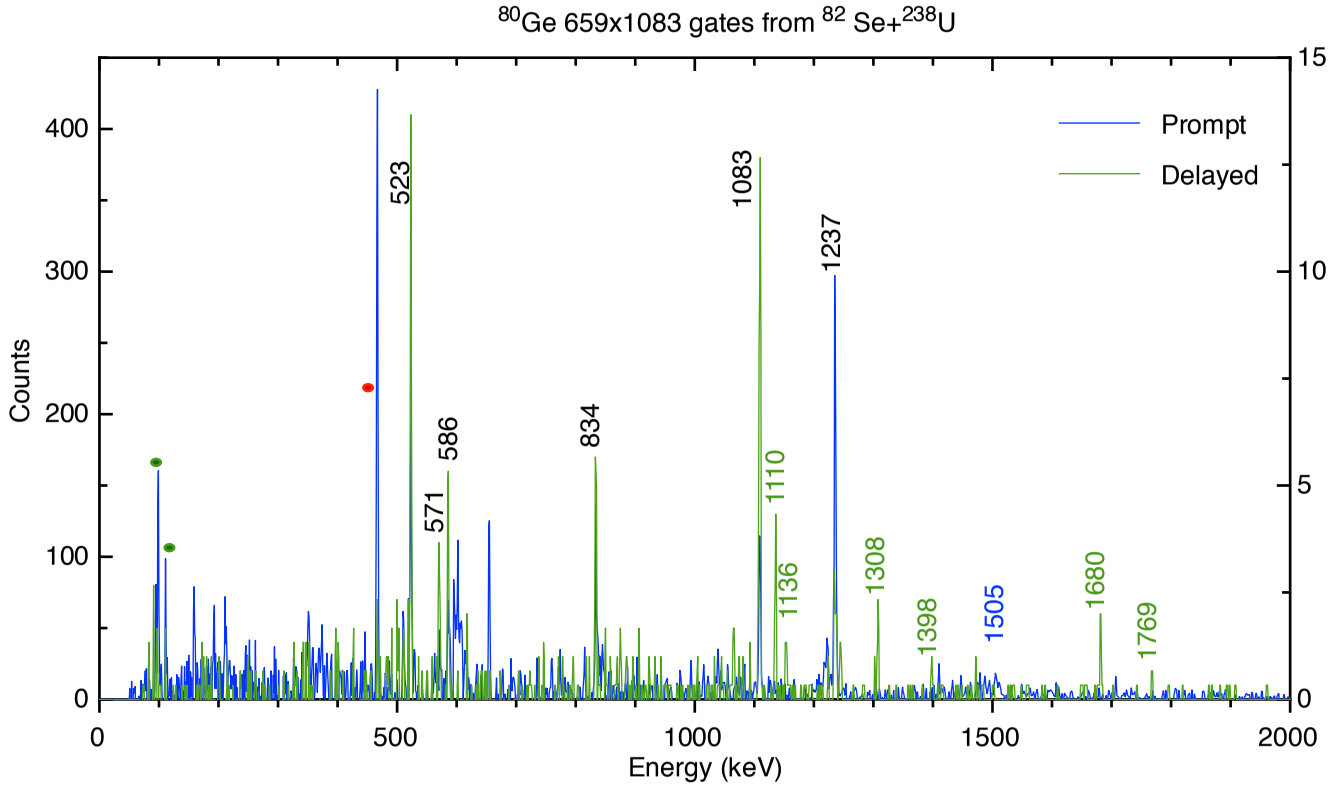


Figure 4.8: Coincidence spectra of 659.4- and 1083.3-keV transitions of $^{80}$Ge in the prompt (blue, left axis) and delayed (green, right axis) data sets.

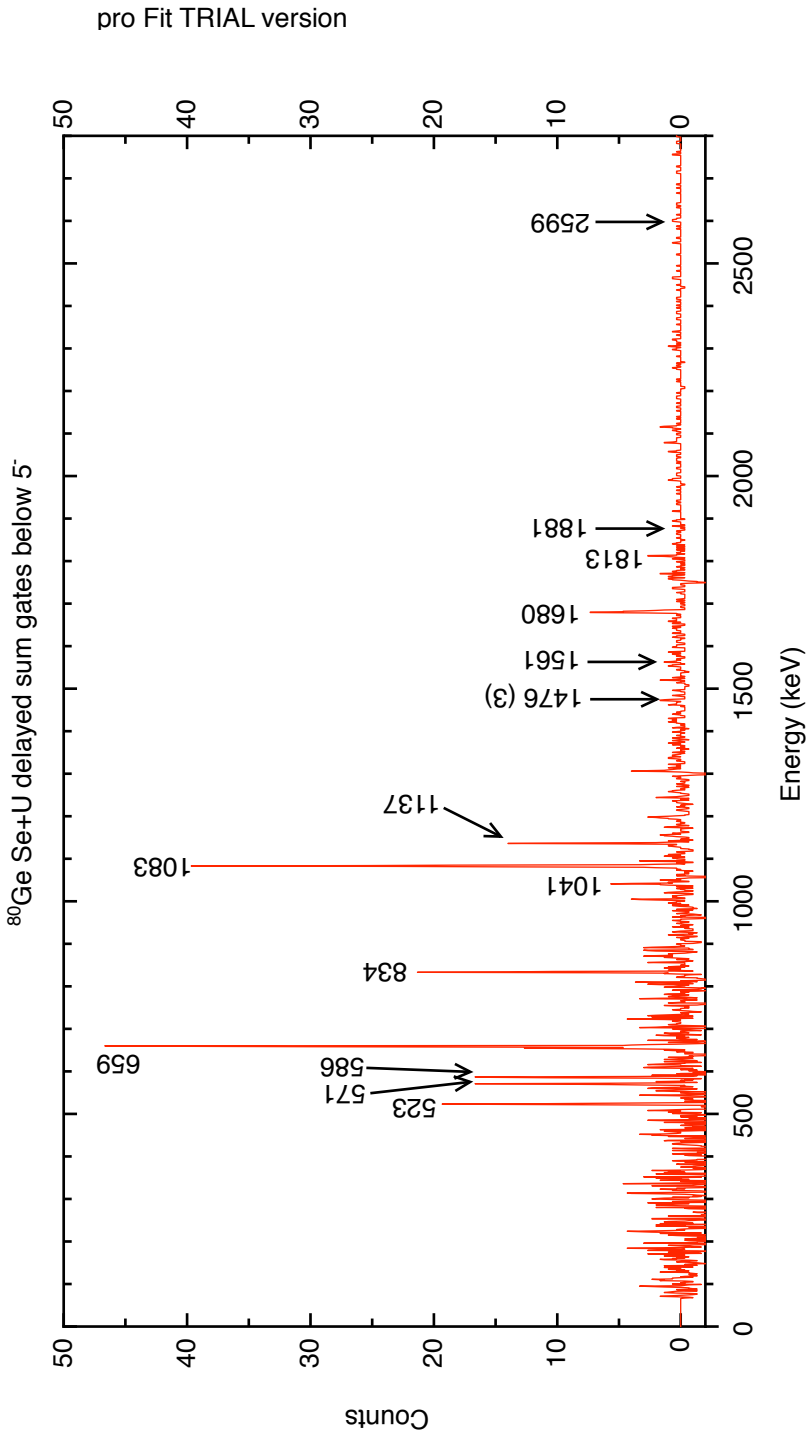


Figure 4.9: Coincidence spectra of transitions below the 2852.5-keV $5^-$ state. This spectrum is the result of summed gates between the 659.4, 1083.3, 1109.8, 523.5, and 586.3 keV transitions in the Se/U data.

### 4.2.3 $^{80}$Ge Levels

Hoff and Fogelberg (HF81) reported an impressive level scheme of $^{80}$Ge in spite of the fact that they were unaware that they were observing the decay of two isomers with relatively close half-lives. This thesis found no issues with the placements in HF81, but many unplaced $\gamma$ rays of that work are now placed.On the other hand, there are several problems with the values reported in the Verney *et al.* work [5]. They incorrectly suggested that a $3^-$ parent feeds $1, 2, 3$ spin states when it should feed $2, 3$, and 4 as first-forbidden non-unique (ffnu) transitions. They also reported the states populated from the high-spin $^{80}$Ga isomer are $\geq 4$ instead of (5,6,7) [5].

The present work provides insight to the $\beta$-decay parent of each state ($6^-$ or $3^-$). Lower-spin levels are populated in the prompt data, but not in the delayed data set. Unless noted with an *****, each of these levels was first identified through $\gamma$ rays observed in the HF81 work. The highest population for $^{80}$Ge were found in the PPP Se/U cube as seen in Fig. 4.7. The energies presented in this section are from the Se/U data set which had a calibration that was slightly different than that of the Ge data. Differences in energies of main $^{80}$Ge transitions are found in Table 4.6. To account for this difference, the uncertainties are increased, but the precise energies for the levels are not relevant for the physical issues involved.

**639 keV,** $0^+$**.** In addition to describing the $^{82,80}$Ge nuclei, the HF81 paper included a detailed level scheme for $^{81}$Ge with only four levels below 1 MeV. Two of these levels are cross-shell intruder $1/2^+$ and $5/2^+$ states. The existence of these low-lying states makes the presence of a $0^+$ intruder state plausible in $^{80}$Ge. The authors mentioned

the strong likelihood that there is a $0_2^+$ level similar to the 1547-keV state of $^{78}$Ge, but it was not populated well enough to be observed [1]. A $0_2^+$ state was identified much later by Gottardo *et al.* [6], at a significantly lower energy of 639 keV. This state has yet to be confirmed by other works and is also not observed in the present work.

**659.4 (1) keV, $2^+$.** The lifetime of this level is currently disputed. It was reported as 16.4(32) ps by Ref. [96] and 22(3) ps by Ref. [89]. This level is reported in the Evaluated Nuclear Data File (ENSDF) as a tentative ($2^+$) state. This data evaluation occurred before the Mané and Verney works, which observed direct feeding by the $3^-$ parent [5, 97]. Ref. [98] measured the $2^+ \rightarrow 0^+$ transition along with its $B(E2)$value. The energy for this transition was determined by a 1083.3/1236.2-keV coincidence gate.

**1574.1 (2) keV, $2^+$.** This state was established by Hoff in his $\beta$ delayed neutron work [92]. The level decays directly by 58% to the ground state and 42% to the $2_1^+$ state. This decay is similar to the $2_1^+$ state in $^{78}$Ge and $^{84}$Kr. The intensities of the 1573.5- and 914.7-keV transitions are of the same order [1, 99], but this thesis is unable to confirm the 1573.3-keV $\gamma$ ray. The energy of this state was determined by the 914.7-keV transition in cross correlation.

**1742.7 (1) keV, $4^+$.** This yrast level decays by a 1083.3-keV transition into the yrast $2^+$ state at 659.4 keV. It is fed directly in $\beta$-decay by the high-spin parent [5]. This agrees with observations in the present work by the amount seen in the DDD spectra. The assigned energy of this state was determined by a 659.4/1236.2-keV gate. **1973.1 keV, $3^+$.** This level decays by a 1313.7-keV transition and a weak

399.0-keV one to the first and second $2^+$ states, respectively. This work proposes a $3^+$ assignment in contrast with the $(4^+)$ $J^\pi$ value assigned by Ref. [5]. Notably, the 1973.1-keV state was not found to decay into the yrast $4^+$ state because it must compete with the energetically favorable 1313.7-keV transition. The Verney group [5] made the $(4^+)$ assignment due to the decay similarity to the $4_2^+$ level in $^{84}$Kr, and also the decay pattern from the jj44b shell-model calculations. They could not attribute the 1973.1-keV state with any certainty to either the high-spin or low-spin $\beta$ parent (Fig. 4 of Ref. [5]). A similar argument for a $3^+$ level could be made due to the similarity of decay to the experimental 1644-keV level in $^{78}$Ge. Faul assigned the 1973-keV level as the $4_2^+$ state. She determined that the 1314-keV transition had an asymmetry value of 6, several times larger than those determined for an $E2$ transition (Table 4.4). This implies that the transition is less likely to have a $\Delta J = 2$ character [4].

**2266.2 (2) keV, $4^+$.** This state decays by 523.4- and a 691.9-keV transitions. It is fed by a 586.3-keV transition from the 2852.5-keV $5^-$ level [4]. Verney *et al.* suggested a $(3^+)$ assignment from the predicted decay pattern of their jj44b and jun45 calculations [5]. If the spin assignment of $5^-$ is correct for the 2852.5-keV state, the 2266.2-keV state cannot have a $3^+$ assignment because that would require a parity change ($\Delta\pi$ =yes) along with a $\Delta J = 2$ spin change. This thesis was able to confirm this level by the 523.4-keV $\gamma$ ray seen in both prompt and delayed data from the Se/U cube. This work was unable to observe the 691.9-keV $\gamma$ ray.

**2852.5 (3) keV, $5^-$.** This state decays by 586.3- and 1109.8-keV $\gamma$ rays observed in both seen in delayed and prompt data. This level is suggested as a $(5^-)$ level by

Table 4.5: $^{80}$Ge excitation energies $E_{lev}$, $\gamma$-ray energies $E_\gamma$, relative intensities $I_{rel}$, and spin-parity assignments $J_i^\pi \rightarrow J_f^\pi$ of initial and final states for $\gamma$ rays placed in $^{80}$Ge from the experimental prompt data. States with reliable reproducibility are shown.

| $E_{lev}$ (keV) | $E_\gamma$ (keV) | $I_{rel}^a$ % | $J_i^\pi \rightarrow J_f^\pi$ |
|---|---|---|---|
| 659.4 | 659.4 | 100(2) | $2_1^+ \rightarrow 0_1^+$ |
| 1574.1 | 914.7 | 12.1(9) | $2_2^+ \rightarrow 2_1^+$ |
| | 1574.1 | | $2_2^+ \rightarrow 0_1^+$ |
| 1742.7 | 1083.3 | 72(2) | $4_1^+ \rightarrow 2_1^+$ |
| 1973.1 | 399.5 | | $3_1^+ \rightarrow 2_2^+$ |
| | 1313.7 | | $3_1^+ \rightarrow 2_2^+$ |
| 2266.2 | 523.5 | 17.8(8) | $4_2^+ \rightarrow 4_1^+$ |
| | 691.9 | | $4_2^+ \rightarrow 2_2^+$ |
| 2852.5 | 586.3 | | $5_1^- \rightarrow 4_2^+$ |
| | 1109.8 | 12.6(8) | $5_1^- \rightarrow 4_1^+$ |
| 2978.9 | 1236.2 | 22.1(1) | $6_1^+ \rightarrow 4_1^+$ |
| 3038.2 | 722.2 | | $5_1^+ \rightarrow 4_2^+$ |
| | 1066.2 | | $5_1^+ \rightarrow 3_1^+$ |
| | 1296.2 | | $5_1^+ \rightarrow 4_1^+$ |
| 3117.4 | 1544.4 | | $\rightarrow 2_2^+$ |
| 3292.2 | 1549.7 | | $(2,3,4) \rightarrow 4_1^+$ |
| 3423.5 | 1157.3 | | $3_1^- \rightarrow 4_2^+$ |
| | 1850.4 | | $3_1^- \rightarrow 2_2^+$ |
| | 2764.3 | | $3_1^- \rightarrow 2_1^+$ |
| 3424.1 | 571.6 | | $\rightarrow 5_1^-$ |
| 3446.0 | 467.1 | 9.5(5) | $8_1^+ \rightarrow 6_1^+$ |
| 3497.6 | 519.8 | 17.8(8) | $\rightarrow 6_1^+$ |
| 3511.3 | 1245.1 | | $\rightarrow 4_2^+$ |
| | 1768.6 | | $\rightarrow 4_1^+$ |
| 3686.9 | 708.0 | | $\rightarrow 6_1^+$ |
| | 834.4 | | $\rightarrow 6_1^+$ |
| 4951.7 | 1505.7 | 7.7(9) | $10_1^+ \rightarrow 8_1^+$ |

[a] Relative intensities from Ref. [4].

Ref. [5] and is also observed in DIS by Ref. [4]. The data in this thesis agree with the determination of a $5^-$ $J^\pi$ value. This is because it is strongly present in the DDD cube. The decay pattern is similar to the decay of the 2646-keV $5^-$ level in $^{78}$Ge.

Unlike that of the $5^-$ state of $^{78}$Ge, this level has eight $\gamma$ rays feeding into it. This is reminiscent of a seniority-four state rather than a $5^-$ state. The transitions feeding from the $5^-$ state can be observed in 659/1083- and 1083/523-keV coincidence gates. The branching ratio of this level was determined using relative intensities in an 834.4/1083.3-keV gated spectrum. The 586.3-keV $\gamma$ ray decays by 28(3) % and the 1109.8 keV transition by 72(3) %.

**2978.9 (3) keV, $6^+$.** This yrast state decays by a 1236.2-keV $\gamma$ ray into the $4_1^+$ state.

**3038.2 (3) keV, $5^+$.** In this work, this level is identified as a $5^+$ state, as it decays to the $4_1^+$, $4_2^+$, and $3_1^+$ levels. By contrast, Ref. [5] could not determine whether this level had a spin-parity of $4^+$ or $5^+$. Since it is directly fed from the high-spin parent, a $J^\pi$ designation of $4^+$ is not possible due to the parity change and a $\Delta J = 2$ change. This level is confirmed via a weak 1066.2-keV transition in a 659.4/1313.7-keV coincidence gate. A few coincidence counts are also observed at 772 keV. The 1294.3-keV $\gamma$ ray could not be confirmed. This is surprising because both the subsequent 523.4- and 1083.3-keV transitions are populated well.

**3117.4 (3) keV, $(2, 3, 4)$.** This level decays by a 1544.4-keV $\gamma$ ray to the $2_2^+$ state, that can be observed in the prompt Se/U and Ge/U data sets. This new transition may correspond to the unplaced 1547.4-keV $\gamma$ ray seen by HF81 [1]. A 1549.7-keV transition is also present in another gate. It is unlikely that HF81 would be unable to observe two $\gamma$ rays near the same energy, because of the quality of their data.

**3292.2 (3) keV, $(2, 3, 4)$.** This level is identified in this work through the decay of a 1549.7-keV $\gamma$ ray to the yrast $4^+$ state. This transition may correspond to the

1547.4-keV $\gamma$ ray that was seen by HF81 [1], but which could not be placed.

**3423.5 (3) keV, $3^-$.** This level decays by three $\gamma$ rays. The first is a 2764-keV line to the $2_1^+$ level which not seen in this work due to lack of a third $\gamma$ ray in coincidence. The second is a 1850.1-keV transition to the $2_2^+$ state which not seen in this work due to the low population of the 1574-keV state. Finally, the third is a 1157.3-keV $\gamma$ ray to the 2266 keV state, with $4_2^+$ $J^\pi$ assignment, seen in a 1083/523-keV coincidence gate. This $3^-$ state has identical decay with the 1644-keV $3_1^-$ level observed in $^{78}$Ge. This thesis agrees with the spin assignment of $3_1^-$ recognized by Verney *et al.* [5], because it is fed from the low-spin $\beta$-decaying parent. The parent can be determined in this thesis because this state is well populated in the prompt data set and not in the delayed data set of the Se/U cube.

**3424.1 (3) keV, $(6^-)$.** This state decays by a 571.6-keV transition to the $5^-$ level at 2852.5 keV. It was assigned as a $5^-$ state by Ref. [5], due to a larger fraction of the feeding by the higher-spin isomer. The 571.6-keV transition is seen in both the prompt and delayed coincidence cubes.

**3446.0 (3) keV, $8^+$.** The lifetime of this state has been variously reported as 2.95(6) ns by Ref. [94] and $> 0.4$ ns by Ref. [2]. The clarity of the isomeric decay spectrum shown by Mach *et al.* [94] leaves little doubt about the isomeric character of this state, which is easily seen in the yrast decay of Fig. 4.7.

**3497.6 (3) keV, $6^+$.** This work is able to confirm this level by the 519.7-keV $\gamma$ ray present in prompt and delayed data from the Se/U cube in a 1236.2/1083.3-keV coincidence gate. In the HF81 work [1], the 2978.9-keV state is populated by the high-spin isomer in $^{80}$Ga, allowing for a spin of $(5, 6, 7)$. The spin was assigned as

$J = 6$, because of its decay pattern.

**3511.3 (5) keV,** $(4^-)$**.** This state decays by 1245.1-keV observed only in delayed data. It also decays by a weak line in prompt and delayed gates of 1083/659 keV by a 1768.6-keV transition. The precise value of the level has a large uncertainty because the 1245.1-keV $\gamma$ ray is only seen in the Se/U DDD data set in both the 659.4/1083.3-keV and 1083.3/523.5-keV coincidence gates. Since the level transitions are weak in prompt data, this level is likely populated by the $3^-$ $\beta$-decay parent and it is a candidate for the $4^-$ level expected in this energy range near the $5^-$ state at 2852.5 keV.**3686.9 (3) keV,** $7^-$**.** This level decays by a strong 834.4-keV transition to the $5^-$ state and also a weak 708.0-keV transition to the $6_1^+$ level. It is strongly fed in $\beta$ decay [1], allowing for a spin possibility of (5,6,7). Two 834 (2)-keV transitions occur in $^{235}$U, one in $^{72}$Ge, and one in $^{83}$Se. In gates set on the 834.4-keV line, a 760.1-keV transition is present. Further investigation shows that this $\gamma$ ray, along with other transitions, are those found in $^{83}$Se.

**3913.7 keV,** $(2, 3, 4)$**.** This state decays by a 1941.5-keV transition, as reported by HF81. [1], but was not seen in this work. Without the 1941-keV transition present in either prompt or delayed data sets, this state is assigned as a daughter of the low-spin $^{80}$Ga parent.

**3983.3 (3) keV,** $(5, 6, 7)$**.** This level decays by an 1130.8-keV $\gamma$ ray to the $5^-$ state at 2853 keV. This state must be from the $6^-$ $\beta$-decay parent since it was observed in $\beta$ decay and feeds a high-spin state. This level was identified in this work in the delayed cube by 659/1110-keV and 1083/586-keV coincidence gates.

**3989.2 (3) keV,** $(5, 6, 7)$**.** This state decays by a 1136.7-keV transition to the

$5^-$ state at 2853 keV. The transition is strong in the delayed data, but not in the prompt data, suggesting that it is a daughter of the high-spin $\beta$ decay parent. The decay into a $5^-$ state also supports this spin assignment.

**4024.2 (16) keV,** $(5, 6, 7)$**.** This level was identified by a very weak 2281.5-keV peak in the delayed cube from a 659/1083-keV gate. A weak 1047.5-keV branch to the $6^+$ state at 2978 keV from the 4024 keV level was reported by HF81 [1], but not observed in this work. This level has a $J^\pi$ assignment of (5,6,7) from the high-spin $\beta$-decay parent.

**4324.7 (16) keV,** $(3^-, 4^+)$**.** This state was seen by Hoff *et al.* [1] to decay by six different $\gamma$ rays with the following energies: 808.5-, 1471.9-, 2351.9-, 2581.4-, and 2750.3-keV. The spin/parity assignments of the states that this level feeds include $2^+$, $3^+$, $4^+$, $4^-$ and $5^-$. Ffnu transitions feed states with $J^\pi$ of $2, 3, 4$. However, it is unlikely this state has a $J^\pi = 4^-$ because of the feeding of the first two $2^+$ levels. In the same manner, a spin of 2 is unlikely because both positive- and negative-parity 4 states are fed. The state also cannot be a $3^+$ level because then the 1472-keV transition to the $5^-$ state would have a parity change as well as a $\Delta J = 2$ change. This thesis identified this level by the 1472.2(10)-keV transition in a 1109/659-keV prompt coincidence gate.

**4413.8 (5) keV,** $(5, 6, 7)$**.** This state decays by a 1562.2-keV $\gamma$ ray to the $5^-$ level at 2852.5 keV in a 586.3/1083.3-keV prompt coincidence gate. It also decays by a 990.8-keV $\gamma$ ray to the 3424.1-keV, $6^-$ state. This is the only instance where the present work does not agree with the $\gamma$-ray placement by HF81 [1]. Their work suggests that this 990.8-keV transition feeds the $3^-$ state, less than 1 keV away.

**4845.7 (7) keV,** $(8^+)$**.** This level was identified in this work through a decay of an 1867.4-keV $\gamma$ ray. This transition was observed by HF81 [1], but could not be placed.

**4951.7 (7) keV,** $10^+$**.** A 1506 keV transition was tentatively placed by Ref. [4]. The present work confirms the previous analysis that this state belongs to the ground-state band.

**4992.7 (7) keV,** $(5, 6, 7)$**.** This state was identified by HF81 [1] to decay by three transitions. The first is a weak 2140.5-keV transition in a 659.4/586.3-keV gate to the 2852.5 keV $5^-$ state. The second is a 1306.9-keV $\gamma$ ray seen in multiple delayed gates of 1083/659-, 586/659-, 586/1083- and 708/1236-keV decaying to the 3686.4 keV $7^-$ state. The final transition at 1004.8-keV transition, not seen in this work, but was identified by Hoff *et al.* [1] as decaying to the 3986.5-keV $(5, 6, 7)$ state.

**5232.7 (7) keV,** $(5, 6, 7)$**.** A 1243.5-keV $\gamma$ ray decays from this level as observed by its coincidence with the 1136.7- and 659.4-keV transitions in the Se/U prompt data.

**5451.3 keV,** $(5, 6, 7)$**.** A 2599-keV $\gamma$ ray was observed in the Se/U prompt data in a gate 586/659-keV. This result confirms the observations from $\beta$ decay.

**5568.0 (7) keV,** $(5, 6, 7)$**.** This state decays by a 1182-keV transition to the $7^-$ state at 3685.9 keV and also a 1154.9-keV line to the $(5, 6, 7)$ state at 4413.2 keV. The 1182-keV transition was the sole $\gamma$ ray identified from this state. This is surprising because, according to the relative intensities from HF81 [1], the 1182-keV transition has 1/4 of the intensity of the 1155-keV line. The 1155-keV transition feeds into the 4413.2 keV state, which decays by a 1157.9-keV $\gamma$ ray that is similar in energy and

very weak.

**5773.2 (7) keV,** $(5, 6, 7)$**.** The two decays from this level are a 1585.3-keV transition to the (5,6,7) state at 3987.9 keV and a 1040.6-keV $\gamma$ ray to the (5,6,7) 4532.6-keV state. These are present in the delayed cube via a 1137/659-keV gate and also 1109/659-keV and 1109/1083-keV coincident gates, respectively. This level must be fed from the $6^-$ $\beta$-decay parent because it decays to high-spin states giving a $J^\pi = (5, 6, 7)$ assignment.

**5800.5 keV,** $(5, 6, 7)$**.** HF81 [1] found this state to decay by three different $\gamma$ rays. These are the 2948.4 keV to the $4_1^+$ state, the 2821.8 keV to the $6_1^+$ state, and the 2114.3 keV to the $(7^-)$ state at 3686.9 keV. The $J^\pi$ value is based on the high-spin level feeding. Although there are sufficient data, $\gamma$-ray energies above 2000 keV have few counts in the Gammasphere data due to the efficiency of the detectors.

**6047.1 keV,** $(2, 3, 4)$**.** HF81 [1] identified this state by its decay through a 5387.8-keV transition to the $2_1^+$ state at 659.1 keV. The energy of this transition is too high to be seen in this work. A tentative $J^\pi$ assignment is (2,3,4), since it feeds a low state, but not any other.

**6155.3 keV,** $(5, 6, 7)$**.** This state was reported to decay by a 4412.6-keV transition to the $4^+$ state by HF81 [1]. The upper limit for Gammasphere spectra is 4000 keV in the prompt data, so it is not seen in this work. A $J^\pi$ assignment cannot be made, but is likely a $(5, 6, 7)$, fed by the high-spin parent. There is a higher likelihood for a transition to lose angular momentum and feed a lower-spin state than a higher-spin one.

Table 4.6: Example $^{80}$Ge excitation energies $E_\gamma$ (keV) observed in the Se/U, Se/Pb, Ge/U, Ge/Pt and Ni/U cubes.

| Se/U | Se/Pb | Ge/U | Ge/Pt | Ni/U |
|---|---|---|---|---|
| 467.1 | 467.1 | 467.0 | 467.1 | 466.6 |
| 523.4 | 523.4 | 523.4 | 522.4 | 522.7 |
| 659.4 | 659.3 | 658.9 | 658.9 | 659.1 |
| 834.4 | 833.8 | 834.0 | – | 834.8 |
| 1083.3 | 1083.8 | 1083.4 | 1084.1 | 1083.7 |
| 1109.7 | 1110.7 | 1109.4 | 1109.1 | 1109.1 |
| 1236.3 | 1236.2 | 1235.8 | 1236.5 | 1235.9 |
| 1505.6 | 1506.8 | 1505.4 | 1505.7 | 1504.9 |

### 4.2.4 Level Configurations

Table 4.7: Possible configurations for states in $^{80}$Ge.

| $E_{\text{lev}}$ (keV) | $J^\pi$ assignment | Particle configuration |
|---|---|---|
| 659.4 | $2^+$ | $\nu g_{9/2}^{-1} g_{9/2}^{-1} \circ \pi f_{5/2}^{+1} f_{5/2}^{+1}$ |
| 1742.7 | $4^+$ | $\nu g_{9/2}^{-1} g_{9/2}^{-1} \circ \pi f_{5/2}^{+1} f_{5/2}^{+1}$ |
| 1973.1 | $3^+$ | $\pi f_{5/2}^{+1} p_{3/2}^{+1}$ |
| 2852.5 | $5^-$ | $\nu p_{1/2}^{-1} g_{9/2}^{-1}$ |
| 2978.9 | $6^+$ | $\nu g_{9/2} g_{9/2}$ |
| 3424.1 | $6^-$ | $\nu g_{9/2}$ + $2p_{1/2}$, $1f_{5/2}$, or $2p_{3/2}$ |
| 3446.0 | $8^+$ | $\nu g_{9/2} g_{9/2}$ |
| 3511.3 | $4^-$ | $\nu g_{9/2}$ + $2p_{1/2}$, $1f_{5/2}$, or $2p_{3/2}$ |
| 3686.9 | $7^-$ | $\nu g_{9/2}^{+1} f_{5/2}^{-1}$ |
| 4950.1 | $10^+$ | $\nu g_{9/2}^{-1} g_{9/2}^{-1} \circ \pi f_{5/2}^{+1} f_{5/2}^{+1}$ |

## 4.3 $^{78}$Ge

### 4.3.1 Background

When this work began, the level structure of $^{78}$Ge was the least well known of the even Ge isotopes between $N = 40$ and $N = 50$. The level schemes that contribute to the structure of $^{78}$Ge are compiled in Fig. 4.10.

The early experiments on the unstable $^{78}$Ge nucleus include mass measurement by Stephans *et al.* [10], half-life determination by Kvale *et al.* [100], and total $\beta$-decay energy determination by Aleklett *et al.* [101]. Interestingly, in their 1977 paper, Aleklett *et al.* refer to a private communication in 1972 between the authors and T. and L. Matsushigue who provided a $\beta$-decay scheme with nine excited states. This scheme was finally published eight years later by an entirely different group (Lewis) [102]. In 1978, Mateja *et al.* conducted a $^{76}$Ge$(t,p)^{78}$Ge experiment to determine the shape transition from oblate to prolate deformation in Ge nuclei [103]. This study followed other results for even mass $^{68-76}$Ge. Three months later, a second (t,p) study for $^{78}$Ge was reported by Ardouin *et al* [104]. New levels identified in these two (t,p) experiments included proposed spin and parity assignments from angular distributions [103,104]. The $J^\pi$ values were not in complete agreement with each other, as seen in Fig. 4.10 and Table 4.8. The discrepancies between these works cannot be fully attributed to the 2 MeV energy difference in the triton beam used.

Three years later, based on the works by Aleklett and the Mateja, Lewis *et*

*al.* published a $\beta$-decay study from $^{78}$Ga $\rightarrow$$^{78}$Ge [102]. The Lewis group assigned a ground-state $J^{\Pi} = 3^{+}$ spin-parity to the $^{78}$Ga parent because they did not observe any direct feeding to the $^{78}$Ge ground state. From this, they could then limit the Ga parent to $2^{-}, 3$, or $4^{-}$. Mateja *et al.* placed a $4^{+}$ level at 2952 keV [103]. This level was observed at 2951.4 keV in this work. This state was also observed by Lewis *et al.* who excluded a $J^{\Pi} = 2^{-}$ for the $\beta$-parent ground state [102]. However the authors hedged their conclusions by also calculating log$f_1t$ values for all transitions that would permit a $2^{-}$ parent to populate a $4^{+}$ level. The population of the proposed $4^{+}$ level would be with a log$f_1t$ of 8.12. The assignment of a $J^{\pi} = 3^{+}$ parent was contradicted in 2011 by Mané *et al.*. They used laser spectroscopy measurements on the even-A Ga nuclei in the region, and this established the ground state of $^{78}$Ga as having a $J^{\pi} = 2^{-}$ [97]. It is possible to exclude certain spin-parity assignments for levels. Table 4.8 contains the level energies from this work. It also includes the log$ft$ and original spin-parity assignments from the Lewis work (and implications from the Mané work), the spin-parity assignments from the (t,p) experiments, and also the spin-parity assignments determined in this thesis. By $\beta$-decay mass separation, Chou *et al.* reported lifetimes of many states, using the analysis reported by Lewis with invalid spin assignments of $(2, 3, 4)$ instead of $(1, 2, 3)$ [105].

Podolyák *et al.* used DIS reactions to determine the yrast band up to the $J^{\pi} = 8^{+}$ state of $^{78}$Ge [3]. These states were reported in an unpublished thesis by Faul [4]. Table 4.9 reproduces the Faul list of single-gated transitions with their relative intensities and asymmetry ratio values. Many of the transitions in the present thesis were first identified by Faul, and the additional information on the

transition's characteristic from the $R_{asym}$ value is further evidence for the spin-parity assignments provided here.

Table 4.8: The $^{78}$Ge levels identified in previous work. The listed level energies are those determined in this work. Arrows are used to indicate possible assignments based on laser-spectroscopy measurements of the parent $^{78}$Ga as a $2^-$ (Ref. [97]).

| $E_{lev}$ (keV) | log$ft$ [102] | $J^\pi$ $\beta$ decay [102] | $J^\pi$ (t,p) [103] | $J^\pi$ (t,p) [56] | $J^\pi$ Forney |
|---|---|---|---|---|---|
| 619.2[a] | 6.44(0.14) | $2^+$ | $2^+$ | $2^+$ | $2^+$ |
| 1186.3[a] | 6.52(0.11) | $2^+$ | $2^+$ | $2^+$ | $2^+$ |
| 1547.1[a] | 9.45[b] | $(0^+)$ | $0^+$,$(4^+)$ | $0^+$ | $0^+$ |
| 1569.8[a] | 8.47[b] | $(4^+)$ | – | $4^+$ | $4^+$ |
| 1644.1[a] | 6.59(0.12) | $(3^+)$ | – | – | $3^+$ |
| 1843[a] | 6.70(10) | $(2^+)$ | $2^+$ | $2^+$ | $2^+$ |
| 2292.0[a] | – | – | $(4^+,5^-)$ | $4^+$ | $4^+$ |
| 2318.9[a] | 8.86[b] | * | $4^+$,$(0^+)$ | $4^+$,$(5^-)$ | $4^+$ |
| 2330.0 | – | – | $4^+$,$(0^+)$ | $4^+$,$(5^-)$ | $0^+$ |
| 2438.4[a] | 6.24(0.06) | $(2^+)$ | $2^+$ | $2^+$ | $2^+$ |
| 2645.8[a] | – | – | $5^-$ | $5^-$ | $5^-$ |
| 2665.0[a] | 5.61(0.05) | $(2^+,3^+,4^+) \rightarrow (1,2,3)^-$ | – | – | $3^-$ |
| 2706[a] | 6.24(0.08) | $(1^+,2^+)$ | – | – | $(1^+)$ |
| 2857.1[a] | 6.14(0.06) | $(2,3,4) \rightarrow (1,2,3)$ | – | $5^-$ | $(2,3)$ |
| 2951.4 | 8.12[b] | $(4^+)$ | $4^+$ | * | $4^+$ |
| 3120.6 | 5.60(0.06) | $(2^+,3^+,4^+) \rightarrow (1,2,3)^-$ | – | – | $2^-$ |
| 3157.2 | – | – | – | $2^+$ | $(4,5,6)$ |
| 3236 | – | – | $3^- + 1^-$ | * | |
| 3295.2 | – | – | | $6^+$ | 6 |
| 3389.2 | 6.11(0.08) | $(2,3,4) \rightarrow (1,2,3)$ | * | – | $2^+$ |
| 3689.3 | 6.17(10) | $(2,3,4) \rightarrow (1,2,3)$ | – | * | $(2,3)$ |
| 4083 | 5.49(0.07) | $(2^+,3^+,4^+) \rightarrow (1,2,3)^-$ | – | – | $2^+$ |
| 4270 | 5.71(0.08) | $(2^+,3^+,4^+) \rightarrow (1,2,3)^-$ | – | – | – |
| 4279.3 | 5.71(0.08) | $(2^+,3^+,4^+) \rightarrow (1,2,3)^-$ | – | – | – |
| 5078.2 | 5.55(0.1) | $(2^+,3^+,4^+) \rightarrow (1,2,3)^-$ | – | – | $3^-$ |

[a] Level observed in Faul thesis [4]
[b] Denotes a log$f_1t$ value from Ref. [102]
– No level observed
* Level observed without $J^\pi$ assignment

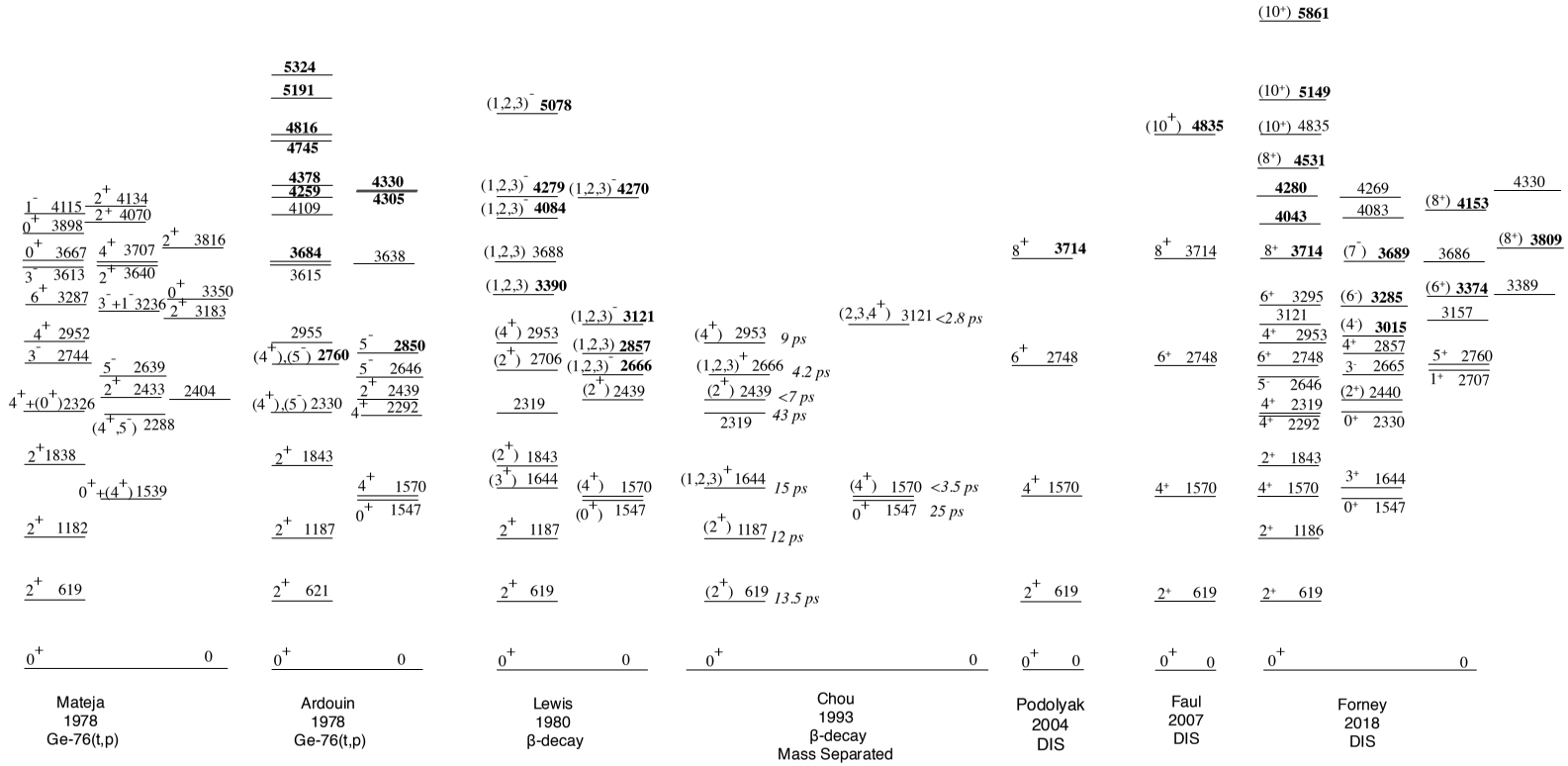


Figure 4.10: Level schemes reported (Refs. [3, 4, 56, 102, 103, 105]) for $^{78}$Ge with energies in keV. Note the known $J^\pi$ value of the $^{78}$Ga parent implies changes must be made to the values in the Lewis [102] and Chou [105] works. Any state with a $(2, 3, 4)$ assignment has been changed to $(1, 2, 3)$. In the Lewis work, states with log$ft$ below 6 were assigned a negative parity.

Table 4.9: Transitions in $^{78}$Ge observed in CLARA-PRISMA experiments from Table 3.3 in the Faul thesis [4].

| $E_\gamma$ (keV) | $I_{\text{rel}}$ | $R_{\text{asym}}$ |
|---|---|---|
| 222.33(12)* | 5.2(1) | |
| 440.17(35) | 15.2(3) | 1.55(22) |
| 457.23(51) | 10.6(2) | 1.23(24) |
| 535.55(89) | 8.6(2) | |
| 566.67(10) | 6.7(1) | |
| 618.87(18) | 100(2) | 1.01(2) |
| 648.17(73) | 6.4(1) | |
| 673.67(19) | 19.2(4) | 0.83(8) |
| 950.41(36) | 54 (1) | 1.47(9) |
| 966.40(10) | 11.2(2) | 1.37(22) |
| 1024.09(78) | 14.2(3) | 1.08(15) |
| 1075.59(96) | 11.6(2) | 0.77(3) |
| 1120.66(18) | 5.9(1) | $> 1$ |
| 1179.34(33) | 33.5(7) | 1.14(11) |
| 1235.39(89)[a] | | |
| 1282.97(16)[a] | | |
| 1330.38(17)[a] | | |

* Likely a contaminant.
[a] Placed in this work

### 4.3.2 Spectra

The level scheme of $^{78}$Ge as observed in this thesis is compiled in Figure 4.11. Figure 4.17 is a partial level scheme including determined relative intensities. The strong yrast transitions are seen in Figure 4.12. Figure 4.13 and 4.14 show the two distinct sequences which feed into the 619.2-keV $2_1^+$ gate through cross-correlations and demonstrate the energies of the expected $E2$ transitions. The placement of the 1236-keV and 1330-keV transitions are shown through coincidence of the 441-keV line in Figure 4.15.

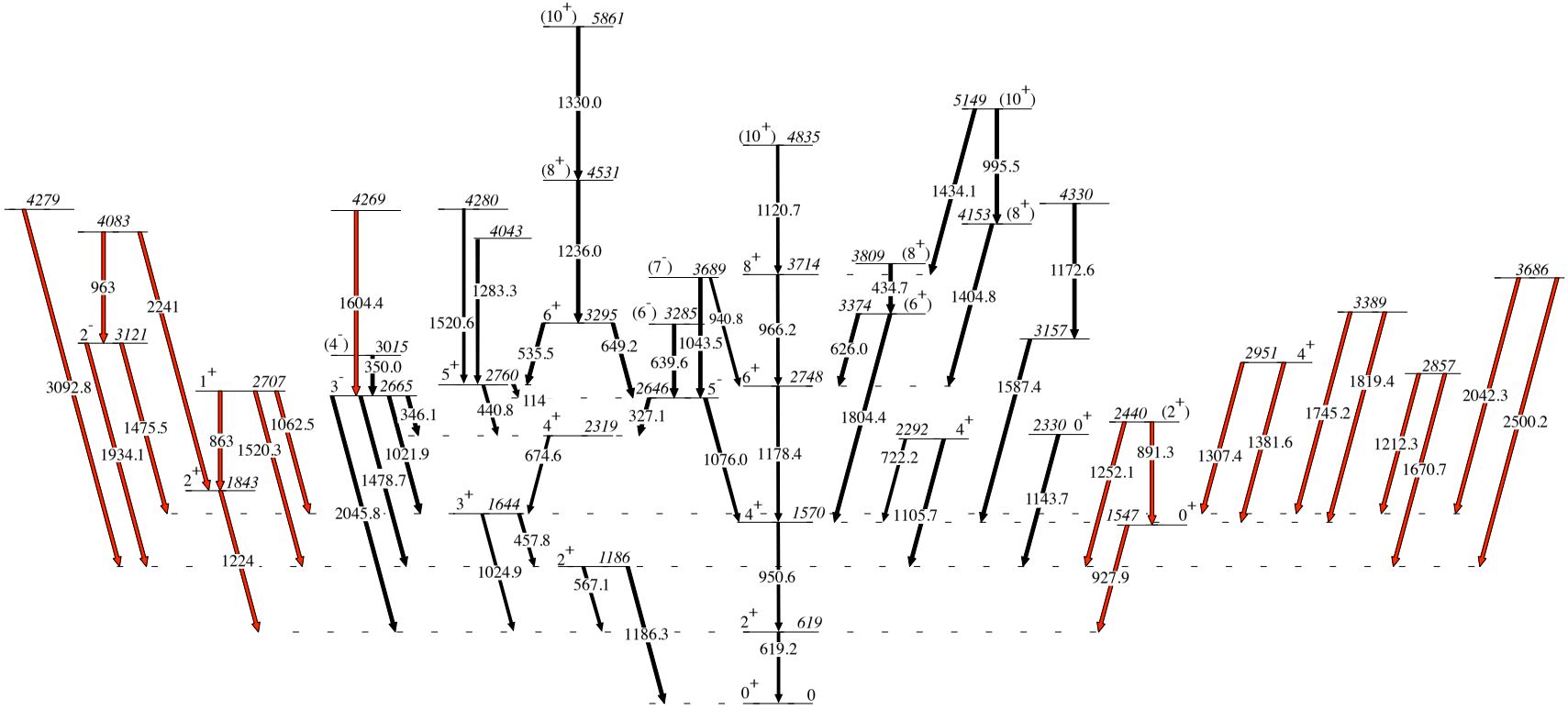


Figure 4.11: The $^{78}$Ge Level scheme compiled in this work with energies in keV. The red transitions are those seen in the delayed cubes.

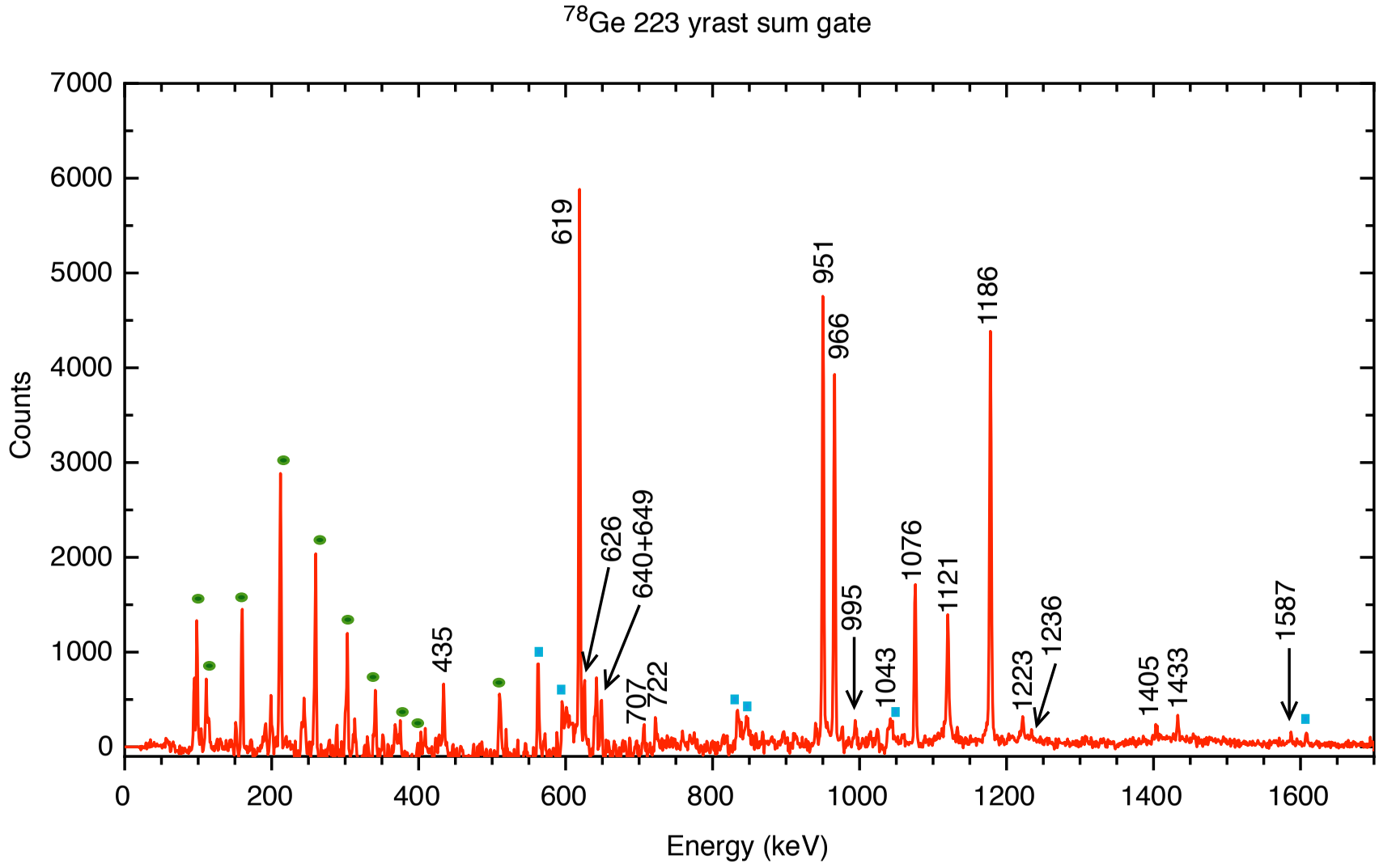


Figure 4.12: Coincidence spectra of the summed gates between the $^{78}$Ge yrast transitions of 619.2, 950.6, 1178.4, 966.2 and 1120.7 keV in the Ge/U data. The green circles mark transitions from uranium, while the blue squares correspond to $\gamma$ rays from the $^{76}$Ge target and the annihilation peak.

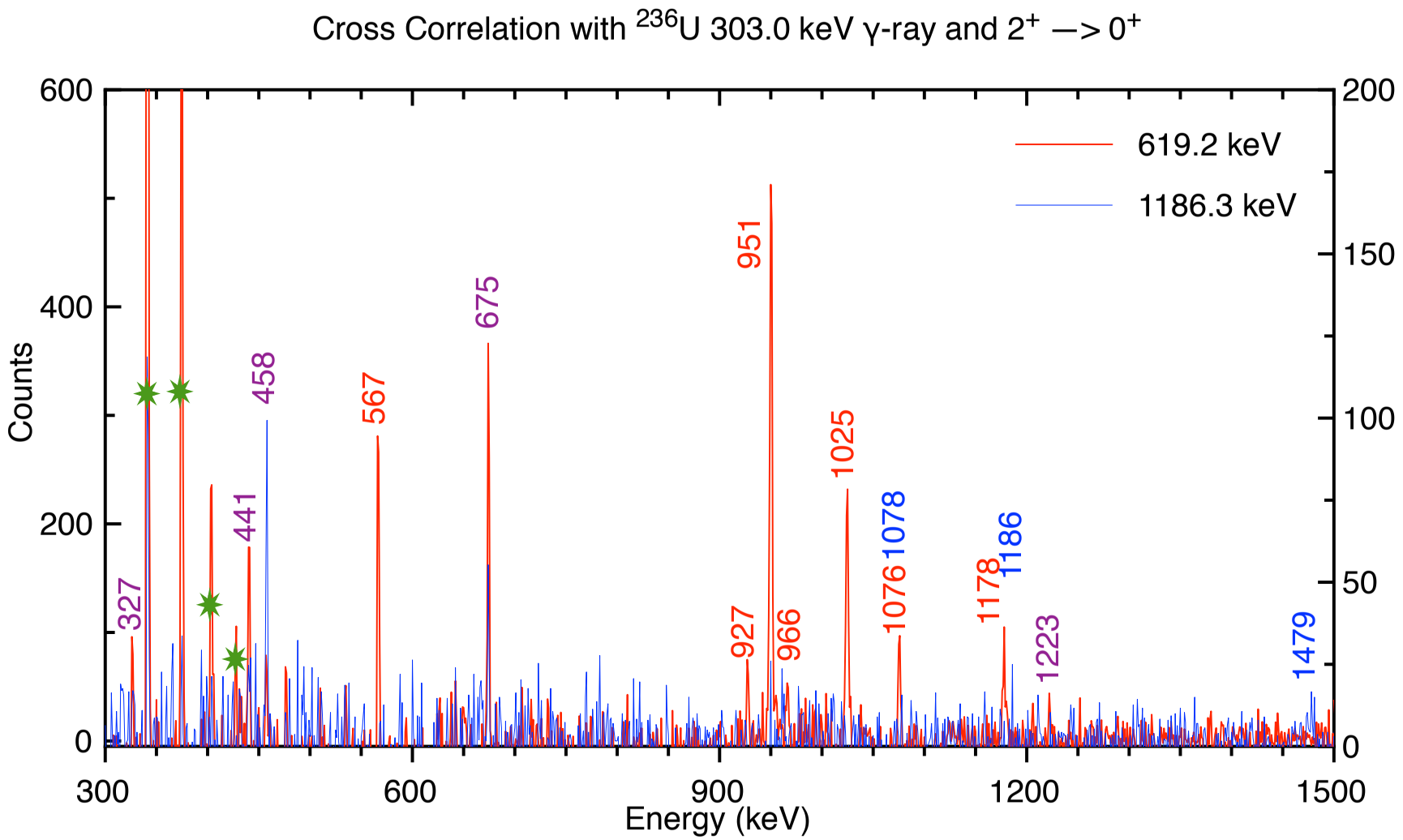


Figure 4.13: Coincidence spectra from the $^{76}$Ge+$^{238}$U data. A gate was set on the cross correlated 303.0-keV transition in $^{236}$U and the $^{78}$Ge $2_2^+ \rightarrow 0^+$ 1186.3 keV (blue) and $2_1^+ \rightarrow 0^+$ 619.2-keV (red) transitions. Peaks labeled in purple are seen in both spectra, whereas peaks with a star are U transitions (lines).

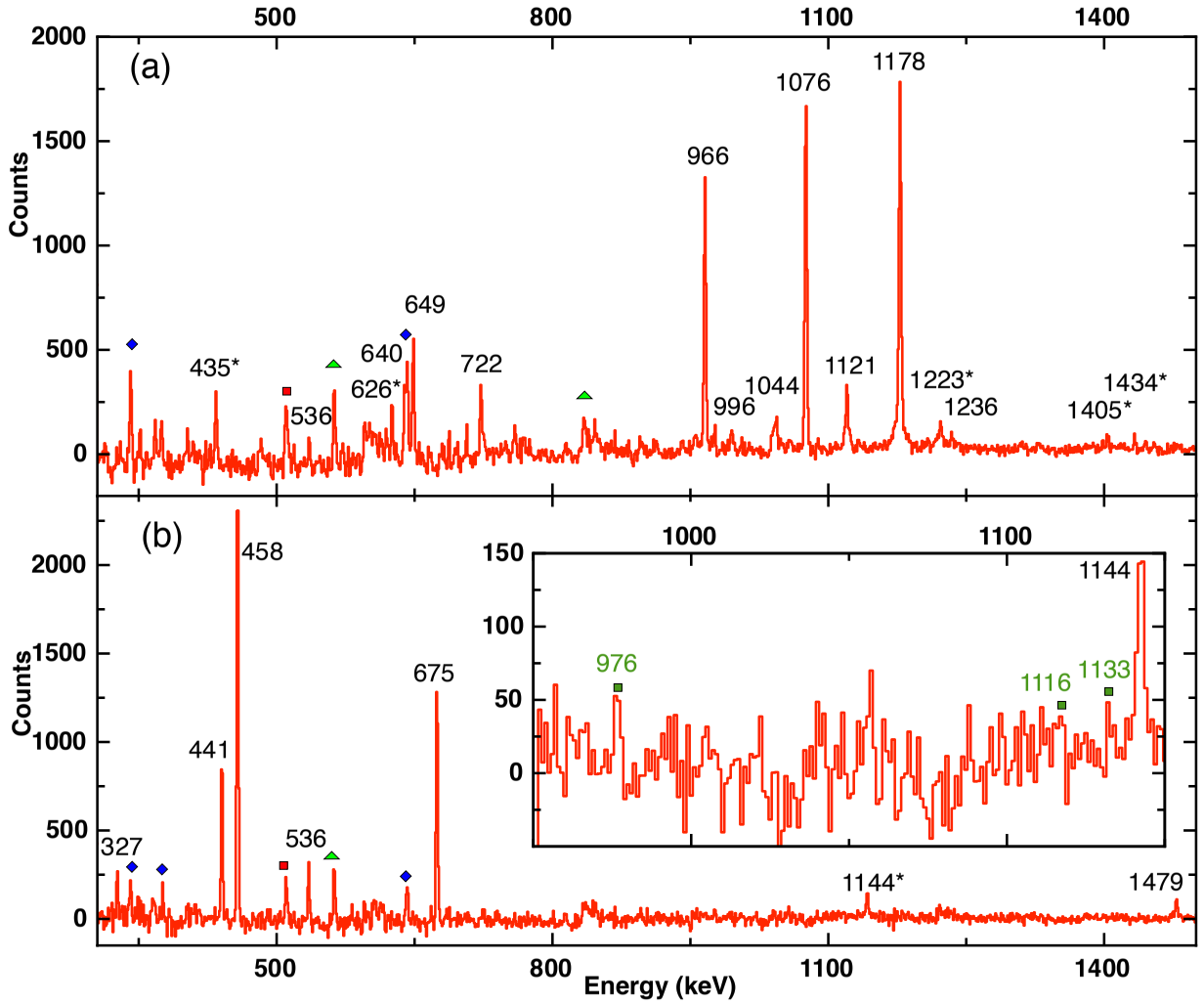


Figure 4.14: Coincidence spectra from the Ge/U data set with $^{78}$Ge $\gamma$ peaks labelled by their energies in keV. (a) Spectrum with a double gate placed on the 950.6-keV, $4_1^+ \rightarrow 2_1^+$ and the 619.2-keV, $2_1^+ \rightarrow 0_1^+$ transitions. (b) Spectrum in coincidence with the 619.2 keV and the 567.1-keV $\gamma$ ray linking the $2_2^+$ and $2_1^+$ states. The inset in (b) is an enlargement shows the absence of the $\Delta J = 2$ crossover transitions. Their locations are indicated by the expected transition energies marked in green. The green triangles in both spectra mark transitions from the $^{76}$Ge beam, while the diamonds correspond to $\gamma$ rays from the $^{238}$U target. A red square marks the positron annihilation peak.

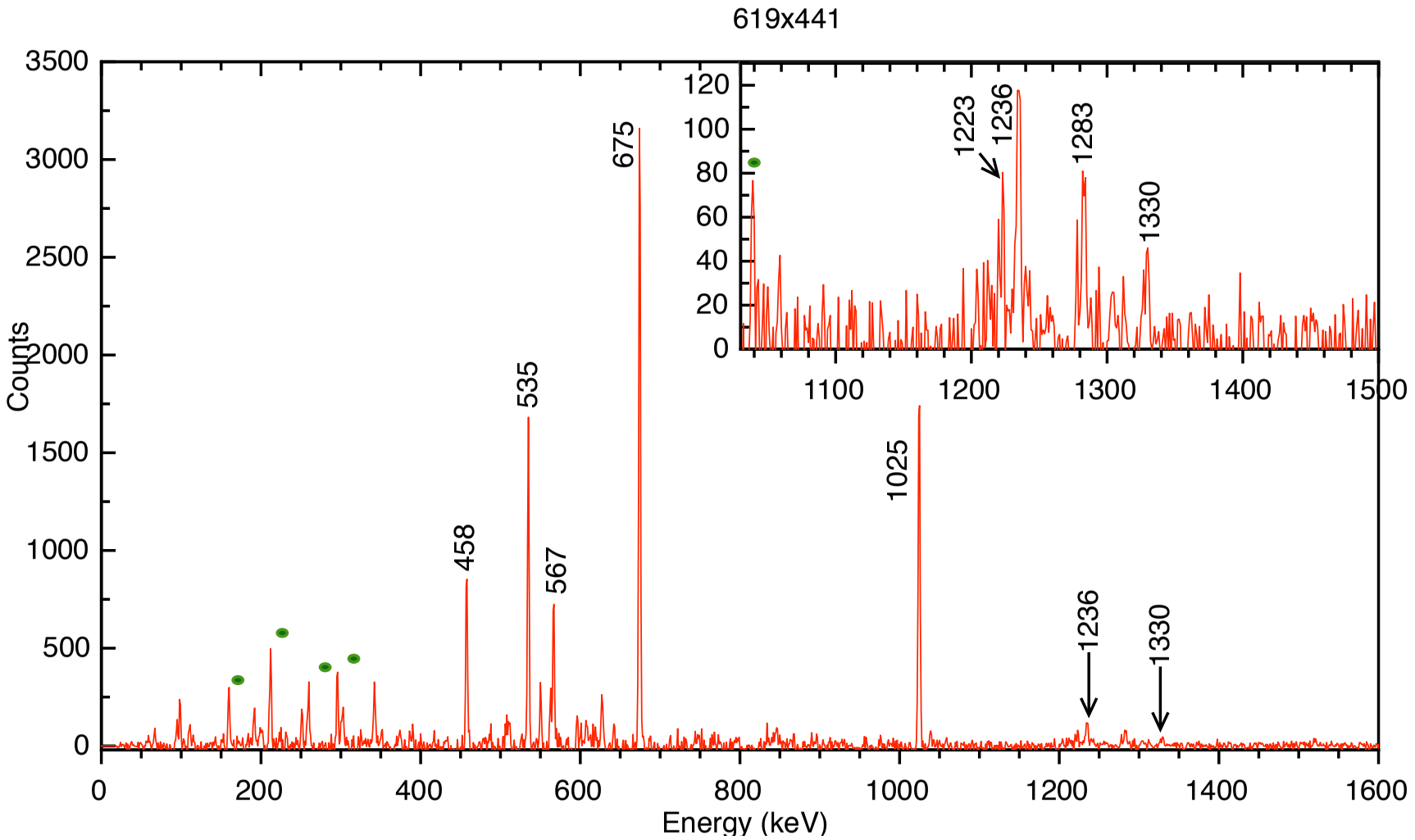


Figure 4.15: Coincidence spectrum of the $^{78}$Ge 619.2-keV, $2_1^+ \rightarrow 0_1^+$ and 440.8-keV, $5_1^+ \rightarrow 4_3^+$ transitions from the $^{76}$Ge+$^{236}$U data. The green circles mark transitions from uranium.

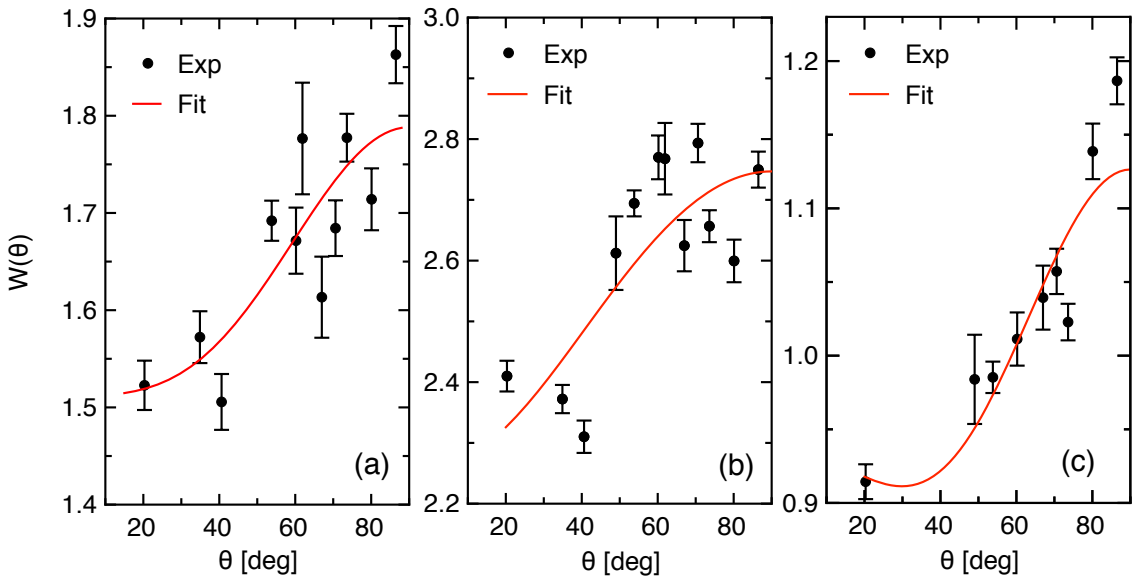


Figure 4.16: Angular correlations measured in the $^{76}$Ge $+^{238}$ U reaction.(a) the 1076.0 keV, $5_1^- \rightarrow 4_1^+$ transition in the 950.6 keV coincidence gate; (b) the 674.8keV, $4_3^+ \rightarrow 3_1^+$ transition in coincidence with the 1024.9-keV $\gamma$ ray; and (c) the 457.8 keV, $3_1^+ \rightarrow 2_2^+$ transition in the 619.2-keV gate. The curves are the result of fits to the data with a conventional expansion in terms of Legendre polynomials, as described in Section 3.6.

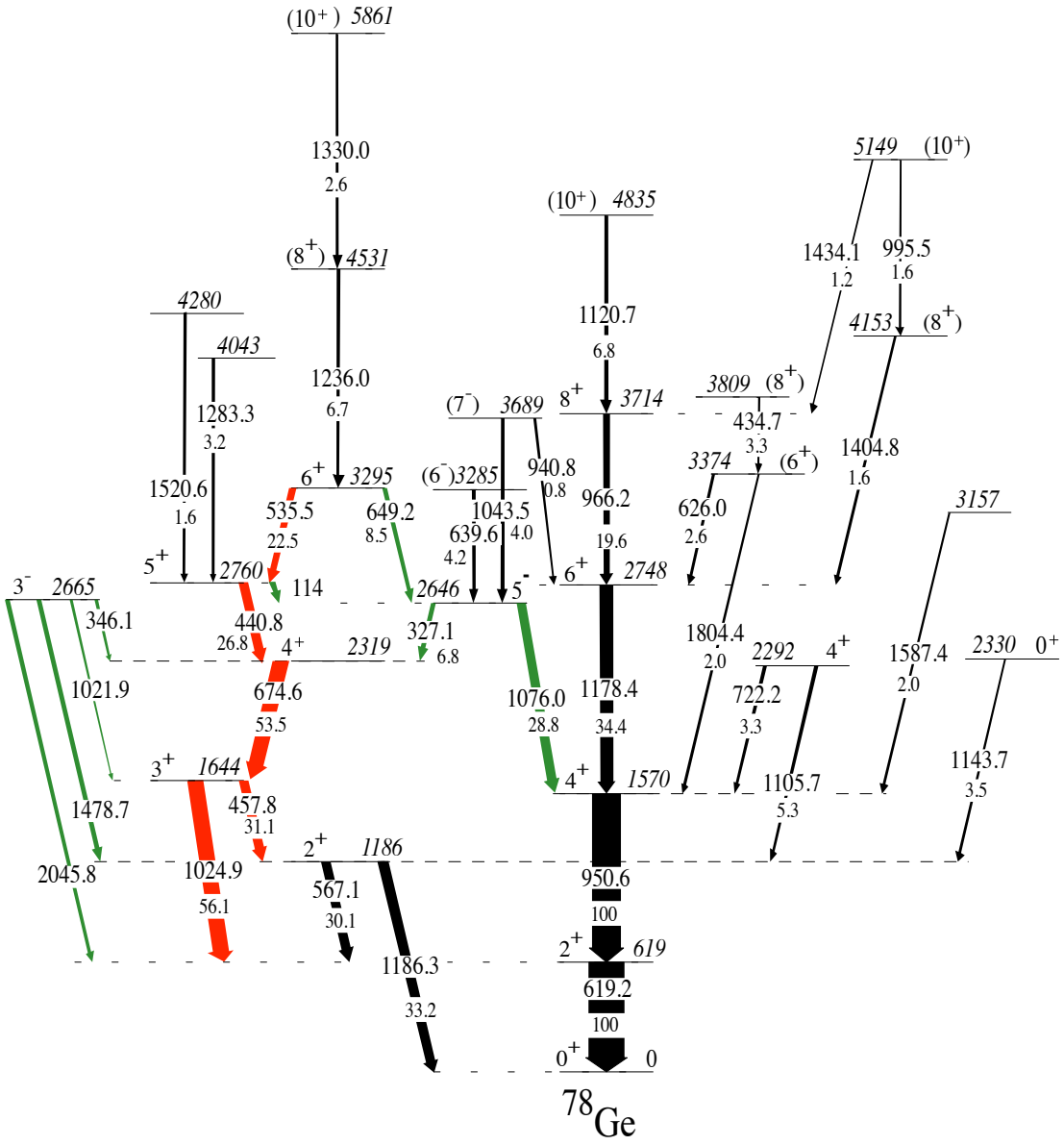


Figure 4.17: Partial level scheme of $^{78}$Ge with relative intensities from the $^{76}$Ge+ $^{238}$U data reported below the transition energy (in keV). Data for $\Delta J = 1$ transitions of the proposed $\kappa$ band are given in red. $E1$ transitions between parity-changing states are given in green. The intensities were corrected to the 950.6 keV intensity in the 619.2-keV gate.

### 4.3.3 $^{78}$Ge Levels

**619.2(1) keV, $2_1^+$.** There is widespread agreement across experimental results describing the energy of this level. The strong yrast $2^+ \rightarrow$ ground-state transition has a $B(E2)$ value of 23.24(190) W.u. as calculated from the 13.5(24) ps half-life adopted by NNDC [28]. It is difficult to separate the 619.2-keV transition from the neutron-capture and neutron scattering peaks in Ge detectors around 600 keV. This complicates its use as a gate in angular correlations and also for the calculation of relative intensities. The neutron peaks cause an artificial increase in counts and over-background subtraction in the transition peak.

**1186.3(1) keV, $2_2^+$.** There are two transitions that are fed from this level. There are the $2_2^+ \rightarrow 0^+$ and the $2_2^+ \rightarrow 2_1^+$, 567.1 keV one. The measured half-life of this level is 12(6) ps [105], where the $B(E2)$ can be calculated as 0.53(18) W.u. for the 1186.3-keV transition and 6.3(21) W.u. for the 567.1-keV transition. Branching ratios were determined from the relative intensities of the 1186.3- and 567.1- keV $\gamma$ rays in a gate of 675- and 441-keV $\gamma$ rays (two higher transitions). The gate produces a 47(5)% to 53(5)% branching ratio, which is in close agreement with the ratio of 47.66% to 52.34% reported in the $\beta$-decay work [102]. The 567.1-keV transition cannot be used in angular correlations, because it is close to the 563-keV transition of $^{76}$Ge (the beam). As a result, the 567 keV peak in the spectrum is next to a section that is heavily subtracted for background.

**1547.1 (3) keV, $0_2^+$.** The Lewis work reports this level to have direct feeding [102].

It is strongly populated in the (t,p) works as a doublet at 1539 keV with a $(4^+)$ [103] and at 1547 keV in Ref. [56]. The level was also reported as a $(4^+ + 0^+)$ doublet in the (d, Li) experiment [51]. The level has a 25 ps half-life [105] leading to a $B(E2)$ value for the 927-keV transition (seen in DIS by Faul, Ref. [4]) to be 1.67 W.u. Low-spin states are difficult to populate in Gammasphere. The 927-keV transition is in coincidence with 891 keV and 619.2-keV transitions in the DDD cube of the Se/U experiment. It is prevalent in cross correlations with transitions in $^{236}$U in the PPP data of the Ge/U cubes.

**1569.8(1) keV, $4_1^+$.** Van den Berg [51] reported a $0^+$ and $4^+$ doublet state, with the $4^+$ level at 1.57 MeV. Although the two levels could not be separated, there appeared to be only a small $L = 0$ component. The 1570 keV level belongs to the yrast sequence and is strongly populated. This level has a half-life of $< 3.5$ ps [105] giving the 950.6 keV a $B(E2)$ of $> 10.51$ W.u. It decays to the $2^+$ state by a 950.6-keV transition. This line is used for the second peak (in addition to the 619.2-keV $\gamma$ ray) to calculate relative intensities for the rest of the transitions in the nucleus.

**1644.1(1) keV, $3_1^+$.** This level was previously observed in $\beta$ decay [102] experiments, but not in the (t,p) reactions as it would require a two-step sequence to populate unnatural parity states. The level decays by two transitions 457.8 and 1024.9 keV with a branching ratio of 36% and 64%, respectively. With a half-life of 15 ps [105], the $B(E2)$ values are 0.08 W.u. for the 457.8 keV gamma and 0.12 W.u. for the 1024.9 keV gamma. In the evaluated nuclear data file (ENSDF) of the National Nuclear Data Center (NNDC), this level is assigned $(2, 3, 4^+)$ from the $\beta$ decay work of Lewis [102], while in the Faul thesis it is assigned as a $(4^+)$ state [4].

A spin/parity of $3^+$ is proposed in this work by angular correlations between the 458 and 619-keV transitions. These have $a_2 = -0.127(0.038)$ and $a_4 = 0.069(0.054)$ values consistent with a nearly pure dipole as seen in Panel C of Fig. 4.16. A verification was made using the 458− and 1186-keV transitions, and this produced values in close agreement. These values are $a_2 = -0.128(0.048)$ and $a_4 = 0.070(0.067)$. Angular correlations of the 1025− and 619-keV $\gamma$ rays indicate a mixed transition (with $a_2 = 0.158(0.026)$ and $a_4 = -0.028(0.036)$. This has a negative slope which is much too large for a pure $E2$ transition. This implies that the maximum $J^\pi$ is a $3^+$, although it could also be a $2^+$. The 1025-keV transition is not a pure dipole transition due to the slope, so cannot be a $3^-$ state.

**1843(1) keV, $2_3^+$.** This level decays by a 1223.5-keV transition to the $2_1^+$ state. There is a 1223 keV contamination peak in the Ge experiments. Therefore, this was confirmed in the Se/U DDD data in coincidence gate with the 619.2 keV transition with the weak 861 keV line, as well as the 2241-keV transitions. A larger uncertainty is added to this level due to the slight differences in energies between the Se and Ge cubes.

**2292.0(3) keV, $4_2^+$.** This level was reported in both (t,p) reactions and (d,Li) experiments [3, 56, 103], but not in $\beta$ decay. The upper limit in $\beta$ decay is consistent with a first-forbidden-unique transition needed to populate a $4^+$ level. In the Gammasphere data, 722.2 and 1105.7-keV transitions were identified in coincidence with 950.6/619.2 and 567.1/619.2-keV gates, respectively.

**2318.9(2) keV $4_3^+$.** This level has been identified strongly in (t,p) reactions and weakly in observed $\beta$ decay [56, 102, 103]. This level has a 43 ps half-life [105]. This

state was initially found to decay by a 674.8-keV transition [4], and was confirmed in this work to only decay by that one transition. This $\gamma$ ray is determined to have a $\Delta J = 1$ based on angular correlations between 674.8− and 457.8-keV transitions (Figure 4.16 Panel b). The $B(E2)$ value of the 674.8-keV transition is either 3.58 or 0.52 W.u. The single mode of decay by an 674.8 keV gamma ray makes it unique when compared to the lighter even-A Ge nuclei which have a $4^+ \rightarrow 2_2^+$ transition. A maximum $B(M1)$ can be calculated by assuming a pure $M1$ transition by using the half-life for this level. That value is less than 0.002 W.u., which indicates the suppression of the $E2$ crossover transition is *not* because the $M1$ component of the $\Delta J = 1$ transition. Instead the $\Delta J = 1$ component dominates the decay and smothers the $E2$ crossover transitions. Below the 0.002 W.u. limit, a partial half-life can be calculated for this level as 2.15 ns. This partial half-life yields a $B(E2)$ upper limit of 0.007 W.u. The $4^+ \rightarrow 2_2^+$ 913-keV $E2$ transition in $^{76}$Ge with a $B(E2) = 18(8)$ W.u. The $\Delta J = 2$ transition is severely quenched when compared to $^{76}$Ge.

**2330.0(3) keV, $0_3^+$.** This level was seen by a doublet in both of the (t,p) experiments [56, 103]. Ardouin *et al.* determined the second level as a $5^-$. The angular distribution in Figure 2 of Ref. [56], indicates that the first two low-angle data points (which are higher), do not align with the fits for an $L = 4$ and $L = 5$ curve (which decrease at low angles). This trend is reminiscent of the data in Ref. [103], and it fits an $L = 0$ assignment for the second level in the doublet. This thesis notes this level is by a 1143.7-keV transition in the double gate on the $2_2^+ \rightarrow 2_1^+ \rightarrow 0_1^+$ cascade. No transitions were found to feed this level in the present study.

**2439.7(3), ($2^+$).** This work is able to confirm the 891.3 keV $\gamma$ ray in the DDD cube of Se/U. The 1252.1-keV transition was also confirmed in the delayed cubes of Se/U, Ge/U, Ge/Pb, Se/Pb and Ge/Pt data sets. The 1819.6-keV transition was not seen in cross-correlation with partner nuclei. There is a second 1819.6(9)-keV $\gamma$-ray at a higher excitation energy that was identified in the $\beta$ decay work. Due to the lack of data on $\gamma$-rays from this level, this work adopts the spin/parity assignment from the $\beta$ decay and both (t,p) works [56, 102, 103].

**2645.8(2) keV, $5_1^-$.** This level has is assigned an $L = 5$ in both (t,p) works [56,103]. It decays by a strong 1076.0-keV transition in DIS [4]. In the present work, angular correlations between the 1076.0-keV and 950.6-keV transitions are found in Figure 4.16 Panel a. These produced an $a_2 = -0.126(0.025)$ and $a_4 = 0.030(0.036)$ values consistent with a dipole transition. In addition to the 1076.0 keV $E1$ transition reported by Faul, a second $E1$ transition with an energy of 327.3 keV also identified by Faul can be placed at this level, decaying to the $4_3^+$ state. The branching ratio of these two transitions is significant. About $81(XXX)\%$ decays into the yrast $4^+$ state and $20(XXX)\%$ decays by 327.3 keV into the $4_3^+$ state. The feeding of a non-yrast $4^+$ level is unusual for negative parity states. In $^{76}$Ge, the $5^-$ state decays to the $4_1^+$ state $97(XXX_{\%}$ of the time, and to the $3^-$ state by only $3(XXX)\%$.

**2665.0(2) keV, $3_1^-$.** This level decays by four $\gamma$ rays which are 346.1, 1021.9, 1478.7, and 2045.8 keV. The lower three transitions were confirmed in multiple data sets in the delayed cubes. The 1478.9-keV transition feeds the 1186.3 keV $2^+$ state and it is strongly present in the prompt spectra. There is a separate 1476 keV $\gamma$-ray

decaying to the 1644 keV $3^+$ state. These two transitions are distinct, since the 1476-keV transition is in coincidence with the $3^+ \rightarrow 2_2^+$ 457.8-keV transition, while the 1479-keV $\gamma$ ray is not. The assignment of a $(2, 3, 4^+)$ was reported by Lewis et al [102], but current analysis allows for the possibility of $(2, 3)$. With a log$ft$ of 5.6, this level is assigned a negative parity state. The (t,p) works should have identified a $3^-$ state, as it is natural parity. The authors did not identify this state because they could not resolve it from the 2646 keV state.

**2706.6(4) keV,** $1^+$ The $\beta$ decay work [102] reports a ground state transition from the 2706.6 keV level. This limits the $J^\pi$ of this state to a $1^+$, $1^-$, and $2^+$. This level was not observed in either (t,p) reaction (which would populate a $1^-$ or $2^+$ state), therefore this state is further limited to a $1^+$. Using the delayed cubes, the 1061.9-keV and 1519.3-keV transitions (feeding the $3_1^+$ and $2_2^+$ states) were seen in multiple data sets. The weak 863-keV $\gamma$ ray (feeding the $2_3^+$ state) was only identified in the delayed Se/U data. No additional $\gamma$ rays were found to populate this state.

**2748.2(2) keV,** $6_1^+$**.** The yrast $6^+ \rightarrow 4^+$ yrast 1178.4-keV transition from this state was seen in DIS by Podolyák [3] as well as Faul [4]. The intensity of the 1178.4-keV $\gamma$ ray is the strongest in the $4 \rightarrow 2 \rightarrow$ ground state. A $J^\pi = 6^+$ was determined in angular correlations as shown in Figure 3.8. This $J^\pi$ assignment was not adopted by either (t,p) study, but both groups reported a $3^-$ level within 10 keV of this level. This $3^-$ state has not been observed in any subsequent work. It is possible that the analysis of the L values in the (t,p) reaction studies mistook a $L = 6$ for a $L = 3$. **2759.7(2) keV,** $5_1^+$**.** This level was first identified by Faul [4], where it was assigned it a spin of either 5 or 7. It had a decay through a 440.8-keV transition

to the 2319 keV state. An additional decay from the 2760 state has been identified in the present work as a 113.9 keV transition to the 2646 keV $5^-$ state. The spin assignment of 7 is excluded because angular correlations suggest the 2319 keV state is a $4^+$. This level decays 93.4$(XXX)$% of the time by the 440.8-keV transition, and 6.4$(XXX)$% of the time by the 113.9 keV. Both (t,p) works identified a level (or doublet) at 2759 keV with $J^\pi = 3^-$ or $(3^-)$,$(4^+)$ (Fig. 4.10). It is quite possible there is another state with lower-spin at or near this energy, but it is not the same state as seen in this work and by Faul.

**2857.0(4) keV,** $(2, 3)$**.** This level is seen in $\beta$ decay [102] through three transitions which are 1212.3, 1670.7, and 2857 keV. Only the 1670.7-keV transition was observed in multiple cubes in the present work. The $5^-$ state reported by Ardouin *et al.* [56] at 2850 keV is almost certainly a different level. This work cannot provide any additional insight to the spin of the state, other than eliminate a possibility of a spin 4 included by Lewis *et al.* [102].

**2951.4(4) keV,** $(4^+)$**.** Ref. [56] assigned this level a $J^\pi = 4^+$, but it is possible that it is a $2^+$, $3^-$ or $4^+$ state. A tentative $(4^+)$ with a log$ft$ of 6.38 was reported in $\beta$ decay in addition to the log$f_1t$ listed as 8.12 [102]. This log$f_1t$ is consistent with a $4^+$ assignment. The decay of this level by 1307.4-keV and 1381.6-keV transitions in multiple delayed cubes is slightly lower in energy compared with those reported in the $\beta$-decay. The 2333.3-keV $\gamma$ ray that feeds the 619.2 keV level reported by the Lewis $\beta$ decay study [102] could not be confirmed in this thesis.

**3015.0(4) keV,** $(4^-)$**.** This state is newly identified through the decay of a 350.0-keV transition into the 2665.0 keV $3^-$ state. As it was not observed in $\beta$ decay, it

likely has a higher spin and is tentatively assigned as the $4^-$ level. No feeding into this state has been identified.

**3120.6(3) keV, $2^-$.** This state was reported in $\beta$ decay as a $(1, 2, 3)$ [102]. It de-excites through three transitions which are 1475.5, 1934.1, and 2501 keV. In the present work, the 2501-keV transition could not be confirmed in a 963/619-keV coincidence gate. The state was confirmed by the 1475.5 keV $\gamma$ ray in the Se/U delayed data. The prominent 1934.1 keV line was observed in all of the Ge and Se delayed cubes. The low log$ft$ of 5.6 measured by Lewis [102] indicates negative parity. This assignment is consistent with the non-observation of the state in the (t,p) reaction studies.

**3157.4(2) keV, $(5^+)$.** This is a newly identified level determined by a 1587.4 keV $\gamma$ ray feeding into the 1644 keV $3^+$ state. A tentative $5^+$ is assigned to this state since it is not observed in the delayed cubes, the (t,p) experiments, nor in the $\beta$ decay study. Therefore it has a spin greater than 3 and a large transition energy, indicating an $E2$. The present work favors a $5^+$ assignment due to the large transition energy. It may also be $4^+$ or $4^-$ state. A $4^+$ level is less likely, since it does not feed any of the $2^+$ levels.

**3285.4(3) keV, $6^{(-)}$.** The level is newly identified from a 639.6-keV transition into the 2645.8 keV $5^-$ level. It is close in energy to the 642.3 keV peak in $^{236}$U. This transition has been confirmed using different beam/target combinations. The proximity of the transition to that of the 642 keV $^{236}$U peak makes it impossible to perform angular correlations in the U data sets. The peak does not have the intensity required for angular correlation measurements in the Pb data sets. A $6^+$

state at 3287 keV was reported by Mateja *et al.* in their (t,p) work [103]. It is likely attributed to the level at 3295 keV instead of this state.

**3295.2(2) keV, $6^+$.** Faul identified this level by a 535.5-keV transition to the 2760 keV level [4]. She did not assigned a spin or parity. The present study found this state to also de-excite by $27(XXX)\%$ to the $5^-$ state at 2646 keV by a 649.2-keV transition. The 649.2 keV $\gamma$ ray was identified by Faul in the whole $\gamma$ spectrum of $^{78}$Ge [4] but was not placed.

**3374.2(2) keV, $(6^+)$.** This state is newly identified in this work. It de-excites directly into the $6_1^+$ and $4_1^+$ by 626.0- and 1804.4-keV transitions.

**3389.2(4) keV, (2,3).** This level was identified as $(1, 2, 3)$ in $\beta$ decay, and not given a spin or parity assignment in (t,p) [103]. It was seen in (t,p), it is likely a $2^+$ or $3^-$. This state de-excites by four transitions which are 532.7, 1745.2, 1819.4, and 2771.2 keV. Only the 1745.2 keV and 1819.4 keV gamma rays were detected in the delayed Se/U data. A possible 4 spin assignment can be eliminated because of laser spectroscopy work [97].

**3686.4(4) keV, (2,3).** This state was identified as a $(1, 2, 3)$ in $\beta$ decay. It was not given a spin or parity assignment in (t,p) [56]. This level de-excites by 2043.1 keV and 2500.1 keV (present in all Ge and Se DDD data).

**3689.3(2) keV, $(7^-)$** The 3689 keV state is observed in the (t,p) experiment of Ref. [56]. The observation indicates that it has a natural parity, so it has a $7^-$ $J^\pi$ assignment. It feeds into the $5^-$ state at 2646 keV by a 1043.5-keV $\gamma$ ray ($84(XXX)\%$), and a 940.8 keV ($16(XXX)\%$) transition into the yrast $6^+$ state. The 940.8-keV $\gamma$ ray has 0.8% of the intensity of the 950.6 keV transition, so it is very weak.

**3714.4(2) keV,** $8^+$**.** Podolyák *et al.* [3] initially identified this state which was later confirmed by Faul [4]. This yrast state decays 100% by a 966.2-keV $\gamma$ ray.

**3808.7(2) keV,** $(8^+)$**.** This newly identified level de-excites to the 3374 keV $(6^+)$ state by a 434.7-keV $\gamma$ ray.

**4043.0(3) keV.** This is possibly the same level as the 4036 keV $5^-$ state reported by the Mateja *et al.* [103]. This level decays by a 1283.3-keV $\gamma$ ray to the 2759.7 keV $5^+$ state.

**4083(1) keV,** $(1,2,3)^-$**.** $\beta$ decay indicates this state has a log$ft$ of 5.5 and it de-excites by 963-, 2241-, and 3464-keV $\gamma$ rays [102]. The 963 and 2241-keV transitions were weakly observed in the present work. This level has large uncertainty because of energy inconsistencies in the different reaction cubes.

**4153.0(2) keV,** $(8^+)$**.** This newly reported state decays to the yrast $6_1^+$ by a strong 1404.8-keV transition.

**4269.4(4) keV,** $(1,2,3)^-$**.**Lewis *et al.* observed this level in $\beta$ decay to de-excite by 1604.4- and 3083-keV transitions [102]. The 1604.4-keV $\gamma$ ray has four times the intensity as the 3083 keV [102]. The lower-energy transition is only weakly observed in the Se/U delayed data in the present work. The log$ft$ of this state is 5.7, which indicates negative parity. Ardouin reported a 4259 keV level, which favors natural spin values of $(1^-)$, $(2^+)$ or $(3^-)$. The absence of ground-state feeding favors a $3^-$ assignment over the $1^-$ or $2^+$ ones.

**4279.1(4) keV,** $(1,2,3)^-$**.** This state is only 10 keV above the prior level. It decays by two transitions, a 1573.4 and a 3092.8 keV [102]. The 1573.4 keV gamma ray (almost half as intense) was not detected in the present study. The 3092.8-keV $\gamma$ ray

was detected in the delayed data with the Ge beam, using Pb, U, and Pt targets. This state has negative parity based on the low log$ft$ of 5.7 reported by the original $\beta$-decay work of Lewis [102]. It is a candidate for spin and parity assignments of $2^-$.

**4280.3(2) keV.** This level feeds the $5^+$ 2760 keV state through a 1520.6-keV $\gamma$ ray. The present work found no further de-excitations of this state. It is $> 1$ keV above the previous level, and it is distinct because it must be at higher spin to feed the $5^+$ state.

**4330.0(3) keV.** This level de-excites by an 1172.6-keV $\gamma$ ray to the 3157.4 keV state. Ardouin observed the 4330 keV level in (t,p), but not the 3157 keV state. This suggests that the 4330.0 keV state has natural parity including $4^+$, $5^-$, $6^+$. This hypothesis depends on the $(5^+)$ designation of the 3157.4 keV state.

**4531.0(3) keV,** $(8^+)$**.** Faul observed a 1235-keV $\gamma$ ray in the $^{78}$Ge spectrum (Figure 3.9 of Ref. [4]), but was not placed in the level scheme. The present study places this transition to decay to the 3295 keV $6_2^+$ state 4.15. A 1236.0-keV $\gamma$ ray coincident with both the 535.5- and the 649-keV transitions has been observed in this study. The 1236 keV transition is only coincident with the ground state band below the $4_1^+$ as it was not observed in a 619/966-keV coincidence gate as performed by Faul (Figure 3.10) and the present thesis. This is in line with the 1236.2-keV $\gamma$ connecting to the g.s.b. through the 1076- and 649.2-keV transitions.

**4835.1(3) keV,** $10^+$**.** This state was identified by Faul [4] as the $(10^+)$ state in the yrast band. It decays by an 1120.7-keV $\gamma$ ray.

**5078 keV,** $(3^-)$**.** This state was not seen in the present work. The log$ft$ of 5.6 measured by Lewis [102] indicates a parity change that can be expected from the

positive parity of the $J^\pi = 2^-$ parent. This state feeds the $2_1^+$ level and also the $4_1^+$ state. The feeding of a $4^+$ state rules out a $J = 1, 2$ spin for this state. This work puts a tentative $J^\pi = (3^-)$, since it was not observed.

**5148.5(3) keV,** $(10^+)$ This newly identified state decays to the yrast $8^+$ level by a strong 1434.1-keV transition and also by a 995.5-keV transition into the 4153 keV $(8^+)$ state. **5861.2(4) keV,** $(10^+)$**.** This state is newly identified in this work. The de-excitation of this state occurs by a 1330-keV transition into the 4531 keV level. Faul observed a 1330-keV $\gamma$ ray, but could not place it [4]. It is seen to be coincident with the 1236 keV transition as well as those in Figure 4.15.

# Chapter 5: Discussion

In this section, the level structures observed in $^{78,80,82}$Ge and adjacent nuclei are discussed in the context of the nuclear shell model. The Ge nuclei are described in shell-model terms relative to the nearest double-magic nucleus, $^{78}_{28}\mathrm{Ni}_{50}$. When compared to Ni, these Ge nuclei are described as having zero, two, or four holes at the top of the *fpg* neutron shell. They also have four proton particles at the bottom of the *fpg* proton shell. As the neutrons are holes and the protons are particles, mixing between states is complex in $^{78}$Ge, when compared to $^{82}$Ge. The use of shell-model codes such as NuShellX provides quantitative results for the calculated nucleon configurations. The predictions made by the shell model can be compared with the observed excited states. Although the decay patterns available, they are presently disregarded.

A discussion of the systematics in a wide Ge isotopic range as well as the $N = 46, 48, 50$ isotones will provide a useful frame of reference to further understand the structural behavior of $^{82,80,78}$Ge nuclei. Nucleon configurations as well as the neutron-hole and proton-particle structures have been previously introduced in Sections 1.14,1.15,1.16.

## 5.1 Ge isotope systematics

The systematics of the even-A Ge nuclei provides insight into the behavior of the isotopes between the $N = 32$ subshell and $N = 50$ shell closure. As discussed in the Chapter 2, $^{72,74,76}$Ge are stable isotopes. Each of these isotopes has features that can be attributed to a degree of triaxiality, or loss of axial symmetry at low energy. As seen in Fig. 5.1, the energy of the $4_1^+$ state in the Ge isotopes is approximately 2.5 times that of the energy of the $2_1^+$ state. This ratio was predicted for $\gamma$-soft nuclei by Wilets and Jean [13]. The measure of staggering, defined in Equation (1.2), provides a negative or positive phase of $S(J)$. This describes the nucleus as tending toward $\gamma$-rigid or $\gamma$-soft. Toh *et al.* postulated evidence for "rigid triaxiality" at low energy in $^{76}$Ge. They based this conclusion from a sequence of levels $2^+$, $3^+$,...$9^+$ with positive staggering values for $S(4)$ and $S(6)$ [34]. Mukhopadhyay *et al.* reported additional structural detail for $^{76}$Ge. They found that the level structure, could be described by large-scale shell-model calculations [55]. There was agreement at energy levels up to about 3 MeV, and included the proposed triaxial states with spins and parities of $2^+, 3^+, 4^+, 5^+$. They authors also noted that density functional theory (DFT) calculations by Nikšic *et al.* could be interpreted as favoring a $\gamma$-soft structure for $^{76}$Ge [106]. Calculations by Nikšić *et al.* showed a large positive value of the $S$ parameter for $^{74}$Ge relative to other Ge nuclei. Sun *et al.* were not able to observe this large value [49]. The unusual features of the structure of $^{72}$Ge were addressed by Ayangeakaa *et al.* in a Coulomb excitation experiment. The results indicated a need to introduce shape coexistence. The authors interpreted that both

shapes could be triaxial, but with negative S values pointing toward $\gamma$ softness [46].

Figure. 5.1 displays the trends of the excited states of interest for the even-A Ge isotopes between $N = 30$ and $N = 50$. The $^{64}_{32}\mathrm{Ge}_{32}$ nucleus has a double $2p_{3/2}$ subshell closure, while the upper limit, $^{82}_{32}\mathrm{Ge}_{50}$ has $\nu 1g_{9/2}$ shell closure. The excited states in Ge isotopes demonstrates the behaviour of the neutrons, and also indicates an evolution of collectivity as neutron orbitals are filled and the proton orbitals invert. This systematic trend suggests that the "$N = 40$" subshell closure observed prominently in $^{68}$Ni has shifted to $N = 38$. This indicates that a gap has developed between the $f_{5/2}$ and $p_{1/2}$ orbitals.

The top panel in Figure 5.1 displays the positive-parity states of the Ge isotopes. The yrast states (shown in red) increase toward $N = 38$. At that point they drop to a minimum in $^{76}_{44}$Ge. Similarly the low-lying positive parity $2_2^+, 3_1^+$ and $4_1^+$ states increase in energy toward $^{70}_{38}$Ge. This indicates a more substantial subshell closure at $N = 38$ instead of $N = 40$. Beyond $N = 38$ the energies decrease in the direction of $^{76}$Ge, and then they increase to the closed $N = 50$ shell closure.

The low excitation energies of the $2_2^+$ and $3_1^+$ states are well recognized of triaxial nuclei. The $2_2^+$ level energy in $^{78}$Ge is similar to the possible triaxial $^{72,74,76}$Ge nuclei. This state increases dramatically in $^{80,82}$Ge. The $3_1^+$ state (green) follows a pattern that is similar to the $2_2^+$ level, with a relatively constant energy difference of $400 - 500$ keV. The spacing of the $4_2^+$ (blue) state follows the same trend as the $2_2^+$ (blue) and $3_1^+$ (green) ones. This continues until $N = 46$, where this excitation energy increase tapers off to become about the $2_2^+$ energy at $N = 50$. The $5_1^+$ (green)

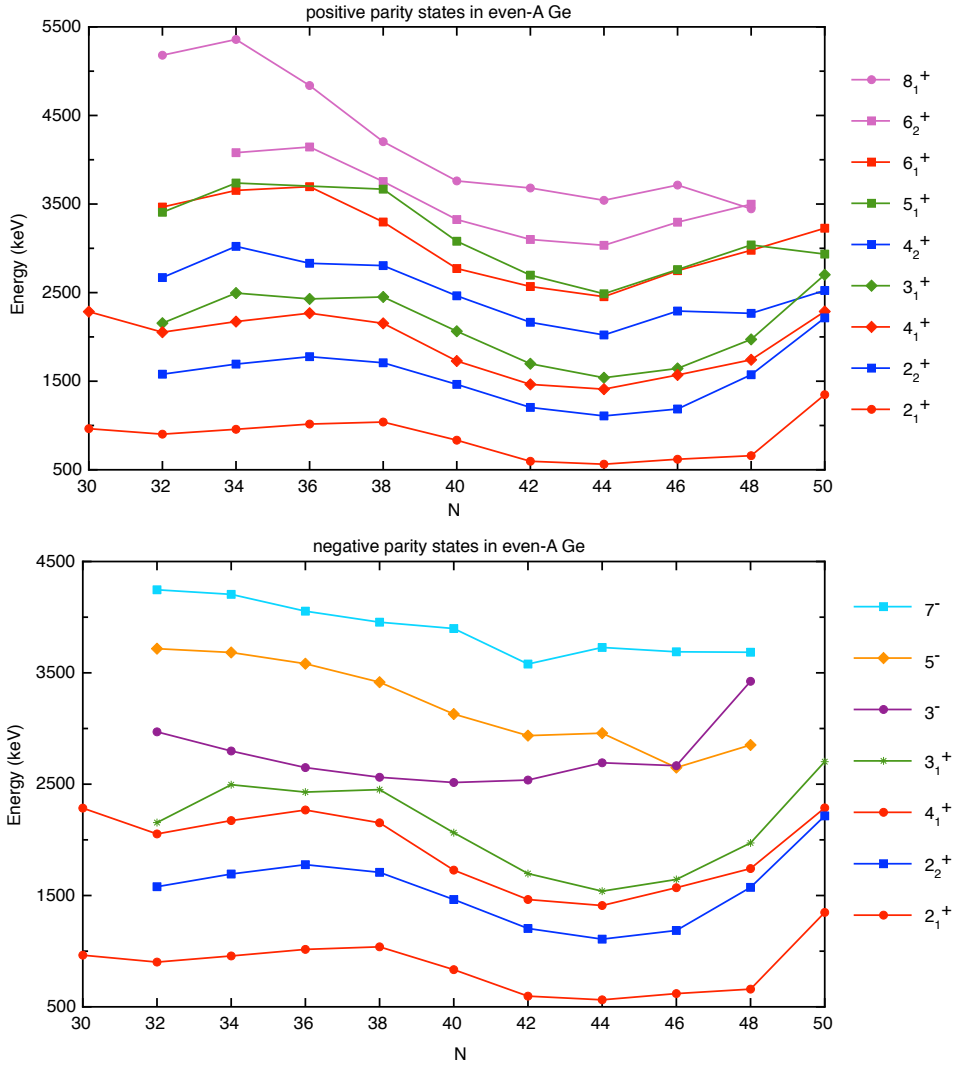


Figure 5.1: Systematics of excited states in even-A Ge nuclei. The energy of the $5_1^+$ state in $^{68}$Ge is unknown.

state drops at $N = 50$ to become close in energy to the $3_1^+$ state. Additionally, the $5_1^+$ state has an energy and trend that is similar to the $6_1^+$ level. The two states become nearly degenerate at $N = 46$. The spacing between the yrast $6_1^+$ and $8_1^+$ states in $^{72}_{40}$Ge is reduced when compared to the spacing in $^{74,76}$Ge. The increase in the $8_1^+$ (pink) energy in $^{78}_{46}$Ge is followed by a decrease in the energy of the (isomeric) state in $^{80}_{48}$Ge. The $8^+$ states in the heavier Ge isotopes can be be characterized by pure $\nu g_{9/2} g_{9/2}$ configurations. The $6_2^+$ (pink) state follow the same trend as the $8_1^+$ level, and this indicates that it might also have $g_{9/2}$ character.

The bottom panel in Fig. 5.1 shows the negative-parity states and also to the low-lying positive-parity ones. These negative-parity levels are associated with neutron configurations. However, the negative parity levels may be subject to collectivity. The energy level of the $7^-$ state in Ge nuclei decreases, with a particularly low value at $^{74}_{42}$Ge. A similar drop is observed in the semi-linear trend of the $5^-$ state occurs at $^{78}_{46}$Ge. The $3^-$ levels have a slightly parabolic trend except $^{78}$Ge, which appears to be an outlier. In $^{78}_{46}$Ge, the $3^-$ and $5^-$ states are nearly degenerate, and they are only 20 keV apart. This drastically different trend in the $3^-$ state could be the result of collectivity in the Ge nuclei associated with the $\pi p_{3/2} g_{9/2}$ configuration. As a proton state, the $3^-$ would be rather insensitive to the neutron number. The lowest $3^-$ states in Ge nuclei occurs in $^{72}_{40}$Ge at 2515 keV and $^{74}$Ge at 2537 keV. Collectivity is at a maximum at $N = 42$ in the Zn, Ge, S, and Kr nuclei (Fig. 2.1) [43]. Collectivity generally decreases near closed shells. This may be the reason that the $3^-$ state is no longer depressed in energy. The trends of the $5^-$ and $7^-$ states suggest that these cases are independent of collectivity.

Trends are identified in the comparison of the experimental level energies in the Ge isotopic chain. Increases in the excitation energy of positive-parity levels occur between $N = 32 - 38$ and $N = 46 - 50$. The only exceptions are the $8_1^+$ and $6^+$ states, which decrease in energy before $N = 38$. The negative-parity states have kinks that break the trends of $3^-$ and $5^-$ states in $^{78}_{46}$Ge. This also occurs in the energy of the $7^-$ level in $^{74}$Ge.

## 5.2 N=50 isotone systematics

The level structure of $N = 50$ isotones has few states when compared with open-shell neighbors. These nuclei have very little collectivity based on their $B(E2)$ values. Therefore, many states can be described as single-particle states within the shell-model framework. With the $\nu g_{9/2}$ shell filled, the lowest energy states result from protons excitations above the $\pi f_{7/2}$ orbital (filled at $Z = 28$). Due to the monopole shift, the $f_{5/2}$ orbital lies at a lower energy than the $p_{3/2}$ one for protons at $N = 50$. The reverse is true at $N = 40$. Protons predominantly occupy the $f_{5/2}$ state, but pairing pushes the second and higher pairs into the $p_{3/2}$ state. There is a narrow 656-keV separation in $^{79}$Cu between the $3/2^-$ excited state and $5/2^-$ ground state (Fig. 1.7). Breaking one pair of protons produces the [pf7] group. Fewer states are accessible for this proton pair with an increase in proton number. As the proton orbital fills, the broken pair must access higher-energy orbitals. Excited states in the $N = 50$ isotones can also be produced by breaking two pairs of protons to create a $5^+$ or $6^+$ state. Another way to form excited states is to promote nucleons across the

closed shell. There is competition between the $f_{5/2}$ or $p_{3/2}$ orbital for the location of the second proton pair at and above $Z = 32$.

The first excited state at well over 1 MeV for the $N = 50$ isotones because of the absence of collectivity. The relatively constant excitation energy of the $2_2^+$ state means that there is little change in the $p_{3/2}f_{5/2}$ pairing energies across the isotones. As seen in Figure 5.2, there are three levels in $^{80}$Zn above the $4^+$ yrast state without $J^\pi$ assignment. The $2_2^+$ level is a candidate for one of the three states higher in energy. These levels may be the $1, 2$, or 3 states created by pairing in the $p$ and $f$ orbitals. These correspond to the $^{82}$Ge 2714-keV ($1_1^+$), 2215-keV $2_2^+$, and 2702-keV $3_1^+$ states. Zn only has two protons in the $f_{5/2}$ orbital so the angular momentum in the nucleus is limited to $1, 2, 3$, or 4. This means $^{80}$Zn can only pair to create a $2^+$ or $4^+$ state, so there is no low-energy $6^+$ level.

The $3_1^+$ levels energies in $^{82}$Ge and $^{84}$Se are identical. The energy in $^{86}$Kr is only 150 keV higher. However, the energy of the $5_1^+$ state increases since it requires breaking two pairs. Only $^{86}$Kr has reported in this region to have $3^-$ and $5^-$ states. These are created by the breaking of a $\pi g_{9/2}$ pair, and the excitation of the second nucleon to a $p$ or $f$ orbital. These states are likely to lie much higher in the other isotones, and have not yet been observed.

## 5.3 $^{82}$Ge

The new data presented in this thesis begins at $^{82}\mathrm{Ge}_{50}$. This nucleus has four protons beyond the double-magic nucleus $^{78}_{28}\mathrm{Ni}_{50}$. $^{82}$Ge has seniority-four states with

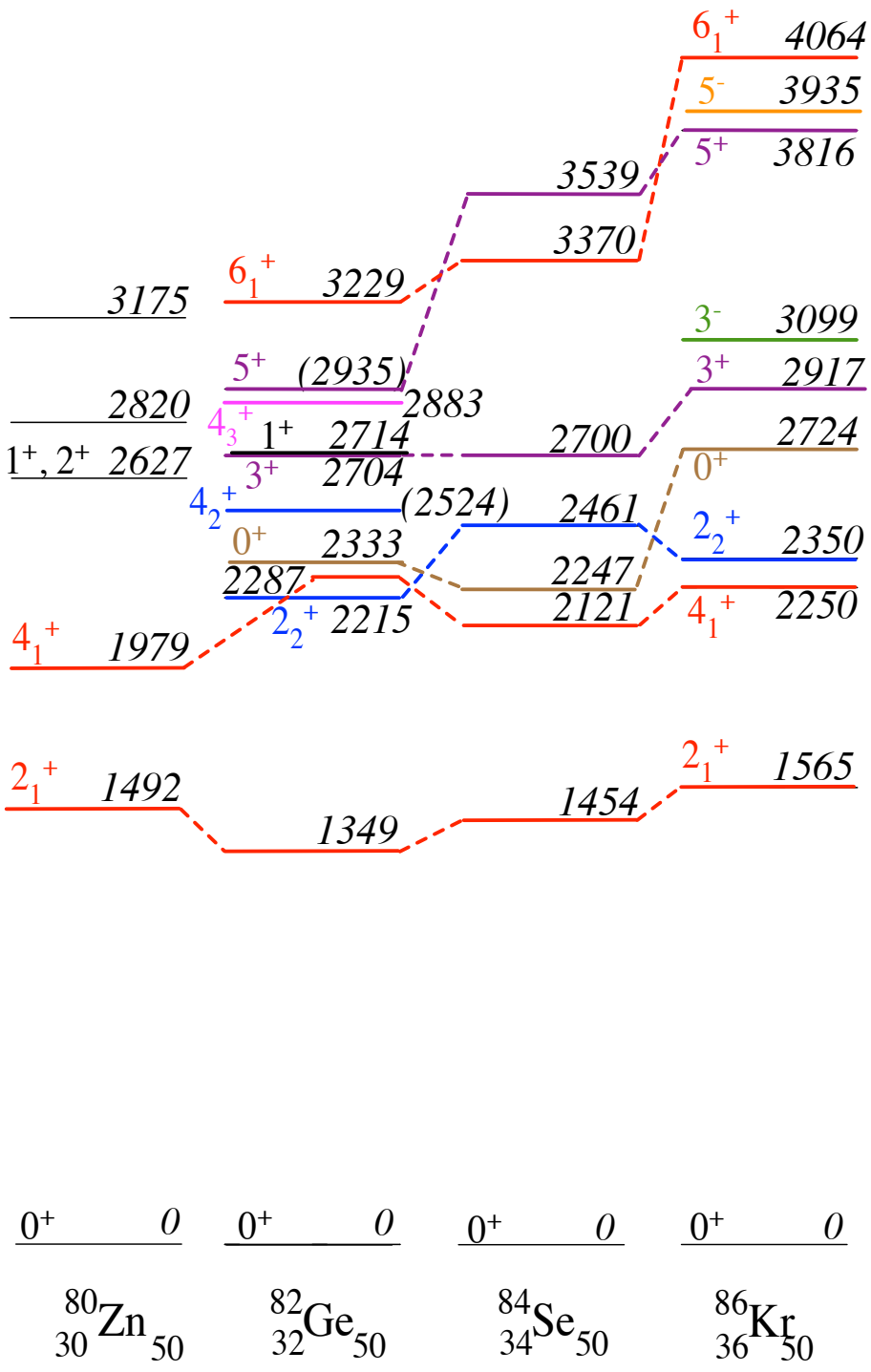


Figure 5.2: Excited states of the $N = 50$ isotones with level energies in keV. An asterisk indicates support for the level will be included in an forthcoming publication [107]. The figure is a compilation of data from the NNDC [28], Refs. [108, 109], and work not covered by the scope of this thesis. Not all levels are shown for Se and Kr. The upper three levels in $^{82}$Ge are beyond the [pf7] group and are either seniority-four levels or neutron-particle-hole excitations across the $N = 50$ closed shell.

higher spin values of $5^+$ and $6^+$ because of the two pairs of protons. Two additional $4^+$ states as well as two $5^+$ and $6^+$ states should be present as a result of the two broken pairs.

This work consolidates the level scheme and confirms transition energies previously reported in $^{82}$Ge. One new transition has been identified. This is the 408.6-keV $\gamma$ ray from the 2935-keV $(5,6)^+$ level. This work also confirms the $6_1^+ \rightarrow 4_1^+ \rightarrow 2_1^+$ doublet at 940 keV.

The connections to the [pf7] configurations in $^{82}$Ge are shown in red in Figure 5.3. They are in reasonable agreement with the NuShellX results. Above 2800 keV, the agreement breaks down and the proposed $4^+, 5^+$ and $6^+$ levels are placed at higher energies in the NuShellX calculations than observed. In the NuShellX code, these state are produced as seniority-four levels. This work favors the jj44b interaction in the case of $^{82}$Ge by the clear indication of the [pf7] group, and the distinct separation of the [pf7] levels from the seniority-four states. However, the jun45 interaction produced a $B(E2)$ value of 17.1 W.u.. That value is half of the jj44b one, and it is much closer to the experimental value of 12.1(21) W.u. Seija and Nowacki [91] argue that the $4^+, 5^+$ and $6^+$ levels arise from breaking the $N = 50$ closed shell to generate a multiplet of states. These configurations are described as $(\nu g_{9/2}^{-1} \circ \nu d_{5/2}^{+1})_{2^+,3^+,4^+,5^+,6^+,7^+}$, and well above 4 MeV. Seija and Nowacki also predict a minimum in the shell gap at $^{82}$Ge by:

$$\Delta = S_{2n}(N = 52) - S_{2n}(N = 50). \tag{5.1}$$

Hakala *et al.* measured this value as 3.1 MeV [110]. These cross neutron-shell

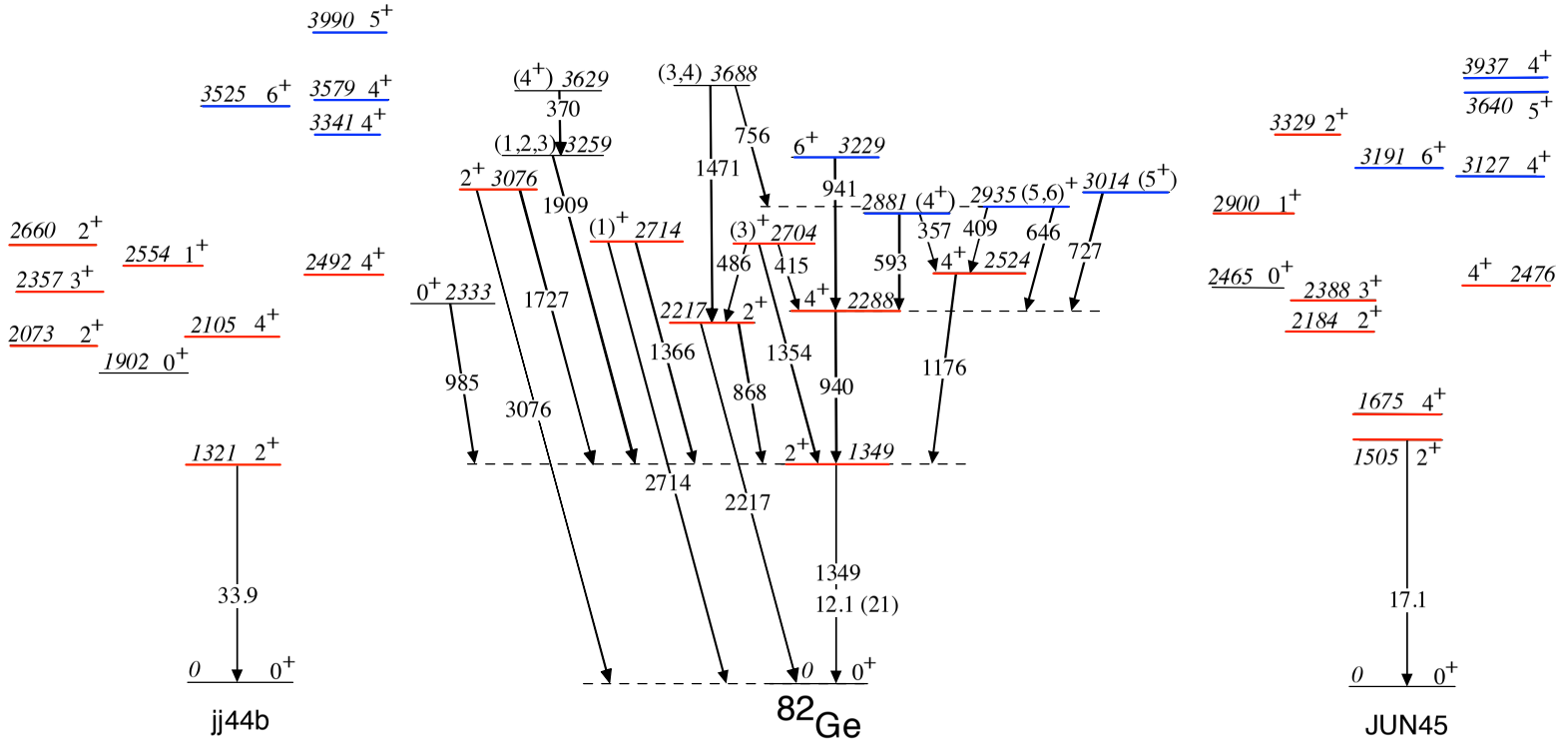


Figure 5.3: Level scheme for experimental levels (center) and theoretical levels using the jj44b (left) and jun45 (right) interactions for $^{82}$Ge. The levels [pf7] group are shown in red and the seniority-four levels in blue. Included are the $B(E2)$ values for the $2_1^+ \rightarrow 0_1^+$ transition in W.u. (Weisskopf units).

states arise from first breaking a valence $g_{9/2}$ neutron pair (requiring about 2MeV). Secondly, the neutrons are moved across the 3-MeV shell gap, placing them at an average of 5 MeV.

Table IV in Verney *et al.* provides an overview of the levels reported in $^{82}$Ge [80]. Remarkably, both the $\beta$ and $\beta$-$n$ decay experiments resulted in common transitions. This implies that the $\beta$-$n$ experiment does not populate higher spins than the $\beta$-decay one. The $\beta$-$n$ decay reported by Winger *et al.* identified two new transitions. These are a 727.6-keV line from a 3014.7-keV level ,and a 596.4-keV $\gamma$ ray from a 2883.4-keV state [111]. However, Verney *et al.* was also able to identify a 728.7-keV $\gamma$ ray in both $\beta$ and $\beta$-$n$ decay [80]. However, Hoff and Fogelberg did not identify this transition [1]. This excludes the 3014.5-keV state from having a higher-spin of $\geq 5$. Due to the proximity of the $^{74}$Ge$(n, n')$ peak at 595.0 keV, Verney *et al.* could not separate the $^{74}$Ge transition from the 596.4-keV $\gamma$ ray reported in Ref. [87]. The 2883.4-keV level spin is not a candidate for an assignment $\geq 5$. The 645.5-keV transition, initially reported in the spontaneous fission experiment (Ref. [76]) was not reported by $\beta$ and $\beta$-$n$ decay experiments, except for the work of Verney *et al.* [80].

A possible yrast sequence reported for $^{82}$Ge by Zhang *et al.* [71] and Podolyák *et al.* [3], was not seen in other experiments. This sequence is actually that of $^{87}Kr$ based on the relative intensities of the transitions. Refs. [3, 71] reported a sequence of 1578 $\rightarrow$ 681 $\rightarrow$ 1348 $\rightarrow$ ground state cascade (Fig. 5.4). This sequence exists in $^{87}$Kr as a 1348 $\rightarrow$ 563 $\rightarrow$ 1267 $\rightarrow$ 681 $\rightarrow$ 1548 one. A 681-keV transition has not been identified in any of the $\beta$ or $\beta$-n experiments on $^{82}$Ge. In a 681/1578-keV

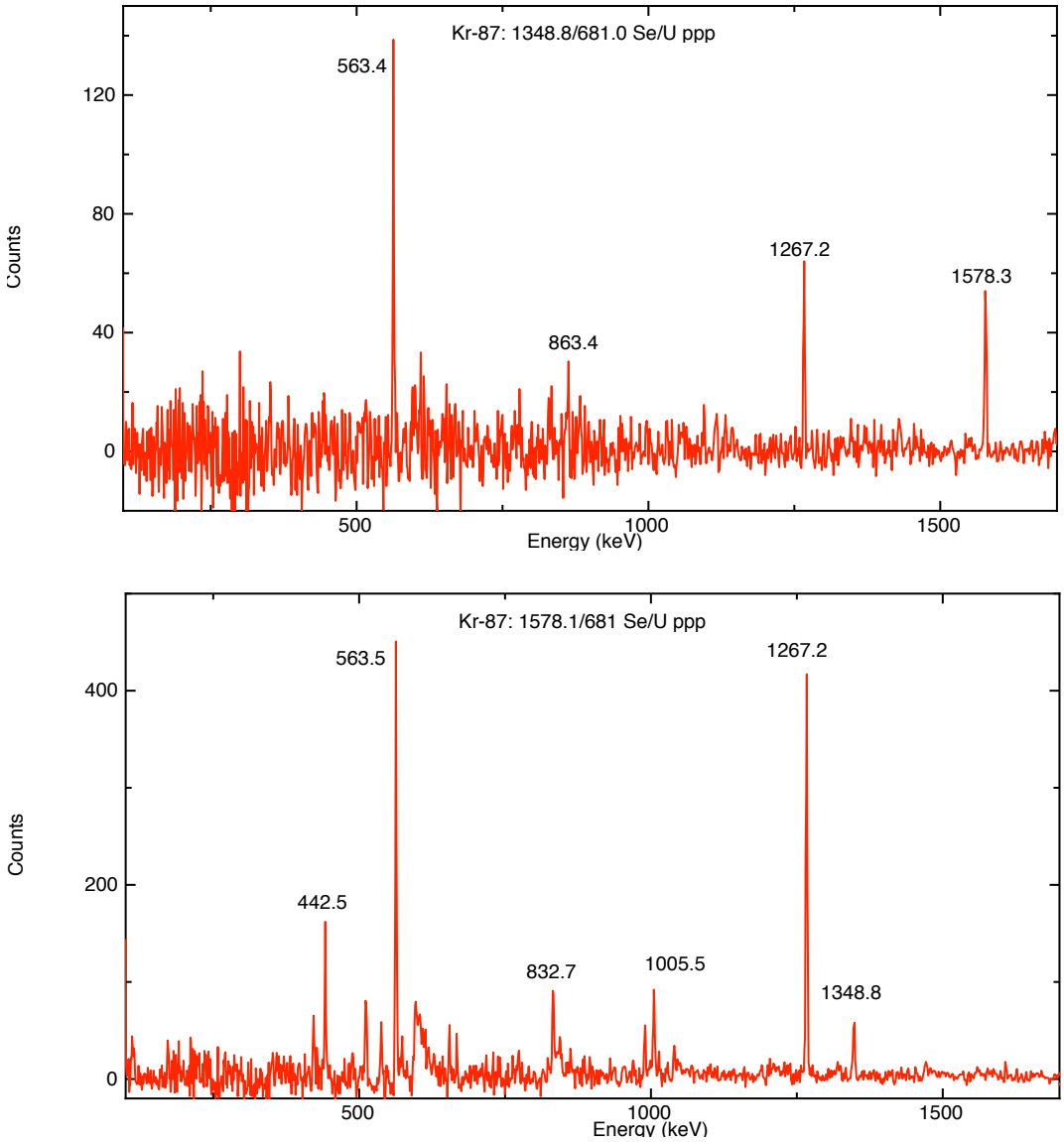


Figure 5.4: Transitions in $^{87}$Kr observed in this work using the Se/U data set. These transitions have been proposed (Refs. [3, 71]) to be in $^{82}$Ge. Transitions seen in 1348.8/681.0-keV and 1573.1/681-keV coincidence gate: the 1348.6-keV $(21/2^-) \rightarrow (17/2^-)$ transition, the 441.8-keV $(19/2^-) \rightarrow (17/2^-)$ link, the 562.9-keV $(15/2^-) \rightarrow 11/2^-$ decay, the 681.2-keV $11/2^- \rightarrow 9/2^+$ $\gamma$ ray and the 1577.6-keV $9/2^+ \rightarrow$ ground state transition.

coincidence gate, the most prominent $\gamma$ ray should be the 1348-keV one if it is the transition to the ground state. However the data indicate that the 1267-keV $\gamma$ ray is the most prominent (Fig. 5.4). This is in accordance with the $^{87}$Kr decay. If the possible sequence reported by Refs. [3, 71] is indeed the $^{82}$Ge yrast sequence, the energy of the $4_1^+$ state would be unusual, as it is below the $2_2^+$ state. Even so, the energy gap between the adopted 2217-keV $2_2^+$ and 2288-keV $4_1^+$ levels of 70 keV would be the smallest in all known Ge nuclei. The presence of the $N = 50$ shell closure in these two states is also persistent and they are at least 500 keV higher in energy than their isotopic counterparts.

This review of the level structure of $^{82}$Ge demonstrates the observed positions of the [pf7] group of levels and their calculated energies, which are in close proximity. The shell model at the closed shell provides a good description of the observed structure up to 2750 keV. The calculated seniority-four levels are higher in energy than the levels observed. This leads to an interpretation that the levels near 3 MeV are neutron particle-hole states, as proposed by Seija and Nowacki [91].

## 5.4 N=48 isotone systematics

The $N = 48$ isotones, have two neutron holes in the $N = 50$ closed shell. They exhibit a $2^+, 4^+, 6^+, 8^+$ sequence by breaking pairs of valence $g_{9/2}$ neutrons. They also exhibit lower-energy negative-parity levels that are constructed by breaking a neutron pair in the $p_{1/2}$, $f_{5/2}$, or $p_{3/2}$ orbital. The energetically favorable configuration forms by breaking a $p_{1/2}$ pair and moving the neutron into an empty $g_{9/2}$

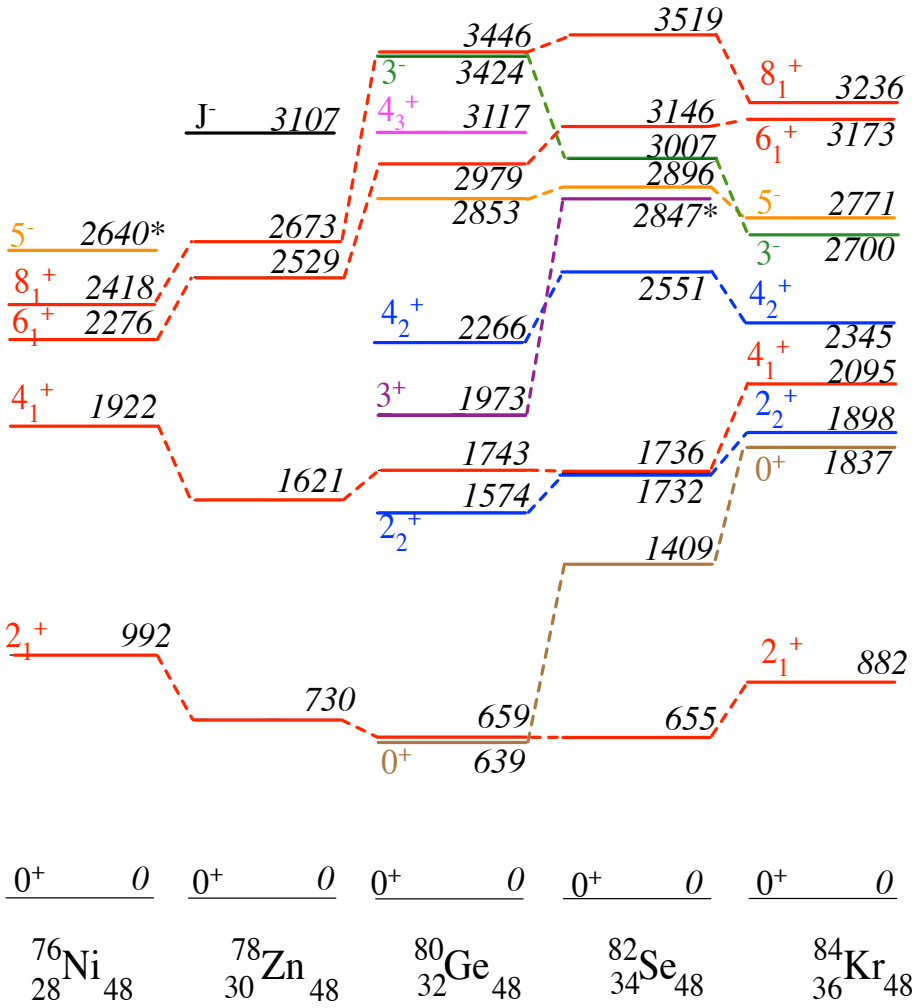


Figure 5.5: Excited states of the $N = 48$ isotones with level energies in keV. An asterisk indicates that the level will be included in an forthcoming publication [107]. The data are from the NNDC [28] and other work not covered by the scope of this thesis. Not all levels are shown. The level at 3107 keV in $^{78}$Zn is fed in allowed $\beta$ decay from a negative-parity Co parent and decays only to the $6^+$ level at 2529 keV. It is likely a negative-parity level with spin 5,6, or 7.

orbital. This generates a doublet of spin $5^-$ and $4^-$. Figure 1.6 shows the candidates for a few of these states in $^{74,76}$Ni.

There is a lack of collectivity in the $N = 48$ isotones. The neutrons are holes and the protons are particles so there is little constructive mixing present. Because of the $Z = 28$ closed shell, the $2_1^+$ and $4_1^+$ states in $^{76}$Ni are higher than the corresponding levels in the other isotones. Makishima *et al.* described the members of the ground state band up to $8^+$ for $^{80}$Ge to $^{94}$Pd as two-hole $(\nu g_{9/2}^{-2})$ states for the $N = 50$ closed shell [2]. The corresponding yrast states of $^{76}$Ni and $^{78}$Zn are found in Figure 5.5. These have systematics resembling those of $Z \geq 36$ whose $8^+ \rightarrow 6^+$ and $6^+ \rightarrow 4^+$ energies are much smaller than those of the Ge and Se isotones. There is a small $8^+ \rightarrow 6^+$ energy difference in the Kr isotone. Makishima *et al.* attributed the energy changes in the $Z \geq 38$ isotones to the proton occupation of the $g_{9/2}$ orbital. They concluded Ge, Se, Kr have proton occupation of the $fp$ orbitals [2]. In Ge and Se, the yrast $2^+$ and $4^+$ states are within a few keV of one another. The yrast $8^+$ and $6^+$ states have similar energy gaps. In the non-yrast states, there is a consistent rise in energy of each level from $^{80}$Ge to $^{82}$Se except in the $3^-$ level. In the shell-model framework, the lowest $3^-$ configuration is attributed to a $\nu g_{9/2} p_{3/2}$ pairing whose energy drops significantly above $N = 32$. At the same time, the lowest $5^-$ state is generated by a $\nu g_{9/2} p_{1/2}$ neutron pair whose energies remain within a couple of hundred keV of one another.

## 5.5 $^{80}$Ge

Only a few levels are available for isotonic $^{78}$Zn as seen in Figure 5.5. A rich $^{80}$Ge data set can be constructed from the GS DIS experiments and the published $\beta$-decay data. This is largely because the $^{80}$Ga $\beta$-decay parents include the isomeric $3^-$ and $6^-$ parents that populate a wide range of levels in $^{80}$Ge.

$^{81}$Ge has two low-energy cross-shell states with $J^\pi = 1/2^+$ and $5/2^+$. The presence of these states makes it reasonable to have a $0^+$ cross-shell intruder in $^{80}$Ge. The low-lying $0_2^+$ state is at 639 keV [6]. The $0_2^+$ state in $^{80}$Ge is depressed by approximately 900 keV below that in $^{78}$Ge, and also about 1700 keV below that in $^{82}$Ge. NuShellX predicts the $0_2^+$ state should be $\sim$ 2000 keV. The 639-keV level is not in the jj44b model space, hence it is called a "cross-shell intruder".

This work establishes the $^{80}$Ge positive-parity sequence up to $J^\pi = 10^+$. The delayed (DDD) Se/U cube indicates that the multi-nucleon transfer reaction creates mostly the $6^-$, $^{80}$Ga parent. This is confirmed by the comparison of the 659/1083- (Fig. 4.8) and 659/914- or 659/1313-keV coincidence spectra. Higher-spin states are more strongly populated in DIS reactions. This provides confidence that within the coincidence spectra, the transitions decaying out of the $6^-$ parent are observed.

There is a missing $4_2^+ \rightarrow 3_1^+$ transition in the $\gamma$-like band of $^{80}$Ge. Verney *et al.* proposed a $J^\pi$ assignment of $\leq 4$ for the 2852- and 1972-keV levels. The energy of the $3^+$ state increases with $N$ as the $N = 50$ shell is approached. In contrast, this work proposes the 2265-keV state as a $4^+$ level and the 2852-keV one as a $5^-$ state. The 2265-keV level feeds the 1742-keV $4_1^+$ state by a 523.5-keV transition.

The 1573.5-keV $2_2^+$ level is fed by a 691.9-keV one.

The Faul work predated the identification of the $J^\pi$ values of the $\beta$-decay parents [4]. She could not place the following transitions: 203.9, 352.0, 374.0, and 385.5 keV. A 399.5-keV transition from the 1973-keV level is the lowest energy $\gamma$ ray reported in the literature. Faul observed the 1313-keV $\gamma$-ray, but not the 399.5-keV transition. Based on the small errors reported in her work, it is unlikely that the 385.5-keV transition is the same $\gamma$ ray as the 399.5-keV line [4]. In the Se/U PPP cube, peaks at 352 and 374 keV are present in a 659/1083-keV gate. They are not included in the level scheme, as they are likely contaminants from another nucleus. The only other lower-energy transition coincident with the 659- and 1083-keV transitions is the the 523.5-keV line from the 2266-keV $4^+$ level (see Fig. 4.8).

Both jj44b and jun45 effective interactions describe the [pf7] states in $^{80}$Ge. The shell-model results are compared with the experimental results of $^{80}$Ge in Fig. 5.6. The $2_1^+, 2_2^+, 3^+, 4_1^+, 4_2^+$ states are calculated in the proper order and they are less than 175 keV from the experimental values. The one low-energy level with no neutron admixture is the $3_1^+$. It is found at 1973 keV, and can be compared with calculated positions at 1996 keV using jun45 and 2119 keV using jj44b. The position of the $3_1^+$ level is critical to the assessment of triaxiality, and it is correctly calculated in $^{80}$Ge with no reference to collectivity or triaxiality.

Both effective interactions depict the yrast sequence well. They include of the small $8^+ \rightarrow 6^+$ transition and the loss of collectivity, as demonstrated by a small $B(E2)$ value. The $10_1^+$ state is predicted in both interactions at a lower energy than

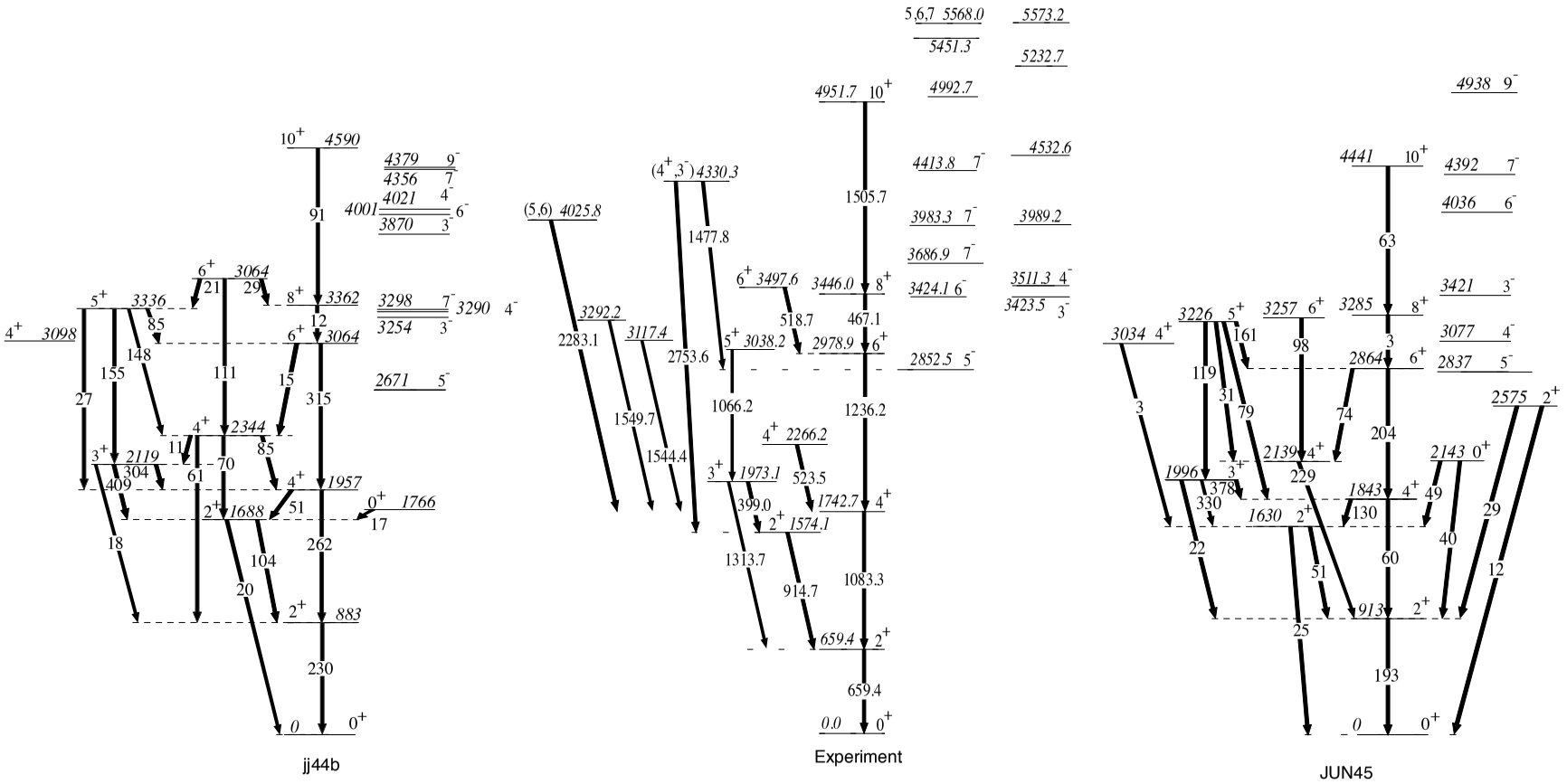


Figure 5.6: Level scheme for experimental levels (center) and theoretical levels using the jj44b (left) and jun45 (right) interaction for $^{80}$Ge. The calculated $B(E2)$ values are given for the calculated levels and they are in units of $10^{-2}e^2b^2$.

the experimental value. The two interactions predict the $3_1^+$ state to be lower in energy than the $4_2^+$ one. This is in agreement with the assignment of the 2266-keV state as a $J^\pi = 4_2^+$. The theoretical jj44b $4_2^+ \rightarrow 4_1^+$ transition is confirmed by the experimental results to decay strongly. However, the same transition in jun45 has a $B(E2) < 10$. Neither interaction predicts a strong $4_2^+ \rightarrow 3_1^+$ transition, and no such transition was observed. The calculated energy of the $5_1^+$ level is much higher than the experimental one. This is close in energy to the $6_1^+$ state. Small transition probabilities are expected between the $6_2^+$ and $5_1^+$ states because of the over-estimation of the $5_1^+$ location. The calculated $5_1^+$ level decays similarly to the measured $5^+$ state at 3038 keV. The only exception is a transition to the $6_1^+$ state, which is about 60 keV in separation.

The theoretical $1_1^+$ states, at 2333 and 2610 keV in jj44b and jun45 (not shown), have no experiment counterparts. The $1_1^+$ level was calculated 112 keV lower than the $4_1^+$ state in the jj44b interaction and 471 keV higher in the jun45 one. Although no $1^+$ level is reported in $^{80}$Ge, $1^+$ levels are found in adjacent $^{78,82}$Ge at 2706 and 2714 keV, respectively. Therefore, the calculated positions are well within the range where a $1^+$ level might be located. Hoff and Fogelberg showed $\gamma$ rays at 2665 and 2008 keV that could be placed as depopulating a possible $1^+$ level at 2666 keV. This is in agreement with the calculated positions.

Many of the transitions in $^{80}$Ge beyond the [pf7] group include a change in parity. Therefore, NuShellX was used to determine the occupation and level energies of the negative-parity states. 61 levels are predicted in the jj44b calculations below 4500 keV, but only 13 have negative parity. Similarly, the jun45 interaction

resulted in 71 levels where 15 had negative parity. Only 23 levels have been identified experimentally, and only seven are identified with negative parity (Fig. 4.5).

The energies of the first three calculated negative-parity states in the jj44 model space agree well with the experimental levels. Both the jj44b and jun45 interactions predict that the lowest negative-parity states are $5^-$, $4^-$ and $3^-$ levels. In this energy range of $\sim 3400$ keV, a $6_1^-$ state has been observed. It is predicted to be $> 4$ MeV with both interactions. These interactions also predict that the first $7^-$ level will be $\sim 600$ keV above the first experimental state.

In summary, in the jj44 model space, the jj44b and jun45 interactions depict the [pf7] states well. They correctly identify the energy range and level order of the first three negative-parity states.

## 5.6 N=46 isotone systematics

The $N = 46$ isotones with 4 holes in the $\nu g_{9/2}$ orbital, can be viewed as mid-shell nuclei. The high energy of the $2_1^+$ state in $^{74}$Ni is due to the closed $Z = 28$ shell. There is an increase in collectivity above $Z = 28$, and this may lead to lower energies for the $2^+$ and $4^+$ states. The $3^+$ state in $^{80}$Se and $^{82}$Kr is nearly identical in excitation energy, but is significantly lower in $^{78}$Ge. Many of the transitions in the positive-parity sequences of $^{80}$Se and $^{82}$Kr have consistent energies. However, the $\gamma$ rays which feed from the negative-parity states are unique in character. The energies in $^{78}$Ge are lower than those of the heavier isotones With the exception of the $0_2^+$ and $4^-$ states. This can be interpreted as a different underlying character in

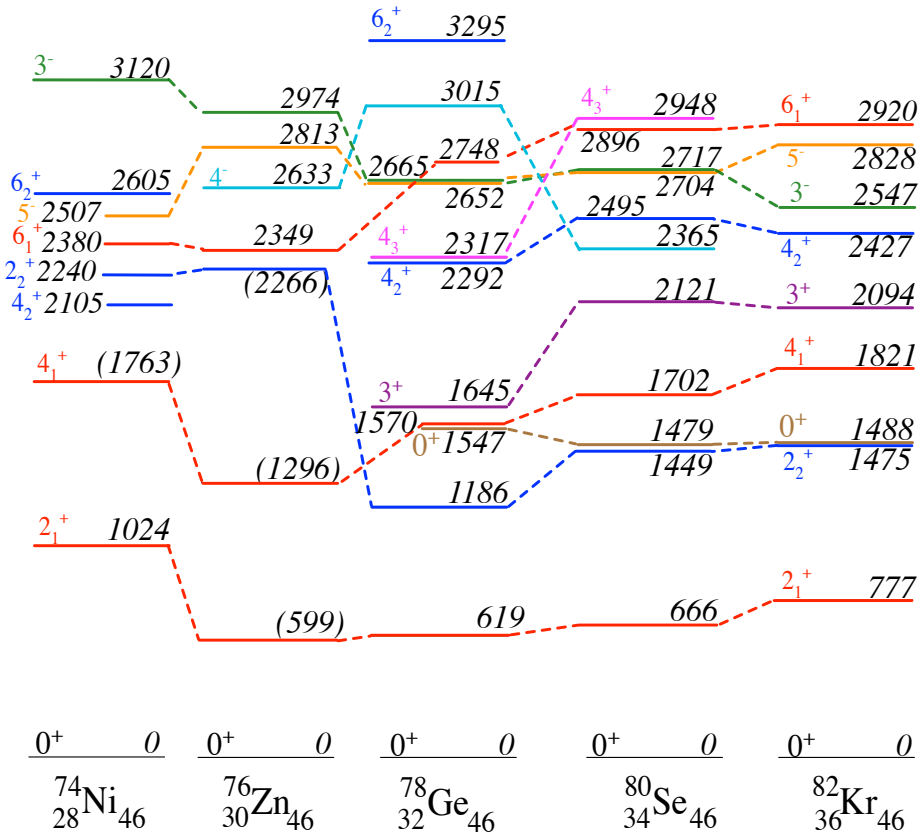


Figure 5.7: $N = 46$ low energy isotonic characteristics. Levels with energies in parenthesis have not been established. The data are taken from NNDC and work not covered by the scope of this thesis. Not all levels are shown.

this nucleus.

The 2240-keV ($2_2^+$) state and 2105-keV $4_2^+$ level in $^{74}$Ni have been reported in separate papers. It is unusual for the $2_2^+$ state to be higher in energy than the $4_2^+$ one. The $2_2^+$ levels in $^{74}$Ni and $^{76}$Zn are close in energy, and they are almost as high as the $4_2^+$ states in other isotones. These factors raise the possibility that the states have been incorrectly identified, and suggests that lower-energy states have been missed.

## 5.7 $^{78}$Ge

The strongest transitions identified within this work come from the PPP data. States with fewer than three coincident $\gamma$ rays are confirmed through cross correlation and delayed spectra. The change in the $J^\pi$ assignment of the $^{78}$Ga $\beta$-decay parent impacts the interpretation of much of the subsequent published work. It also affects the assignment possibilities of ten states [102]. Direct population via allowed and first-forbidden transitions is limited to $1, 2$ or 3. The $4^+$ levels are populated through first-forbidden unique transitions, and the $5^-$ levels could be fed directly only by highly-inhibited third-forbidden unique transitions. The states observed in the (t,p) works are largely low-spin levels with natural parity of: $0^+$, $1^-$, $2^+$, $3^-$, and so on. These observations, along with angular correlations (Figs. 3.8, 4.16), provide insight into the presently-proposed $J^\pi$ assignments.

Below 3 MeV, the 2744-, 2759-, and 2850-keV levels seen in (t,p) reactions with spin-parity assignments of $3^-$, $[(3^-), (4^+)]$, and $5^-$, cannot be reconciled with

present observations. The closest levels from $\beta$ decay are a $1^+$ state at 2706 keV and a $(2,3)$ level at 2857 keV. Above 3 MeV, there is little overlap between DIS and (t,p) data sets. This is because most levels populated in the (t,p) reaction are low-spin levels with little overlap with the higher-spin levels populated in the DIS reactions. The levels observed within this energy range based on GS data are the 2748-keV $6_1^+$ state, and a 2760-keV $5^+$ one. The (t,p) experiments designate these states as the lowest-energy $3^-$ levels in contrast with the $\beta$-decay $3^-$ state at 2665 keV.

### 5.7.1 The $\kappa$ band

The double-coincidence gate on the non-yrast 567-keV $2_2^+ \rightarrow 2_1^+$ $\gamma$ ray with the 619.2-keV $2_1^+ \rightarrow 0_1^+$ transition produces a distinct sequence. It includes the 1644-, 2319-, 2760-, and 3295-keV levels with the respective spin-parity assignments of $3^+$, 4, $5^+$, $6^+$. In $^{72,74,76}$Ge, similar sequences built on the $2^+$ have been labelled a $\gamma$ bands (see Sec 5.7.3.1) [34, 46, 49]. They have been interpreted as a "softness" toward loss of axial symmetry. However, the decay pattern of the $^{78}$Ge sequence is unique, so it is labelled the "$\kappa$(kappa)-band", short for $\kappa\alpha\iota\nu o\acute{\upsilon}\rho\gamma\iota o\varsigma$, "new" in Greek. In $^{78}$Ge, the low excitation energy of the $2_2^+$ and $3^+$ states may that indicate these states are non-axially symmetric. This leads to an important question. Does this sequence indicate rigid triaxiality in $^{78}$Ge?

This sequence of levels is quantitatively different from similar sequences in the neighboring Ge and Se nuclei, since the decay proceeds strictly through $\Delta J = 1$

transitions. The half-life measured by Chou *et al.* [105] for the $4^+_\kappa$ level can be used to show that the transition rate for this $\Delta J = 1$ transition is very low. This implies the $\Delta J = 2$ transitions are inhibited by the quantum matrix elements of the state, not by the speed of the $\Delta J = 1$ transition. This characteristic is critical to the interpretation, therefore a step-by-step explanation follows. Chou *et al.* measured the lifetime ($\tau$) of the $4^+_\kappa$ level as 62(8) ps [105]. Through the relation of $t_{1/2} = ln(2) * \tau$, the half-life of this state is 43.0(5.5) ps. This gives an upper limit for the transition probability ($B(E2)$) for the 1133-keV $4^+_\kappa \rightarrow 2^+_\kappa$ $E2$ cross-over $\gamma$ ray. It also can be used to estimate the $B(E2)$ value for the 674.6-keV $\Delta J = 1$, $4^+_\kappa \rightarrow 3^+_\kappa$ transition. The measured upper limit for the branching ratio of the unobserved 1133-keV transition is $\leq 2\%$, which indicates a partial half-life of 2.15(28) ns. A 15.3 ps half-life can be inferred for this transition using the Weiskopf estimate. This half-life, in turn, yields a $B(E2)$ upper limit of 0.007(1) W.u. This limit can be compared to the value of $B(E2) = 18(8)$ W.u. [105] for the 913-keV, $4^+_\gamma \rightarrow 2^+_\gamma$ cross-over transition in $^{76}$Ge. This highlights the difference in character between the bands in the two nuclei (Fig. 5.9). Estimates are also possible for the $B(E2)$ and $B(M1)$ values for the 674.6-keV $\Delta J = 1$ $4^+_\kappa \rightarrow 3^+_\kappa$ transition. If the $E2/M1$ mixing is determined to be 50%, partial $M1$ and $E2$ half-lives of 86 ps would be deduced. The calculated Weiskopf half-lives for $M1$ and $E2$ transitions are 72 fs and 20 ps, respectively. These lead to $B(M1)$ and $B(E2)$ estimates of 0.0085(2) and 2.4(1) W.u., respectively for the comparable transitions in $^{76}$Ge. Note that the maximum $B(M1)$ value for $^{78}$Ge would be 0.0017 W.u., or of the same order as in $^{76}$Ge. If the transition were to be pure of $E2$ character, the $B(E2)$ value would

double to 4.8 W.u. The cross-over $\gamma$ rays are *not* missing in the $\kappa$ band, but may result from the especially fast $\Delta J = 1$ transitions.

Zamfir and Casten [24] found the separation between the $5^+_\gamma$ and $3^+_\gamma$ states was a reliable measure of the collective frequency for $\gamma$ bands. There are few states with similar spins and parities with which to mix, so there are few chances for perturbation. The $5^+_\kappa \rightarrow 3^+_\kappa$ transition energ for the $\kappa$ band at 1116 keV is large. However, it is still well below the calculated $5^+_\gamma \rightarrow 3^+_\gamma$ separation of 1391 keV in $^{78}$Ge. It is also above the 948-keV one observed value in $^{76}$Ge, and in line with the calculated value in $^{76}$Ge. The comparisons between calculated and observed levels in $^{76}$Ge, shown in Fig. 7 of Ref. [55]. They reveal the same trend in which the observed levels are well below their calculated counterparts. This holds for both the ground-state band and $\gamma$ band, but with branching from the $\gamma$ band levels well described by the calculations. Above the $3^+$ state in the $\kappa$ band ($3^+_\kappa$), there are no cross-over transitions feeding into the ground-state band.

Two theories of deformed nuclei were proposed by Wilets and Jean, and also Davydov and Fillipov. They state that the $\Delta J = 2$ crossover intra-band transitions tend toward zero as $\gamma$ approaches 30° for both vibrational and rotational structures. The quenching of the $\Delta J = 2$ transitions in $^{78}$Ge was measured using relative intensities as described in Section 3.6.1. Upper limits for the branching ratios (Tab. 5.1) can be inferred from the relative intensities of the missing transitions to those in Figure. 4.17.

Another "indicator" of the rigidity of the non-axial structures is the staggering parameter (Discussed in Chapter 1). Table 5.2 lists these values for the $\kappa$-band

Table 5.1: Upper limit intensities of missing $E2$ transitions in $^{78}$Ge.

| $E_{i,\text{lev}}$ (keV) | $E_\gamma$ (keV) | $E_{f,\text{lev}}$ (keV) | Relative Intensity upper limit | % Branching ratio upper limit |
|---|---|---|---|---|
| 3295 | 976* | 2319 | 2.5 | 7.4 |
| 2760 | 1116 | 1644 | 0.1 | 0.3 |
| 2760 | 1190 | 1570 | 0.6 | 2.2 |
| 2319 | 1700 | 619 | 0.1 | 0.2 |
| 2319 | 1134 | 1186 | 0.6 | 1.1 |
| 2319 | 749 | 1570 | 0.6 | 1.1 |

* indicates the transition intensity is inflated by contamination in spectra from the 976.5 keV transition in the $^{76}$Ge beam.

Table 5.2: Staggering values $S(J)$ observed in the even $_{32}$Ge and $_{34}$Se isotopes for $J = 4, 5, 6$.

| | $^{78}$Ge$_{46}$ | $^{76}$Ge$_{44}$ | $^{74}$Ge$_{42}$ | $^{72}$Ge$_{40}$ |
|---|---|---|---|---|
| $S(4)$ | 0.35 | 0.09 | -0.04 | -0.24 |
| $S(5)$ | -0.40 | -0.03 | 0.11 | 0.26 |
| $S(6)$ | 0.20 | 0.15 | 0.14 | -0.35 |
| | $^{80}$Se$_{46}$ | $^{78}$Se$_{44}$ | $^{76}$Se$_{42}$ | $^{74}$Se$_{40}$ |
| $S(4)$ | -0.36 | -0.25 | -0.16 | -0.53 |
| $S(5)$ | | 0.25 | 0.15 | 0.4 |
| $S(6)$ | | -0.17 | 0.03 | -0.28 |

sequence in $^{78}$Ge along with those of the $^{72,74,76}$Ge isotopes and the $^{74,76,78,80}$Se isotones. The absolute $S(J)$ values for $^{78}$Ge are larger than the values of the other nuclei listed. The phases of $^{76}$Ge and $^{78}$Ge have positive staggering values for $S(4)$ and $S(6)$, which contrast to those of $^{72,74}$Ge and all of the Se isotones. On the strict basis of phase, $^{76}$Ge has been proposed to have rigid triaxiality. The $^{72,74}$Ge nuclei have been also interpreted as $\gamma$-soft [34] on the basis of staggering value. This is because there is no inclusion of $\Delta J = 2$ cross-over transition in this interpretation. What is clear from the staggering values of $^{78}$Ge is that the energy spacing of the

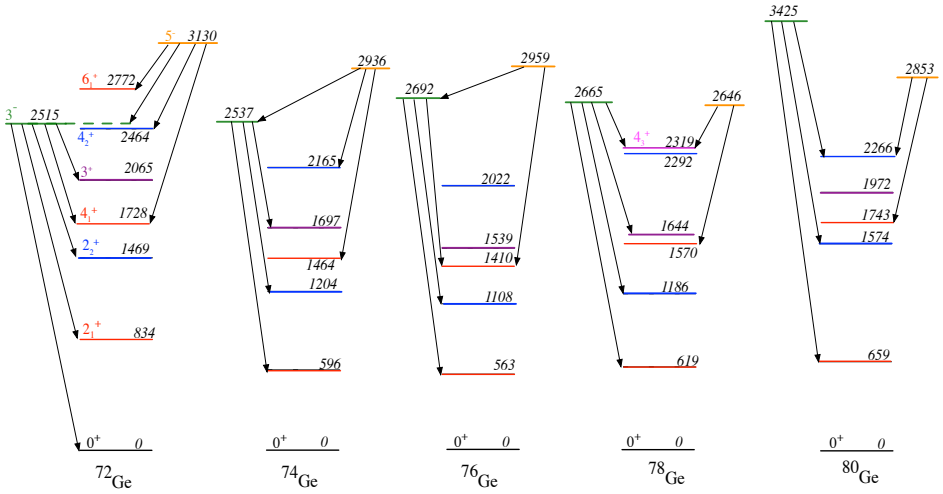


Figure 5.8: Decay of the $3^-$ and $5^-$ states in even-A $^{72-80}$Ge.

$\kappa$ band is not in line with the $J(J+1)$ characteristic of a symmetric rotor. The spacing is irregular, which is more typical of oblate structures at higher excitation energies.

### 5.7.2 $E1$ transitions in and out of the $\kappa$ band

If the $\kappa$ band is considered to indicate triaxiality or shape coexistence in $^{78}$Ge, the strong $E1$ transitions which connect this sequence to the ground state band through negative-parity states, must be considered in detail. The negative-parity states in $^{78}$Ge result from breaking $\nu g_{9/2}$ pair into a negative parity orbital $(p, f, h)$. The $5^-$ level can be populated either by a $g_{9/2}f_{5/2}$ or $g_{9/2}p_{1/2}$ coupling (Tab. 1.4). The lowest $3^-$ state has mixed character, resulting from collective excitations and two-particle neutron structures. The $5^-$ state at 2646 keV and the $3^-$ one at 2665 keV are the lowest negative-parity states in the nucleus. Above $N = 40$, the $5^-$

level decreases in energy to reach a minimum at 2646 keV in $^{78}$Ge (Fig. 5.1). At this point it has lower excitation energy than the $3^-$ level. In $^{80}$Ge, the $5^-$ state rises to an excitation energy seen in $^{74,76}$Ge. However, it remains lower than the $3^-$ level, which has increased dramatically by $\sim 550$ keV.

The $5^-$ state in $^{78}$Ge is fed by a 649.2-keV transition from the $6^+_\kappa$ state with an $I_{rel} = 8.5(4)$. It is also fed by a 113.9-keV $\gamma$ ray from the $5^+_\kappa$ state with an $I_{rel} = 3.2(7)$. The $5^-$ state decays back into the the $\kappa$ band by a 327.1-keV transition with an $I_{rel} = 6.8(5)$ (Fig. 4.17). There is significant additional feeding into the $5^-$ level from by the 3285- and 3689-keV states and others states not yet observed. The 1076-keV decay into the $4^+_1$ state has an intensity of $I_{rel} = 28.8(4)$. The intensity carried by the 1076-keV transition is only 16% smaller than the intensity of the $6^+_1 \rightarrow 4^+_1$ 1178.8-keV one. Both of these transitions are easily seen in a double gate on the $4^+_1 \rightarrow 2^+_1$ and $2^+_1 \rightarrow$ g.s. coincidence spectrum (Panel (a) of Fig. 4.14).

In $^{78}$Ge, the $3^-$ state has been well characterized through $\beta$-decay as only $\sim 20$ keV above the $5^-$ level [102]. The $3^-$ state feeds the $2^+_2$, $3^+_\kappa$, and $4^+_\kappa$ states by a combined 73(13)% of the decay, while the remaining percentage feeds into the $2^+_1$ level. No feeding was found into the $4^+_1$ state, suggesting that the $3^-$ may be in the same potential well as the $\kappa$ band if shape coexistence were found to exist. Feeding from the $3^-$ and $5^-$ states is a major contributor to the intensity of the $\kappa$ band. The cause of the inversion of the two states cannot be clearly identified. It could be a significant factor in their ability to feed both the ground state band above $2^+$, and the $\kappa$ band.

A comparison of the decay characteristics of the $3^-$ and $5^-$ states in the Ge

isotopes is found in Fig. 5.8. The $5^-$ level feeds into the $4_1^+$ state in all isotopes. This $5^-$ state has been found to also feed the $3^-$ level Below $N = 46$. In $^{76,78}$Ge, the $5^-$ level does not feed the $4_2^+$ state at all. Instead, in $^{78}$Ge, decays into the $4_3^+$ state. The $4_2^+$ level is only fed by the $3^-$ state in $^{82}$Ge, even though it is energetically available to the $4_2^+$ state in $^{74-78}$Ge. The $3^-$ level in $^{78}$Ge decays to the $4_3^+$ state instead of to the $4_2^+$ level. This must be caused by a factor other than energy, since the two $4^+$ states are less than 40 keV apart. This is another example of the selective decay.

The $3^-$ energies in $^{76}$Ge and $^{78}$Ge are very similar at 2692 and 2665 keV, respectively. The branching pattern of the two nuclei is shown in Table 5.3. The half-life of the $3^-$ level in $^{76}$Ge is 0.231(20) ps [55]. While the level in $^{78}$Ge it is 4.2(25) ps [105], which is 18.2 times slower. The transition rates of $3^- \rightarrow 2_2^+$ $\gamma$ ray are quite similar even though they have different branching ratios. The main transition out of the $3^-$ state in $^{76}$Ge is to the $2_1^+$. The counterpart in $^{78}$Ge has three times that value. Although the $3^- \rightarrow 2_1^+$ $\gamma$ rays have similar energy in the two nuclei, the transition in $^{78}$Ge is significantly slower as seen from its partial half-life. The $3^- \rightarrow 2_1^+$ transition is hindered by a factor of 200 based on the ratio of the $B(E1)$ values. Since the $E1$ transition to the $2_1^+$ state is suppressed in $^{78}$Ge, decay within the $\kappa$ band can compete.

Table 5.3: $3^-$ decay and in $^{76}$Ge and $^{78}$Ge. The $B(E1)$ values were determined by using the half-lives of the $3^-$ states as 0.231(20) ps [55] in $^{76}$Ge and 4.2(25) ps [105] in $^{78}$Ge. The branching ratios (B.R.) for each transition (from Refs. [55, 102]) are used in conjunction with the half-life of the state to determine the partial half-lives for each transitions (partial $t_{1/2}$). The calculated partial half-life (calc $t_{1/2}$) was determined using Weiskopf estimates. The $E1$ reduced transition probability is calculated from the ratio of the calculated partial half-life to the partial half-life. This $B(E1)$ value offers a measure of hindrance of the transition between the two states.

| $^{76}$Ge | | | | | |
|---|---|---|---|---|---|
| Transition | $E_\gamma$ (keV) | B.R. | partial $t_{1/2}$ (ps) | calc. $t_{1/2}$ (ps) | $B(E1)$ |
| $3^- \rightarrow 4_1^+$ | 1282.35(5) | 10.7(7) | 2.16(19) | $1.78 * 10^{-2}$ | $8.25 * 10^{-3}$ |
| $3^- \rightarrow 2_2^+$ | 1593.93(3) | 5.4(6) | 4.28(37) | $9.44 * 10^{-5}$ | $2.21 * 10^{-5}$ |
| $3^- \rightarrow 2_1^+$ | 2129.34 | 83.9(33) | 0.275(24) | $3.89 * 10^{-5}$ | $1.41 * 10^{-4}$ |
| $^{78}$Ge | | | | | |
| Transition | $E_\gamma$ (keV) | B.R. | partial $t_{1/2}$ (ps) | calc. $t_{1/2}$ (ps) | $B(E1)$ |
| $3^- \rightarrow 4_3^+$ | 346.1(1) | 25.8(38) | 16.2(97) | $8.9 * 10^{-3}$ | $5.48 * 10^{-4}$ |
| $3^- \rightarrow 3_1^+$ | 1021.9(1) | 6.0(15) | 70(42) | $3.46 * 10^{-4}$ | $4.92 * 10^{-6}$ |
| $3^- \rightarrow 2_2^+$ | 1478.7(2) | 40.7(27) | 1.03(61) | $1.14 * 10^{-4}$ | $1.11 * 10^{-5}$ |
| $3^- \rightarrow 2_1^+$ | 2045.8(2) | 27.4(27) | 15.3(91) | $4.30 * 10^{-5}$ | $2.80 * 10^{-6}$ |

### 5.7.3 How unique is the $\kappa$ band sequence?

The degree of uniqueness of the $\kappa$ band can be assessed experimentally or theoretically by its modes of decay.

**1. Experimental Approach**: The level and decay structure found in the $\kappa$ band can be compared with similar levels in other even-A Ge nuclei, and isotonic, $N = 46$ nuclei (Section 5.7.3.1).

**2. Theoretical Approach**: The degree of agreement between the experimental findings in $^{78}$Ge and the calculated values produced by shell-model calculations and other theory can determine if the $\kappa$ band characteristics are reproducible (Sec-

tion 5.7.4).

#### 5.7.3.1 $\kappa$ band in comparison to neighboring nuclei

A comparison of the structure of $^{78}$Ge with its isotonic ($N = 46$) and isotopic ($Z = 32$) neighbors emphasizes the similarities and differences which make the $\kappa$ band unique.

$^{74}_{28}$**Ni**: Little is known of the structure of the nucleus except members of the yrast band and a $(3^-)$ state at 3120 keV. Unlike the $2^+_2$ state in $^{78}$Ge, the $(2^+_2)$ state in $^{74}$Ni is above the yrast $4^+_1$ state. The $(2^+_2)$ and $(3^-)$ states decay directly to the $0^+$ ground state without de-excitation into other states. The $4^+_1$ state of $^{74}$Ni is nearly equivalent in energy to the $4^+_1$ one of $^{78}$Ge. However, this does not resolve the occurrence of the $\kappa$ band.

$^{76}_{30}$**Zn**: The structure of $^{76}$Zn is vastly different and few states are known. The location of a low $(2^+_1)$ state at 596 keV is similar to the other $N = 46$ isotones. A $4^+_1$ state at 1296 keV is followed by a tentative $2^+_2$ state at 2292 keV. The depression of the $4^+$ level and the strong elevation of the $(2^+_2)$ state produce strong differences between $^{76}$Zn and $^{78}$Ge.

$^{80}_{34}$**Se**: The $E_4/E_2$ ratio in $^{80}$Se (Fig. 5.9) is above that of the 2.5 prediction of an asymmetric rotor, like $^{78}$Ge. The $2^+_2$ state of $^{80}$Se is pushed higher by the additional two protons. The states feed into the $2^+_2$ level are also higher than their $^{78}$Ge counterparts. The $4^+$ state of this sequence is notable as the third $4^+$ level in the nucleus, identical to the one in $^{78}$Ge. Unlike $^{78}$Ge, this $4^+_3$ state in $^{80}$Se decays by

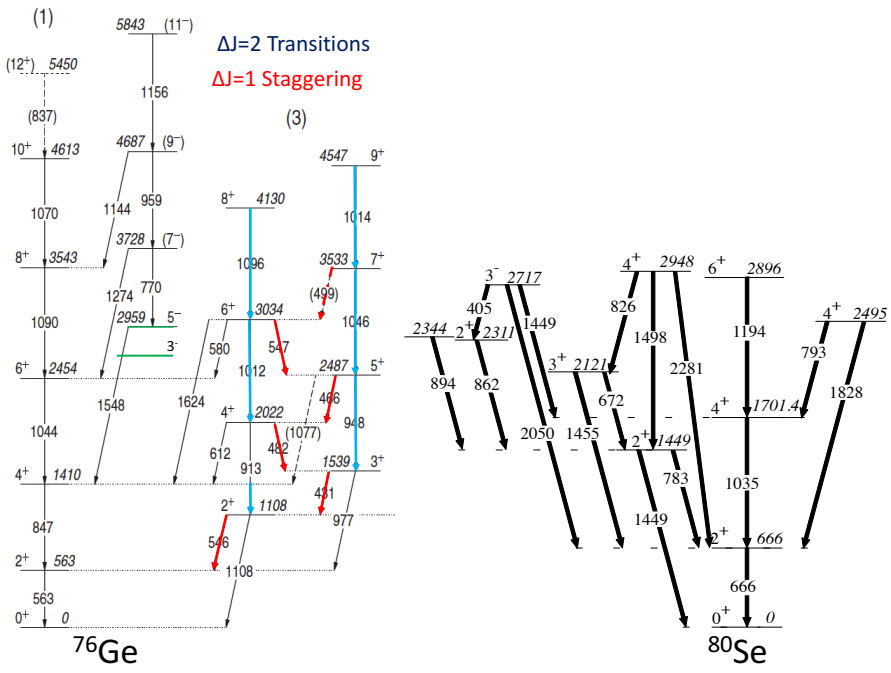


Figure 5.9: Partial level schemes for $^{76}$Ge [34] and $^{80}$Se [107] to highlight the structures built on the $2_2^+$ levels. In the $^{80}$Se scheme, the intensities of transitions from the $2_2^+$ state have been included. These were reported in the $\beta$ decay of $^{80}$As.

two $\Delta J = 2$ transitions to the lowest $2^+$ states in addition to a $\Delta J = 1$ transition to the $3_1^+$ level. The $3_1^+$ state decays in a identical manner to its counterpart in $^{78}$Ge.

$^{82}_{36}$**Kr**: The decay of the $3_1^+$ level at 2094 keV in $^{82}$Kr feeds the $2_1^+$, $2_2^+$, $4_1^+$ and $(2_3^+)$ states. The $(4_2^+)$ state decays to the $2_1^+$, $2_2^+$, $4_1^+$, and $3_1^+$ levels. The $4_3^+$ level in $^{82}$Kr decays to all the lower-lying states, including the $(4_2^+)$ state, *except* for the $3_1^+$ level. Any hypothesis for why the $(4_3^+)$ state does not decay to the $3_1^+$ level is beyond the scope of this thesis. In summary, a $\gamma$ band consists of states with spins $2^+, 3^+, 4^+$, and $5^+$, but without $4_2^+ \rightarrow 3_1^+$ and $5_1^+ \rightarrow 4_2^+$ $\Delta J = 1$ transitions [28].

$^{72}$**Ge**: The $\gamma$ band of $^{72}$Ge has both $\Delta J = 1$ and $\Delta J = 2$ transitions. The $2_2^+$

state at 1464 keV decays with a 87(10)% branching ratio to the $2_1^+$ state. This is significantly larger than the $\sim 50\%$ probability in $^{78}$Ge. The $2_2^+$ state also exhibits a small branch to the low-lying $0_2^+$ state at 691 keV. Both the $3_1^+$ level and the $4_2^+$ state have a small branch to the $4_1^+$ state.

**$^{74}$Ge**: Up to the $5^+$ state, $^{74}$Ge exhibits a $\gamma$ band with intra-band $\Delta J = 1$ and $\Delta J = 2$ transitions. It also has inter-band transitions to the yrast sequence. The $6_2^+$ state at 3315 keV has been reported to solely feed the $4_\gamma^+$ level [49]. However, there is evidence that it also feeds the yrast $6^+$ state by a 764.4-keV transition and the $5_\gamma^+$ level by a 618.9-keV one in the GS data [107]. The $(7_1^+)$ level does not feed any $6^+$ state, but only the $5_\gamma^+$ one. This breaks down feeding found in the $\gamma$ band sequence above 3 MeV. The $3_1^-$ and $5_1^-$ states feed both positive-parity sequences (yrast and $\gamma$ band).

**$^{76}$Ge**: A $\gamma$ band up to $6^+$ has been reported [34] with $\Delta J = 1$ and $\Delta J = 2$ intra-band transitions. It also has inter-band transitions with the yrast sequence (Fig. 5.9). Higher spins, up to $9^+$, have been attributed to the $\gamma$ band, but with only intra-band $\Delta J = 2$ transitions observed. The energy spacing of the $\gamma$-band states is similar to the spacing of the $\kappa$ band in $^{78}$Ge. The branching ratios of the $3_1^+$ state in the two nuclei are similar with about 40% decaying to the $2_2^+$ state. Above the $3_1^+$ state, the level structure of the two nuclei are different. The $5_1^-$ level in $^{76}$Ge lies much higher than the $5_1^+$ state. In fact, the negative-parity states in $^{76}$Ge feed only the yrast sequence, and not the $\gamma$ band.

**$^{80}$Ge**: There is no clear sequence of states built upon the $2_2^+$ level in $^{80}$Ge. The $3_1^+$ has been observed, but no $4^+$ state has been found to decay into it. The $5_1^+$ state at

3038 keV decays into the $4_1^+$, $4_2^+$ and $3_1^+$ levels, but could not be confirmed in this work.

**$^{82}$Ge**: The $3_1^+$ state is higher in energy than the $4_2^+$ state. This precludes the $4_2^+$ level as a member of a $\gamma$-like band. A 180-keV, $4_3^+ \rightarrow 3_1^+$ transition was not observed. Such a low-energy $\gamma$ ray would be hindered as discussed in Section 4.2.2. In both $^{82}$Ge and $^{80}$Ge, the lowest $3^+$ level is well reproduced as a part of the [pf7] group and it can be described as a unique structure consisting of a $f_{5/2}$ proton coupled to a $p_{3/2}$ proton.

### 5.7.4 Theoretical descriptions of $^{78}$Ge

The structure and shape of $^{78}$Ge have been investigated using three categories of models. These include the interacting boson model (IBM) [112–115], self-consistent mean-field (SCMF) models [52, 106, 114, 116–118], and shell models [35, 36, 119–123]. $^{78}$Ge has also been studied for the existence of triaxiality and shape deformation by various theoretical means including the shell model [119, 120, 122, 124], density functional theory (DFT) [49, 106, 125], mean field approach [126], and also an algebraic description [127]. Refs. [49, 104, 114, 117, 128] report that there is prolate deformation in $^{78}$Ge with $\beta \sim 0.2$. The IBM-2 configuration mixing approach predicted shape coexistence with a prolate ground band and a spherical excited band [127]. Ardouin *et al.* performed Hartree-Fock (HF) calculations on the Ge nuclei and they found a possible oblate to prolate shape transition of the ground

state between $N = 36$ and $N = 46$ [56]. Their work characterizes the $0_2^+$ state in even-even Ge nuclei as non-collective. They also determined that $^{76}$Ge and $^{78}$Ge were both prolate rotators and that $^{74}$Ge has maximum triaxiality ($\gamma \sim 30°$) by the Davydov model [52]. Nilsson, Ragnarsson, Larsson, and Sheline proposed triaxial shell closures at $N = 44, 46$ and $Z = 32$, making the Ge isotones magic and $^{76,78}$Ge double-magic nuclei.

Nikšić *et al.* used relativistic Hartree-Bogoliubov (RHB) triaxial quadrupole energy maps. They found an axially symmetric minimum on the prolate axis for $^{76-80}$Ge [106]. They also reported that the $^{78-80}$Ge nuclei have a $\gamma$-soft potential due to the calculated staggering values [106]. Yoshinga and Hiashiyama also found evidence for $\gamma$-softness in $^{78}$Ge by their neutron contour plot of the potential energy surface using Nilsson states [129]. Hsieh *et al.* concluded that the $4_3^+$ state of $^{78}$Ge is dominated by the N-1-boson-plus-two-$f_{5/2}$-fermions configuration. They used IBM with fermion pair model calculations [112], but did not include the state in a triaxial band.

It is possible to compare the experimental levels from this thesis to the theoretical levels produced by Yoshinga and Hiashiyama [129]. The experimental levels are generally in close agreement with the shell model (SM) and generator coordinate method (GCM) triaxial calculations. They attributed the 1186-keV $2_2^+$ and 2319-keV $4_3^+$ non-yrast states to the $\gamma$ band. The authors used the $6^+$ level at 3287 keV published in the (t,p) work as the experimental yrast state [103]. They did not use the published $6_1^+$ energy of 2748 keV. The calculated yrast $6^+$ state in all models is therefore too high. Yoshinga and Hiashiyama calculated the $3^+$ level at energies of

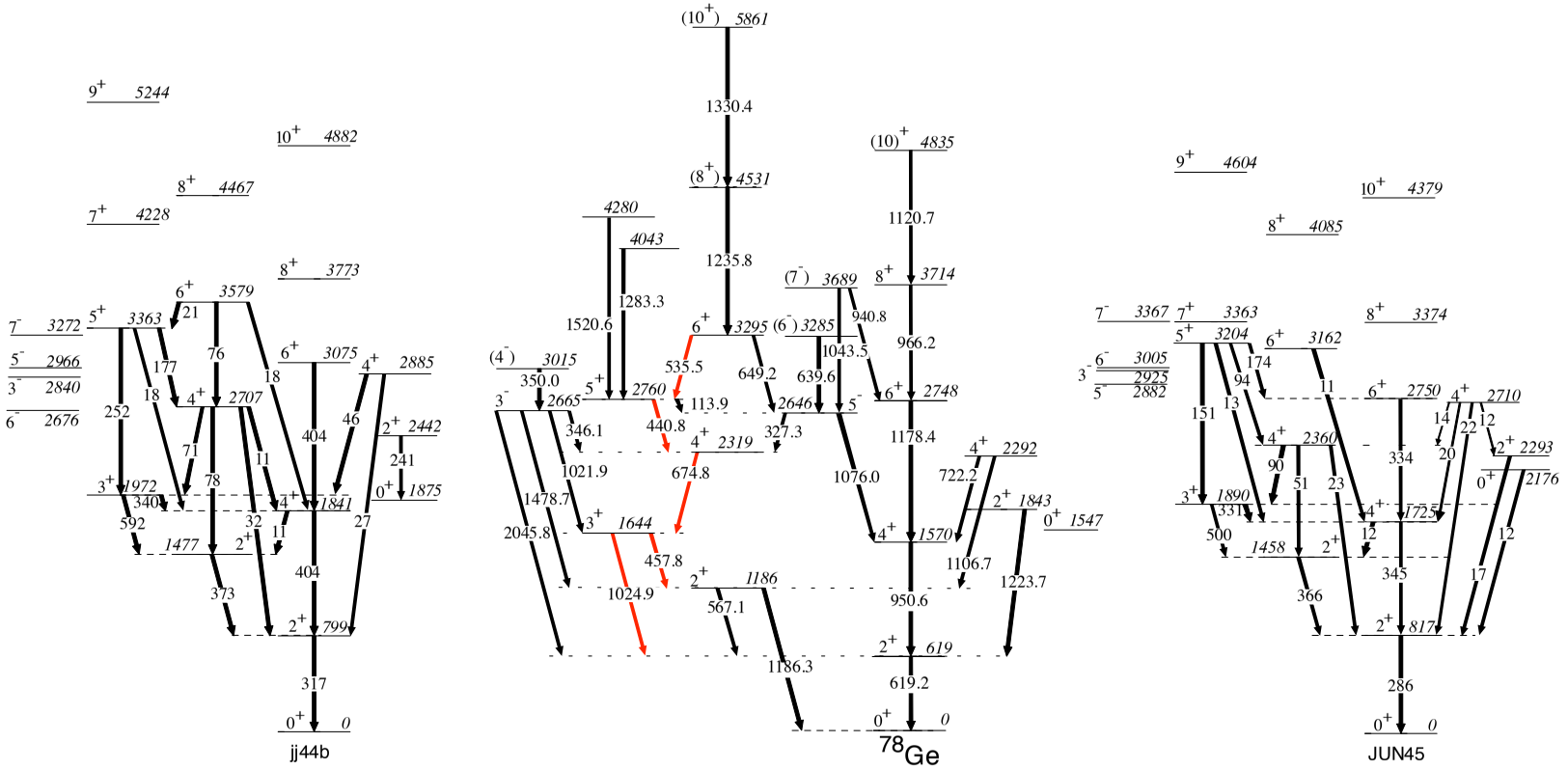


Figure 5.10: $^{78}$Ge experimental levels and transition energies (center) and NuShellX level energies and $B(E2)$ values in the jj44b (left) and jun45 (right) model spaces.

$\sim$ 1700 and $\sim$ 2130 keV for the SM and triaxial GCM. The axial GCM predicts the $3^+$ state around 2500 keV. This thesis reports the $3^+$ state is at 1644 keV, in strong agreement with the SM calculation. The $5^+_\kappa$ state is observed at 2760 keV, which is only a few keV below the $6^+_1$ state. The SM predicts the $5^+$ and $6^+_1$ levels to be at the same energy around $\sim$ 3150 keV. The GCM calculations predict the $5^+$ level at several hundred keV above the yrast $6^+$, and also above 3 MeV. The energies of the yrast $8^+$ or $10^+$ states had not been determined when Yoshinga and Hiashiyama conducted their study. They predicted the $8^+_1$ level at about 300 keV too high (in SM and triaxial GCM) and at 700 keV too high in axial GCM. They also predicted the $10^+_1$ level well in the SM and triaxial GCM, a value just below 4 MeV.

All of the theoretical works for $^{78}$Ge show no indication that the nucleus is unique in missing the $\Delta J = 2$ transitions in the $\kappa$ band. The shell-model calculations in this thesis using the NuShellX jj44b and jun45 interactions are presented in Fig. 5.10 with the calculated $B(E2)$ values. The $^{78}$Ge levels from the NuShellX calculation represent a smooth evolution of a similar structure to $^{76}$Ge [55]. In $^{78}$Ge the calculated position of the $8^+$ level, largely a $(g_{9/2})^2$ configuration, is well reproduced. The lower-energy members of the ground-state band are systematically well above the experimental level energies. The lowest seniority-four state, the $10^+_1$ level, has a calculated value within 50 keV of the experimental value.

Both models predict a band built on the $2^+_2$ state. The levels are located higher in energy than their experimental counterparts. In both instances, the band includes strong $\Delta J = 2$ transitions in the $\kappa$ band. In the models, the $6^+_2$ level decays 98% to the ground state band. Multiple decay modes from the $4^+_\kappa$ level

are present in the theoretical results. This is in contrast to the single transition identified experimentally. It is important to emphasize that the $4^+$ level of the $\kappa$ band is the $4_3^+$ state. It is not the $4_2^+$ one as is the $4_\gamma^+$ state in other Ge nuclei. The $4_3^+$ state is calculated at 2886 keV with the jj44b and 2710 keV with the jun45 interactions. This does not have the decay pattern that feeds the $3_1^+$ and $2_2^+$ states. The $4_3^+$ state is predicted to feed the ground state band with a branching ratio $> 90\%$. The theoretical $3_1^+$ state has a high transition probability to the $4_1^+$ level.

The $6_\kappa^+ \rightarrow 5_1^- \rightarrow 4_1^+$ cascade has not been observed in any other nucleus in this region. These strong $E1$ transitions are another unusual feature in the decay of $^{78}$Ge. This is the only instance of linking observed between the $\kappa$ band and yrast sequence above the $2_2^+$ state. The $3_1^-$ level observed in $\beta$ decay feeds all accessible levels of the $\kappa$ band but not the yrast states. The calculated level energies for the $3^-$ level at 2676 keV and $5^-$ state at 2942 keV are compressed in energy. However they appear more compressed in experiment. NuShellX does not describe branching between negative- and positive-parity levels. As a result, a different method must be used to investigate the strong $E1$ decay. The $5^-$ state in the jj44b calculation is close to the $6_1^+$ level. This is in agreement with experimental results. Neither model predicts the $3^-$ state to be the first excited negative-parity state. The jun45 calculation returns it at a higher energy than the $5^-$ state.

The staggering phase and amplitude can be determined for the models using levels calculated by NuShellX. These values, along with 5DCH values from Ref. [49] demonstrate that these models do not reflect the behavior of the $\kappa$ band in $^{78}$Ge accurately. This phenomenon ca be clearly seen as a difference in staggering in

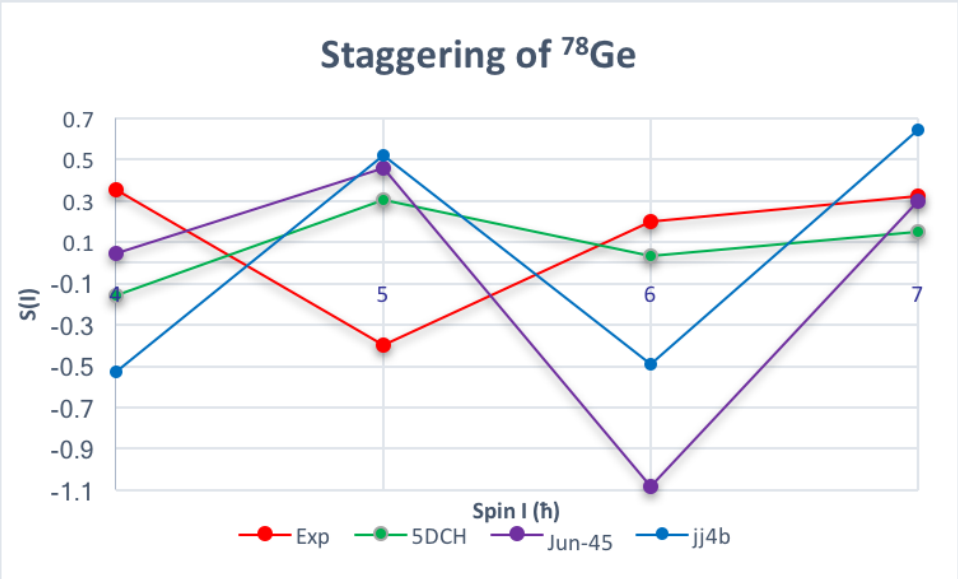


Figure 5.11: Experimental and theoretical staggering in $^{78}$Ge. 5DCH values from Ref. [49], jj44b and jun45 values provided in this work.

Figure 5.11.

Since the shell model fails to describe the $\kappa$ band, another approach is necessary. These include calculations within the Davydov-Filippov-Rostovsky (DFR) model at higher excitation energies [19, 20]. The decay pattern and $B(E2)$ values for a rigid-triaxial rotor with $\gamma = 30°$ are found in Fig. 5.12. These energies have been normalized to a $2_1^+ \rightarrow 0$ transition of 619 keV. The $2_2^+$ and $3_1^+$ levels have the low excitation energies expected for a rigid triaxial nucleus. The model predicts a strong transition from the $2_2^+$ level to the $2_1^+$ state and also a completely suppressed transition to the ground state. The nonzero $B(E2)$ value reported experimentally in $^{78}$Ge is contrary to the value predicted by this model. It also contradicts that experimentally found in neighboring $^{76}$Ge [34]. Similarly, the $3_1^+$ state decay is hindered to the $2_1^+$ state. The difference between the energies of the $3_1^+$ and $4_1^+$ states

in the model is twice the value found experimentally. This explains explaining why a $3_1^+ \rightarrow 4_1^+$ transition is not hindered. Although the $4_1^+$ state is represented well in the model, the higher-spin yrast level energies are over-predicted.

The DFR model predicts three $4^+$ levels. These are found higher in energy than their nearly-degenerate experimental counterparts. The lowest becomes the second excited state in the ground-state rotational band. The calculated state at 3509 keV has an inhibited decay to the $3^+$ level. The branching is similar to those for the $4_2^+$ level observed experimentally at 2292 keV. The calculated 4128-keV $4_3^+$ state, on the other hand, has a strong branch to the $3_1^+$ level with inhibited transition strength to the other lower-energy $2_{1,2}^+$ and $4_1^+$ levels. This is in agreement with experimental results. The decay of the $4_3^+$ level indicates a large $B(E2)$ value to the 3509-keV $4_2^+$ state. These states are observed 17 keV apart. A transition that is this small cannot be measured with Gammasphere. Two $5^+$ levels are also predicted by the model. The upper state exhibits a strong branch to the calculated $4_3^+$ level. It has an inhibited transition strength to other, lower-energy $4^+$ levels. The experimental equivalent of the DFR-predicted $5^+$ state at 3715 keV could not be identified from transitions coincident with the 2292-keV $4_2^+$ state or the 1644-keV $3_1^+$ state. A $6_2^+$ state was predicted with a strong branch to the second $5^+$ level. This is similar to the observations for the 3295-keV $6^+$ level. No transitions were measured to feed the 2292-keV state. This complicates the character of the decay from the predicted 6192-keV $6^+$ state.

The staggering behavior is another feature of the states calculated in the DFR model. The $3_1^+$ state is closer to the $2_2^+$ state than to the $4_3^+$ level. However the

$5_2^+$ state is closer to the $6_2^+$ level than to the $4_3^+$ state. The $5_1^+$ and $4_2^+$ states are close in energy, as expected in the $\gamma$ band of a rigid triaxial rotor. The implication of using the $6_2^+$ and $4_3^+$ state is that both $S(3)$ and $S(4)$ will have negative values, which destroys the phase of the staggering. The staggering amplitude predicted by the DFR model is also 3 to 8 times higher than the experimental amplitude. This poses a significant question. Can staggering be used as an indicator of triaxiality if the triaxial band does not use the $4_2^+$ and $5_1^+$ states?

The DFR model demonstrates inhibited $\Delta J = 2$ transitions within the $\kappa$ band. It also includes the $4_3^+$ state in this band instead of the $4_2^+$ state. The DFR model describes the $\kappa$ band in agreement with experimental data. The only exception to this is found in the high excitation energies.

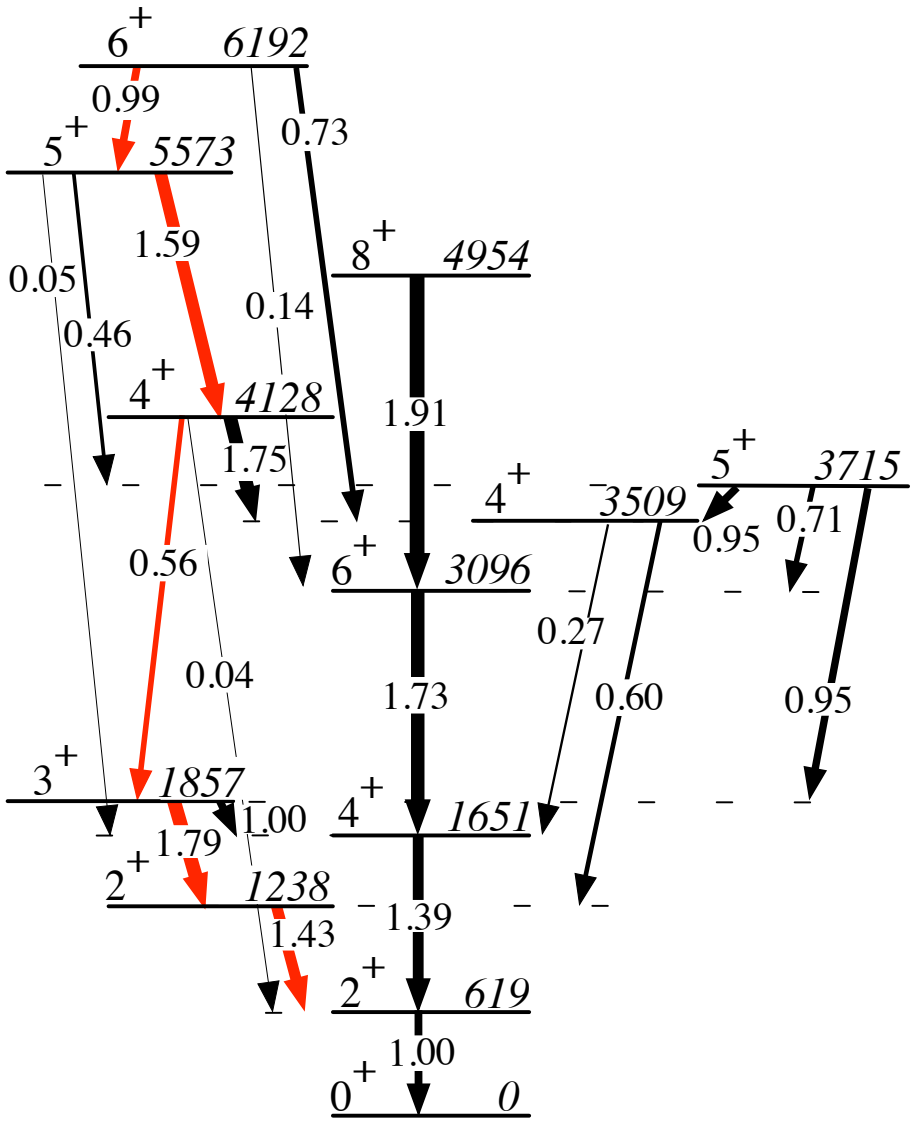


Figure 5.12: B(E2) and energy level calculations for $^{78}$Ge with $\gamma = 30°$ in the Davydov-Filippov-Rostovsky model with energies normalized to the experimental $2_1^+ \rightarrow 0^+$ transition. The transitions in red depict the equated $\kappa$-band transitions. Transitions not shown have a $B(E2)$ value of 0. The energy values are scaled to the experimental $2^+$ state.

# Chapter 7: Conclusion

This thesis has examined the nuclear structure of $^{82,80,78}$Ge through deep inelastic reactions. This work has confirmed many previously reported results and has significantly expanded level scheme of $^{78,80}$Ge. The [pf7] group is shown to adequately characterize the low-lying $^{82}$Ge structure. The higher-energy states appear to excitations across the $N = 50$ shell. The [pf7] group is also present within the $^{80}$Ge nucleus. The higher-energy states in $^{80}$Ge are not necessarily due to cross-shell excitations. They are due to additional configurations provided by the two neutron holes in the $N = 50$ shell. The $^{78}$Ge structure has noteworthy characteristics such as the $\kappa$ band, identified within this work. The presence of this sequence additional questions. These questions include the significance of the $4_3^+$ state within the sequence, the presence of shape coexistence, and the role of $E1$ transitions which populate both the $\kappa$ and the ground state band.

## 7.1 $^{82}$Ge Conclusions

The results of this thesis show a concurrence with previously reported levels of $^{82}$Ge. This study demonstrates the strength of multi-nucleon transfer reactions and the power of the coincidence method using the Gammasphere array. The re-

sults included a new transition of 408.6 keV from the 2935 keV level, and also the population of the yrast 940 keV doublet.

In $^{82}$Ge, the jj44 model space reproduces the [pf7] group, which is the seven states made through configurations in the $p_{3/2}$ and $f_{5/2}$ orbitals. Little collectivity has been observed in $^{82}$Ge as the states can be described by the [pf7]. The jj44 model space has reached its limit beyond the [pf7] as it cannot account for the density of states observed near 3 MeV. This is because the calculations do not describe cross-shell states in this model space. Additional investigations which compare even and odd $N = 50$ nuclei in this region will be available in a forthcoming publication [107].

The positions of the first seven states of $^{82}$Ge are accurately calculated by NuShellX. These results are consistent with the structure and calculations for isotonic $^{80}$Zn. The proposed higher-spin $5^+$ and $6^+$ states in $^{82}$Ge at 2935 and 3014 keV, are well below the predicted energies. These states are likely excitations across the $N = 50$ shell. This permits a test of the fidelity of the jj44 model space. An alternative approach was proposed by Seija and Nowacki [91]. They treat these states as arising from promotion of a single $g_{9/2}$ neutron across the $N = 50$ shell into a $d_{5/2}$ orbital. Their calculations place these states at 3170 and 3370 keV, respectively. These are reasonably close to the observed positions. NuShellX locates these states over 3500 keV.

The population of $^{82}$Ge in the available data from GS DIS was limited. Future investigation of the higher-spin states, and also states above 3 MeV will require a larger production of the nucleus. One such method would be a repetition of the DIS experiment using a $^{82}$Se beam with a thick target, but with a longer run-time. A

second approach would be to use a neutron-rich radioactive ion beam to populate more lower-lying states.

## 7.2 $^{80}$Ge Conclusions

The reactions used in this work to study the level structure of $^{80}$Ge were well-suited to the study of higher-spin levels. The $3^+$ assignment of the 1973 keV state compared to the previous $J^\pi = 4^+$ assignment, brings to light a set of states with $2^+, 3^+, 4^+, 5^+, 6^+$. This sequence is reminiscent of the $\gamma$-band in $^{72-76}$Ge and other nuclei. However, unlike the $\gamma$ bands of those nuclei, this set of states does not decay as a continuous sequence. The decay favors feeding into the ground state band.

The population of the $6^-$ $^{80}$Ga parent within the DDD data set is a clear indicator of $\beta$-decay parent. By contrast the isomer separation technique used by Verney *et al.* provided ambiguous values [5]. The intense decay into the $5^-$ state at 2852.5 keV may prove to be a significant aspect of this nucleus. Chou *et al.* [105] performed lifetime measurements for such states in $^{78}$Ge. It would be useful if a similar study were performed on $^{80}$Ge.

The observed structure up to about 3.7 MeV is in reasonable agreement with the NuShellX calculations. The NuShellX code reflects the experimental [pf7] states as well as the first few negative parity states. Two holes in the $g_{9/2}$ orbital can account for many of the states below the large shell gap at $N = 50$. Since these states are reflected by the code, they also exhibit very little collectivity.

## 7.3 $^{78}$Ge Conclusions

At the beginning of this study, the level structure of $^{78}$Ge was poorly understood among the even-even Ge nuclei. Moreover, the levels populated in $\beta$ decay were accorded an incorrect range of spin and parity possibilities. This was due to the incorrect assignment of the ground-state spin and parity for parent $^{78}$Ga. Among the nuclei studied, this was the only nucleus where additional information was available from (t,p) reaction measurements.

The most important result in this thesis work has been the identification of the $\kappa$ band. This is a band whose decay properties are not found elsewhere among low-energy excited levels in any nucleus. The energies of the members of this sequence appear similar to sequences labeled as $\gamma$ bands in lighter nuclei. However, the absence of $\Delta J = 2$ crossover transitions is not reproduced in any model proposed so far. The numerous $E1$ transitions in and out of the $\kappa$ band are the second feature of interest in $^{78}$Ge. The significance of this feature awaits further work.

The NuShellX calculations fit the observed levels in $^{78}$Ge without the inclusion of the $\kappa$ band. It has configurations beyond those in the jj44 model space. This could be an example of shape coexistence in the nucleus. The $\kappa$ band seems to be in a separate potential well, with a different shape for which no apparent parameterization is applicable. The inhibited inter-band $\Delta J = 2$ transitions are characteristic of the second shape, while the absence of transitions into the ground-state band is an indication of a significant potential barrier between the two shapes.

There are three $4^+$ states at low energy in $^{78}$Ge. The $4^+_3$ level belongs to the

$\kappa$ band. The $4^+$ level of $\gamma$ bands in lighter-Ge nuclei are the $4_2^+$ state. Further investigation will shed light as to the inclusion of the $4_3^+$ state rather than the $4_2^+$ level in $\gamma$-like sequences. This idea already has served to alter the interpretation of the structure of isotonic $^{80}$Se [107].

The results for the $\kappa$ band have been published as a Physical Review Letter in May 2018 [57]. It is possible to envision a number of new experiments that can be undertaken to improve the knowledge of the level structure of $^{78}$Ge.

# Appendix A:

## A.1 Ge DIS runs

To explore the germanium isotopes within these runs, a simple neutron transfer is required, not requiring the energies provided by this deep-inelastic collision.

### A.1.1 $^{76}$Ge beam on $^{238}$U target

Two runs, labeled gsfma223 and gsfma241 were run with this beam/target combination. The gsfma241 run was run at a higher energy beam, and has poorer statistics. The gsfma223 run done by Stefanescu *et al.* (described in Ref. [130]), provided the main data for the analysis within this work. With a $^{238}$U target, there are a series of low-energy Uranium transitions present.

Setting a gate in gsfma223 on two transitions in $^{78}$Ge, transitions from the complimentary $^{236}$U nucleus will be present. For example, a gate on the two lowest yrast transitions in $^{78}$Ge: 619.2 and 950.6 keV, returns a spectrum with the $^{236}$U transitions: 104.2 (E2) (doublet), 151.2 (E2), 160.2 (E2), 198.9 (E2), 212.5 (E2), 260.1 (E2), 303.3 (E2), 403.3 (E2), 642.6 (E1[+M2+E3]), 687.9 (E1), 956.2 keV. $^{238}$U transitions are also present: 995.3, 1042.3, 1454.8 keV. The transitions with energies

of 341.5, 1222.5 ($^{238}$U), 1234.9, 1328.4 keV are found in both the uranium nuclei and germanium. The peaks of 94.9, 98.8, 104.2, 111.4, 114.9, 351.8, 368.5, 375.2, 410.0, 434.4, 519.0, 535.5, 562.8*, 596.4, 625.8, 639.5, 649.0, 707.0, 722.5, 759.4, 834.6, 846, 913, 940.8, 966.2, 977.1, 1076.0, 1120.7, 1133, 1178.4, 1433.2, 1445.8, 1587.8, 1608.5, 1804.6 are yet to be accounted for. There a few other possibilities where these transitions come from: leak-through from the $^{76}$Ge beam or $^{238}$U target (like the starred 562.8-keV peak); or another nucleus that shares coincident transitions of 619.2 and 950.6 keV.

To be aware if two coincident transitions are in multiple nuclei, the NNDC [28] has an option to search nuclear levels and gammas. For example, investigating what other nuclei have coincident 619.2- and 950.6-keV transitions, a range with $\pm$1.0 keV of these two energies are input with a coincidence of 1 ns, return 7 nuclei with these coincidences. With the GS data, the energies usually only vary by $< 0.5$ keV between data sets, so $\pm$1.0 keV is a conservative range. This group of nuclei is beneficial to be aware of to prevent attributing transitions that belong to another nucleus. The likelihood of making some of these nuclei in the multi-nucleon transfer reaction can vary, as well as the high-spin levels that cause the decay of one of the transitions of interest. For example, there exists a 619.8-keV transition from a $(39/2^+)$ level coincident with a 951.2-keV $(23/2^+)$ transition in $^{163}_{71}$Lu$^{92}$. In order to make this nucleus in the $^{76}$Ge on $^{238}$U reaction, a very deep-inelastic reaction would be necessary, which would produce high spins. Looking into the list of levels in $^{163}$Lu, the $(39/2^+) \rightarrow (35/2^+)$ 619.8 keV transition would be followed by a 312.0-keV $(35/2^+) \rightarrow (31/2^+)$ transition. Since this 312.0 keV coincident transition is not

present in our spectrum, the coincidence in our spectra does not belong to the $^{163}$Lu nucleus.

One of the more challenging transitions to reconcile in $^{78}$Ge is the known 1223-keV transition from the $\beta$-decay work [102]. There is a $2^+ \rightarrow$ ground state 1223.8-keV $\gamma$ ray in $^{238}$U. With a gate on a 1223.8keV line and its coincident 768.3-keV transition in $^{238}$U, five transitions appear quite strong: 620.5, 647.0, 725.4, 769.6, and 834.4 keV. Using the gamma search of NNDC, 620.5-, 647.6-, 725.7-, and 835.2-keV transitions occur in $^{98}$Zr along with a 1222.9-keV line. There is no 768.3-keV transition, but that is accounted for because it occurs in the $^{238}$U nucleus. This complication indicates that any data set with a Uranium target cannot be used to correctly place the 1223-keV transition.

### A.1.2 $^{76}$Ge beam on a $^{208}$Pb target

The gsfma245 data set, or $^{76}$Ge beam on a $^{208}$Pb target, provides another set of data to confirm transitions in the other data sets. The main $^{206}$Pb lines are the 880.9-keV $4_1^+ \rightarrow 2_1^+$ and 803.0-keV $2_1^+ \rightarrow 0_1^+$ transitions. The same 619.2-950.6 keV gate, as shown as an example in the previous section returns a number of peaks. In the $^{206}$Pb and $^{208}$Pb nuclei: 343.6, 537.1, 663.8, 802.9, 880.9 keV. Unplaced transitions include: 75.3, 85.0, 114.0, 168.0, 184.2, 316.6, 324.6, 403.3, 434.0, 458.1, 546.1, 562.8, 567.8, 618.5, 626.0, 639.7, 649.1, 683.7, 703.8, 722.4, 759.4 keV. The presence of the 458.1-keV transition in the yrast gate is troubling, since we have proposed elsewhere in this work that it is not coincident with the 950.6-keV transition. There

are four possibilities to account for its presence: that there is a 458.1-keV $\gamma$ ray that has not been identified in the lead nuclei, that there is a second 458.1-keV transition within our Ge nucleus, that the 458.1-keV $\gamma$ ray is in another nucleus, or there is leak-through occurring because of the gate. It is highly unlikely that there is a 458.1-keV transition in the lead nucleus, because it has been studied extensively for many decades. A second 458.1 keV transition in the $^{78}$Ge nucleus can be checked in other data sets, and was not seen in the $^{76}$Ge on $^{238}$U experiment. The NNDC website is a useful tool to see if there exists a 458.1 keV $\gamma$ ray in coincident with our other two transitions, but there is no nucleus that has these three transitions coincident in the database. The last possibility is most likely, that there is some contamination in this nucleus. Another supporting factor for this possibility is that there is a second 618.5-keV peak in this gate–and a transition 617.6-(4) keV in $^{206}$Pb. The 617.6-keV transition feeds into the 1166.4-keV level which has a lifetime. This may cause the leak-through because it causes the prompt data to be contaminated by delayed transitions. Even with leak-through, this data set can be very useful to confirm the presence of other transitions in the $^{78}$Ge nucleus, but it cannot be used as the main data set.

### A.1.3 $^{76}$Ge beam on a $^{198}$Pt target

Unlike lead or uranium, platinum has fewer low-energy transitions. In the same 619.4-950.9 keV gate (energies are slightly different in this data set), peaks appear with energies (within 1 keV): From $^{196}$Pt: 316.2, 332.7, 340.9, 355.5, 393.2,

687.3, 441.3 keV. From $^{198}$Pt: 368.3, 407.1, 375.1, 578.2 keV.

The unplaced transitions are: 66.1, 113.7, 181.9, 184.6, 191.3, 204.5, 295.7, 321.3, 328.1, 433.8, 446.8, 467.9, 482.8, 521.1, 528.4, 550.4, 562.8, 599.7, 604.9, 627.6, 639.7, 649.0, 722.9, 727.4, 758.7, 846.8, 966.7, 1076.4, 1121.0, 1179.0, 1236.0, 1329.5, 1404.9, 1433.7, 1587.9, 1805.1, 2052.7 keV. Notice, that since the energies of our gates are slightly different because the calibration is slightly off, the energies of our coincident $\gamma$ rays differ as well.

## A.2 Spin Assignments Via Angular Correlation Measurements

This section is a continuation of Section 3.6. The angular momentum in DIS experiments is not aligned strongly with the beam direction. The angular distribution of detectors in Gammasphere allows for correlations between successive $\gamma$ rays. Pairs of detectors in the Gammasphere array with similar angles between them are compiled into bins for analysis which make up the angular correlation matrices of Fig. 3.7. The statistics of each of these bins varies dramatically, e.g. bin 4 and 7 have the lowest statistics. The goal is to account for the number of coincident $\gamma_2$ transitions within each detector occurring with the same timestamp as a $\gamma_1$ transition. The nature (quadrupole or dipole) of one of the two transitions should be known to conduct an angular correlation.

Coincidence matrices are sorted by the twelve bins, each with similar angles. These angle dependent matrices have been background subtracted to correct for Compton back-scattering and to allow for the assumption of a relatively constant

background for ease of peak fitting. For each matrix, a gate on $\gamma_1$ with a size on the order of $\sim$ 7 keV is created using the "damm" program from a "*.cmd" file Table A.1. This gate is determined from where the peak of $\gamma_1$ occurs in the total projection of a matrix, in spectral files with names such as: "ACmat01_xproj.spe" opened with RadWare program gf3. The "damm" program is called, then the command: cmd *.cmd is executed. This reads the *.cmd file and builds "gate655x.spk" and "gate655y.spk" files which will contain all coincidences from each of the twelve matrices. The "damm" procedure must be conducted for each matrix gate.

Table A.1: Example of a *.cmd file. Setting a gate around a $\gamma$ ray to conduct an Angular Correlation. Example for a gate at 655 keV with a channel (1 keV) width of 6. One *.cmd file is written for each matrix (our setup has 12) for each gate

| Code | Description |
|---|---|
| in ACmat01.his | The input is the histogram for the AC matrix 1 |
| ou gate655x.spk, new | Designating and creating an output spectral file for the x-axis. The ", new" is only used for the first cmd file. |
| nuid 01 | Creates a new id number |
| z1 | First buffer |
| z2 | Second buffer |
| gxa 1,653,658 | Setting the gate on the x-axis: step of 1, $E_{min}, E_{max}$ |
| ou | output |
| ou gate655y.spk, new | Creating an output spectral file for the y-axis. The ", new" is only used for the first cmd file. |
| nuid 01 | Creates a new id number |
| z1 | First buffer |
| z2 | Second buffer |
| gya 1,652,658 | Setting the gate on the y-axis: step of 1, $E_{min}, E_{max}$ |
| o2 | Writes the output |
| end | End of command file |

The spectrum for each gate (saved as *.spk) is presented using the gf3 RadWare function. The x-axis and y-axis information in the *.cmd file is identical, so either

*x.spk or *y.spk can be used. The command is: gf3 *.spk. There is a series of questions to fix values such as the shape (Gaussian, skewed Gaussian) of the peak, the linear (B) or quadratic (C) nature of the background [65]. The initial values used in this work are B =0, C=0, R=5, Beta = 0.2, Step = 0.25. These values can be adjusted after a fit is created to reflect the data more appropriately. Each spectrum (1-12) is displayed individually, and the peak area of $\gamma_2$ is fit with similar range in each matrix. A $\chi^2$ for the fit is provided as well as information on each peak fit within the region of interest. The peak area of $\gamma_2$ as well as its associated error in each matrix is noted and saved in a *.raw text file. In this work, screen shots of each fit were saved. The areas and errors of the *.raw file are corrected for detector efficiency, using $\gamma_1$ and $\gamma_2$ using a function in RadWare *corr*16 to become a *.dat file. With the command:

corr _feb16 *.raw *.dat

This *.dat file lists the converted efficiency values to $\theta$, $\omega(\theta)$, and $\sigma[\omega(\theta)]$, as the angle, the fit from Equation 3.1, and the error in the value of $\omega(\theta)$. The gnuplot program is then opened and the $\omega(\theta)$ equation (Eq. 3.2), here designated f(x), is loaded by the command:

f(x) = a*(1 + b*(1.5*cos(22*x/(7*180))**2 - 0.5) + c*(35*(cos(22*x/(7*180)))**4 - 30*(cos(22*x/(180*7)))**2 + 3)/8) .

Next, the *.dat file is fit to the f(x) by the command:

fit f(x) '*.dat' u 1:2:3 via a,b,c .

The final iteration of $a_{22}$ and $a_{44}$ coefficients (b and c parameters in gnuplot) of the Legendre polynomial and their errors are returned (Fig. A.1). Lastly, the command:

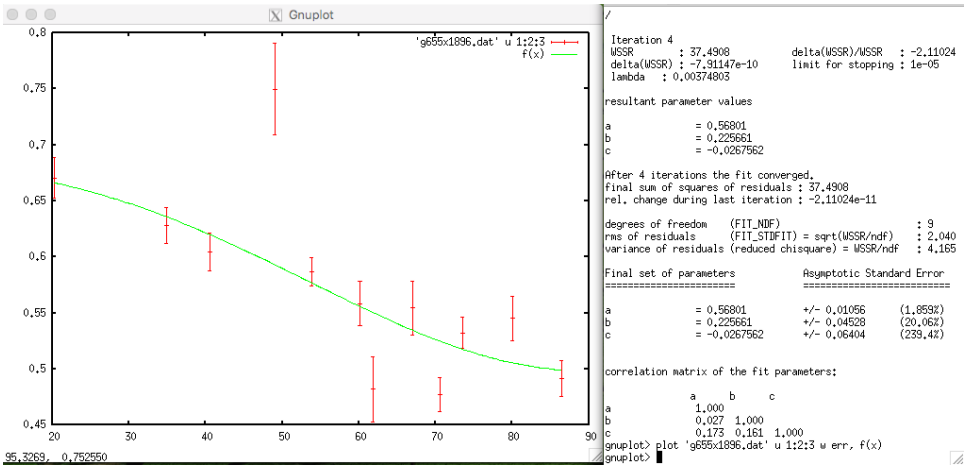


Figure A.1: Angular Correlation data from g655x1896.dat file plot (left) and fit of $\omega(\theta)$ (right) in the gnuplot program. Included in the fit are the determination of the $a_{22}$ (b) and $a_{44}$ (c) coefficients.

plot 'g966x1120V2.dat' u 1:2:3 w err, f(x)

will plot the data points and the fit. An example for the $\gamma_1 = 655.0$ keV $\gamma_1 = 1896$ keV $^{82}$Se transitions are shown in Fig. A.1. This example offers some insight into the limitations of our data. Notice the fourth and seventh data points are far off the fit. As seen in Fig. 3.7, the fourth and seventh bins have the fewest number of detector combinations, therefore the lowest statistics. For other points that fall significantly off an obvious trend (data point 9), the screen shot of that fit may be revisited and the data point may not be included in the final fit for the determination of $a_{22}$ and $a_{44}$. If, like the example in Fig. A.1, there is a negative correlation between the angles, it means that $\gamma_1$ and $\gamma_2$ are of the same nature, in this case, both are quadrupole in character. If the two transitions were of different natures, e.g., dipole and quadrupole, with the increase of angle (x-axis) there would be an increase in the $\omega(\theta)$ (y-axis).

# Bibliography


[1] P. Hoff and B. Fogelberg. Properties of strongly neutron-rich isotopes of germanium and arsenic. *Nuc. Phys. A*, 368(2):210 – 236, 1981.

[2] A. Makishima, M. Asai, T. Ishii, I. Hossain, M. Ogawa, S. Ichikawa, and M. Ishii. $(\nu g_{9/2}^{-2})_{8^+}$. *Phys. Rev. C*, 59:R2331–R2333, 1999.

[3] Zs. Podolyák, S. Mohammadi, G. De Angelis, Y. H. Zhang, M. Axiotis, D. Bazzacco, P. F. Bizzeti, F. Brandolini, R. Broda, D. Bucurescu, E. Farnea, W. Gelletly, A. Gadea, M. Ionescu-Bujor, A. Iordachescu, Th. Kroll, S. D. Langdown, S. Lunardi, N. Marginean, T. Martinez, N. H. Medina, B. Quintana, P. H. Regan, B. Rubio, C. A. Ur, J. J. Valiente-Dobon, and P. M. Walker. Structure of neutron-rich nuclei from deep-inelastic reactions. *Int. J. Mod. Phys.*, E13:123, 2004.

[4] T. Faul. Etude de la structure des noyaux riches en neutrons autour du noyau doublement magique $^{78}$Ni. Theses, Université Louis Pasteur - Strasbourg I, 2007.

[5] D. Verney, B. Tastet, K. Kolos, F. Le Blanc, F. Ibrahim, M. C. Mhamed, E . Cottereau, P. V. Cuong, F. Didierjean, G. Duchene, S. Essabaa, M. Ferraton, S. Franchoo, L. H. Khiem, C. Lau, J. F. Le Du, I. Matea, B. Mouginot, M. Niikura, B. Roussiere, I. Stefan, D. Testov, and J. C. Thomas. Structure of $^{80}$Ge revealed by the $\beta$ decay of isomeric states in $^{80}$Ga: Triaxiality in the vicinity of $^{78}$Ni. *Phys.Rev. C*, 87:054307, 2013.

[6] A. Gottardo, D. Verney, C. Delafosse, F. Ibrahim, B. Roussière, C. Sotty, S. Roccia, C. Andreoiu, C. Costache, M.-C. Delattre, I. Deloncle, A. Etilé, S. Franchoo, C. Gaulard, J. Guillot, M. Lebois, M. MacCormick, N. Marginean, R. Marginean, I. Matea, C. Mihai, I. Mitu, L. Olivier, C. Portail, L. Qi, L. Stan, D. Testov, J. Wilson, and D. T. Yordanov. First evidence of shape coexistence in the $^{78}$Ni region: Intruder $0_2^+$ state in $^{80}$Ge. *Phys. Rev. Lett.*, 116:182501, 2016.

[7] J.S. Lilley. *Nuclear Physics: Principles and Applications*. John Wiley & Sons, New York, NY, 2009.

[8] V.M. Strutinsky. Shell effects in nuclear masses and deformation energies. *Nuclear Physics A*, 95(2):420 – 442, 1967.

[9] V. F. Weisskopf. Radiative transition probabilities in nuclei. *Phys. Rev.*, 83:1073–1073, 1951.

[10] G. Stephans, S. Mordechai, and H. T. Fortune. Masses of $^{78}$Ge and $^{78}$As. *Phys.Rev.*, C24:1785, 1981.

[11] F. Yang and J. Hamilton. *Modern Atomic and Nuclear Physics*. World Scientific, Hackensack, NY, 2010.

[12] A. Aprahamian, D. S. Brenner, R. F. Casten, R. L. Gill, and A. Piotrowski. First observation of a near-harmonic vibrational nucleus. *Phys. Rev. Lett.*, 59:535–538, 1987.

[13] L. Wilets and M. Jean. Surface oscillations in even-even nuclei. *Phys. Rev.*, 102:788–796, 1956.

[14] G. Scharff-Goldhaber and J. Weneser. System of even-even nuclei. *Phys. Rev.*, 98:212–214, 1955.

[15] Ben R. Mottelson. Collective motion in the nucleus. *Rev. Mod. Phys.*, 29:186–190, 1957.

[16] A. Bohr and B. Mottelson. Collective and individual-particle aspects of nuclear structure. *Kgl. Danske Videnskab. Selskab Mat. Fys. Medd*, 27(16), 1953.

[17] W. Nazarewicz, J. Dudek, R. Bengtsson, T. Bengtsson, and I. Ragnarsson. Microscopic study of the high-spin behaviour in selected A $\sim$ 80 nuclei. *Nuc. Phys. A*, 435(2):397 – 447, 1985.

[18] S. Gardner. Tom Brady offered $1M fine, turned down alternative to Deflategate suspension, per report. *USA Today*.

[19] A. S. Davydov and G. F. Filippov. Rotational states in even atomic nuclei. *Nuc. Phys.*, 8:237 – 249, 1958.

[20] A. S. Davydov and V. S. Rostovsky. Relative transition probabilities between rotational levels of non-axial nuclei. *Nucl. Phys.*, 12(1):58 – 68, 1959.

[21] R.F. Casten. *Nuclear Structure from a Simple Perspective*. Oxford University Press, New York, NY, 1990.

[22] T. Fényes. *Structure of Atomic Nuclei*. Akadémiai Kiadó, Budapest, 2002.

[23] K.S. Krane. *Introductory Nuclear Physics*. Wiley & Sons, New York, NY, 1998.

[24] N. V. Zamfir and R. F. Casten. Signatures of $\gamma$ softness or triaxiality in low energy nuclear spectra. *Phys. Lett. B*, 260(3):265 – 270, 1991.

[25] E. A. McCutchan, D. Bonatsos, N. V. Zamfir, and R. F. Casten. Staggering in $\gamma$-band energies and the transition between different structural symmetries in nuclei. *Phys. Rev. C*, 76:024306, 2007.

[26] M. Bender, P.-H. Heenen, and P.-G. Reinhard. Self-consistent mean-field models for nuclear structure. *Rev. Mod. Phys.*, 75:121–180, 2003.

[27] B. H. Wells. *Green's Function Monte Carlo Methods*, pages 311–350. Springer US, Boston, MA, 1987.

[28] National Nuclear Data Center (NNDC). http://www.nndc.bnl.gov.

[29] Y. Shiga, K. Yoneda, D. Steppenbeck, N. Aoi, P. Doornenbal, J. Lee, H. Liu, M. Matsushita, S. Takeuchi, H. Wang, H. Baba, P. Bednarczyk, Zs. Dombradi, Zs. Fulop, S. Go, T. Hashimoto, M. Honma, E. Ideguchi, K. Ieki, K. Kobayashi, Y. Kondo, R. Minakata, T. Motobayashi, D. Nishimura, T. Otsuka, H. Otsu, H. Sakurai, N. Shimizu, D. Sohler, Y. Sun, A. Tamii, R. Tanaka, Z. Tian, Y. Tsunoda, Zs. Vajta, T. Yamamoto, X. Yang, Z. Yang, Y. Ye, R. Yokoyama, and J. Zenihiro. Investigating nuclear shell structure in the vicinity of $^{78}$Ni: Low-lying excited states in the neutron-rich isotopes $^{80,82}$Zn. *Phys. Rev. C*, 93:024320, 2016.

[30] L. Olivier, S. Franchoo, M. Niikura, Z. Vajta, D. Sohler, P. Doornenbal, A. Obertelli, Y. Tsunoda, T. Otsuka, G. Authelet, H. Baba, D. Calvet, F. Château, A. Corsi, A. Delbart, J.-M. Gheller, A. Gillibert, T. Isobe, V. Lapoux, M. Matsushita, S. Momiyama, T. Motobayashi, H. Otsu, C. Péron, A. Peyaud, E. C. Pollacco, J.-Y. Roussé, H. Sakurai, C. Santamaria, M. Sasano, Y. Shiga, S. Takeuchi, R. Taniuchi, T. Uesaka, H. Wang, K. Yoneda, F. Browne, L. X. Chung, Z. Dombradi, F. Flavigny, F. Giacoppo, A. Gottardo, K. Hadyńska-Klęk, Z. Korkulu, S. Koyama, Y. Kubota, J. Lee, M. Lettmann, C. Louchart, R. Lozeva, K. Matsui, T. Miyazaki, S. Nishimura, K. Ogata, S. Ota, Z. Patel, E. Sahin, C. Shand, P.-A. Söderström, I. Stefan, D. Steppenbeck, T. Sumikama, D. Suzuki, V. Werner, J. Wu, and Z. Xu. Persistence of the $z = 28$ shell gap around $^{78}$Ni: First spectroscopy of $^{79}$Cu. *Phys. Rev. Lett.*, 119:192501, 2017.

[31] J. M. Daugas, T. Faul, H. Grawe, M. Pfützner, R. Grzywacz, M. Lewitowicz, N. L. Achouri, J. C. Angélique, D. Baiborodin, R. Bentida, R. Béraud, C. Borcea, C. R. Bingham, W. N. Catford, A. Emsallem, G. de France, K. L. Grzywacz, R. C. Lemmon, M. J. Lopez Jimenez, F. de Oliveira Santos, P. H. Regan, K. Rykaczewski, J. E. Sauvestre, M. Sawicka, M. Stanoiu, K. Sieja,

and F. Nowacki. Low-lying isomeric levels in $^{75}$Cu. *Phys. Rev. C*, 81:034304, 2010.

[32] C. Petrone, J. M. Daugas, G. S. Simpson, M. Stanoiu, C. Plaisir, T. Faul, C. Borcea, R. Borcea, L. Cáceres, S. Calinescu, R. Chevrier, L. Gaudefroy, G. Georgiev, G. Gey, O. Kamalou, F. Negoita, F. Rotaru, O. Sorlin, and J. C. Thomas. Nearly degenerate isomeric states of $^{75}$Cu. *Phys. Rev. C*, 94:024319, 2016.

[33] O. Arndt, S. Hennrich, N. Hoteling, C. J. Jost, B. E. Tomlin, J. Shergur, K.-L. Kratz, P. F. Mantica, B. A. Brown, R. V. F. Janssens, W. B. Walters, B. Pfeiffer, A. Wöhr, S. Zhu, R. Broda, M. P. Carpenter, B. Fornal, A. A. Hecht, W. Królas, T. Lauritsen, T. Pawłat, J. Pereira, D. Seweryniak, I. Stefanescu, J. R. Stone, and J. Wrzesiński. Structure of neutron-rich odd-mass $^{127,129,131}$In populated in the decay of $^{127,129,131}$Cd*. *Acta Phys. Polonica B*, 40:437–446, 2009.

[34] Y. Toh, C. J. Chiara, E. A. McCutchan, W. B. Walters, R. V. F. Janssens, M. P. Carpenter, S. Zhu, R. Broda, B. Fornal, B. P. Kay, F. G. Kondev, W. Królas, T. Lauritsen, C. J. Lister, T. Pawłat, D. Seweryniak, I. Stefanescu, N. J. Stone, J. Wrzesiński, K. Higashiyama, and N. Yoshinaga. Evidence for rigid triaxial deformation at low energy in $^{76}$Ge. *Phys. Rev. C*, 87:041304, 2013.

[35] S. E. Larsson, G. Leander, I. Ragnarsson, and N. G. Alenius. Collective motion and deformed shell structure in the doubly even fp shell nuclei. *Nuc. Phys. A*, 261(1):77 – 92, 1976.

[36] I. Ragnarsson, S. G. Nilsson, and R. K. Sheline. Shell structure in nuclei. *Phys. Rep.*, 45(1):1 – 87, 1978.

[37] R. V. F. Janssens, B. Fornal, P. F. Mantica, B. A. Brown, R. Broda, P. Bhattacharyya, M. P. Carpenter, M. Cinausero, P. J. Daly, A. D. Davies, T. Glasmacher, Z. W. Grabowski, D. E. Groh, M. Honma, F. G. Kondev, W. Królas, T. Lauritsen, S. N. Liddick, S. Lunardi, N. Marginean, T. Mizusaki, D. J. Morrissey, A.C. Morton, W. F. Mueller, T. Otsuka, T. Pawłat, D. Seweryniak, H. Schatz, A. Stolz, S. L. Tabor, C. A. Ur, G. Viesti, I. Wiedenhöver, and J. Wrzesiński. Structure of $^{52,54}$Ti and shell closures in neutron-rich nuclei above $^{48}$Ca. *Phys. Lett. B*, 546(1):55 – 62, 2002.

[38] M. Rosenbusch, P. Ascher, D. Atanasov, C. Barbieri, D. Beck, K. Blaum, Ch. Borgmann, M. Breitenfeldt, R. B. Cakirli, A. Cipollone, S. George, F. Herfurth, M. Kowalska, S. Kreim, D. Lunney, V. Manea, P. Navrátil, D. Neidherr, L. Schweikhard, V. Somà, J. Stanja, F. Wienholtz, R. N. Wolf, and K. Zuber. Probing the $N = 32$ shell closure below the magic proton number $Z = 20$: Mass measurements of the exotic isotopes $^{52,53}$K. *Phys. Rev. Lett.*, 114:202501, 2015.

[39] A. T. Gallant, J. C. Bale, T. Brunner, U. Chowdhury, S. Ettenauer, A. Lennarz, D. Robertson, V. V. Simon, A. Chaudhuri, J. D. Holt, A. A. Kwiatkowski, E. Mané, J. Menéndez, B. E. Schultz, M. C. Simon, C. Andreoiu, P. Delheij, M. R. Pearson, H. Savajols, A. Schwenk, and J. Dilling. New precision mass measurements of neutron-rich calcium and potassium isotopes and three-nucleon forces. *Phys. Rev. Lett.*, 109:032506, 2012.

[40] F. Wienholtz, D. Beck, K. Blaum, Ch. Borgmann, M. Breitenfeldt, R.B. Cakirli, S. George, F. Herfurth, J.D. Holt, M. Kowalska, S. Kreim, D. Lunney, V. Manea, J. Menendéz, D. Neidherr, M. Rosenusch, L. Schweikhard, A. Schwenk, J. Simonis, J. Stanja, R.N. Wolf, and K. Zuber. Masses of exotic calcium isotopes pin down nuclear forces. *Nature*, 498(7454):346–9, 2013.

[41] S. N. Liddick, P. F. Mantica, R. Broda, B. A. Brown, M. P. Carpenter, A. D. Davies, B. Fornal, T. Glasmacher, D. E. Groh, M. Honma, M. Horoi, R. V. F. Janssens, T. Mizusaki, D. J. Morrissey, A. C. Morton, W. F. Mueller, T. Otsuka, J. Pavan, H. Schatz, A. Stolz, S. L. Tabor, B. E. Tomlin, and M. Wiedeking. Development of shell closures at $N = 32, 34$. I. $\beta$ decay of neutron-rich Sc isotopes. *Phys. Rev. C*, 70:064303, 2004.

[42] G. Gürdal, E. A. Stefanova, P. Boutachkov, D. A. Torres, G. J. Kumbartzki, N. Benczer-Koller, Y. Y. Sharon, L. Zamick, S. J. Q. Robinson, T. Ahn, V. Anagnostatou, C. Bernards, M. Elvers, A. Heinz, G. Ilie, D. Radeck, D. Savran, V. Werner, and E. Williams. Measurements of $g(4_1^+, 2_2^+)$ in $^{70,72,74,76}$Ge: Systematics of low-lying structures in $30 \leq Z \leq 40$ and $30 \leq N \leq 50$ nuclei. *Phys. Rev. C*, 88:014301, 2013.

[43] M. Bernas, Ph. Dessagne, M. Langevin, J. Payet, F. Pougheon, and P. Roussel. Magic features of $^{68}$Ni. *Phys. Lett. B*, 113(4):279 – 282, 1982.

[44] Y. Toh, T. Czosnyka, M. Oshima, T. Hayakawa, H. Kusakari, M. Sugawara, A. Osa, M. Koizumi, Y. Hatsukawa, J. Katakura, N. Shinohara, and M. Matsuda. Multiple Coulomb excitation of a $^{76}$Ge beam. *J. Phys. G*, 27(7):1475–1480, 2001.

[45] E. Padilla-Rodal, A. Galindo-Uribarri, C. Baktash, J. C. Batchelder, J. R. Beene, R. Bijker, B. A. Brown, O. Castaños, B. Fuentes, J. Gomez del Campo, P. A. Hausladen, Y. Larochelle, A. F. Lisetskiy, P. E. Mueller, D. C. Radford, D. W. Stracener, J. P. Urrego, R. L. Varner, and C.-H. Yu. $B(E2)\uparrow$ measurements for radioactive neutron-rich Ge isotopes: Reaching the $N = 50$ closed shell. *Phys. Rev. Lett.*, 94:122501, 2005.

[46] A. D. Ayangeakaa, R. V. F. Janssens, C. Y. Wu, J. M. Allmond, J. L. Wood, S. Zhu, M. Albers, S. Almaraz-Calderon, B. Bucher, M. P. Carpenter, C. J. Chiara, D. Cline, H. L. Crawford, H. M. David, J. Harker, A. B. Hayes, C. R. Hoffman, B. P. Kay, K. Kolos, A. Korichi, T. Lauritsen, A. O. Macchiavelli, A. Richard, D. Seweryniak, and A. Wiens. Shape coexistence and the role of axial asymmetry in $^{72}$Ge. *Phys. Lett. B*, 754:254–259, 2016.

[47] K. Heyde and J. L. Wood. Shape coexistence in atomic nuclei. *Rev. Mod. Phys.*, 83:1467–1521, 2011.

[48] M. Sugawara, Y. Toh, T. Czosnyka, M. Oshima, T. Hayakawa, H. Kusakari, Y. Hatsukawa, J. Katakura, N. Shinohara, M. Matsuda, T. Morikawa, A. Seki, and F. Sakata. Multiple coulomb excitation of a $^{70}$Ge beam and the interpretation of the $0_2^+$ state as a deformed intruder. *The European Physical Journal A - Hadrons and Nuclei*, 16(3):409–414, 2003.

[49] J. J. Sun, Z. Shi, X. Q. Li, H. Hua, C. Xu, Q. B. Chen, S.Q. Zhang, C. Y. Song, J. Meng, X. G. Wu, S. P. Hu, H. Q. Zhang, W. Y. Liang, F. R. Xu, Z. H. Li, G. S. Li, C. Y. He, Y. Zheng, Y. L. Ye, D. X. Jiang, Y. Y. Cheng, C. He, R. Han, Z. H. Li, C. B. Li, H. W. Li, J. L. Wang, J. J. Liu, Y. H. Wu, P. W. Luo, S. H. Yao, B. B. Yu, X. P. Cao, and H. B. Sun. Spectroscopy of $^{74}$Ge: From soft to rigid triaxiality. *Phys. Lett. B*, 734(0):308 – 313, 2014.

[50] H. T. Fortune. Coexistence and $B(E2)$ values in $^{72}$Ge. *Phys. Rev. C*, 94:024318, 2016.

[51] A. M. Van Den Berg, R. V. F. Janssens, G. T. Emery, A. Saha, and R. H. Siemssen. First excited $0^+$ states in the germanium isotopes via the Se($d$,$^6$ Li) reaction. *Nucl. Phys. A*, 379(2):239 – 255, 1982.

[52] D. Ardouin, R. Tamisier, M. Vergnes, G. Rotbard, J. Kalifa, G. Berrier, and B. Grammaticos. Systematics of the proton stripping reaction on $^{69,71}$Ga, $^{75}$As, $^{79,81}$Br isotopes and nuclear structure of the Ge-Se isotopes. *Phys. Rev. C*, 12:1745–1761, 1975.

[53] S. Sen, S. E. Darden, R. C. Luhn, N. O. Gaiser, G. Murillo, and J. Ramirez. Evidence of a shape transition in even-A Ge isotopes. *Phys. Rev. C*, 31:787–799, 1985.

[54] W.B. Walters. Structure of $^{74}$Ge. *Bull. Am. Phys. Soc.*, pages 62 #11, JB 8, 2017.

[55] S. Mukhopadhyay, B. P. Crider, B. A. Brown, S. F. Ashley, A. Chakraborty, A. Kumar, M. T. McEllistrem, E. E. Peters, F. M. Prados-Estévez, and S. W. Yates. Nuclear structure of $^{76}$Ge from inelastic neutron scattering measurements and shell model calculations. *Phys. Rev. C*, 95:014327, 2017.

[56] D. Ardouin, C. Lebrun, F. Guilbault, B. Remaud, E. R. Flynn, D. L. Hanson, S. D. Orbesen, M. N. Vergnes, G. Rotbard, and K. Kumar. Structure of $^{78}$Ge from the $^{76}$Ge(t, p)$^{78}$Ge reaction. *Phys. Rev. C*, 18:1201, 1978.

[57] A. M. Forney, W. B. Walters, C. J. Chiara, R. V. F. Janssens, A. D. Ayangeakaa, J. Sethi, J. Harker, M. Alcorta, M. P. Carpenter, G. Gürdal, C. R. Hoffman, B. P. Kay, F. G. Kondev, T. Lauritsen, C. J. Lister, E. A. McCutchan, A. M. Rogers, D. Seweryniak, I. Stefanescu, and S. Zhu. Novel

$\Delta J = 1$ sequence in $^{78}$Ge: Possible evidence for triaxiality. *Phys. Rev. Lett.*, 120:212501, 2018.

[58] H. Breuer, A. C. Mignerey, V. E. Viola, K. L. Wolf, J. R. Birkelund, D. Hilscher, J. R. Huizenga, W. U. Schröder, and W. W. Wilcke. Charge and mass exchange in $^{56}$Fe-induced reactions at 8.3 Mev/nucleon. *Phys. Rev. C*, 28:1080–1103, 1983.

[59] A. D. Hoover, J. R. Birkelund, D. Hilscher, W. U. Schröder, W. W. Wilcke, J. R. Huizenga, H. Breuer, A. C. Mignerey, V. E. Viola, and K. L. Wolf. $^{165}$Ho + $^{56}$Fe reaction at $E_{\text{lab}} = 462$ Mev. *Phys. Rev. C*, 25:256–277, 1982.

[60] J. Eberth and J. Simpson. From Ge(Li) detectors to gamma-ray tracking arrays 50 years of gamma spectroscopy with germanium detectors. *Progress in Particle and Nuclear Physics*, 60(2):283 – 337, 2008.

[61] I.-Y. Lee. The gammasphere. *Nuc. Phys. A*, 520(Supplement C):c641 – c655, 1990. Nuclear Structure in the Nineties.

[62] P. Fallon. Gamma-ray tracking school. online.

[63] N. Hoteling. Structure of the Fe isotopes at the limits of the *pf* shell. Thesis, University of Maryland, 2007.

[64] D. Radford. Radware.

[65] D. Radford. Notes on the use of the program gf3.

[66] D. Radford. Escl8r and levit8r: Software for interactive graphical analysis of hpge coincidence data sets.

[67] S.J. Robinson. How reliable are spins and -values derived from directional correlation experiments? *Nuclear Instruments and Methods in Physics Research Section A: Accelerators, Spectrometers, Detectors and Associated Equipment*, 292(2):386 – 400, 1990.

[68] H.W. Taylor, B. Singh, F.S. Prato, and R. McPherson. A tabulation of gamma-gamma directional-correlation coefficients. *Atomic Data and Nuclear Data Tables*, 9(1):1 – 83, 1971.

[69] B.A. Brown and E. Simpson. Talent course resources. online.

[70] J. A. Winger. Shell model studies of the $N = 50$ isotones in the $^{78}$Ni 'doubly magic' region. *Retrospective Theses and Dissertations*, 11660, 1987.

[71] Y. H. Zhang, Zs. Podolyák, G. de Angelis, A. Gadea, C. Ur, S. Lunardi, N. Marginean, C. Rusu, R. Schwengner, Th. Kroll, D. R. Napoli, R. Menegazzo, D. Bazzacco, E. Farnea, S. Lenzi, T. Martinez, M. Axiotis, D. Tonev, W. Gelletly, S. Langdown, P. H. Regan, J. J. Valiente-Dobon,

W. von Oertzen, B. Rubio, B. Quintana, N. Medina, R. Broda, D. Bucurescu, M. Ionescu-Bujor, and A. Iordachescu. Stability of the $N = 50$ shell gap in the neutron-rich Rb, Br, Se, and Ge isotones. *Phys. Rev. C*, 70:024301, 2004.

[72] M. P. Carpenter, F. G. Kondev, R. V. F. Janssens, N. Hoteling, T. L. Khoo, T. Lauritsen, C. J. Lister, D. Seweryniak, X. Wang, S. Zhu, R. Broda, B. Fornal, A. Galindo-Uribarri, A. Ibanez, E. Padilla-Rodal, and J. P. Ureggo-Blanco. Study of $N = 50$ nuclei near $^{78}$Ni using deep inelastic reactions. Technical Report ANL-07/29, Physics Division Argonne National Laboratory, 2006.

[73] T. Rzaca-Urban, W. Urban, J. L. Durell, A. G. Smith, and I. Ahmad. New excited states in $^{82}$Ge: Possible weakening of the $N = 50$ closed shell. *Phys. Rev. C*, 76:027302, 2007.

[74] E. Sahin. Investigation of nuclear shell structure far from stability in the region of $^{78}$Ni. In *Proc. Nuclear Physics and Astrophysics: From Stable Beams to Exotic Nuclei*, 2008.

[75] J. A. Winger, K. P. Rykaczewski, C. J. Gross, R. Grzywacz, J. C. Batchelder, C. Goodin, J. H. Hamilton, S. V. Ilyushkin, A. Korgul, W. Królas, S. N. Liddick, C. Mazzocchi, S. Padgett, A. Piechaczek, M. M. Rajabali, D. Shapira, E. F. Zganjar, and J. Dobaczewski. New subshell closure at $N = 58$ emerging in neutron-rich nuclei beyond $^{78}$Ni. *Phys. Rev. C*, 81:044303, 2010.

[76] J. K. Hwang, J. H. Hamilton, A. V. Ramayya, N. T. Brewer, Y. X. Luo, J. O. Rasmussen, and S. J. Zhu. Possible excited deformed rotational bands in $^{82}$Ge. *Phys. Rev. C*, 84:024305, 2011.

[77] E. Sahin, G. de Angelis, A. Gadea, G. Duchene, T. Faul, D. R. Napoli, E. Farnea, J. J. Valiente-Dobon, R. Orlandi, D. Mengoni, F. Della Vedova, R. P. Singh, C. Ur, F. Recchia, M. N. Erduran, M. Bostan, S. Erturk, S. Aydin, K. T. Wiedemann, A. M. Stefanini, S. Lenzi, S. Lunardi, N. Marginean, L. Corradi, E. Fioretto, G. Montagnoli, F. Scarlassara, P. Mason, S. Szilner, D. Ackermann, G. Pollarolo, J. R. B. Oliveira, T. Byrski, D. Curien, B. Gall, F. Haas, O. Dorwaux, J. Robin, M. Nespolo, F. Azaiez, G. De France, A. Algora, X. Liang, F. Nowacki, Y. H. Zhang, and X. H. Zhou. Nuclear structure far from stability at the $N = 50$ shell closure. In *Proc. Frontiers in Nuclear Structure*, 2008.

[78] M. F. Alshudifat, R. Grzywacz, M. Madurga, C. J. Gross, K. P. Rykaczewski, J. C. Batchelder, C. Bingham, I. N. Borzov, N. T. Brewer, L. Cartegni, A. Fijalkowska, J. H. Hamilton, J. K. Hwang, S. V. Ilyushkin, C. Jost, M. Karny, A. Korgul, W. Królas, S. H. Liu, C. Mazzocchi, A. J. Mendez, K. Miernik, D. Miller, S. W. Padgett, S. V. Paulauskas, A. V. Ramayya, D. W. Stracener, R. Surman, J. A. Winger, M. Wolinska-Cichocka, and E. F. Zganjar. Reexamining Gamow-Teller decays near $^{78}$Ni. *Phys. Rev. C*, 93:044325, 2016.

[79] D. Testov, D. Verney, B. Roussiere, J. Bettane, F. Didierjean, K. Flanagan, S. Franchoo, F. Ibrahim, E. Kuznetsova, R. Li, B. Marsh, I. Matea, Yu. Penionzhkevich, H. Pai, V. Smirnov, E. Sokol, I. Stefan, D. Suzuki, and J. N. Wilson. The $^{3}$He long-counter TETRA at the ALTO ISOL facility. *Nucl. Instrum. Methods Phys. Res.*, A815:96, 2016.

[80] D. Verney, D. Testov, F. Ibrahim, Yu. Penionzhkevich, B. Roussiere, V. Smirnov, F. Didierjean, K. Flanagan, S. Franchoo, E. Kuznetsova, R. Li, B. Marsh, I. Matea, H. Pai, E. Sokol, I. Stefan, and D. Suzuki. Pygmy gamow-teller resonance in the $N = 50$ region: New evidence from staggering of $\beta$-delayed neutron-emission probabilities. *Phys. Rev. C*, 95:054320, 2017.

[81] J. C. Hill, J. A. Winger, F. K. Wohn, R. L. Gill, A. Piotrowski, Xiangdong Ji, and B. H. Wildenthal. Is the region above $^{78}$Ni doubly magic (question). In *Contrib. Proc. 5th Int. Conf. Nuclei Far from Stability*, 1987.

[82] X. Ji and B. H. Wildenthal. Effective interaction for $N = 50$ isotones. *Phys. Rev. C*, 37:1256–1266, 1988.

[83] X. Ji and B. H. Wildenthal. Shell-model calculations for the energy levels of the $N = 50$ isotones with $A = 80 - -87$. *Phys. Rev. C*, 40:389–398, 1989.

[84] O. Perru, F. Ibrahim, O. Bajeat, C. Bourgeois, F. Clapier, E. Cottereau, C. Donzaud, M. Ducourtieux, S. Gales, D. Guillemaud-Mueller, C. Lau, H. Lefort, F. Le Blanc, A. C. Mueller, J. Obert, N. Pauwels, J. C. Potier, F. Pougheon, J. Proust, B. Roussiere, J. Sauvage, O. Sorlin, and D. Verney. Decay of neutron-rich Ga isotopes near $N = 50$ at PARRNe. *Yad. Fiz.*, 66:1467, 2003.

[85] G. J. Farooq-Smith, A. R. Vernon, J. Billowes, C. L. Binnersley, M. L. Bissell, T. E. Cocolios, T. Day Goodacre, R. P. de Groote, K. T. Flanagan, S. Franchoo, R. F. Garcia Ruiz, W. Gins, K. M. Lynch, B. A. Marsh, G. Neyens, S. Rothe, H. H. Stroke, S. G. Wilkins, and X. F. Yang. Probing the $_{31}$Ga ground-state properties in the region near $Z = 28$ with high-resolution laser spectroscopy. *Phys. Rev. C*, 96:044324, 2017.

[86] B. Cheal, J. Billowes, M. L. Bissell, K. Blaum, F. C. Charlwood, K. T. Flanagan, D. H. Forest, S. Fritzsche, Ch. Geppert, A. Jokinen, M. Kowalska, A. Krieger, J. Krämer, E. Mané, I. D. Moore, R. Neugart, G. Neyens, W. Nörtershäuser, M. M. Rajabali, M. Schug, H. H. Stroke, P. Vingerhoets, D. T. Yordanov, and M. Žáková. Discovery of a long-lived low-lying isomeric state in $^{80}$Ga. *Phys. Rev. C*, 82:051302, 2010.

[87] J. A. Winger, C. J. Gross, K. P. Rykaczewski, J. C. Batchelder, C. Goodin, R. Grzywacz, J. H. Hamilton, S. V. Ilyushkin, A. Korgul, W. Królas, S. N. Liddick, C. Mazzocchi, S. Padgett, A. Piechaczek, M. M. Rajabali, D. Shapira, and E. F. Zganjar. Nuclear structure studies near $^{78}$Ni at the HRIBF. In *Book of Abstracts*, 2008.

[88] O. Perru. Etude des fermetures de couches $N = 40$ et $N = 50$ dans les noyaux riches en neutrons, 2004.

[89] H. Iwasaki, N. Aoi, S. Takeuchi, S. Ota, H. Sakurai, M. Tamaki, T. K. Onishi, E. Takeshita, H. J. Ong, N. Iwasa, H. Baba, Z. Elekes, T. Fukuchi, Y. Ichikawa, M. Ishihara, S. Kanno, R. Kanungo, S. Kawai, T. Kubo, K. Kurita, S. Michimasa, M. Niikura, A. Saito, Y. Satou, S. Shimoura, H. Suzuki, M. K. Suzuki, Y. Togano, Y. Yanagisawa, and T. Motobayashi. Intermediate-energy coulomb excitation of the neutron-rich Ge isotopes around $N = 50$. *Eur.Phys.J. A*, 25:Supplement 1, 415, 2005.

[90] A. Gade, T. Baugher, D. Bazin, B. A. Brown, C. M. Campbell, T. Glasmacher, G. F. Grinyer, M. Honma, S. McDaniel, R. Meharchand, T. Otsuka, A. Ratkiewicz, J. A. Tostevin, K. A. Walsh, and D. Weisshaar. Collectivity at $N = 50$: $^{82}$Ge and $^{84}$Se. *Phys. Rev. C*, 81:064326, 2010.

[91] K. Sieja and F. Nowacki. Three-body forces and persistence of spin-orbit shell gaps in medium-mass nuclei: Toward the doubly magic $^{78}$Ni. *Phys. Rev. C*, 85:051301, 2012.

[92] P. Hoff. The population of excited states in residual nuclei via delayed neutrons. *Nuc. Phys. A*, 359(1):9 – 35, 1981.

[93] R. Lică, N. Mărginean, D. G. Ghiţă, H. Mach, L. M. Fraile, G. S. Simpson, A. Aprahamian, C. Bernards, J. A. Briz, B. Bucher, C. J. Chiara, Z. Dlouhý, I. Gheorghe, P. Hoff, J. Jolie, U. Köster, W. Kurcewicz, R. Mărginean, B. Olaizola, V. Paziy, J. M. Régis, M. Rudigier, T. Sava, M. Stănoiu, L. Stroe, and W. B. Walters. Low-lying isomeric states in $^{80}$Ga from the $\beta^-$ decay of $^{80}$Zn. *Phys. Rev. C*, 90:014320, 2014.

[94] H. Mach, P. M. Walker, R. Julin, M. Leino, S. Juutinen, M. Stanoiu, Zs. Podolyák, R. Wood, A. M. Bruce, T. Bäck, J. A. Cameron, B. Cederwall, J. Ekman, B. Fogelberg, P. T. Greenless, M. Hellström, P. Jones, W. Klamra, K. Lagergren, A.-P. Leppänen, P. Nieminen, R. Orlandi, J. Pakarinen, P. Rahkila, D. Rudolph, G. Simpson, J. Uusitalo, and C. Wheldon. Application of ultra-fast timing techniques to the study of exotic and weakly produced nuclei. *J. Phys. G*, 31(10):S1421, 2005.

[95] C.-A. Wiedner, R. Haupt, W. Saathoff, J. Haas, R. Gyufko, K.R. Cordell, S.T. Thornton, R.A. Cecil, and R.L. Parks. Mass excesses of $^{79}$As, $^{81}$As, and $^{80}$Ge. *Nuc. Phys. A*, 411(1):151 – 160, 1983.

[96] B. Grapengiesser, E. Lund, and G. Rudstam. Survey of short-lived fission products obtained using the isotope-separator-on-line facility at studsvik. *J. Inorg. Nucl. Chem.*, 36:2409, 1974.

[97] E. Mané, B. Cheal, J. Billowes, M. L. Bissell, K. Blaum, F. C. Charlwood, K. T. Flanagan, D. H. Forest, Ch. Geppert, M. Kowalska, A. Krieger,

J. Krämer, I. D. Moore, R. Neugart, G. Neyens, W. Nörtershäuser, M. M. Rajabali, R. Sánchez, M. Schug, H. H. Stroke, P. Vingerhoets, D. T. Yordanov, and M. Žáková. Ground-state spins and moments of $^{72,74,76,78}$Ga nuclei. *Phys. Rev. C*, 84:024303, 2011.

[98] S. Iwasaki, T. Marumori, F. Sakata, and K. Takada. Structure of the anomalous $0^+$? excited states in spherical even-even nuclei with N or Z $\sim$40. *Prog. Theor. Phys.*, 56(4):1140–1155, 1976.

[99] C. M. Baglin. Nuclear data sheets for $A = 81$. *Nuclear Data Sheets*, 79(3):447 – 638, 1996.

[100] E. Kvale and A. C. Pappas. Half-life and decay properties of $^{78}$Ge. *Nucl.Phys.*, 74:27, 1965.

[101] K. Aleklett, E. Lund, G. Nyman, and G. Rudstam. Total $\beta$-decay energies and masses of short-lived isotopes of zinc, gallium, germanium and arsenic. *Nucl. Phys. A*, 285(1):1 – 18, 1977.

[102] D. A. Lewis, John C. Hill, F. K. Wohn, and M. L. Gartner. Decay of mass-separated $^{78}$Ga to levels in even-even $^{78}$Ge. *Phys. Rev. C*, 22:2178–2185, 1980.

[103] J. F. Mateja, L. R. Medsker, H. T. Fortune, R. Middleton, G. E. Moore, M. E. Cobern, S. Mordechai, J. D. Zumbro, and C. P. Browne. $^{76}$Ge$(t,p)^{78}$Ge. *Phys. Rev. C*, 17:2047–2052, 1978.

[104] C. Lebrun, F. Guilbault, D. Ardouin, E. R. Flynn, D. L. Hanson, S. D. Orbesen, R. Rotbard, and M. N. Vergnes. $^{72,74,76}$Ge. *Phys. Rev. C*, 19:1224–1235, 1979.

[105] W.-T. Chou, D. S. Brenner, R. F. Casten, and R. L. Gill. Level lifetime measurements and the structure of neutron-rich $^{78}$Ge. *Phys. Rev. C*, 47:157–162, 1993.

[106] T. Nikšić, P. Marević, and D. Vretenar. Microscopic analysis of shape evolution and triaxiality in germanium isotopes. *Phys. Rev. C*, 89:044325, 2014.

[107] A. M. Forney, W. B. Walters, et al. To be published.

[108] D. Wilmsen. Nuclear structure studies with neutron-induced reactions: fission fragments in the $N = 50-60$ region, a fission tagger for FIPPS, and production of the isomer Pt-195m. Theses, Normandie Universite, 2017.

[109] J. Litzinger, A. Blazhev, A. Dewald, F. Didierjean, G. Duchêne, C. Fransen, R. Lozeva, K. Sieja, D. Verney, G. de Angelis, D. Bazzacco, B. Birkenbach, S. Bottoni, A. Bracco, T. Braunroth, B. Cederwall, L. Corradi, F. C. L. Crespi, P. Désesquelles, J. Eberth, E. Ellinger, E. Farnea, E. Fioretto, R. Gernhäuser, A. Goasduff, A. Görgen, A. Gottardo, J. Grebosz, M. Hackstein, H. Hess, F. Ibrahim, J. Jolie, A. Jungclaus, K. Kolos, W. Korten, S. Leoni, S. Lunardi,

A. Maj, R. Menegazzo, D. Mengoni, C. Michelagnoli, T. Mijatovic, B. Million, O. Möller, V. Modamio, G. Montagnoli, D. Montanari, A. I. Morales, D. R. Napoli, M. Niikura, G. Pollarolo, A. Pullia, B. Quintana, F. Recchia, P. Reiter, D. Rosso, E. Sahin, M. D. Salsac, F. Scarlassara, P.-A. Söderström, A. M. Stefanini, O. Stezowski, S. Szilner, Ch. Theisen, J. J. Valiente Dobón, V. Vandone, and A. Vogt. Transition probabilities in neutron-rich $^{84,86}$Se. *Phys. Rev. C*, 92:064322, 2015.

[110] J. Hakala, S. Rahaman, V. V. Elomaa, T. Eronen, U. Hager, A. Jokinen, A. Kankainen, I. D. Moore, H. Penttila, S. Rinta-Antila, J. Rissanen, A. Saastamoinen, T. Sonoda, C. Weber, and J. Aysto. Evolution of the $N = 50$ shell gap energy towards $^{78}$Ni. *Phys. Rev. Lett.*, 101:052502, 2008.

[111] J. A. Winger, John C. Hill, F. K. Wohn, R. Moreh, R. L. Gill, R. F. Casten, D. D. Warner, A. Piotrowski, and H. Mach. Decay of $^{80}$Zn: Implications for shell structure and r-process nucleosynthesis. *Phys. Rev. C*, 36:758–764, 1987.

[112] S. T. Hsieh, H. C. Chiang, and Der-San Chuu. Structure of even Ge isotopes by means of interacting boson model with a fermion pair model. *Phys. Rev. C*, 46:195–200, 1992.

[113] A. R. Subber. Nuclear structure of even-even Ge isotopes by means of interacting boson models. *Turk. J. Phys.*, 35:43, 2011.

[114] K. Nomura, R. Rodríguez-Guzmán, and L. M. Robledo. Structural evolution in germanium and selenium nuclei within the mapped interacting boson model based on the Gogny energy density functional. *Phys. Rev. C*, 95:064310, 2017.

[115] S. Abood, A. Saad, A. Kader, and L. Najim. Nuclear structure of the germanium nuclei in the interacting boson model (IBM). *J. Pure & Applied Science*, 4(3):63–73, 2013.

[116] J. Dobaczewski, W. Nazarewicz, J. Skalski, and T. Werner. Nuclear deformation: A proton-neutron effect? *Phys. Rev. Lett.*, 60:2254–2257, 1988.

[117] M. Lebois, D. Verney, F. Ibrahim, S. Essabaa, F. Azaiez, M. C. Mhamed, E. Cottereau, P. V. Cuong, M. Ferraton, K. Flanagan, S. Franchoo, D. Guillemaud-Mueller, F. Hammache, C. Lau, F. Le Blanc, J. F. Le Du, J. Libert, B. Mouginot, C. Petrache, B. Roussiere, L. Sagui, N. de Sereville, I. Stefan, and B. Tastet. Experimental study of $^{84}$Ga beta decay: Evidence for a rapid onset of collectivity in the vicinity of $^{78}$Ni. *Phys. Rev. C*, 80:044308, 2009.

[118] J. A. Sheikh, N. Hinohara, J. Dobaczewski, T. Nakatsukasa, W. Nazarewicz, and K. Sato. Isospin-invariant Skyrme energy-density-functional approach with axial symmetry. *Phys. Rev. C*, 89:054317, 2014.

[119] N. Yoshinaga, K. Higashiyama, and P. H. Regan. High-spin structure of neutron-rich Se, As, Ge, and Ga isotopes. *Phys. Rev. C*, 78:044320, 2008.

[120] M. Honma, T. Otsuka, T. Mizusaki, and M. Hjorth-Jensen. New effective interaction for $f_5pg_9$-shell nuclei. *Phys. Rev. C*, 80:064323, 2009.

[121] A. Gade et al. Collectivity at $N = 40$ in neutron-rich $^{64}$Cr. *Phys. Rev. C*, 81:051304, 2010.

[122] S. F. Shen, S. J. Zheng, F. R. Xu, and R. Wyss. Stability of triaxial shapes in ground and excited states of even-even nuclei in the A $\sim$ 70 region. *Phys. Rev. C*, 84:044315, 2011.

[123] J. G. Hirsch and P. C. Srivastava. Shell model description of Ge isotopes. *J. Phys. Conf. Ser.*, 387:012020, 2012.

[124] G. H. Bhat, W. A. Dar, J. A. Sheikh, and Y. Sun. Nature of $\gamma$ deformation in Ge and Se nuclei and the triaxial projected shell model description. *Phys. Rev. C*, 89:014328, 2014.

[125] L. Gaudefroy, A. Obertelli, S. Péru, N. Pillet, S. Hilaire, J. P. Delaroche, M. Girod, and J. Libert. Collective structure of the $N = 40$ isotones. *Phys. Rev. C*, 80:064313, 2009.

[126] K. Higashiyama and N. Yoshinaga. Application of the generator coordinate method to neutron-rich Se and Ge isotopes. In *Int. Nuclear Physics Conf. 2013*, 2014.

[127] E. Padilla-Rodal, O. Castanos, R. Bijker, and A. Galindo-Uribarri. IBM-2 configuration mixing and its geometric interpretation for germanium isotopes. *Revista Mexicana de Fisica*, 52:57 – 62, 2006.

[128] P. Möller, A.J. Sierk, R. Bengtsson, H. Sagawa, and T. Ichikawa. Nuclear shape isomers. *Atomic Data and Nuclear Data Tables*, 98(2):149 – 300, 2012.

[129] N. Yoshinaga and K. Higashiyama. Band structure of neutron rich Se and Ge isotopes. *Journal of Physics: Conference Series*, 445(1):012032, 2013.

[130] I. Stefanescu, W. B. Walters, R. V. F. Janssens, S. Zhu, R. Broda, M. P. Carpenter, C. J. Chiara, B. Fornal, B. P. Kay, F. G. Kondev, W. Królas, T. Lauritsen, C. J. Lister, E. A. McCutchan, T. Pawłat, D. Seweryniak, J. R. Stone, N. J. Stone, and J. Wrzesiński. Identification of the $g_{9/2}$-proton bands in the neutron-rich $^{71,73,75,77}$Ga nuclei. *Phys. Rev. C*, 79:064302, 2009.